Faculty of Engineering

Department of Chemical, Environmental and Civil Engineering

Nottingham Transportation Engineering Centre

PRODUCTION AND CHARACTERISATION OF WASTE LIGNIN AND BIODIESEL-DERIVED RESIDUES AS POTENTIAL BITUMEN MODIFIERS

by

Ana I. Weir (BSc, MSc)

Supervised by

Prof C.E. Snape, Prof G.D. Airey, Dr. C.N. Uguna, Dr. A. Jiménez del Barco Carrión

Thesis submitted to the University of Nottingham for the degree of Doctor of Engineering

March 2022

Abstract

Most pavements around the world are built with asphalt comprising bituminous binders derived from fossil fuels. Bitumen traditionally fulfils the role of a binder in asphalt mixtures and provides tensile resistance and cohesion to the mixture. The binder's rheological and adhesive properties allow these asphalt mixtures to withstand daily stresses such as traffic loads and environmental conditions without suffering excessive damage. Growing environmental concerns surrounding petroleum-derived bitumens have motivated the search for biobinders (binders manufactured from biomass) to be used in asphalt mixtures. In particular, waste biomass products are of interest due to their availability and impact on sustainability, but they generally need to be thermochemically treated before being used as biobinders. Biobinders have shown great potential to reduce bitumen demand and have exhibited good performance in terms of resisting common distresses affecting roads. However, detailed characterisation is still needed before they can be used in practice. The main objective of this project was to produce and characterise binders manufactured from waste biomass that can be used in pavements and encourage the development of sustainable and environmentally friendly solutions in pavement engineering. In this context, the focus of this project was to understand the chemical and rheological properties of waste lignin and biodiesel-derived residues in order to assess their suitability as potential biobinders. For this purpose, biobinders were produced via hydrothermal liquefaction and/or pyrolysis to obtain a higher viscosity bio-bitumen product.

The research initially focused on the production and rheological characterisation of a lignin-containing paper waste residue via hydrothermal liquefaction (HTL). Although far too low yields of the paper waste biobinder were produced via HTL, these early results revealed that these biobinders are soft materials with lower stiffness compared to conventional bitumens. With further testing, a potential application for this material could be enhancing high-temperature performance due to an increased elastic response at these temperatures. Following this, the research centred on investigating the chemical and rheological properties of two biodiesel-derived residues before and after thermal treatment labelled Biofuel Oils (BFO). A comprehensive chemical characterisation was undertaken on the neat biomaterials before blending with bitumen in order to characterise the differences between the residues. This then led to the bio-modification of three penetration grade bitumens and the analysis of

their rheological and ageing characteristics. The results showed that hydrothermal liquefaction is not an appropriate thermochemical treatment for the production of a higher viscosity biobinder from BFO materials due to the thermal decomposition of higher molecular weight compounds. However, the BFO can be upgraded to a higher viscosity product via thermal (pyrolytic) treatment to distil off lower molecular weight compounds.

The rheological testing revealed that the addition of the BFO (original or pyrolysed) softens the bitumens by decreasing the complex modulus and increasing the viscous response. However, there is an increased stiffness and elastic response in the pyrolysed BFO compared to the starting materials. Although the biomodified bitumens showed the same ageing tendency as conventional materials, ageing occurred at a faster rate, which can be considered the main drawback of their performance.

In light of the results obtained for the materials studied, the BFO can be considered a promising material in the improvement of low temperature cracking and fatigue performance due to the decrease in stiffness and increase in viscous response compared to aged or low penetration grade bitumens including recycled asphalt mixtures. With further research, a possible application for the higher viscosity pyrolysed BFO could be as an additive for warm mix asphalt pavements due its softer consistency than conventional materials. As a result, future work could focus on the implications of scale-up in the laboratory to produce higher quantities of the pyrolysed BFO for comprehensive asphalt mixture work.

Acknowledgments

First and foremost, I would like to thank my supervisors Prof. Colin Snape, Prof. Gordon Airey and Dr. Clement Uguna for all their help and support throughout this EngD. Without their guidance, this thesis would not have been possible.

This research is part of the Carbon Capture and Storage and Cleaner Fossil Energy Centre for Doctoral Training and the Nottingham Transportation Engineering Centre research group at the University of Nottingham. I would like to acknowledge the Engineering and Physical Sciences Research Council (EPSRC) and Tarmac, a Cement Roadstone Holdings company, for providing financial support for this project. I would also like to acknowledge Argent Energy UK Ltd. for providing the BFO materials. Thank you all for your involvement in this project.

During the development of this thesis I had the chance to collaborate with some fantastic individuals. Thanks to all my colleagues and technicians for your support throughout these years. A special mention to my mentor Dr. Ana Jiménez del Barco Carrión for your incredible support. I would also like to thank Dr. José M. Hidalgo for undertaking SIMDIS analysis, Kevin Butler for undertaking ^{13}C NMR and Max Edney for the collection of the LDI-MS data.

Last but certainly not least, I would like to thank my family and friends, near and far, for all their love and encouragement. A special mention to my fiancé, Richard Seely, for always listening to me, particularly these last few months! If it weren't for this experience, we would not have met. I wouldn't have been able to do this without you.

To Abuelo, for inspiring me to keep learning.

Declaration

I declare that the contents and the work described in this thesis were performed at the University of Nottingham, Faculty of Engineering from August 2017 to December 2021. I hereby certify that this thesis is my own and has not been submitted in whole or in part to any other university or any other educational association for a higher degree.

Ana I. Weir

March, 2022

We declare that the contents and the work described in this thesis were performed at the University of Nottingham, Faculty of Engineering from August 2017 to December 2021 and under our supervision.

Prof Colin. E. Snape

Prof Gordon D. Airey

Dr. Clement N. Uguna

Contents

^{13}C NMR	Carbon-13 Nuclear Magnetic Resonance
^{1}H NMR	Proton Nuclear Magnetic Resonance
AGC	Automatic Gain Control
BBOT	2,5-Bis(5-tert-butyl-2-benzo-oxazol-2-yl) thiophene
BBR	Bending Beam Rheometer
BBS	Binder Bond Strength
BFO	Biofuel Oil
CCS CFE	Carbon Capture and Storage and Cleaner Fossil Energy
$CDCl_3$	Deuterated Chloroform-d
CO	Carbon monoxide
CO_2	Carbon dioxide
DBE	Double Bond Equivalence
DBP	Dibutyl phthalate
DMA	Dynamic Mechanical Analysis
DSR	Dynamic Shear Rheometer
EA	Elemental Analysis
EI	Electron Impact Ionization Detector
EIBP	Environmental Impact of Biomass Pre-processing
EMS	Epoxidized Soybean Soyate
EPSRC	Engineering and Physical Sciences Research Council
F20TPP	Iron (III) porphyrins
FAME	Fatty acid methyl esters
FBP	Final Boiling Point
G*	Complex Modulus
GC	Gas chromatograph
GC-MS	Gas Chromatography-Mass Spectrometry
H_2	Hydrogen
H_2O	Water
HTC	Hydrothermal Carbonisation
HTF	Horizontal High-temperature Furnace
HTL	Hydrothermal Liquefaction
IBP	Initial Boiling Point
IRS	Indirect Tensile Strength
ITSM	Indirect Tensile Stiffness Modulus
Jnr	Non-recoverable creep compliance
LAS	Linear Amplitude Sweep
LCA	Life Cycle Assessment
LDI-MS	Laser Desorption Ionisation Mass Spectrometry
MALDI MS	Matrix-assisted Laser Desorption Ionisation Mass Spectrometry
MFP	Molecular Formula Prediction
MSCR	Multiple Stress Creep Recovery
N_2	Nitrogen
N_f	Number of Cycles
nmRC	Nanoscale and Microscale Research Centre
NTEC	Nottingham Transportation Engineering Centre

Pa.s	Pascal-second
PATTI	Pneumatic Adhesive Testing Instrument
PAV	Pressure Ageing Vessel
PBA	Polybutyl acrylate
PEA	Polyethyl acrylate
PG	Performance Grade
PMA	Polymethyl acrylate
PMB	Polymer-modified bitumen
PTTSP	Partial Time-Temperature Superposition Principle
R%	Percentage Recovery
RA	Recycled Asphalt
RAP	Reclaimed Asphalt Pavement
RCAT	Rotating Cylinder Ageing Test
RPM	Revolutions Per Minute
RTFOT	Rotating Thin Film Oven Test
SBS	Styrene-butadiene-styrene
SD	Standard Deviation
SEC	Size-exclusion Chromatography
SHRP	Strategic Highway Research Program
SIM	Selected Ion Monitoring
SIMDIS	Simulated Distillation
sME	Saturated fatty acid methyl ester
SP	Softening Point
TFOT	Thin Film Oven Test
TGA	Thermogravimetric analysis
THF	tetrahydrofuran
TIC	Total Ion Chromatogram
TMS	Tetramethylsilane
TTSP	Time-Temperature Superposition Principle
uME	Unsaturated fatty acid methyl ester
VECD	Viscoelastic Continuum Damage Theory
VOCs	Volatile Organic Compounds
WLF	William-Landel-Ferry
WMA	Warm Mix Asphalt
Wt. %	Weight percentage

List of figures

List of tables

1. Introduction

1.1. Background of the thesis

Most bituminous binders used for pavements are derived from fossil fuels. Their function is to provide the road with a smooth and impermeable surface to ensure road safety. For years, bituminous pavement mixtures have been derived from petroleum and have been able to withstand daily stresses such as climate changes and heavy traffic loads, without suffering excessive damage.

Asphalt mixtures are typically composed of two components: aggregates and binder. Aggregates are mineral particles such as sand, gravel and crushed stone that are used with a binding medium (i.e. bitumen) to form an asphalt mixture. Aggregates provide the mixture with resistance to compression due to friction between them, while binders keep the aggregates bound providing tensile resistance and cohesion to the mixture (Thom, 2008).

Bitumens or modified bitumens are the most common materials used as binders in asphalt mixtures. Due to growing environmental concerns, the past few years has seen a surge in the development of new materials made from alternative renewable sources to be used in asphalt mixtures. Consequently, the concept of biobinders is becoming more popular in the field as a potential effective solution to conventional binders. Biobinders is a broad term for asphalt binder alternatives derived from biomass. They can be derived from any biological origin including algae, swine manure and waste residues. According to the literature, they can be used as bitumen extenders, modifiers and potentially as direct bitumen replacements. They can also be used in combination with recycled asphalt (RA) pavements in order to restore some of the original properties of reclaimed asphalt binders (Hill et al., 2013). So far, biobinders have shown great potential to reduce bitumen demand and have exhibited good performance in terms of resisting common distresses affecting roads. Within this framework, the feasibility of various waste biomaterials available in large quantities are studied in this project in order to assess their suitability as potential biobinders for road construction. “Production and characterisation of waste lignin and biodiesel-derived residues as potential bitumen modifiers” is part of the Carbon Capture and Storage and Cleaner Fossil Energy (CCS CFE) CDT and the Nottingham Transportation Engineering Centre (NTEC) research groups at the University of Nottingham.

1.2. Aims and Objectives

The primary motivation behind this study is to promote the use of binders and mixtures containing biobinders in order to encourage the development of more sustainable and environmentally friendly solutions in pavement engineering. For this purpose, the overall aim of the thesis is to study the potential of waste lignin and biodiesel-derived residues for the partial replacement of traditional bitumens, through the study of their chemical and rheological properties.

The specific objectives are as follows:

1. To investigate the generation of a higher viscosity biobinder from waste feedstocks using thermochemical conversion methods at laboratory-scale.

2. To provide a thorough chemical characterisation of the biodiesel-derived feedstocks and the thermally generated biobinders.

3. To evaluate the rheological properties of biobinders and blends of biobinders with petroleum bitumen.

4. To maximise the content of biobinders through the study and optimisation of their blends with bitumen.

5. To study the ageing effects of the biobinders as well as some performance-related properties.

6. To investigate the suitability of these biomaterials as potential bitumen modifiers or additives and compare their behaviour to conventional binders.

In this thesis, it was important to focus on a detailed analysis of the neat biomaterials as many biobinder studies concentrate on the study of the biobinder once already mixed with bitumen.

1.3. Outline of the thesis

This thesis is divided into ten chapters. Chapter 1 introduces the motivations behind this project as well as the aims and objectives. Chapter 2 reviews the existing literature about the various topics addressed: biomass thermochemical treatments to produce biobinders, asphalt binders, mixtures, biobinders, recycled asphalt and the mechanical and rheological performance of those materials. Part of Chapter 2 has been published as a Review paper in *Construction and Building Materials* (Weir et al., 2022). Chapter 3 displays the experiment technique and methodologies used while Chapters 4 to 9 present the results and discussion obtained during the development of the thesis. Chapter 4 studies the hydrothermal treatment and rheological characterisation of a paper waste residue. Chapter 5 deals with the hydrothermal liquefaction and pyrolysis of biodiesel-derived waste residues (BFO). In Chapter 6, a detailed chemical fingerprinting of the biodiesel-derived residues is presented. Chapter 7 displays the rheological characterisation of the BFOs, while Chapters 8 and 9 present the rheological properties of BFO blended with bitumen and some performance-related rheological characterisation, respectively. Finally, Chapter 10 outlines the conclusions drawn and recommendations for further research.

Journal Publication

WEIR, A., JIMÉNEZ DEL BARCO CARRIÓN, A., QUEFFÉLEC, C., BUJOLI, B., CHAILLEUX, E., UGUNA, C. N., SNAPE, C. & AIREY, G. 2022. Renewable binders from waste biomass for road construction: A review on thermochemical conversion technologies and current developments. *Construction and Building Materials,* 330**,** 127076.

Conference proceedings

WEIR, A.I., AIREY, G., SNAPE, C. and JIMÉNEZ DEL BARCO CARRIÓN, A., 2020, December. Rheological Characterisation of Modified Bitumens with Biodiesel-Derived Biobinders. In *RILEM International Symposium on Bituminous Materials* (pp. 1563-1569). Springer, Cham.

1.4. Description of materials

1.4.1. Paper waste

The paper waste residue studied was grey in colour and supplied by Tarmac, a CHR company and comes from the Kings Lynn paper mill located near the Norfolk coast. Kings Lynn paper mill manufactures newsprint and corrugated base paper from 100% recycled paper (Palm, 2022). The proximate analysis of the paper waste residue is presented in Table 1.

Table 1: Proximate analysis of the paper waste feedstock.

Moisture (wt. %)	Volatile Matter (wt. %)	Fixed Carbon (wt. %)	Ash (wt. %)
1.0	49.3	1.4	48.4

1.4.2. Biofuel Oil (BFO)

The biofuel residual oil (BFO) studied is shown in Figure 1. When referring to the BFO, for brevity, the prefix “bio” is used throughout this thesis instead of “vegetal-derived”. This biofuel was supplied by Argent Energy UK Ltd, who produce commercial grade biodiesel with the BFO being the residual material left after biodiesel distillation. Argent Energy produce biodiesel using a combination of waste animal and vegetable oils and fats, such as used cooking oil from restaurants and grease from wastewater. Their biodiesel process produces high quality biodiesel from a range of variable raw materials following the European standard EN14214 using methanol as the solvent to produce fatty acid methyl esters (FAME) or biodiesel (Argent, 2022). The by-products produced during this process are glycerine, potassium sulphate which can be used as a fertiliser, and the Biofuel Oil. BFO is a chocolate brown, soft (low viscosity) liquid sold mostly as a renewable heavy fuel oil for the shipping industry. It is composed of a wide range of species, including but not limited to long chained methyl ester molecules, mono, di and triglycerides, waxes, and both oxidized and oligomerised oils. The BFO has also been treated with 2% water and 1% phosphoric acid to strip out metals and other solids. According to Argent Energy, this treatment is used to make the BFO more fluid at ambient temperature. Both the treated and untreated BFO have been used in this study. There is an abundance of BFO available to use for research purposes as Argent Energy produce these materials on an industrial scale (Argent, 2022), unlike the products obtained via hydrothermal carbonisation (HTC) or hydrothermal liquefaction (HTL) of other biomass feedstocks.

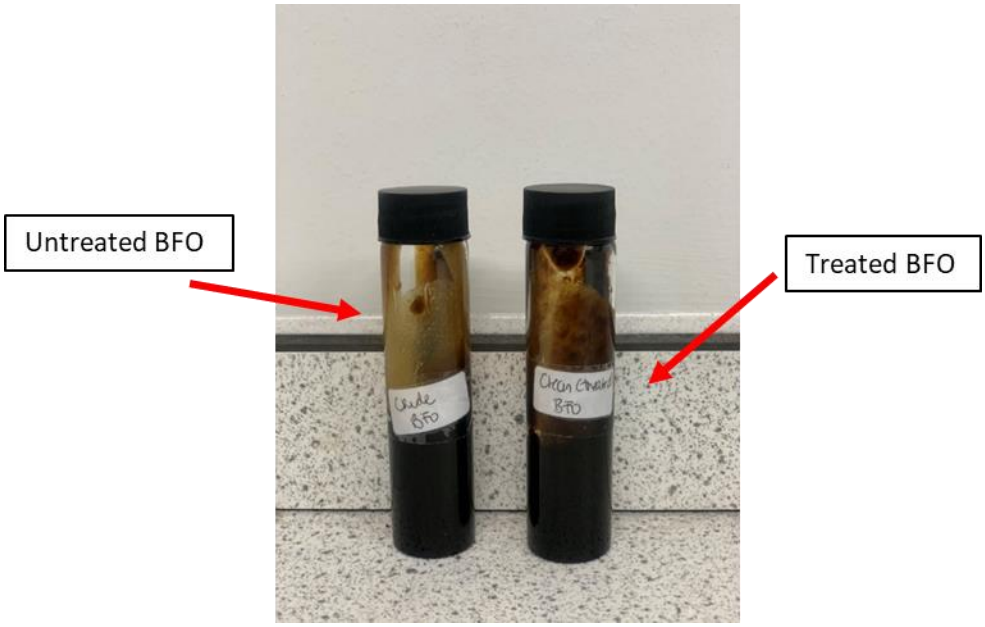

Figure 1: Biofuel Oil, referred to as BFO. The BFO has been treated with 2% water and 1% phosphoric acid to strip out metals and other solids. According to Argent Energy, this treatment is used to make the BFO more fluid at ambient temperature.

1.4.3. Control samples for rheological testing

Five conventional penetration grade bitumens ranging from hard to soft have been used as reference in the master curve plots. These are a 10/20, 20/30, 40/60, 70/100 and 100/150 pen bitumens. Three of these bitumens were selected as base binders for the biomodified blends. Two hard penetration grade bitumens (20/30 and 10/20 pen) were selected in terms of the blend with the soft BFO materials. A common 40/60 penetration grade bitumen was also used for the blending of the pyrolysed BFO. Argent Energy's commercial-grade biodiesel was also used as a control against the BFO. A basil-infused vegetable oil was also tested to compare its viscosity pattern with the BFO.

1.4.4. Biobinder Blends

Due to the liquid nature (low viscosity) of the BFO it cannot be used as a complete substitute for petroleum bitumen. Therefore in order to study the feasibility of using BFO in asphalt mixtures as a bitumen extender or modifier, it was blended with three base binders (10/20, 20/30 and 40/60 penetration grade bitumens) to produce nine laboratory blended modified bitumens as shown in Table 2. The BFO/bitumen blends were produced by heating the base bitumen up to 160 °C and then mixing the required BFO content by mass through simple mechanical stirring. No bitumen blends were made with the paper waste bio-bitumen, as

there was no prospect of generating a large enough amount of sample for testing over a short period of time (please refer to Chapter 4, section 4.1). As a result the material was considered to be preliminary testing.

The BFO/bitumen blends were tested on a Dynamic Shear Rheometer (DSR) to evaluate their rheological properties, including viscosity and ageing. Performance-based rheological testing was also carried out for the pyrolysed BFO untreated blend (labelled B10HTF+40/60, Chapter 9).

Table 2: Composition of BFO and bitumen blends.

Blend name	Bitumen type	BFO type	BFO content
B10T+10/20	10/20 pen	Treated	10%
B10U+10/20	10/20 pen	Untreated	10%
B5T+20/30	20/30 pen	Treated	5%
B5U+20/30	20/30 pen	Untreated	5%
B2.5T+20/30	20/30 pen	Treated	2.5%
B2.5U+20/30	20/30 pen	Untreated	2.5%
B50T+20/30	20/30 pen	Treated	50%
B50U+20/30	20/30 pen	Untreated	50%
B10HTF+40/60	40/60	Pyrolysed BFO untreated	10%

2. *Literature Review*

2.1. Introduction

Most bituminous binders used for pavement materials are derived from fossil fuels (Peralta et al., 2012). Petroleum bitumens and modified bitumens (bitumens designed to change the performance of straight run bitumen altered by one or more chemical agents such as polymers, waxes and crumb rubber) (Self, 2015), are the most common materials used as binders in asphalt mixtures. In Europe, the overall consumption of bitumen remains high and relatively stable, varying from 12.89 million tonnes in 2016 to 10.74 million tonnes in 2019 (EAPA, 2020). In addition, bitumen and asphalt mixture demand is predicted to further increase after years of low spending and will be driven by increased expenditure on road maintenance to accommodate for repair backlogs (The Freedonia Group, 2021). In the US, the production of hot and warm mix asphalt mixtures has been on the rise since 2016 due to increased construction activity, highlighting their high demand for bitumen and bituminous mixtures (Figure 2) (EAPA, 2020). Fortunately, efforts to use more sustainable materials in all areas of construction have greatly increased (Olaoye et al., 2021). This rise in production coupled with the urge to minimise the usage of fossil fuels has developed a drive to produce binders from alternative sources globally, particularly from bio-renewable materials or biobinders.

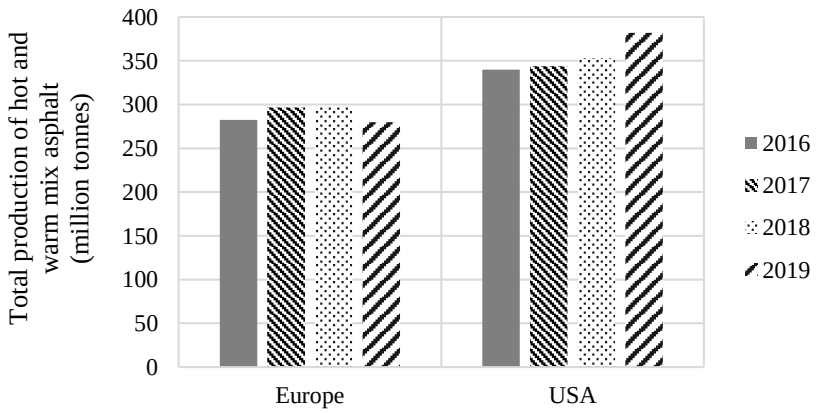

Figure 2: Total production of hot and warm mix asphalt (in million tonnes) between 2016 and 2019 (EAPA, 2020).

Biobinders are defined as asphalt binder alternatives made from non-petroleum-based renewable sources, which should not impact on food production, and have environmental and economic benefits (Peralta et al., 2012). They can be produced from a range of sources

including vegetable oils, algae and swine manure (Ingrassia et al., 2019). Not only do they have the potential to reduce petroleum bitumen demand, biobinders have also exhibited good performance in terms of resisting the common distresses affecting pavements depending on their composition (Ingrassia et al., 2019). Therefore they are receiving increasing attention in pavement engineering as effective alternatives to petroleum-based binders.

Manufacturing biobinders from biomass has gathered interest in recent years in light of environmental concerns with conventional bituminous binders. According to the US National Academy of Sciences, approximately 550 million dry tons per year of cellulosic biomass can be produced by 2020 without any major impact on food production or the environment (Council, 2009, Perlack, 2011). Fossilised biomass, like bitumen, has been heavily exploited for decades as coal and oil. The burning of fossil fuels uses 'old' biomass and converts it to 'new' CO_2, contributing to increased greenhouse gas emissions. On the other hand, burning 'new' biomass contributes no new CO_2 to the atmosphere as the released CO_2 is absorbed and recycled back into replanted biomass through photosynthesis in a cyclical process; this balance makes 'new' biomass carbon neutral (McKendry, 2002a, Zhang et al., 2007). Unlike fossil fuels, biomass is abundantly available around the world on a renewable basis, either through natural processes or as a by-product of human activities i.e. organic wastes (Isa, 2015, McKendry, 2002a).

2.1.1. Biomass sources

Sources of biomass can be categorised into four main groups: woody plants and agricultural products, herbaceous plants/grasses (all perennial crops), aquatic plants and manures (waste biomass) (McKendry, 2002a). Within this grouping, biomass sources can be further subdivided into those with high- and low-moisture contents. 'Dry' biomass such as wood chips and sawdust are naturally more suited for gasification, pyrolysis or combustion, whereas aquatic plants and manures are inherently high moisture materials and therefore more suited to 'wet' processing techniques (McKendry, 2002a). The herbaceous plant sugarcane has a high-moisture content and so would be suitable for a 'wet' conversion process. On the other hand, switchgrass, another herbaceous plant, has a much lower moisture content. Apart from moisture content, other factors should be considered when selecting an appropriate

conversion method, especially in relation to those sources of biomass which lie between 'wet' and 'dry'. These include:

1. Moisture content (intrinsic and extrinsic)
2. Calorific value
3. Proportions of fixed carbon and volatile components
4. Ash/residue content
5. Alkali metal content
6. Cellulose/lignin ratio

For 'dry' biomass conversion processes such as pyrolysis, the first five properties are of interest while for 'wet' processes like hydrothermal liquefaction (HTL) the moisture content and the cellulose/lignin ratio are the most important (McKendry, 2002a).

Over the last decade, there has been an increase in biobinder development technologies from biomass that are applicable to road construction. These technologies have evolved taking into account the available biomass and physico-chemical treatment needed to be applied to reach an optimum, consistent state. Biomass used as a source of road biobinders can be divided in two categories: liquid hydrophobic (mainly lipidic) biomass and solid biomass that needs to be converted (i.e. pyrolysed or liquefied). Liquid biomass includes vegetable oils and wood by-products such as pine rosin and pitch. Today, major full-scale developments have been made with this type of biomass where the processes are mainly physical blending and well-known chemical modifications such as transesterification of vegetable oil and polymerisation of rosin (Colas, 2004b, Pasquier, 1997, Pinomaa, 1991). Considering the global consumption of bitumen, liquefied biomass cannot cover the demand alone as there are many other competing uses including the increasing demand to produce biofuels and chemicals such as biodiesel and bioethanol (Demirbaş, 2001). This is why more studies have shifted the focus to the second category (solid biomass). Conventional agricultural and wood by-products can provide large quantities of biomass so long as they are not used for the food industry. Depending on the moisture content of biomass, two main types of thermochemical processes can be used: solvent liquefaction and pyrolysis.

Using biogenic sources for biobinder production can help reduce emissions and diverts the biomass away from combustion and into sustainable development. In terms of producing

asphalts with novel biomaterials, waste biomass products are particularly interesting. Recycling biomass waste products can minimise waste destined for landfill and reduce greenhouse gas emissions by substituting the biowaste into conventional asphalt binders (Azahar et al., 2016). Life cycle assessment (LCA) in the road industry is an important tool used to measure and compare the key life-time environmental impacts of asphalt products and laying processes (Bird et al., 2004). This includes energy consumption and greenhouse gas emissions. The production of 1 tonne of bitumen (including crude oil production, transport, refinery and storage) amounts to a total of approximately 226 kg of CO_2 emissions to the atmosphere (European Bitumen Association, 2012). As more novel materials and laying techniques emerge, LCA provides a framework for assessing the environmental benefits of biobinders and so researchers and LCA practitioners should focus on expanding the current databases to accommodate these novel materials (Huang et al., 2009). Albeit novel, biobinders have proven to be beneficial in reducing emissions. One study which investigated the production of a biomodified binder via HTL from swine manure observed a significant reduction in greenhouse gases with an 81% drop in CO_2 emissions, whilst also reducing the emission factors of the conventional binder in the mixture (Figure 3) (Samieadel et al., 2018). Similarly, the index for the Environmental Impact of Biomass Pre-processing (EIBP) is a comparable method to LCA that includes carbon footprint reduction and pollutant impacts from by-products and residuals (Tao et al., 2020). It is considered to be a more feasible method to make a more generalised comparison between various pre-combustion processes, including HTL, pyrolysis, gasification and anaerobic digestion. A lower EIBP value suggests a better environmental impact. In this study, the anaerobic digestion process has the lowest EIBP for most feedstocks studied, whereas HTL had the highest values. Despite this, HTL had an “extremely high environmental impact improvement potential” (Tao et al., 2020). The authors found no strong correlations between energy conversion efficiency and EIBP and concluded that environmental impact should be considered separately when optimising biomass pre-combustion processes.

This review attempts to provide a link between biomass thermochemical conversion technologies and their respective products that may be used as biobinders in pavement engineering. For this purpose, firstly, the main biomass thermochemical conversion technologies are compared, and a review of the parameters influencing liquefaction products

is provided. Next, it presents an overview of the recent biobinder studies reported in literature with an emphasis on the feedstock used and their performance-related properties. The studies are classified depending on the technology used to obtain the biobinder, including a specific section dedicated to the use of biobinders with recycled asphalt. The limitations to why biobinders have not been produced at industrial scale are also presented. Based on this, summary tables of the currently known properties of different biobinders have been compiled from the literature. The tables aim at providing a quick but insightful way of identifying potential biobinder feedstocks with certain desirable properties and help researchers identify gaps and potential research opportunities in the field.

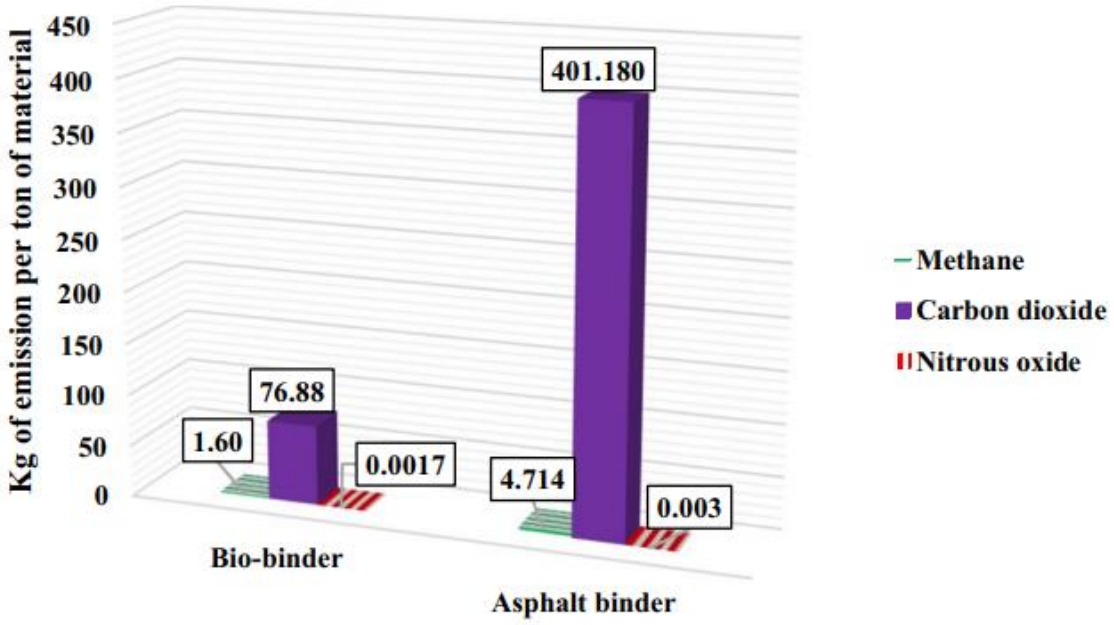

Figure 3: Greenhouse gas emissions from an HTL-derived swine manure biobinder compared to a conventional asphalt binder (Samieadel et al., 2018).

2.2. Comparison of main biomass thermochemical conversion technologies

The main biomass thermochemical conversion technologies for biofuels and chemicals are gasification, pyrolysis and solvent liquefaction. The conversion of carbon-containing solids at high temperatures (700-1000 °C) and under oxygen-starved conditions is referred to as thermal gasification (Brown and Zhang, 2019). Biomass gasification for the purpose of producing biobinders for road construction has not been studied and is therefore not relevant

in this case. As a result, the focus in this section is on pyrolysis and solvent liquefaction as these are the techniques primarily used to produce biobinders.

Pyrolysis and liquefaction are two direct methods considered to be both time saving and relatively simple, and so they are used extensively (Bridgwater, 2012). They are comparable technologies as they both extract bio-based intermediate products, referred as a bio-oil or biocrude product respectively. There are complex reaction pathways associated with these technologies and currently many research groups are focusing on understanding them (Dimitriadis and Bezergianni, 2017).

Although similar, there are considerable differences between these two conversion technologies. During pyrolysis, biomass is decomposed in the absence of oxygen within temperature and heating rates ranging from 300-900 °C (Guo et al., 2015) and less than 0.005 °C/s to more than 10,000 °C/s respectively (Collard and Blin, 2014). Pyrolysis can be classified as slow, intermediate, fast and flash pyrolysis depending on the operating conditions, with fast and slow pyrolysis being the most commonly used processes (Brown and Zhang, 2019). Slow pyrolysis operates at relatively low heating rates and temperatures with long residence time. The main target product is often solid char i.e. traditional charcoal making process (Al Chami et al., 2014). Intermediate and fast pyrolysis use moderate to high heating rates and temperatures, with fast pyrolysis characterised by shorter residence time. Flash pyrolysis uses the highest heating rates and shortest residence time, with a reaction time only lasting several seconds or less. Flash pyrolysis requires the use of special reactors and a sample particle size of approximately 105-250 μm (Goyal et al., 2008, Zhang, 2016).

In pyrolysis, low temperatures and long residence times favour the production of char, whereas high temperatures and long residence times favour the production of the gaseous products. If the purpose is to maximise the yield of the liquid product (bio-oil), moderate temperatures, high heating rates and short residence times are required (Al Chami et al., 2014, Demirbas, 2005). Pyrolysis oil or bio-oil, recovered from the condensable vapours and aerosols produced during the process, is composed of a complex mixture of oxygenated organic compounds, including alcohols, aldehydes, esters, saccharides, phenolic compounds, carboxylic acids and lignin oligomers (Brown and Zhang, 2019). Bio-oil usually has a high yield of 70-80 wt. % (Zhang, 2016).

Liquefaction, also referred to as solvent liquefaction, converts biomass into liquid fuels by processing in a hot, pressurised liquid environment for a period of time, in order to break down the solid biopolymeric structure to mainly liquid components (Elliott et al., 2015). Various solvents can be utilised such as water and methanol, non-polar solvents like toluene and tetrahydronaphtalene and ionic liquids like 1-ethyl-3-methylimidazolium chloride (Brown and Zhang, 2019). Solvent liquefaction undertaken in water is typically referred to as hydrothermal processing, hydrothermal liquefaction or hydrous pyrolysis. It is particularly attractive for wet feedstocks that are handled as slurries. Unlike pyrolysis, HTL does not require feedstock drying, therefore saving on high dewatering costs. This in turn increases the economic return of fuel production largely due to the wet nature of biomass feedstocks (Dimitriadis and Bezergianni, 2017).

Solvent liquefaction can produce fractionated and hydrolysed plant polymers (Allen et al., 1996), partially deoxygenated liquid product (biocrude) (Elliott et al., 1991) or syngas (gasification product) (Elliott et al., 2004). As reaction temperature increases, pressure must be increased in order to avoid the boiling of the water in the biomass (Figure 4). Extraction of high-value plant chemicals including resins, phenolics, phytosterols and fats occur at around 100 °C. At around 200 °C and 20 atm, fractionation of biomass takes place to yield cellulose, lignin and hemicellulose degradation products like furfural. According to Elliott et al. (2015), a further increase in temperatures and pressures (300-350 °C, 120-180 atm) can hydrolyse the cellulose to glucose and more extensive chemical reactions take place, yielding a hydrocarbon-rich liquid product known as biocrude. For the purpose of biobinders, the biocrude liquid is the desired product. It is important to note that although visually resembling bio-oil, biocrude has a lower oxygen content and is less miscible in water, making it more amenable to hydrotreating (Elliott et al., 2015). Gas products with a significant fraction of methane are primarily achieved at around 600-650 °C and 300 atm (Brown and Zhang, 2019).

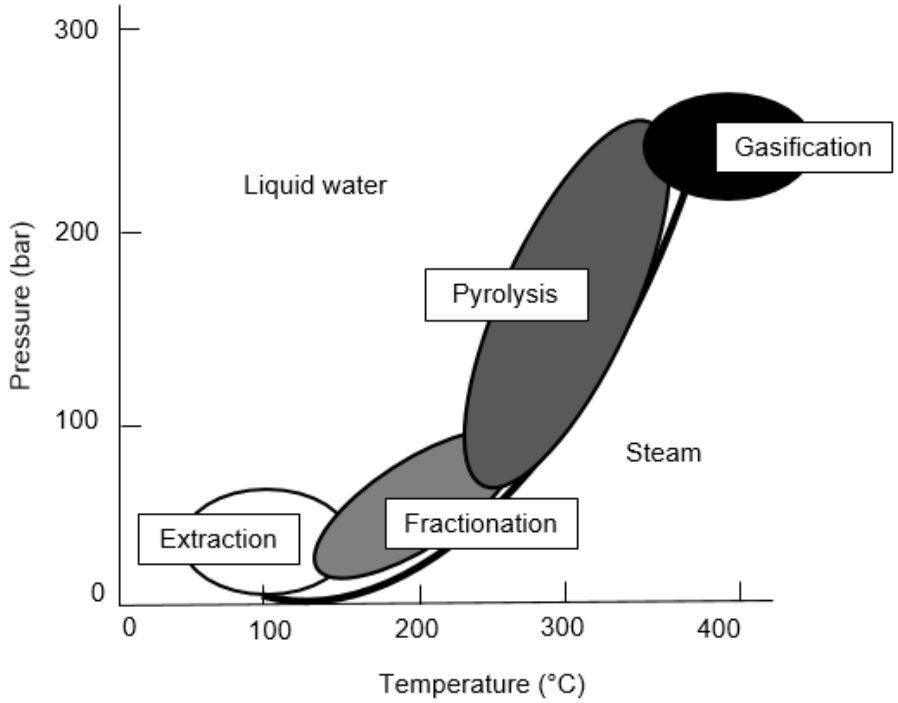

Figure 4: Temperature/pressure regimes for hydrothermal processing (Brown and Zhang, 2019).

The use of catalysts is not common in pyrolysis, whilst the solvents used during liquefaction can act as catalysts and deliver premium products in comparison to those acquired through pyrolysis (Dimitriadis and Bezergianni, 2017). Additionally, the biocrude oil produced from liquefaction is far more stable and less corrosive than the one obtained from fast pyrolysis. This is due to a higher heating value and lower oxygen and moisture content. Equipment handling and storage costs are therefore reduced (Bensaid et al., 2012, Dimitriadis and Bezergianni, 2017, Haarlemmer et al., 2016, Lédé et al., 2007). The less oxygenated and more stable liquefaction product could therefore be more easily stored, transported and upgraded (Boateng and Mullen, 2013). Studies report that pyrolysis oils can contain between 35-50% oxygen on a water free basis (Doassans-Carrère et al., 2014, Haarlemmer et al., 2016, Zhang et al., 2007). In comparison, HTL biocrude produced from a continuous-flow reactor contains between 5 and 18% oxygen for lignocellulosic, macro and microalgal biomass feedstocks (Elliott et al., 2015, Elliott et al., 2014, Elliott et al., 2013, Jazrawi et al., 2013, Tews et al., 2014). The high-water content found in the fast pyrolysis product is also a major concern as it would be immiscible with hydrocarbon products including bitumen. As a result, a lower

moisture content in the product yield is desirable, such as those achieved via HTL. Overall, liquefaction can be considered a more competitive technology for biomass conversion to bio-bitumen-like products than pyrolysis, as indicated by their typical parameters in Table 3 proposed by Dimitriadis and Bezergianni (Dimitriadis and Bezergianni, 2017).

However, the high-pressure conditions during liquefaction raise investment costs of the equipment units. Solvent liquefaction has some key engineering challenges that must be overcome in order to make this technology commercially viable. These include the continuous feeding of biomass slurries into high-pressured reactors, efficient energy integration and product separation from solvent (Brown and Zhang, 2019).

Table 3: Typical hydrothermal liquefaction and pyrolysis parameters for biomass conversion (Dimitriadis and Bezergianni, 2017).

Parameter	Pyrolysis	Liquefaction
Drying	Necessary	Unnecessary
Pressure (MPa)	0.1 – 0.5	5 – 20
Temperature (° C)	370 – 526	200 – 400
Catalyst	No	Sometimes
Heating Value	Low (~17 MJ/kg)	High (~30 MJ/kg)
Oxygen Content	High	Low
Water Content	High	Low
Viscosity	Low	High
Upgrade	Hard	Easy

Both pyrolysis and liquefaction product yield and quality are governed by a range of factors, including biomass feedstock, temperature, pressure, catalyst and residence time. These parameters are highly dependent on the chemical characteristics of the feedstock such as the ratio of protein, lipid and carbohydrate fractions present in the biomass (Dimitriadis and Bezergianni, 2017). As liquefaction can provide a more stable product in high yields with relatively low oxygen contents than pyrolysis, it therefore seems to be more suited for the production of biobinders and so it is important to examine it in more detail in order to optimise the technology. As a result, the following section focuses on the effects of the operating parameters that come into play in solvent liquefaction.

2.3. Liquefaction Operating Parameters

Biocrude product yields vary considerably according due to the nature of the biomass feedstock and the operating parameters during liquefaction, such as temperature and

pressure. Each parameter is inter-connected with one another, but their effects are ultimately influenced by the biomass feedstock. Each biocrude product must therefore be individually studied, even if the starting material is the same. The key operating parameters that affect liquefaction products are summarised in Table 4. It is important to note that these studies were not conducted for the sole application of road biobinders. However, it is useful to understand the influence of HTL parameters on product yield, and it is safe to assume they will affect biobinder production in a similar way.

Table 4: Summary of liquefaction parameters and their effects on product yield.

Liquefaction parameter	Main factors affecting biocrude yield
Temperature	• Can have a substantial effect on both product yield and properties of liquefaction biocrude • No ideal set temperature for a potential biobinder as product depends heavily on biomass feedstock and all operating parameters involved • General consensus that increasing reaction temperature increases yield up to a certain point, where the biocrude yield then begins to level off or decrease (Dimitriadis and Bezergianni, 2017), with some attributing a decrease in yield with temperatures over 300 °C to a competition between hydrolysis and repolymerisation reactions involved in the liquefaction process (Zhong and Wei, 2004, Sun et al., 2010)
Pressure	• High pressure increases solvent density, with the resulting high-density medium penetrating efficiently into molecules of biomass components, resulting in enhanced decomposition and extraction • The rate of biomass dissolution can be controlled by maintaining pressure above the critical point, helping to boost the favourable reaction pathways to increase oil or gas yields (Akhtar and Amin, 2011) • The effect of pressure on product yield becomes negligible once supercritical conditions for liquefaction are achieved (Akhtar and Amin, 2011)
Catalyst	• Mostly used to reduce char formation and boost biocrude yield by reducing condensation and/or repolymerisation reactions of intermediate products (Dimitriadis and Bezergianni, 2017) • Catalyst selection dependent on feedstock used. Selection can have either a positive or negative effect on the desired chemical reactions (Xu and Etcheverry, 2008)

	• Different types of catalysts can influence yield even if the same feedstocks are used (Xu and Etcheverry, 2008, Wang et al., 2013), highlighting the importance of studying each liquefaction product (and potential biobinder) individually
Residence time	• Similarly dependent on feedstock used and other parameters involved • Short residence times (a few minutes rather than tens of minutes) have been reported to decompose biomass effectively and produce high yields for algal and evergreen-type feedstocks (Akhtar and Amin, 2011, Qu et al., 2003, Valdez et al., 2012) • Like temperature, increasing residence time can increase biocrude yields until a certain threshold (Xu and Etcheverry, 2008, Dimitriadis and Bezergianni, 2017, Xu and Lancaster, 2008) • This levelling-off possibly accounted to cracking of the liquid products to gases and the formation of char (Xu and Etcheverry, 2008)
Solvent	• Water is the most popular solvent used in HTL due to being readily available, environmentally benign and inexpensive. Water acts as a solvent, a reactant and a catalyst during HTL, making the process significantly different from pyrolysis (Toor et al., 2011) • Organic solvents such as methanol and ethanol have lower boiling and critical points than those of water and so milder reaction conditions can be used (Singh et al., 2015) • High molecular weight products have been obtained from organic solvents in comparison to water for the liquefation of pinewood and algae (Liu and Zhang, 2008, Singh et al., 2015), while others have reported lower yield biocrude products with organic solvents, such as Cheng et al. (2010), who studied the liquefaction of white pine sawdust, reinforcing the idea of treating each feedstock individually, even if it comes from the same type of biomass • Combining more than one solvent has also been explored, and Cheng at al. (2010) was able to show the advantage of using co-solvent systems over single solvents to produce a greater product yield and biomass conversion • Hydrogen-donor solvents like tetralin can also enhance the yield of liquid products (Akhtar and Amin, 2011, Li et al., 2016)
Biomass-to-solvent ratio	• Generally, the optimum biomass-to-solvent ratio varies according to the feedstock used and the operating parameters (Vassilev et al., 2015).

	• Most types of biomass contain water and due to its threefold functionality, many researchers have evaluated the overall effect of biomass-to-water content • Similar to temperature and residence time, biocrude yield increases with increasing biomass/water ratio until a certain point, with a too-high water content ratio being undesirable (Jin et al., 2013). • Smaller ratios can sometimes lead to higher heavy oil yields (Qu et al., 2003).

2.4. Summary and findings

Liquefaction biocrude products are overall found to be both more deoxygenated and hydrophobic and contain less water than pyrolysis oils. They are physically less dense but in fact more viscous than the latter (Elliott et al., 2015). As a result, they are more suited for the production of biobinders. Operating parameters during liquefaction are all closely interrelated, and each play a key part in determining yields. For instance, temperature, residence time and biomass-to-solvent ratio generally increase yield until a certain threshold. The liquefaction process mechanisms and interactions between the parameters have not been clarified much in the literature, although three major steps take place: depolymerisation followed by decomposition and recombination (Toor et al., 2011). These processes along with the critical parameters explained above vary extensively according to the feedstock used. As biomass is a complex mixture of carbohydrates, lignin, proteins and lipids, the reaction chemistry and mechanisms of biomass liquefaction are consequently also complex (Gollakota et al., 2018, McKendry, 2002a, McKendry, 2002b). This coupled with the variability of feedstocks makes it difficult to predict what happens during and after liquefaction. This is a challenge that exists in this field and the complexities of the critical parameters should be studied individually for each feedstock (Gollakota et al., 2018).

2.5. Asphalt mixtures for pavements

Asphalt mixtures are compound materials made of four components: aggregates, binder, filler and air voids. Aggregates are mineral particles such as sand, gravel and crushed stone that are used with a binding medium (i.e. bitumen) to form an asphalt mixture. Aggregates provide the mix with resistance to compression due to friction between them, while binders keep the aggregates bound, providing tensile resistance and cohesion to the mixture. Filler, or filler

aggregate, are the finest granular particles (<0.063 mm). Finally, air is distributed throughout a compacted asphalt, and fills the voids that remain between the aggregate skeleton and the binder (Thom, 2008, Pavement Interactive, 2013). Air void content is a key consideration when designing asphalt mixtures, as they can have a significant effect on the asphalt's service life. When the air void content is too high, the mixture may exhibit additional permeability to air and water, resulting in moisture damage and age hardening (Sarker, 2015).

In general, the main features affecting the design and performance of asphalt mixtures are aggregate, binder and air void content properties. These features can vary, providing a range of mixture types. Different countries can also have distinctions between asphalt mixtures. In the UK there are 8 types of mixtures: asphalt concrete, asphalt concrete for very thin layers, stone mastic asphalt, hot rolled asphalt, soft asphalt, mastic asphalt, porous asphalt and mixtures containing recycled asphalt. All of these mixtures vary in aggregate gradation, binder content and functionality (Airey et al., 2016, British Standards, 2005).

The main distresses affecting asphalt mixtures are caused by the loads they are exposed to during their service life due to traffic and climate conditions. Cracking, deformation or rutting, fatigue and moisture damage are the four key distresses.

Cracking is a complex phenomenon associated with stresses induced in the asphalt layers by wheel loads, temperature changes or both (Figure 5). It occurs when the tensile and related strain induced by traffic and/or temperature change exceed the breaking strength of the mixture. Cracking that results from extreme cold is usually referred to as low temperature cracking, whilst cracking that develops from thermal cycling is known as thermal fatigue cracking. Thermal cracking is related to the relaxation capabilities of binders, for instance when they become too stiff to withstand thermally induced stress. Thermal cracking is also associated with the nature of the binder, and its risk increases with age of the pavement as a result of oxidation or time-dependent physical hardening (Xu et al., 2015).

Figure 5. Longitudinal crack in a major UK motorway (Xu et al., 2015).

Deformation (rutting) results from plastic deformation in the asphalt mixture due to repetitive loading of traffic. Severe rutting can occur under the high shearing stresses imposed by breaking, turning, accelerating, overloading traffic, or long and steep sloping road sections. The primary factors inducing plastic deformation is the composition of the mixture as well as stress and temperature. Plastic deformation is greatest at high service temperatures, for which 70 °C is taken as the maximum in situ temperature. At such temperatures, the cumulative effect of repeated loading is determined by the binder viscosity. During the 1976 hot UK summer, it has been estimated that deformation in the wheel tracks of hot rolled asphalt surfaces was between two and four times the rate of an average UK summer (Xu et al., 2015).

Fatigue cracking is the result of the accumulation of damage due to extensive loading cycles. It consists of two main phases, crack initiation and crack propagation, both caused by tensile strains generated in the pavement by traffic, temperature variations and construction

practices. According to Read (1996), the fatigue properties of bituminous mixtures cannot be studied in isolation, and stiffness should also be considered as it determines the magnitude of the tensile strength experienced by the material.

Moisture damage is one of the main causes of failure in asphalt mixtures (Figure 6). It results in loss of strength, stripping, ravelling, fatigue damage and permanent deformation. In other words, the intrusion of moisture into the pavement structure can induce a loss of the adhesive bonding between aggregates and binder and/or loss of cohesive strength, resulting in one or more of the distresses mentioned above. Anti-stripping agents such as hydrated lime and polymers have been commonly used to increase the pavement's resistance against water penetration, thereby reducing the hydrophilic properties of the aggregates and changing the major electrical charges of the aggregate surface (Hamzah et al., 2015).

Ravelling Potholing

Figure 6. Moisture induced damage in asphalt mixtures (Hamzah et al., 2015).

2.6. Bitumen in asphalt mixtures

2.6.1. Bituminous binders

Bitumen is the most common binder used for asphalt mixtures. It was defined in 1990 by the British Standard (BS 3690 Part 3) and is reproduced here in verbatim:

"A viscous liquid, or a solid, consisting essentially of hydrocarbons and their derivatives, which is soluble in trichloroethylene and is substantially non-volatile and softens gradually when heated. It is obtained by refinery processes from petroleum, and is also found as a

natural deposit or as a component of naturally occurring asphalt, in which it is associated with mineral matter".

This definition establishes the main features of bitumen: its chemical composition ("hydrocarbons and derivatives"), its viscoelasticity and temperature and time dependent relationship between applied stresses and resultant strains ("viscous liquid or solid that softens when heated") (British Standards, 1990).

The role of bitumen is crucial in defining many aspects of asphalt road performance, such as strength and stiffness, permanent deformation and cracking, as it is responsible for the viscoelastic behaviour of all bituminous materials (Airey et al., 2016).

Elemental analysis of bitumen manufactured from a range of crude oils shows that most bitumens contain:

Carbon 82-88%

Hydrogen 8-11%

Oxygen 0-1.5%

Sulphur 0-6%

Nitrogen 0-1%

The chemical composition of bitumen is extremely complex, as it varies according to the source of crude oil and chemical modification induced during the manufacturing process and ageing in service. Generally, bitumen structure is divided into two groups: asphaltenes and maltenes (Figure 7). Asphaltenes are highly polar, high molecular weight molecules (ranging from 1000 g/mol to 100000g/mol) and generally consist about 5 to 25% of the bitumen mass. They play an important role as a higher asphaltene content produces a harder binder. Conventional bitumen increases its asphaltene content with ageing, increasing its molecular weight (Lesueur, 2009). The maltenes can be subdivided into saturates, aromatics and resins. Saturates consist of straight and branched-chain aliphatic hydrocarbons with cycloaliphatic compounds, forming 5-20% of bitumen. Aromatics comprise the lowest molecular weight naphthenic compounds in bitumen, representing a large proportion of the dispersion medium for the asphaltenes, forming about 40-65% of the bitumen mass. Resins are dark brown in colour, semi-solid, polar in nature and strongly adhesive. They are generally 13 to 25% of

bitumen, and their proportion to asphaltenes influences the gelatinous character of the bitumen (Lesueur, 2009, D'Melo, 2015).

The most common method to characterize bitumen is through rheological studies. However, it is important to study both the constitution and structure of the material as they determine the rheological characteristics of bitumen at a particular temperature. Thereby, to understand changes in bitumen rheology, it is crucial to understand how composition and structure interact to influence rheology (D'Melo, 2015).

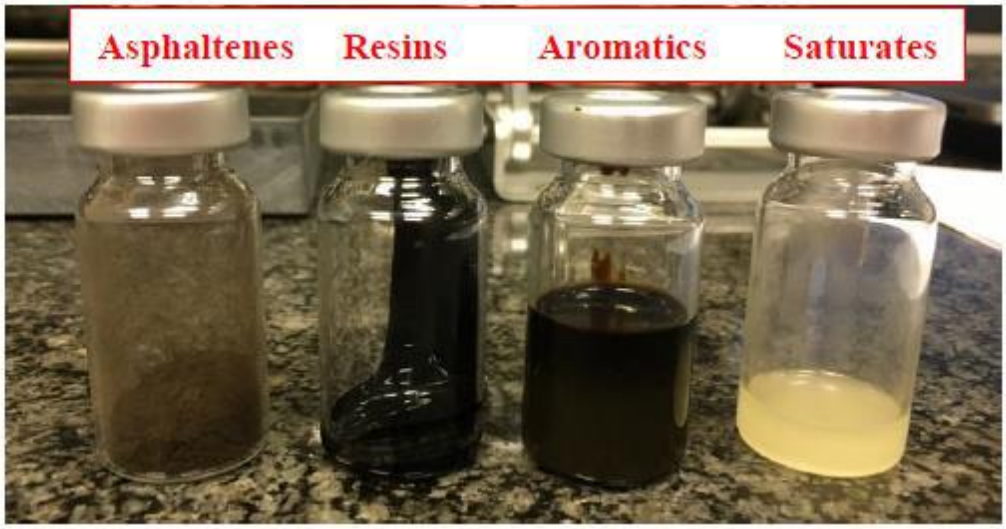

Figure 7. Bitumen fractions, obtained through SARA analysis (Jimenez del Barco Carrion, 2017).

2.6.2. Bitumen Rheology

Bitumen is a thermoplastic, viscoelastic liquid that behaves as a glass-like elastic solid at low temperatures and/or during rapid loading (short loading times - high loading frequencies) and as a viscous (Newtonian) fluid at high temperatures and/or during slow loading (long loading times - low leading frequencies). Bitumen's response to stress is dependent on both the temperature and loading time, and thus the rheology of bitumen is defined by its stress/strain/time/temperature response (Airey et al., 2016).

Amongst the physical properties of bitumen, primary emphasis is given to study its rheological behaviour. Rheology (derived from the Greek, translating literally as *rheos* (flow) and *logy* (science)), is the study of the flow of matter (Yusoff et al., 2011). As a result, bitumen rheology

can broadly be defined as the fundamental measurements associated with the flow and deformation characteristics of bitumen (Airey, 1997).

Bitumen is responsible for the viscoelastic behaviour of asphalt mixtures, and therefore is a key player in determining road performance, particularly resistance to deformation and cracking (Di Benedetto et al., 2004). The relationship between binder properties and asphalt mixtures is a major study area in pavement engineering, as testing binders is both less time and material consuming than testing asphalt mixtures. Therefore, predicting the performance of asphalt mixtures from binder testing is hugely beneficial (Jimenez del Barco Carrion, 2017).

2.6.3. Dynamic Shear Rheometry

Most of the materials studied in this thesis have been studied using a Dynamic Shear Rheometer (DSR). Dynamic Shear Rheometers (DSRs) are used to study bitumen rheology at a wide range of loads, frequencies (number of cycles per second) and temperatures. The principles involved in DSR testing are illustrated in Figure 8, where a rounded sample of bitumen is sandwiched between a spindle and a base plate located inside a temperature control system. The spindle is allowed to rotate at different frequencies in order to apply alternating stresses and strains to the sample whilst the base plate remains fixed during testing. The test can be either stress or strain controlled, but the usual condition used for determining the dynamic rheological properties of bitumen is the controlled strain. This helps to ensure the strains are within the viscoelastic region (Peterson et al., 1994). The DSR controls torque (T) and displacement (θ) and therefore calculates stress and strain according to Equation 1 and Equation 2:

$$\tau_r = \frac{2T}{\pi r^3} \qquad \textit{Equation 1}$$

$$\gamma_r = \frac{r\theta}{h} \qquad \textit{Equation 2}$$

where τ_r is the maximum applied stress, T is the torque (N·m), and r is the specimen radius (m). γ_r is the maximum resultant strain, θ is the displacement (rad), and h is the height of the sample (m), also known as the gap.

As the DSR equipment has a minimum and maximum torque capacity, bitumen testing requires the use of different plate sizes in order to measure data accurately. There are two common geometries used, a 25mm (used for high temperatures) and an 8mm geometry (used for low temperatures).

From this data, shear complex modulus (G*) and phase angle are obtained for the temperatures and frequencies tested. The ratio of the maximum (shear) stress to maximum strain is called the complex modulus (|G*|), also known as the stiffness (Equation 3). It is a quantitative measurement of a material's total resistance to deformation when the bitumen is subjected to shear loading:

$$G^* = \frac{\sigma_{max}}{\gamma_{max}} \qquad \textit{Equation 3}$$

where G* is the complex modulus in Pa, σ is the peak applied stress and γ is the measured strain.

The higher the complex modulus, the higher the resistance of the binder to deformation. The phase angle (δ) is the measure of the viscoelastic behaviour of bitumen, defined as the phase difference between the stress and the strain. It is also called the loss angle or the phase lag. A purely elastic material has a phase angle of zero, whereas a purely viscous material has a phase angle of 90 °. Between these two extremes the material behaviour can be considered to be viscoelastic in nature with a combination of viscous and elastic responses (Taylor and Airey, 2015).

Complex modulus and phase angle are closely related. Complex modulus is made up of two components, the elastic (storage, G') and viscous (loss, G") modulus; these are separated by means of the phase angle, as seen on Figure 9. The storage modulus describes the amount of energy that is stored and released elastically in each oscillation. It is referred as the elastic component of the complex modulus. The loss modulus, also known as the viscous modulus, is the average dissipated energy rate in the dynamic test (Airey, 1997). Complex modulus and phase are sensitive to temperature and loading time (frequency). Thus, these properties are studied over a wide range of temperatures and frequencies in the DSR.

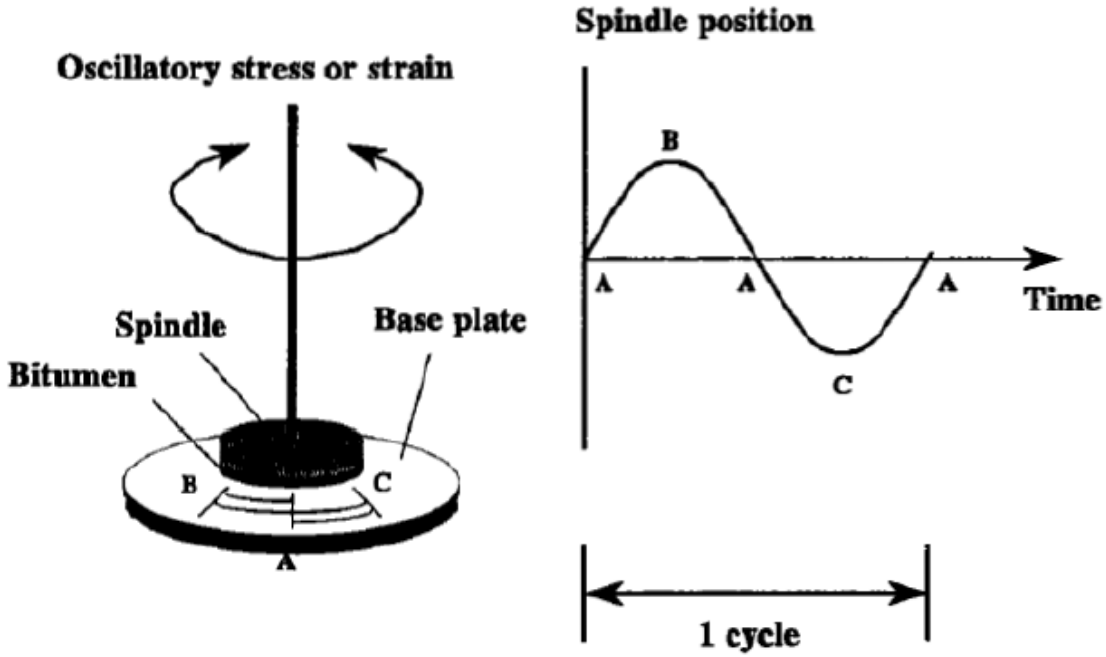

Figure 8. Principles of operation of a Dynamic Shear Rheometer. The spindle oscillates about its own axis such that a radial line through point A moves to point B, reverses back to point A and moves to point C, followed by a further reversal movement back to point A. These set of movements comprise one smooth, continuous cycle which can be continuously repeated during the test (Airey, 1997).

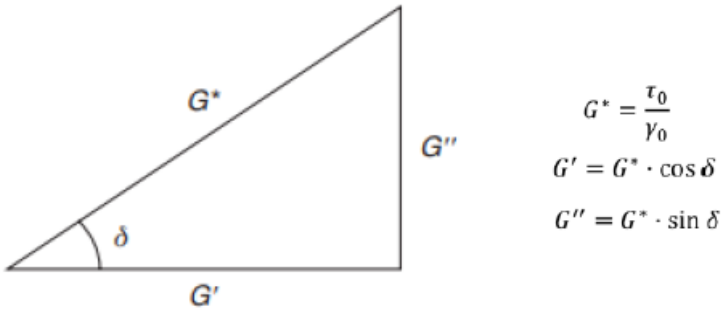

Figure 9. Relationship between the shear modulus and the phase angle (Taylor and Airey, 2015).

Another component that can be defined is the complex viscosity or complex dynamic shear viscosity, η* (Pascal-second/Pa.s). It is a viscosity value obtained from dynamic oscillatory tests and is defined as the ratio of the complex modulus and the angular frequency (ω) (Equation 4):

$$\eta^* = \frac{G^*}{\omega}$$ *Equation 4*

Similar to complex modulus, complex viscosity includes two component parts: the dynamic, or real, viscosity (η'), and the storage viscosity (η") which represents the out-of-phase or imaginary component of the complex viscosity (Equation 5):

$$\eta^* = \eta' + i\eta"$$ *Equation 5*

2.6.4. Representation of rheological data

In order to study the rheological properties of bituminous materials, the data obtained from testing needs to be presented in a useful form. One of the main ways to present rheological data is the construction of master curves, which allow the measurements done at different temperatures to fit a smooth curve over a range of frequencies using shift factors. The representation of a continuous master curve of the binder behaviour at a reference temperature is enabled by the Time-temperature superposition principle (TTSP) (Equation 6). TTSP can be expressed as (Dobson et al., 1969):

$$G(\omega, T) = G(\omega a(T), T_r)$$ *Equation 6*

where G is the modulus (G', G" or G*), ω is the loading frequency, a(T) is the shift factor, T is the temperature and T_r is the reference temperature.

Shift factors are the amount of shifting required at each temperature along the logarithmic frequency axis to form a master curve (Yusoff et al., 2011). They are temperature dependent and can be obtained either manually or by following different mathematical equations. The William-Landel-Ferry (WLF) (Equation 7) and the Arrhenius equation (Equation 8) are two empirical equations commonly used to determine shift factors.

$$loga(T) = -\frac{C_1(T - T_r)}{C_2 + (T - T_r)}$$ *Equation 7*

$$loga(T) = \frac{-E_a}{2.303R}\left(\frac{1}{T} - \frac{1}{T_r}\right)$$ *Equation 8*

Where a(T) is the shift factor at a temperature (T), T_r is the reference temperature, C_1 and C_2 are empirically derived parameters. E_a is the activation energy of the binder, R is the universal gas constant (8.314 J/Kmol). The parameters of both the WLF and Arrhenius equations can help provide an insight into the molecular structure of bitumen (Marateanu and Anderson, 1996).

The rheology of bitumen becomes more complex with the addition of polymers and biomaterials and they can breakdown the TTSP and affect the construction of smooth master curves. This is termed thermorheological complexity. Partial time-temperature superposition principle (PTTSP) is an alternative shifting procedure developed by Olard and Di Benedetto (2003) that allows the construction of master curves for thermorheologically complex materials.

2.6.5. Bituminous binders' modification

The primary role of bitumen modifier is to improve some of the properties that conventional bitumens accord to asphalt mixtures, such as increasing resistance to deformation at high temperatures without adversely affecting other properties. Desirable characteristics of modified binders include a higher softening point, greater viscosity, greater elastic recovery, and improved cohesive strength and ductility (Yildirim, 2007).

Polymers are the most common modifying agents. The use of these materials in asphalt mixtures was patented in 1843 and since then, they have become common practice worldwide as they improve targeted aspects of the performance of roads (Yildirim, 2007, Rodrigues and Hanumanthgari, 2015). Bitumens that have been modified are referred to as polymer-modified bitumens (PMBs).

The degree of modification is always dependent on the nature of the base bitumen and polymer and the compatibility of the materials. Common polymers used are styrene-butadiene-styrene (SBS), recycled crumb rubber, polyethylene, and lignin.

SBS is currently the most common modifier of bitumen and consists of a block copolymer that increases bitumen elasticity thereby increasing viscosity, complex modulus and elastic response (Rodrigues and Hanumanthgari, 2015, Airey, 2003). As a result, SBS modification improves rutting and cracking resistance in asphalt mixtures (Kalantar et al., 2012, Singh et al., 2013).

2.6.6. Bituminous binders' ageing

Ageing (hardening) is one of major factors affecting pavement deterioration and shortening road service life. Ageing affects binder behaviour and has direct consequences on common distresses such as rutting and fatigue (Lu and Isacsson, 2002, Ali et al., 2013).

Age hardening can take place during the manufacture, laying and service life of the asphalt pavement due to its exposure to the elements. In other words, when bitumen is laid in the form of an asphalt mixture in the road, it is considered to have already aged and its properties will differ from its original form.

Similar to common organic substances, bitumen is affected by the presence of oxygen, ultraviolet radiation and changes in temperature (Preston and O'Nions, 2015). The four dominant factors that influence bitumen ageing are oxidation, volatilisation, exudation and physical hardening, with oxidation being the most significant cause (Karlsson and Isacsson, 2006). Ageing influences bitumen chemistry and rheology. Conventional bitumens become stiffer and more elastic due to changes in their chemical composition and structure. In this instance, the asphaltene content increases and consequently hardens the binder (Lesueur, 2009). With ageing, the complex modulus increases as the phase angle decreases, making the bitumen more solid-like (Figure 10). However, the process of ageing and its effect on physical and performance-related properties depends on the binder's nature and composition and should be carefully studied (Karlsson and Isacsson, 2006, Lu and Isacsson, 2000).

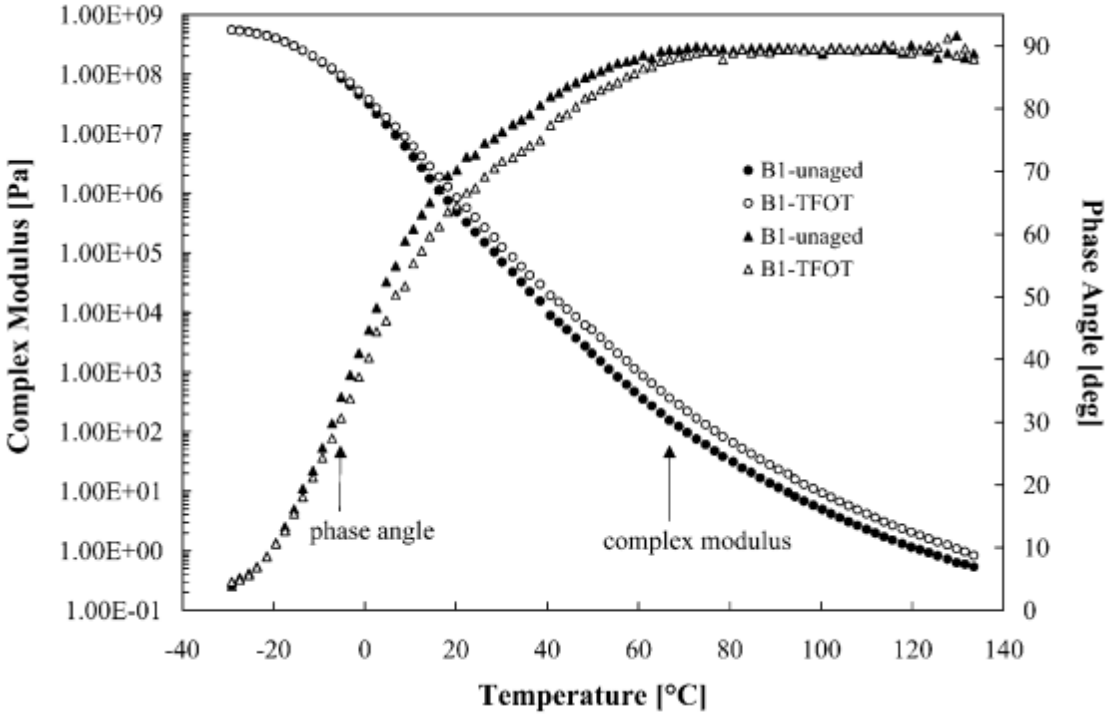

Figure 10. Effect of ageing on bitumen rheology (Lu and Isacsson, 2002).

Polymer-modified bitumens have shown differences in their rheological characteristics in comparison to conventional bitumens. Airey (2003) noted that at high temperatures, the PMBs became more viscous rather than more elastic, resulting in 'softer' binders after ageing, attributed to the degradation of the polymer.

Similarly, Ruan et al. (2003) concluded ageing diminished the effectiveness of the polymer by improving asphalt ductility. This was the result of stiffening of the base bitumen and degradation of the polymer network. Wu et al. (2009) also stated that with ageing, the polymer network is so significantly impaired that eventually, the rheological and mechanical properties of the PMB tended to be similar to that of the aged conventional bitumen.

Bitumen ageing is studied by distinguishing two types of ageing: short-term ageing is associated with the loss of volatile components and oxidation of bitumen during the manufacture of the asphalt mixture, and long-term ageing, which simulates the progressive oxidation of the bitumen in service.

After some time of service life, depending on pavement conditions and road wearing, pavements need to be maintained and sometimes replaced due to significant damage. In this case, bituminous pavements are removed through milling (Figure 11).The by-product after milling is known as Reclaimed Asphalt Pavement (RAP) and is the recycled product of the aged asphalt mixture (West, 2010).

Used for decades, RAP can offer environmental and economic benefits, as its use decreases the amount of new material needed for the construction and maintenance of roads. RAPs also decrease costs related to processing virgin materials and help to reduce disposal issues like landfill space (Al-Qadi et al., 2007, Zaumanis et al., 2014a).

Figure 11. Milling machine removing asphalt pavement layers as part of road rehabilitation (West, 2010).

2.7. Ageing Test Methods

The most frequently used short-term ageing tests are the Thin Film Oven Test (TFOT) and Rotating Thin Film Oven Test (RTFOT). In regards to long-term ageing, the Pressure Ageing Vessel (PAV) test and the Rotating Cylinder Ageing Test (RCAT) have shown the greatest results in simulating the process that takes place in the field (Airey, 2003). RTFOT and PAV are the most widely used methods.

2.7.1. Thin Film Oven Test (TFOT)

Designed to evaluate the hardening of bitumen (ageing) during plant mixing. In principal, a film of bituminous binder is heated in an oven at 163 ^{o}C for 5 hours in a layer that is 3.2 mm thick (British Standards, 2014a).

2.7.2. Rotating Thin Film Oven Test (RTFOT)

An improved version of the TFOT test that simulates more accurately what happens to a bitumen during mixing (Hveem et al., 1963). During RTFOT, a moving film of bituminous binder is heated in an oven to a specified temperature (normally 163 ^{o}C) for a specific time with a constant supply of air (British Standards, 2014b). This test helps to ensure that all the bitumen is exposed to heat and air and the continuous rotation helps to better reproduce the conditions in an asphalt plant (Preston and O'Nions, 2015).

2.7.3. Pressure Ageing Vessel (PAV)

Used to simulate long-term, in-service oxidative ageing of bitumen in the field. In the test, a static film of binder is heated to a specified temperature (between 80 and 115 ^{o}C) under a specified air pressure (usually 2.1 MPa) for a given period of time (British Standards, 2012). In order to evaluate the effects of this ageing procedure, the binders must be analysed in their neat (virgin) state and after RTFOT and RTFOT+PAV.

2.7.4. Rotating Cylinder Ageing Test (RCAT)

Another long-term ageing test, the RCAT test involves a rotating film of binder being heated to a specified temperature (90 ^{o}C) under a specified rotation and oxygen flow (1 r/min, 4.5 l/h respectively) for a given period of time. Other conditions can be used for research purposes. The ageing effects are evaluated on the residual binder after testing. However, as samples can be taken at intermediate exposure times, the ageing process can be monitored on the basis of a kinetic approach (British Standards, 2007).

Bitumen ageing is commonly quantified by measuring a conventional binder property before and after an ageing procedure. As a result, the Ageing Index is usually defined as the ratio of viscosity of the aged bitumen, η_a, to the viscosity of the virgin bitumen, η_o. It is not a

fundamentally defined parameter, as it can be the ratio of any two values (e.g. viscosity, stiffness, penetration, etc.) measured at different times. Its generic form can be expressed as shown in Equation 9 (Preston and O'Nions, 2015).

$$Ageing\ Index = \frac{P_{aged}}{P_{unaged}} = \frac{\eta_a}{\eta_o} \qquad \textit{Equation 9}$$

where: P_{aged} = a physical property measured on the aged binder (after any of the ageing methods above), P_{unaged} = the same physical property measured on the unaged bitumen.

2.8. Routine and Mechanical Properties of bitumens

Bitumen (and its response to stress) is complex and dependent on both temperature and loading time. As a result, the nature of any bitumen test must be interpreted in relation to the nature of the material. There is a wide range of tests performed on bitumens; the most common ones are described below.

2.8.1. The Penetration Test

Known as a measure of bitumen stiffness. A needle of specified dimensions penetrates a bitumen sample under a known load and temperature for a fixed period of time. The result of the test is expressed as the distance (in decimillimetres, dmm or 0.1 mm) that the needle penetrates vertically into the sample. The lower the penetration value, the harder the bitumen and vice versa. As a standard, the operating parameter is usually 25 °C, when the binder is semi-solid but the test can be obtained at different temperatures (European Standards, 2015, Koenders, 2015).

2.8.2. The Fraass breaking point Test

One of the few tests that can describe the behaviour of bitumens at very low temperatures (as low as -30 °C). It determines the temperature at which bitumen reaches a critical stiffness and cracks, termed as the Fraass breaking point (Koenders, 2015).

2.8.3. The softening point test

Another property commonly used to determine the consistency of a penetration grade. It can be defined as the temperature at which a bitumen changes consistency and begins to be more fluid-like. In this test, a small steel ball is placed on a bitumen sample contained in a brass ring, and the set-up is then suspended in a glass beaker with water or glycerine (depending on the expected softening point: water for a softening point <80 ^{o}C and glycerine for a SP> 80 ^{o}C). When water is used, the sample is conditioned at 5 ^{o}C and when glycerine is used, the initial temperature is 30 ^{o}C. Temperature is then increased at 5 ^{o}C per minute. As the bitumen softens it eventually deforms and the softening point is recorded as the temperature at which the bitumen surrounding the ball touches a sensor below the ring (Koenders, 2015).

2.9. Binder specifications

Bitumen is available in a variety of grades. Specifications are used worldwide to define these grades to meet the needs of climate, application, loading conditions and end use. They are usually based on a sequence of standard tests that define the properties of each grade such as viscosity, solubility, hardness and durability (M. Vondenhof, 2015).

In Europe, bitumens and polymer-modified bitumens are specified according to the properties mentioned in the previous section. Bitumens are usually denominated by their penetration value: for example 40/60 pen bitumen has a penetration that ranges from 40 to 60 inclusive. This is expressed in decimillimeters and is known as penetration grading (British Standards, 2009). In Australia, bitumens are classified on the basis of their viscosity at 60 ^{o}C and expressed in Pa.s (i.e. bitumen class 170).

However, these binder specifications have limitations when used in asphalt mixtures. As a result, the Strategic Highway Research Program (SHRP) in the United States developed a new binder specification system called the 'Superpave' (superior performing pavements), which categorises grades of bitumen according to their performance characteristics in different environmental conditions, with the motivation to produce pavements that perform well in service. This specification classifies binders regarding their field performance for some of the more common distresses such as rutting, fatigue and thermal cracking. Binders are denominated by the initials PG (Performance Grade) followed by two temperatures, one positive and one negative, which define the range of temperature for which the binder should

adequately perform. For instance, a PG64-12 binder would suitably behave between 64 ^{o}C and -12 ^{o}C (M. Vondenhof, 2015).

2.10. Biobinders

There are three ways in which biobinders can be utilised to decrease the demand of petroleum-based bitumen: (1) as bitumen modifiers (<10% bitumen replacement), (2) as bitumen extenders (20-75% bitumen replacement), and (3) as a direct alternative binder (100% replacement) (Airey et al., 2008, Aziz et al., 2015, Metwally and Raouf, 2010, Sun et al., 2017b). According to the literature, most current studies focus on using biobinders as modifiers, and adding <10% to the mixture (Mamat et al., 2015). This is perhaps because of the increase in uncertainty in rheological properties when higher amounts of biobinder are used. Research is still vital to use biobinders as bitumen extenders or direct replacements (Aziz et al., 2015), and therefore there is a need to study further these materials in order to maximise their potential.

Biobinders can be produced from a range of natural resources including agricultural crops, municipal wastes, forestry by-products, sugar, molasses and rice, natural tree and gum resins, natural latex rubber and vegetable oils, amongst many others (Peralta et al., 2012). However, Kluttz (2012) highlighted some issues around substituting other materials for some or all of the bitumen in conventional mixtures. He pointed out that the alternative binder should have predictable properties regarding rheology, adhesion to aggregates, coating behaviour in a mix plant and flow characteristics during construction. Kluttz (2012) further added other less obvious assumptions to take into consideration such as predictable leaching characteristics, water solubility, interactions with fuels or oils, environmental issues, odour, mixing with virgin binders and interaction with contiguous mixes. All of these points should serve as starting points when evaluating a new material for a pavement binder. It is important to note that bituminous binders and biobinders greatly differ in terms of their chemical compositions and properties. Bitumen is mostly composed of hydrocarbon molecules with some heterocyclic species and functional groups containing sulphur, nitrogen and oxygen atoms (Romberg et al., 1959, Traxler, 1936). On the other hand, biobinders are generally composed of a mixture of fatty acid derivatives with an array of compounds, including aromatic and nitrogenous

compounds, esters, aldehydes and ketones (Zhang et al., 2017). This difference in chemical composition presents an added challenge with the development of biobinders, and stresses the importance of characterizing the chemical properties of the biobinder prior to blending with bitumens.

When dealing with the blend of bitumen and biobinders, mixing speed and temperature are important parameters to consider in order to obtain a homogeneous, consistent material that could mimic the rheological properties of petroleum bitumen. Table 5 presents the mixing conditions used by different authors when working on the partial replacement of petroleum-based binders.

Table 5: Main mixing conditions used in biobinder studies.

Mixer type	Temperature (°C)	Mixer speed (rpm)	Time (min)	Type of biomass	Reference
Shear mixer	120	5000	20	Pyrolysed oil	(Raouf and Williams, 2010c)
Shear mixer	180	4000	45	Used oil	(Sun et al., 2017a)
Ribbon mixer	125	3000	30	Tall oil	(Owerhall et al., 2016)
Mechanical mixing	125	3000	30	HTL oil from manure	(Mills-Beale et al., 2012)
High speed shear mill	145	3000	5	HTL oil from manure	(Mills-Beale et al., 2012)
Mechanical stirrer	150	2000	0.1 ml each minute	Agricultural waste dissolved in ethylene glycol	(Caro et al., 2016)
Low shear mixing reactor	160	1500	60	Dehydrated sap	(Gondim, 2017)

The following section presents current biobinder studies organised according to the thermochemical technique employed to make the biobinder (where applicable and mentioned). A summary has been compiled from the literature displaying the currently known properties of various biobinders (Appendix A). It aims at providing a quick but insightful way of identifying potential biobinder feedstocks with certain desirable properties and help researchers identify gaps and potential research opportunities in the field. In

addition, Table 6 to Table 10 present a short summary of Appendix A, with key improvement and drawback properties of each biobinder.

2.10.1. Pyrolysis-based biobinder studies

Wood-derived pyrolysis oils have been shown to enhance high temperature stability and elasticity, fatigue and rutting resistance (Yang et al., 2014, Yang and You, 2015) and have been recommended as good bitumen modifiers or extenders. Bio-oils can be successfully combined with other waste materials such as crumb rubber from used tires at lower temperatures (around 125 °C) than those used for blending traditional bitumens, with the developed bio-bitumens performing as well or better than conventional asphalt mixtures with ground tire rubber, in terms of rutting, fatigue, moisture sensitivity and low temperature cracking (Peralta et al., 2012, Williams et al., 2015).

Similarly, commercially made biobinders such as Eco-Biopave™, made from a mixture of rosin oil, pyrolysed waste materials and natural rubber (Figure 12) have also shown better behaviour at high temperatures with limited emissions of volatile organic compounds (VOCs), as well as good properties against fatigue and cracking after short-term ageing (Owerhall et al., 2016). However, in order for the technology to be freely applicable, sufficient commercial production of fractionated bio-oil and bio-oil pavement trials are necessary to further understand the ageing mechanisms of these new materials.

Figure 12: On the left, biobinder test road section near Adelaide, Australia. On the right, the Ecopave™ biobinder cross-section specimen (EcoBiopave™, 2004b, EcoBiopave™, 2004a).

Biobinders developed from switchgrass bio-oil, oak wood and corn stover blended at under 10% with bitumen can also result in improvement of the rutting parameter (|G*|/sinδ) of the base bitumen (Williams et al., 2009). In particular, it has been noted that the rheology of

switch grass bio-oils is similar and comparable to that of bituminous binders and can therefore be considered a feasible alternative solution (Raouf and Williams, 2010b, Williams et al., 2017, Yang and You, 2015) . However, such bio-oils cannot be used as direct replacements on their own due to their low viscosity and high-water content, and therefore require upgrading. Low fractions of biobinders (~10% or less) tend to show the most promising results in terms of improving binder performance without lowering viscosity too much, ensuring a stable performance. Yang et al. (2017) suggest that increasing the bio-oil fraction decreases the compatibility with petroleum bitumen, as adding higher dosages increases conglomeration of the asphaltenes, leading to possible stiffening effects or loss of elastic behaviour.

There are studies that have also found promising results with higher blending proportions of biobinders (up to 50% replacement), making the case for treating each biobinder individually and trialling different proportions. Both Mohammad et al. (2013) and Yang and Suciptan (2016) manufactured biobinders using up to 50% fast pyrolysis bio-oil obtained from pine wood chips. The biomodified mixtures had rutting performance that was similar or better than that of the base binder. In the case of Mohammad et al. (2013), almost all the mixtures had adequate moisture susceptibility and showed improved low-temperature performance. However, the mixtures with biobinders revealed less fracture resistance at intermediate temperatures.

Similarly, Zhang et al. (2017) studied how a styrene-butadiene-styrene (SBS) modified binder with pyrolysis-derived bio-oil added up to 20% can improve high temperature performance. After RTFOT ageing, temperature sensitivity was lower than that of the base binder but increased with increasing bio-oil content. On the other hand, rutting resistance increased in comparison to the base binder and improved with increasing bio-oil content. Overall, the high temperature performance of SBS-bio-modified binders is promising in this study, but further work is needed to improve its performance and investigate its modification mechanisms as well as storage stability. This emphasises the need for characterising binders before and after ageing, as the biggest challenge with biobinders lies with their ageing susceptibility. Table 6 presents a summary of the pyrolysis-derived biobinder studies with the primary property improvements and drawbacks.

Table 6: Summary of pyrolysis-derived biobinder studies.

Biobinder	Replacement	Key property improvement	Key property drawback/reduction	References
Oakwood and crumb rubber	100% binder replacement	None	None	(Peralta et al., 2012)
Oakwood and crumb rubber	20% binder extender	Fatigue & moisture damage	None	(Williams et al., 2015)
Switchgrass oil	100% binder replacement	None	Temperature susceptibility	(Raouf and Williams, 2010a)
Pine wood biomass	Up to 50% binder extender	Rutting & thermal cracking resistance	Viscosity	(Mohammad et al., 2013)
Japanese cedar chips	2, 8, 25 and 50% binder modifier and extender	Rutting resistance & temperature susceptibility	Thermal cracking resistance	(Yang and Suciptan, 2016)
Oakwood, switchgrass and corn stover oils	3-9% binder modifier	Rutting resistance	Thermal cracking resistance	(Williams et al., 2009)
Waste wood resources	5 and 10% binder modifier	Fatigue resistance	None	(Yang et al., 2014)
Waste wood resources	5 and 10% binder modifier	Rutting resistance & temperature susceptibility	None	(Yang and You, 2015)
Waste wood resources in the form of wood chips, sawdust and shavings	2, 5 and 10% binder modifier	None	Ageing resistance	(Yang et al., 2017)
SBS-modified bio-oil	1% SBS, 5-20% bio-oil (binder modifier and extender)	Rutting, temperature susceptibility & ageing resistance	Viscosity	(Zhang et al., 2017)

2.10.2. Liquefaction-based biobinder studies

HTL-derived biocrude from swine manure has been shown to enhance low temperature performance, decrease the rate of ageing, and allow for reduced mixing and compaction temperatures due to the decrease in viscosity, when used at <10% by weight of the base binder (Fini et al., 2011, Fini et al., 2012, Mills-Beale et al., 2012, You et al., 2011, Fini and Buehler, 2012). The addition of the HTL biocrude from swine manure can yield a more robust binder against oxidation compared to bio-oil from pyrolysis of corn stover or miscanthus (Fini et al., 2017). A life cycle analysis was carried out to determine the environmental impact (Samieadel et al., 2018). Even though only 10% of swine manure biocrude was added to the bituminous binder, the energy consumption was reduced by half and the global warming potential index improved by 7.8%. In other words, this process reduces the emission of carbon dioxide by 5 times compared to the production of bitumen from petroleum. Life cycle studies such as this one present an area of opportunity for biobinders in order to quantitatively show the benefits of their implementation in asphalt binders, and discovering their future potential.

Similarly to pyrolysis oils, HTL biocrudes combined with other modifiers have exhibited good performance. Swine manure biocrude modified with crumb rubber, Gilsonite, SBS and polyphosphoric acid at low proportions (<10%) show improved low temperature performance and enhanced temperature sensitivity, although results become less obvious at higher temperatures (Fini et al., 2013, Aflaki et al., 2014).

Algae-derived biocrudes are also very popular biobinders. Studies that display the potential of microalgae and HTL to produce binders for pavements, show how the rheological behaviour of the developed biocrude is heavily affected by the operating conditions used.

Dhasmana et al. (2015) produced bio-crude from HTL at 300 °C of different algae feedstocks including spirulina, a nanoalgae strain and swine manure. Although all the biobinder blends exhibited similar viscoelastic properties before and after ageing, the algae-derived biobinders were stiffer than those obtained from swine manure. Other algae biobinder studies have claimed a rheologically simple material with similar viscoelastic properties to bitumen, if lower temperature ranges (240-260 °C) are used (Borghol et al., 2018, Audo et al., 2015). High molecular weight species that fragment at the higher temperature result in less viscous material that is no longer thermorheologically simple. It is crucial to preserve these heavy

species which appear to function similarly to asphaltenes and resins in petroleum derived binders. Future work involves studying how the properties of the hydrophobic fraction vary with microalgae strain. This would be helpful in understanding how the main elements and their molecular weight distributions impact the final biobinder viscosity profile. Once the most suitable microalgae residues are chosen, an assessment of their economic viability for road pavement compared to the petroleum distillation process would be beneficial. Table 7 presents a summary of the liquefaction-derived biobinder studies with key property improvements and drawbacks.

Table 7: Summary of liquefaction-derived biobinder studies.

Biobinder	Replacement	Key property improvement	Key property drawback/reduction	References
Biocrude from swine manure	2, 5 and 10% binder modifier	Thermal cracking & ageing resistance	None	(Fini et al., 2011, Fini et al., 2012)
Biocrude from swine manure	2, 5 and 10% binder modifier	Thermal cracking resistance	None	(You et al., 2011)
Biocrude from swine manure	2, 5 and 10% binder modifier	Low temperature performance, moisture damage & thermal cracking resistance	None	(Fini and Buehler, 2012)
Biocrude from swine manure with crumb rubber	5, 10 and 15% crumb rubber blended with 5% biobinder	Thermal cracking resistance & temperature susceptibility	None	(Fini et al., 2013)
Biocrude from swine manure	2, 5 and 10% binder modifier	Thermal cracking resistance	None	(Aflaki et al., 2014)
Biocrude from swine manure	5% binder modifier	Rutting, ageing, temperature	None	

		susceptibility & thermal cracking resistance		(Mills-Beale et al., 2012)
Swine manure, miscanthus pellets, corn stover and wood pellets	10% binder modifier	Rutting	Ageing resistance	(Fini et al., 2017)
Biocrude from swine manure	10% binder modifier	None	None	(Samieadel et al., 2018)
Spirulina sp. algae (microalgae), swine manure, and nanoalgae	Studied as virgin biobinder and blended biobinder with PG 64-22 bitumen in a 1:8 ratio	Thermal cracking resistance & moisture damage	Ageing resistance	(Dhasmana et al., 2015)
Scenedesmus sp. Microalgae	100% binder replacement	Similar rheological properties to that of bitumen	None	(Borghol et al., 2018)
Spirulina sp. Residues	100% binder replacement	Temperature susceptibility	None	(Audo et al., 2015)
Household food waste	5 and 10% binder modifier	Temperature susceptibility	None	(Mahssin et al., 2019)

2.10.3. Biobinder and recycled asphalt studies

The use of bio-oils and biocrude as rejuvenators for recycled asphalt mixtures have also been a focus in recent years. Increasing the recycled asphalt (RA) content is environmentally valuable since it reduces long distance aggregate transport and amount of new bitumen needed in asphalt mixtures (Blanc et al., 2019a, Santos et al., 2018, Santos et al., 2017). In order to make the most of the RA, researchers use new binders and/or additives that re-activate the aged binder by increasing its viscous fraction (Jiménez del Barco Carrión et al., 2015, Blanc et al., 2019a, Lo Presti et al., 2016). In this case, bio and conventional rejuvenators typically improve cracking performance (fatigue and low temperature behaviour) but can be detrimental to rutting performance. Table 8 presents a summary of the biobinder studies with recycled asphalt with the main property enhancements and drawbacks.

Biobinders from swine manure and pongamia oil have been considered suitable rejuvenators with RA, with improved rutting and fatigue resistance and adequate thermal stability (Mogawer et al., 2016, Nayak and Sahoo, 2017a). Apart from swine manure, other studies have examined thermochemically treated wood, miscanthus and corn stover with RA, with the objective of understanding how feasible these mixtures could be in cold regions prone to thermal cracking. Results showed that the presence of biobinders improved fracture resistance, and overall it was observed that the biomodified RA mixtures exhibited better low-temperature cracking behaviour to that of conventional hot-mix asphalt (Hill et al., 2013, Hill et al., 2018).

Nevertheless, limited data on accelerated pavement testing is currently available as most studies are restricted to laboratory evaluations (Blanc et al., 2019b, Ding et al., 2019, Mogawer et al., 2013, Tran et al., 2017, Zaumanis et al., 2014b). One study that has undertaken a full scale accelerated pavement test was Blanc et al. (2019b), where three mixtures were designed incorporating 50% RA content with three innovative bio-materials and compared with a reference high modulus asphalt mixture. They were tested for one year in order to speed up rutting and fatigue cracking. The authors concluded that all three bio-mixtures present similar or better performance than the control and confirmed that they can be effectively used in road construction, but further investigation should focus on long-term monitoring to evaluate ageing performance.

Fatty acids from vegetabe oils like soybean and sunflower oils have also been shown to soften aged bitumen (Seidel and Haddock, 2012, Somé et al., 2016). Field investigations have found the biomodified mixtures to have adequate performance after 5 years of service, despite the biomodified binders being more sensitive to ageing than traditional binders. Nevertheless, the authors agree that five years is not long enough to draw definitive conclusions.

The use of biobinders to enhance the properties of petroleum bitumen has been a topic of discussion over several years, however there is limited knowledge on the adhesion properties of bitumens blended with biobinders. Gong et al. (2017) and Jiménez del Barco Carrión et al. (2019) looked at characterizing the adhesion behaviour of bio-modified bitumen using contact angle measurement and surface free energy. Gong et al. (2017) used dosages of 1%, 2%, and 3% of bio-modifier (produced from natural bean oil) with two base binders. They found that the adhesion properties depended on the compatibility between the biobinder

and base bitumen used. Jiménez del Barco Carrión et al. (2019) combined biobinders with RA binders and concluded that biobinders had great potential to maintain moisture damage resistance of such type of asphalt mixtures. As a result, it is critically important to characterize these properties for innovative materials used.

A main conclusion drawn from RA studies is that high amounts (i.e. 50% RA) could be incorporated into asphalt mixtures with suitable biobinders, restoring their rheological properties and enhancing the performance of the mixture (Jiménez del Barco Carrión et al., 2017, Jiménez del Barco Carrión et al., 2017, Chailleux et al., 2018, Jiménez del Barco Carrión et al., 2019, Sotoodeh-Nia et al., 2019). Such bio-derived mixtures with RA can sufficiently pass the design requirements for pavements and perform well at low, intermediate and high temperatures without the need of neat bitumen (Manke et al., 2019).

Table 8: Summary of recycled asphalt and biobinder studies.

Biobinder	Replacement	Key property improvement	Key property drawback/reduction	References
Bio-rejuvenator SYLVAROAD™ Biobinder Biophalt® Bio-additive Epoxidized Soybean Soyate (EMS)	Up to ~5% added to mixtures with 50% RA	Rheological properties including complex modulus and phase angle, fatigue, rutting, thermal cracking resistance & durability in field	None	(Blanc et al., 2019a, Blanc et al., 2019b)
Rejuvenator A (regenerated oil and a Fischer-Tropsch wax) and Rejuvenator B (highly viscous material free of polycyclic aromatic hydrocarbons)	6,12 and 18% Rejuvenator A and 9, 18 and 27% Rejuvenator B added to RA mixture	Thermal cracking, rutting & fatigue resistance	None	(Jiménez del Barco Carrión et al., 2015)
Waste vegetable oil, waste vegetable grease, organic oil, distilled tall oil, aromatic extract and waste engine oil	12% added to RA mixture	Rutting, fatigue & thermal cracking resistance	Viscosity, moisture damage & ageing resistance	(Zaumanis et al., 2014b)
Bio-rejuvenator SYLVAROAD™	6.8% added to mixtures with 50% RA	Thermal cracking, rutting & ageing resistance (short-term ageing)	None	(Tran et al., 2017)

Rejuvenators BituTech RAP SonneWarmix RJT and RJ	9.28% added to mixtures containing 35 and 40% RA	Fatigue, thermal cracking & ageing resistance	Viscosity, rutting & moisture damage	(Mogawer et al., 2013)
Crumb rubber with a commercial rejuvenator	3, 5 and 7% rejuvenator added to mixtures containing 0, 30 and 50% RA	Fatigue, thermal cracking & moisture damage	Rutting resistance	(Ding et al., 2019)
Crude tall oil and soybean oil derivative	3 and 6% added to mixtures containing 50% RA	Thermal cracking resistance	Ageing resistance	(Sotoodeh-Nia et al., 2019)
Bio-rejuvenator SYLVAROAD™ Biobinder Biophalt® Bio-additive Epoxidized Soybean Soyate (EMS)	Up to 2.8% biobinder added to mixtures containing 50% RA	Rheological properties including complex modulus, rutting, fatigue, thermal cracking, moisture damage & ageing resistance	None	(Chailleux et al., 2018)
Biobinder Biophalt®	1.7% added to mixtures containing 50% RA	Rutting & thermal cracking resistance	None	(Manke et al., 2019)
Swine manure	5% biobinder added to mixtures containing 40% RA	Fatigue, thermal cracking resistance, temperature susceptibility & durability in field	Viscosity	(Mogawer et al., 2016)
Swine manure	% biobinder added to mixtures of 0, 15 and 45% RA	Thermal cracking resistance & temperature susceptibility	Viscosity	(Hill et al., 2013)
Swine manure, corn stover, miscanthus and wood pellets	5 and 10% biobinder added to mixtures with 0, 15 and 45% RA	Thermal cracking, temperature susceptibility & ageing resistance	Viscosity	(Hill et al., 2018)

Pongamia oil and a composite oil made from castor oil and coke oven gas	5, 10 and 15% binder modifier	Rutting, fatigue & temperature susceptibility	Viscosity	(Nayak and Sahoo, 2017a, Nayak and Sahoo, 2017b)

2.10.4. Miscellaneous biobinder studies

Some studies are considered miscellaneous in the sense that they do not adhere or refer to one specific thermochemical technology. Materials such as algae (Chailleux et al., 2012), residues from the forestry industry, waste cooking oils, some agricultural wastes and natural fibres such as sugarcane, rice husk and hemp as well as synthetic binders have been used as bitumen modifiers at different percentages (Martínez-Echevarría-Romero et al., 2015, Caro et al., 2016, Ingrassia et al., 2019).

Overall, the materials have shown adequate rheological performance and improve some mechanical properties compared to bitumen (see Annex A for details). They seem to perform better at lower temperatures than conventional bitumens, due to their increased workability, making them more suited to be used in colder climates or as fluxing agents for stiff binders such as those found in recycled asphalt (de Toulouse, 2010, Avantium, 2018). This renders the study of high-temperature performance more critical with biobinders (Wen et al., 2012, Sun et al., 2016, Gong et al., 2016). When ageing was considered, most of them revealed faster ageing rates (Pouget and Loup, 2013, Xue et al., 2014). Ageing of biomodified binders and mixtures is therefore an unavoidable issue which needs to be carefully studied. A summary of the miscellaneous biobinder studies' key properties is shown in Table 9.

Table 9: Summary of miscellaneous biobinder studies.

Biobinder	Replacement	Key property improvement	Key property drawback/reduction	References
Microalgae	100% binder replacement	None	None	(Chailleux et al., 2012)
Forestry industry by-products	5.7%	None	Ageing resistance	(Pouget and Loup, 2013)

Waste cooking oil	10,30 and 60% binder modifier and extender	Rheological properties & thermal cracking resistance	Fatigue & rutting resistance	(Wen et al., 2012)
Biodiesel by-product from waste cooking oil (as aged binder rejuvenator)	2-8% binder modifier	Fatigue & thermal cracking resistance	Rutting & moisture damage	(Sun et al., 2016)
Biodiesel by-product from waste cooking oil (as aged binder rejuvenator)	1.5,1.75 and 2% binder modifier	Fatigue & thermal cracking resistance	Rutting & moisture damage	(Gong et al., 2016)
Soy fatty acids	1 and 3% binder modifier	Rheological properties including viscosity and complex modulus	None	(Seidel and Haddock, 2012)
Waste coffee grounds	2-8% binder modifier	None	Ageing resistance	(Zofka and Yut, 2012)
Vinasse	10% binder modifier	Rheology & fatigue resistance	None	(Martínez-Echevarría-Romero et al., 2015)
Rice husk and wood sawdust	10 and 20% binder modifier and extender	Rutting resistance	Ageing resistance	(Xue et al., 2014)
Plant resin fluxed with monoalkyl esters from	0.5 and 5% binder modifier	Rheological properties including complex modulus &	Ageing resistance	(Somé et al., 2016)

vegetable and animal oils		durability in field (after 5 years)		
Sugarcane bagasse, corncobs and rice husk	1 and 2% binder modifier	Rutting & ageing resistance	Moisture damage	(Caro et al., 2016)
Natural bean oil	1-3% binder modifier	None	None	(Gong et al., 2017)

2.10.5. Synthetic binder studies

Synthetic binders have also been studied as alternative binders. Although these are not derived from natural sources and have not been studied extensively, they can still affect the rheological properties of asphalt binders. In particular, Airey and Mohammed (2008) investigated the rheological properties of polyacrylate binders, which consisted of polyethyl acrylate (PEA), polymethyl acrylate (PMA) and polybutyl acrylate (PBA). Results indicated that PEA could simulate a 'soft' 100/150 penetration grade bitumen, while PMA showed stiff 10/20 penetration grade bitumen characteristics. Airey et al. (2008) further studied these binders and blended the polyacrylates with conventional bitumens, which were found to be rheologically similar to SBS polymer modified bitumens.

Bio-rejuvenators manufactured from cotton oil and the plasticizer dibutyl phthalate (DBP) have also been used to restore the properties of conventional and SBS-modified binders (Gong et al., 2016, Zhu et al., 2017). Results showed that the 10% dosage of bio-rejuvenator helps to restore workability and rutting resistance of the long-term aged bitumen to original levels. Low-temperature cracking and fatigue resistance also improved but not to the level of the virgin conventional and SBS-modified bitumens. A summary of these studies is presented in Table 10.

Table 10: Summary of synthetic binder studies.

Biobinder	Replacement	Key property improvement	Key property drawback/reduction	References
Polyethyl acrylate (PEA), polymethyl acrylate (PMA) and polybutyl acrylate (PBA)	100% binder replacement	Rheological properties including complex modulus and phase angle	None	(Airey and Mohammed, 2008)
Polyethyl acrylate (PEA), polymethyl acrylate (PMA) and polybutyl acrylate (PBA)	25-75% binder extender	Rheological properties including complex modulus and phase angle	None	(Airey et al., 2008)
Cotton oil by-product and dibutylphthalate (DBP) (as aged binder rejuvenator)	5 and 10% binder modifier	Viscosity, thermal cracking & fatigue resistance	Rutting resistance	(Zhu et al., 2017)

2.11. Current limitations of biobinders

Although the field of biobinders has drastically taken off in the last ten years, the use of bio-derived additives to enhance petroleum bitumen has been around for much longer. The first patent dealing with the production of an alternative binder based on compounds partially derived from biomass was published in 1991 in the US (Pinomaa, 1991). This binder was obtained from a mixture of natural or modified vegetable resins (tall oil, wood, or turpentine) and was considered an added-value product with high abrasion resistance. Since then, various companies have developed such biobinders based on oils, resins and polymers. The key benefit is reduced asphalt manufacturing process temperatures compared to petroleum binders, corresponding to significant energy reductions (Colas, 2004a, Eiffage, 2007, Eurovia, 2010, Shell, 2010, Colas, 2004b, Valagro, 2011).

At present, essentially all studies (academic or commercial) that use biobinders in road construction are limited to small-batch production, and so bio-bitumen, whether blended with bituminous binders or not, cannot compete with traditional bitumen. One of the key obstacles to the deployment of biobinders compared to conventional binders is their price.

Indeed, the price of vegetable binders is equivalent to that of synthetic binders and is 3 to 10 times higher than that of petroleum bitumen (Yvelines, 2011). This results in an asphalt mixture approximately four times more expensive than the traditional product. Unlike bitumen, it can be safe to assume that the price of biobinders will not be affected by the volatile price of crude oil. A high oil price coupled with further development of renewable technologies will result in a favourable environment for developing biobinders at a much larger scale. Due to the fact that the biobinder technologies are at an early stage, its price is unlikely to fall until a commercial market has been developed and economies of scale take off.

In addition, the process of manufacturing biobinders and then combining them with bitumen tends to be time-consuming and stability of the biobinders is a major issue. Each biobinder has to be carefully studied in detail to understand its chemical and rheological properties, as well as their ageing mechanisms. This building of knowledge is what will help make biobinders more acceptable for widespread use in the future.

Carrying out more studies that look at the sustainability impact and overall carbon footprint of biobinders in comparison with bitumen, such as LCA, will also help build the case for biobinders. In order to help LCA to be useful as a decision-making tool for practitioners and road administrations, cradle-to-grave analysis should be performed, and therefore, more data about the durability of asphalt mixtures containing biobinders should be produced, including full-scale trials and trial sections.

2.12. Conclusions and final remarks

This review aimed, for the first time, to bring together studies across different disciplines and investigate their effects on biobinders for road construction.

The utilisation of biomass is beneficial to the environment and society as a sustainable form of energy. A vast range of biomass feedstocks can be thermochemically treated and the derived products subsequently used for various applications, including biobinders for road construction. Its availability worldwide makes it an attractive option for researchers looking to find more environmentally-friendly alternatives to bituminous binders.

Liquefaction and pyrolysis are two effective biomass thermochemical conversion technologies that can be used to produce biobinders. Unlike pyrolysis, liquefaction does not

require feedstock drying, saving on high drying costs. The recovered products seem to be more stable and less corrosive than the ones obtained from pyrolysis, due to lower oxygen and moisture contents and higher heating values, and are therefore more suitable as biobinders for asphalt mixtures.

However, liquefaction is considered a less developed technology than pyrolysis and so understanding the effects of the operating parameters is essential to optimise biocrude yields and ultimately advance the process. Product yield and quality are impacted by a range of factors, including temperature, pressure, residence time and type of biomass source. These parameters are highly reliant on the nature of the feedstock as well as each other and can vary extensively. Numerous complex reactions take place during the conversion of biomass into biocrude products. The wide variation in different feedstock types and reaction conditions generates a broad but fragmented spectrum of knowledge and makes it essential to individually study each material to produce biobinders.

The concept of biobinders has definitely gained momentum in pavement engineering and a range of studies have been carried out evaluating their influence on asphalt mixture performance. Biobinders have shown promising performance as bitumen modifiers and extenders. They can enhance the chemical and mechanical properties of conventional asphalt binders. Extensive research has been found on these categories, but less confident results are found in terms of total replacement of conventional bitumen.

The review carried out reveals that biobinder behaviour is dependent on biomass composition. While some biobinders improved rutting resistance, others improved fatigue cracking. However, most biobinders seem to enhance low temperature performance and lower the viscosity of the bitumen. There are no reports of a single biobinder improving all of the desired performance parameters. Therefore, before these materials can be further implemented, their performance in asphalt mixtures needs to be always fully characterised in terms of their chemical, rheological, mechanical and ageing properties. These need to be tested over a whole range of service temperatures depending on the behaviour and nature of the biobinder. Due to their recent use, most of the studies found are focused on laboratory properties. In order to provide confidence to the use of these materials, more data about

long-term performance and durability are required; and attention should be paid to future issues such as their recyclability.

Biobinders that are available in large quantities such as through industrial processes, i.e. waste feedstocks, are more attractive in terms of commercial viability than those derived from more involved processes. Due to their availability, these are more likely to become a practical reality in the near future. Comprehensive environmental assessment tools like LCA and EIBP should be incorporated when studying thermochemical processes and biobinders as they can highlight potential research opportunities and help provide a clearer picture of where the technology is heading in the long term. Environmental impact studies should consider the whole life cycle of asphalt mixtures containing biobinders, accounting for their impact during the whole service life of the pavement. For this purpose, future research should focus on their long-term performance and recyclability.

Finally, the price and length of time required to make biobinders are major barriers limiting their widespread use. Current biobinder materials are mostly used for research purposes either at lab or pilot-scale, and so are not presently found at industrial scale. For these reasons, successfully produced biobinders almost exclusively apply to small cycle and pedestrian paths, sidewalks and car parks. Nevertheless, there is a great opportunity for biobinder production costs to decrease as the technology becomes mainstream, their combination with reclaimed asphalt to reduce the final price of the mixture and also for the implementation of a more bio-based and circular economy in the future, where suitably efficient bio-products can then compete and capture markets dominated by petroleum bitumen.

3. Theory and Methods

3.1. Hydrothermal liquefaction experiments and product recovery

Hydrothermal liquefaction experiments were undertaken using both the paper waste and the BFO feedstocks at various temperatures to generate a bio-bitumen or biobinder. This biobinder would subsequently be used with conventional bitumens and characterised in terms of their chemical and rheological properties.

The paper waste runs were performed at 320 and 360 °C for one hour, and the BFO runs at 300-360 °C for 4 hours. The liquefaction experiments were performed using a Parr 4740 series stainless steel (75 mL cylindrical) pressure vessel connected to a pressure gauge rated to 690 bars. Photographs of the assembled reactor and HTL equipment are shown in Figure 13 and Figure 14. Heat is applied by means of a fluidised sand bath (connected to a compressed air source) which is controlled by an external temperature controller. Temperature is also monitored by an additional K-type thermocouple connected externally to a computer, which records the temperature every 10 seconds. Firstly, distilled water used is de-gassed by bubbling nitrogen gas through for about 15 minutes in order to remove dissolved gases such as oxygen and carbon dioxide. The biomass feedstock (either the BFO or the paper waste) was first weighed and transferred into the vessel, after which the water needed for the experiment was measured and introduced into the vessel. The biomass to water ratio used was 1:2.5 by weight. It is important to note that the paper waste was kept in the freezer to avoid bacterial degradation, and is defrosted overnight before every experiment was undertaken. Similarly, the BFO materials are refrigerated for the same purpose. After the addition of sample and water, the pressure vessel was assembled and the pressure gauge attached to the vessel. The experimental set up was then flushed for about 20 minutes with nitrogen gas at 2 bar to reduce the oxygen content in the system, after which the reactor head space was filled with nitrogen gas at 1 bar to keep the system relatively inert during the experiment. The sand bath was pre-heated to the required temperature and left to equilibrate. After equilibration of the sand bath, the pressure vessel was lowered onto the sand bath and the experiment was left to run for the required time. At the end of the run the sand bath was switched off and the reactor immediately removed from the sand bath and allowed to cool to ambient temperature before product recovery. After generated gas collection (procedure described later in section 3.6.1), oil floating on top of the water after

the experiment (for experiments that generated expelled oil), was collected with the aid of a spatula after which the water was decanted into a beaker.

For the paper waste experiments, the expelled oil and the reactor content was then transferred to a round bottom flask by washing the spatula containing the expelled oil and the pressure vessel with toluene to recover any product stuck to the wall of the vessel. The recovered expelled oil and reactor content in toluene was then extracted via reflux using a Dean-Stark apparatus overnight (Figure 15). After reflux, the set-up was allowed to cool and the unconverted biomass residues were then separated from the biocrude (toluene soluble) by filtration using a 0.5µm glass fibre filter paper, after which the filtrate(bio-bitumen/toluene mixture) was transferred to a round bottom flask for rotary evaporation. The residue is left to dry under a fume cupboard and the weight subsequently recorded. The bio-bitumen/toluene mixture is gently rotary evaporated (to almost dry) at 85 ° C / 200 mbar and transferred to a pre-weighed glass vial using a pasture pipette. The vial is left to air dry in a fume cupboard to remove any leftover solvent. This is then termed “paper waste biobinder”.

Regarding the generated biocrude from the BFO, after decanting the water, the biocrude is scraped into a round bottom flask and the reactor is rinsed with dichloromethane and methanol to remove excess product and water. Similarly to the paper waste, the bio-bitumen/dichloromethane/methanol mixture is gently rotary evaporated at 85 °C / 200 mbar and transferred to a glass jar. The BFO biocrudes are left to dry in a fume cupboard for 3 weeks until a constant weight is reached through the removal of any water and low boiling point organic compounds. The final dried product is then used for chemical and rheological characterisation.

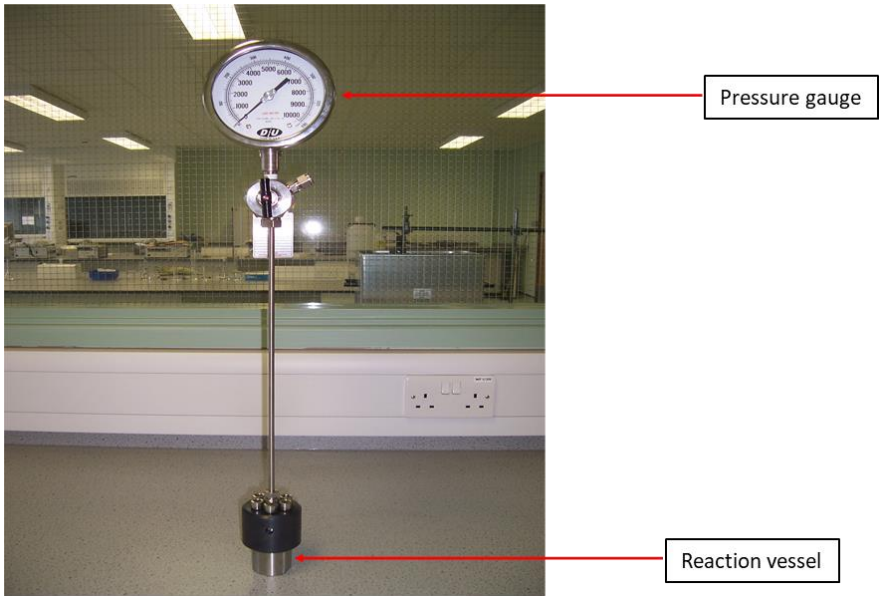

Figure 13: Photograph of assembled reactor for HTL.

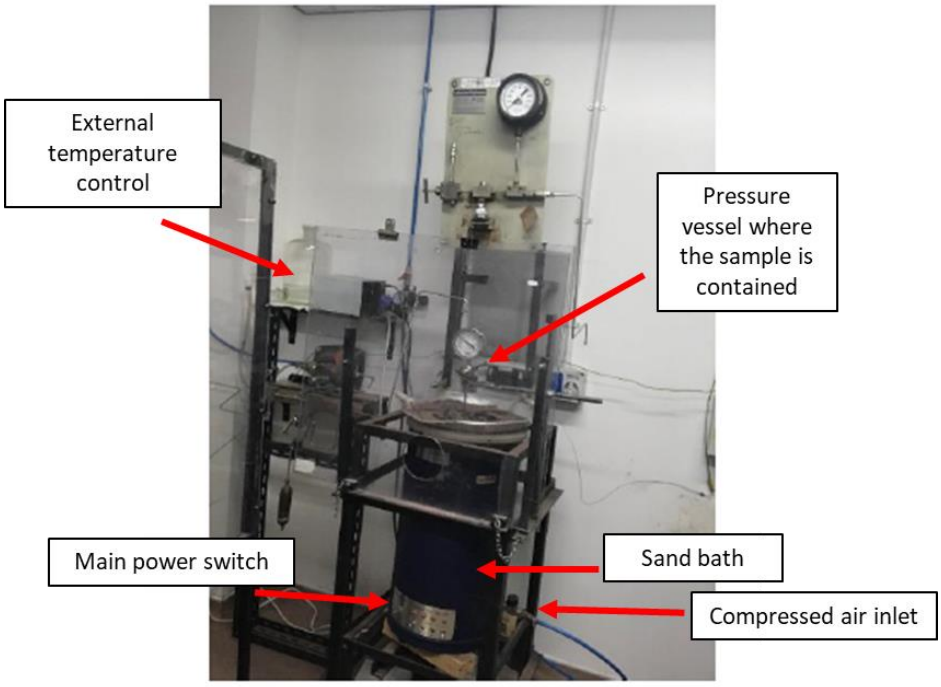

Figure 14: Photograph of hydrous pyrolysis (hydrothermal liquefaction) equipment.

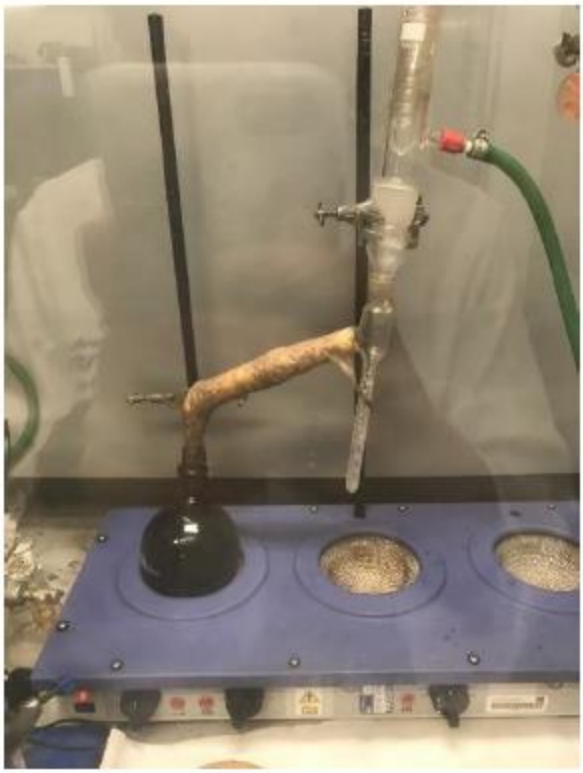

Figure 15: Reflux of paper waste biocrude using a Dean-Stark apparatus to collect water.

3.2. Pyrolysis using a high-temperature horizontal furnace

In addition to hydrothermal liquefaction, a second method was tried in order to increase the viscosity of the BFO materials and to produce a more suitable biomodifier. Pyrolysing the material using a horizontal high-temperature furnace (HTF) in a flow of nitrogen at atmospheric pressure is less severe than hydrothermal liquefaction at high pressures. This is essentially a crude distillation where the material is heated in an inert environment in order to evaporate off the lower molecular weight compounds. A higher mass loss is desired as this increases the viscosity of the remaining product. The pyrolysis was performed by using between 10-15g of BFO. The BFO was placed in a pre-weighed ceramic boat which was heated in a horizontal tube furnace (Elite Thermal Systems Limited, Figure 16) to the desired temperature at a heating rate of 5 °C/min in a flow of nitrogen (1 L/min). The sample was kept at the desired temperature for a specific length of time (either 1 hr or 5 hrs). Following the run, the sample was cooled down to room temperature and removed from the furnace. It was then weighed and transferred to a glass jar. Repeat runs were carried out for the experiment which gave the greatest percentage mass loss, i.e. the heaviest material. These were

subsequently combined before carrying out the chemical and rheological characterisation. For convenience, this is referred to as 'pyrolysed BFO' in this thesis.

Figure 16: Pyrolysis equipment using a high-temperature horizontal furnace (HTF).

3.3. Thermogravimetric analysis

Thermogravimetric analysis (TGA), an analytical technique used to identify the combustion profile of a material, was carried out on the BFO starting materials, their liquefaction products and the biodiesel products which were used as controls. An inert environment (N_2) will cause pyrolysis and the chemical decomposition of organic materials. Switching to a reactive gas such as oxygen (air) allows for the combustion of carbon in order to identify its proportion in a material.

3.3.1. Experimental

The proximate analyses were performed in a Discovery TGA Q500 V20.13 Build 39 (TA Instruments) using the following method. Approximately 65 mg of sample was loaded in a platinum pan 4mm deep and 10mm in diameter. It was then heated from ambient temperature to 110 °C with a heating rate of 20 °C/min and kept at this temperature for 30 minutes under N_2 with a flow rate of 50 ml/min to remove moisture. From this point, the sample was further heated to 950 °C with a heating rate of 20 °C/min under the same nitrogen flow rate, and kept for 30 minutes to remove the volatile matter, before changing to air to

combust the fixed carbon at a flow rate of 50 ml/min for 30 minutes. TGA results are displayed in the initial sample characterisation section (6.1.1).

3.4. Elemental Analysis

Elemental analysis (EA), an analytical technique used to determine the chemical composition of a material, was carried out on the BFO materials, their liquefaction products, the pyrolysed BFO and the biodiesel control samples. EA, also called CHNS analysis, provides a means for the rapid determination of carbon, hydrogen, nitrogen and sulphur in a material given as a percentage by mass. It requires high temperature combustion in an oxygen-rich environment, where the accurately weighed aliquot of a sample is combusted to decompose it into gases CO_2, N_2, H_2O and SO_2. Quantification of each element requires calibration by using a high purity micro-analytical standard, such as 2,5-Bis(5-tert-butyl-2-benzo-oxazol-2-yl) thiophene (BBOT). A wide variety of sample types can be tested, including solids, liquids, polymers, and volatile and viscous samples. The analyser can be set up in various configurations depending on the application, such as CHN, CNS, N, or CHNS. In this case, the CHN configuration was used as it was assumed that no inorganic elements were present.

3.4.1. Experimental

The ultimate analysis was performed on a Leco CHN-628 instrument. A schematic of the equipment is presented in Figure 17. Approximately 0.075 g of sample placed in tin foil cups were dropped into the vertical combustion furnace from an automated sample carousel (A) to the combustion tube (B) held at approx. 1000 °C. Combustion gases, mainly CO_2, H_2O and N_2 are swept in a constant helium flow to the reduction tube (C), which is held at approx. 700 °C. Unwanted gas species are removed when the gasses pass one or more chemical traps (D). The species of interest (CO_2, H_2O, and N_2) are then chromatographically separated in a column (E) at 40-100 °C and detected sequentially by a detector (F), each yielding a peak in abundance at different times (G). This is the basis for estimating the abundance of the elements C, H and N in each sample. The analyses were repeated three times to reduce any systematic error. Elemental analysis results are displayed in section 6.1.2.

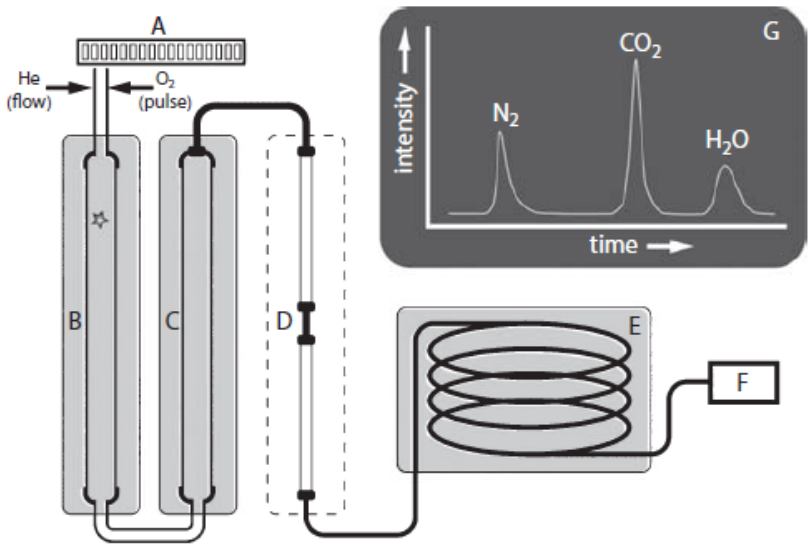

Figure 17: Schematic of an elemental analyser with vertical combustion furnace (Bird et al., 2017).

3.5. Gas chromatography and mass spectrometry (GC-MS)

Gas chromatography-mass spectrometry (GC-MS) is the combination of gas chromatography and a mass spectrometer. The gas chromatograph separates the components in a mixture according to their volatility and mass and the mass spectrometer provides information that helps to structurally identify those components (Figure 18). GC-MS is one of the most well-established analytical tools available for the study of complex samples. The prepared sample is injected through an injection port, and is then vapourised and passed through the GC column with a carrier gas (usually helium). Separation of the components takes place and the eluted components are detected and recorded on a chromatogram. Height and area of the peaks are directly proportional to the concentration of the compound within the sample. The components are then hit with an electron impact allowing them to fragment into cations. The fragment ions are filtered by mass through an electromagnetic field and a mass spectrum is created. The components can be detected either in full scan mode (scan) or by selected ion monitoring (SIM), in which a selected mass fragment (m/z) value characteristic of a particular compound or group of compounds is monitored. The spectrum shows each individual component within the sample and is the blueprint of its chemical identity.

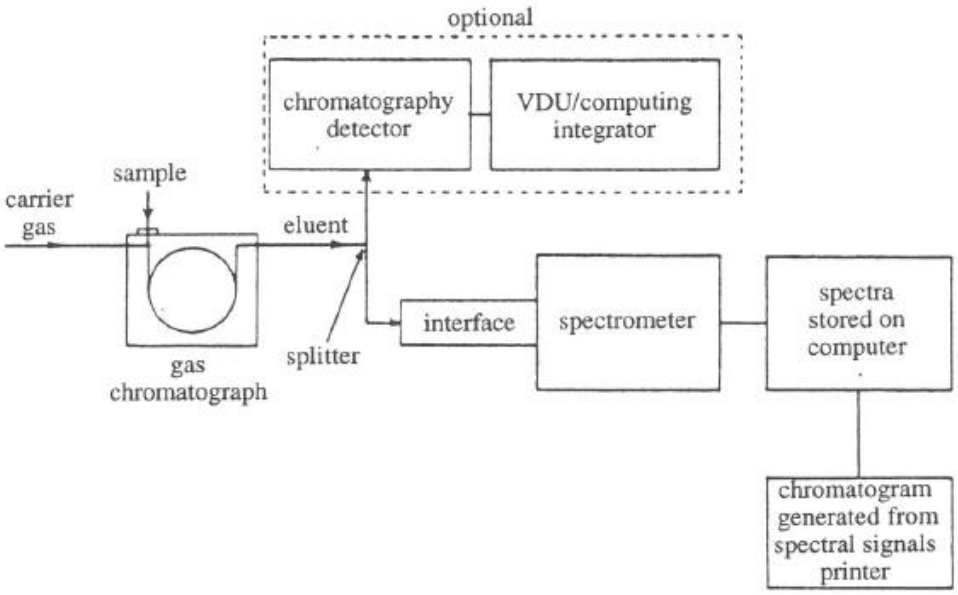

Figure 18: Schematic diagram of a gas chromatograph-mass spectrometer (Fifield and Kealey, 2000).

3.5.1. Experimental

Aliquots of treated and untreated biofuel oils (BFOs), hydrothermal liquefied BFOs, a pyrolysed BFO, undistilled (crude) and distilled biodiesel were dissolved in 1 ml of dichloromethane and analysed on an Agilent GC-MS (7890B GC; 5977A MSD), with a single quadrupole mass spectrometer and an electron impact ionization detector (EI). The GC injector was kept at 280 °C, and the injection split ratio and the injection volume were 10:1 and 1 µl, respectively. The products were separated with a DB-1701 MS column (60 m × 0.25 mm i.d. × 0.5 µm film thickness, Agilent Technologies, Inc., USA). The temperature ramp of the GC column oven began with a constant temperature step at 50 °C for 2 min and then increased by a rate of 4 °C/min up to a final temperature of 280 °C which was held constant for 20 min. Helium (99.99% purity) was used as a carrier gas with a 1.2 ml/min volume flow. The MS ionization mode was electron impact at 70 eV and the mass scan range was from 29 to 450 m/z. The eluted components were monitored in full scan mode during analysis. The various product compounds were identified by comparing all chromatogram spectra to the NIST mass spectral search programme and the Wiley mass spectrum library. The GC-MS results are presented in section 6.3.

3.6. Gas chromatography

3.6.1. Experimental

Gases generated during the hydrothermal liquefaction experiments were collected with the aid of a gas tight syringe at ambient temperature via a connector by opening the gauge block valve and transferred to a gas bag (after the total volume had been recorded), and immediately analysed on a Clarus 580 gas chromatograph (GC) fitted with a FID and TCD detectors operating at 200 °C. The hydrocarbon gases were analysed by injecting 100 μl of gas samples (split ratio 10:1) onto the FID at 250 °C with separation performed on an alumina plot fused silica 30 m x 0.32 mm x 10 μm column, with helium as the carrier gas. The oven temperature was programmed from 60 °C (13 min hold) to 180 °C (10 min hold) at 10 °C min^{-1}. Individual hydrocarbon gas yields were identified and quantified in relation to C_1-C_5 gases (injected separately) as an external gas standard. The non-hydrocarbon gases (H_2, CO and CO_2) were analysed by injecting 500 μl onto the TCD. Separation was performed on a Haysep N6 packed column (60–80, 7_ ×1/8_sulfinert), using Argon as the carrier gas. The oven temperature was programmed from 60 °C (13 min hold) to 160 °C (2 min hold) at 10 °C min^{-1}. The H_2, CO, and CO_2 yields were also identified and quantified in relation to their individual gas standards (injected separately) as a mixture of external gas standard. The gas analysis results are presented in section 6.2.

3.7. ^{13}C Nuclear Magnetic Resonance

Comparable to proton NMR (^1H NMR), ^{13}C Nuclear magnetic resonance (NMR) spectroscopy is used to determine the type and number of carbon atoms in organic compounds. The major isotope of carbon, C-12, is not magnetically active and is therefore not detectable by NMR. C-13 carbons comprise of approximately 1% of all carbon atoms, which are magnetically active with a ½ spin quantum number. This very low natural abundance gives an overall sensitivity of ^{13}C absorption to be about 1/5700 compared to ^1H (natural abundance of 99.984%). As a result, very weak signals were produced and ^{13}C NMR was not popular before 1970 (Yadav, 2013). Since then with the advancement of technology and the rise of Fourier transform NMR, ^{13}C NMR has become a routine tool for structure determination. It is a valuable analytical technique that provides information about the structure of the carbon skeleton in organic molecules, such as those found in the BFO materials. In a typical ^{13}C NMR spectrum, the number of peaks relate to the number of carbon environments and their position (chemical

shift, δ value) corresponds to the type of carbon present in the sample. Chemical shifts for selection of carbon functionalities are presented in Table 11 and Table 12 .

Table 11: Carbon chemical shift classification, based on (Clark, 2014)

Type of carbon	Chemical shift range (ppm)
C=O (ketones)	205-220
C=O (aldehydes)	190-200
C=O carboxyl (esters and carboxylic acids)	170-185
C in aromatic rings	125-150
C=C (alkenes)	115-140
RCH_2OH	50-90
RCH_2Cl	40-45
RCH_2NH_2	37-45
R_3CH	25-35
CH_3CO-	20-30
R_2CH_2	16-25
RCH_3	10-15

Table 12: Simplified version of the carbon chemical shift classification relevant to BFO, based on (Clark, 2014)

Type of carbon	Chemical shift range (ppm)
C-C	0-50
C-O	50-100
C=C	100-150
C=O	150-200

3.7.1. Experimental

Carried out as a service by the Department of Chemistry at the University of Nottingham, ^{13}C-NMR spectra were acquired on a Bruker Avance AV(III)400HD spectrometer with a 5mm BBFO probe. The samples were prepared as 10% solutions in deuterated chloroform-d ($CDCl_3$) with 1% tetramethylsilane (TMS) as the reference material. TMS is assigned a chemical shift value of 0 ppm so all the chemical shifts are assigned relative to TMS. The NMR spectra were processed using MestReNova (version 11.0.0-17609) developed by Mestrelab Research S.L. Having excluded signals from $CDCl_3$ and TMS, the signal intensities were integrated, normalised to 100 % and presented according to the chemical shift ranges in Table 11 and Table 12. The parameters used during the NMR runs are presented in Table 13.

Table 13: Table 1. Instrument parameters for ^{13}C NMR.

Parameter	Value
Nucleus	^{13}C
Bruker pulse sequence	zgpg30
Spectrometer frequency (MHz)	100.61
Receiver gain	196.1
Pulse width (microseconds)	10.0000
Relaxation delay (seconds)	1.0000
Working temperature (Kelvin)	298
Number of scans	512
Spectra width (ppm)	238.9

3.8. Laser desorption ionisation mass spectrometry

Laser desorption ionisation mass spectrometry (LDI-MS) is a 'soft' ionisation analytical technique that uses laser energy to create gaseous ions from large molecules with minimal fragmentation. Mixtures of organic macromolecules or large synthetic polymers and biopolymers can be ionised, including non-volatile molecules. The most common ionisation format is for the analyte molecules to carry a single positive (1+) ionisation charge. Considered a soft mode of ionisation, the complete molecular ions remain intact when ionised, as opposed to other MS techniques such as secondary-ion mass spectrometry (SIMS) which generates more ion fragments and observes smaller molecules. This makes the direct mass spectrometry of complex mixed samples possible, such as the BFO materials. LDI-MS is a matrix-free desorption method which does not require a matrix to be mixed with the analyte and co-crystallise, making LDI-MS ideal for the analysis of low molecular weight compounds

(<1500 m/z). In this work an OrbitrapTM was used as the mass analyser, this is a high mass resolving power analyser (> 180,000 for a peak at *m/z* 200) compared to other mass analysers such as a time-of-flight analyser used in conjunction other LDI MS ionization sources. Orbitraps rely on observing the fluctuation of an electric field caused by oscillation of trapped ions around the central spindle. The frequency of the oscillation is dependent on the ions m/z value, allowing distinction of ions by their m/z value for accurate identification (Edney et al., 2020, Silina and Volmer, 2013).

3.8.1. Experimental

The LDI-MS experiments were run as a service by the Nanoscale and Microscale Research Centre (nmRC) at the University of Nottingham. The original BFO (untreated) and the pyrolysed BFO were prepared for laser desorption ionization mass spectrometry (LDI-MS) by dissolving the 10 mg of the solute in 5 ml of tetrahydrofuran (THF) to make a 2 mg/ml concentration solution. 0.5 µL of sample was spotted on an ABI Opti-TOF 192 target plate using a dried-droplet spotting technique. A Q Exactive HF mass spectrometer (QE HF, Thermo Fisher Scientific, Bremen, Germany) was coupled to a AP-MALDI source (MassTech Inc., Columbia, MD). Target-ng software (MassTech) was used to control the XY stage motion and operation of the laser. The source utilized a diode-pumped solid-state laser (λ = 355 nm) operating at a 0.1−10 kHz repetition rate. Maximum laser pulse energy was 3 µJ at 1 kHz repetition rate. A beam attenuator was used to adjust laser energy, in both cases the laser energy was 9.6 % and the laser was operated in a spiral raster mode (distance = 0.05 µm). The voltage applied between the MALDI plate and inlet capillary of mass spectrometer was 4 kV. The distance between the plate and the capillary was 3 mm. The inlet capillary was set to 400 °C. Each dried-droplet spot was scanned with a 50 µm wide laser spot. The signals from each spot were integrated over 15 s. Mass spectra were acquired in a positive-ion mode with mass resolution up to 180,000 at m/z 200 and a mass range of m/z 150−1500. An automatic gain control (AGC) target was set to 5×10^6 with 200 ms maximum injection time. Data was acquired and analyzed using Tune and Xcalibur software (Thermo Fisher Scientific, Waltham, MA).

3.9. Simulated Gas Chromatography Distillation

Distillation is the process of separating components in a mixture by using selective boiling points and condensation, in order to separate products and remove impurities. The most common type of distillation is the classical laboratory distillation set up, where a heat source heats up the liquid to a certain boiling point, the liquid then evaporates and the produced vapour is cooled and condensed to form a distillate. This method of conventional distillation has certain drawbacks, including lack of automation, precision and reproducibility from operator bias and errors in volume measurement and costly vacuum distillation equipment (Bachler et al., 2010). Large sample volumes (> 100 ml) and long measurement times can also be an issue. On the other hand, simulated distillation (SIMDIS) by gas chromatography is a fully automated process that is reproducible, reliable and offers high precision and fast analysis times. More importantly, small sample volumes are used in SIMDIS, so it is perfect for limited sample amounts such as in the case of the pyrolysed BFO.

3.9.1. Experimental

The simulated distillation analysis was carried out at the ORLEN UniCre Research Institute in the Czech Republic, to determine the boiling point distribution of the BFO untreated material, its liquefaction product at 350 °C, the pyrolysed BFO product obtained at 300 °C for 5 hrs and both control biodiesel samples (crude and distilled). The SIMDIS was performed on a high-temperature gas chromatograph using the standard ASTM D7169 method, which determines the boiling point distribution up to 720 °C (n-C_9 up to n-C_{100}) (ASTM D7169, 2020).

3.10. Rheological characterisation of bio-materials and bitumen blends

One of the primary analytical techniques used in analysing dynamic oscillatory data involves the construction of master curves using the interrelationship between temperature and frequency to produce a continuous rheological parameter curve at a reduced frequency scale. The principle used to relate the equivalency between time and temperature and thereby produce a smooth rheological master curve is known as the time-temperature superposition principle (TTSP) (Ferry, 1980) or the partial time-temperature superposition principle (PTTSP) if testing thermorheologically complex materials such as the neat paper waste residue (Olard and Di Benedetto (2003). Due to the expected thermorheologically simple behaviour of the base bitumens and the BFO biomodified blends, TTSP has been used in this study to construct master curves of the blends at a reference temperature of 25 °C.

In addition to the complex modulus and phase angle master curves for the base bitumen and biobinder blends, five reference penetration grade bitumens have also been included in the master curve plots. These reference master curves have been produced by means of the 2S2P1D mechanical model developed by researchers at the Ecole Nationale des Travaux Publics de l'Etat (ENTPE) and used successfully to represent the complex modulus and phase angle values for these standard penetration grade bitumens at a reference temperature of 25 °C (Yusoff et al., 2013, Airey et al., 2016). The 2S2P1D Model, an abbreviation of the combination of two springs, two parabolic creep elements and one dashpot, is a model based on the generalisation of the Huet-Sayegh Model and used to describe the rheological properties of binders and asphalt mixtures (Olard and Di Benedetto, 2003, Olard et al., 2003, Delaporte et al., 2007, Pellinen et al., 2007, Yusoff et al., 2011).

3.10.1. Experimental

Dynamic mechanical analysis (DMA) was performed on the base bitumens and the blended modified bitumens using a Malvern Instruments Kinexus Pro+ rotational rheometer. The Dynamic Shear Rheometer (DSR) tests were performed under controlled-strain loading conditions using frequency sweeps between 0.1 and 10 Hz between 10 and 70 °C (with 5 °C increments). The neat paper waste biobinders were tested on the 8mm parallel plate geometry due to the limited quantities available, while the neat BFO materials were tested using the 25mm parallel plate geometry. For the BFO-bitumen blend samples, the tests between 10 and 40 °C were undertaken using the 8mm parallel plate geometry and from 25 to 70°C with a 25mm diameter, both with a 1 mm gap. For each binder, only one of the two testing geometries at each of the overlapping temperatures of 25, 30, 35 and 40 °C was selected for detailed rheological analysis. The selection was based on eliminating errors in the DSR rheological data associated with testing artefacts such as machine compliance. The correct geometries (and related rheological parameters) were selected by ensuring that the rheological data determined over the entire temperature and frequency range produced smooth and continuous Black Space diagram curves (Airey, 2002b). A fixed strain of 0.5% was used for all runs. The control basil-infused salad oil was tested using the cup and bob geometry from 25 to 140 °C with 0.1 to 100 s^{-1} shear rates. The basil-infused oil was used because it is a simple, near single origin oil.

3.11. Predicted penetration and softening points

To characterise the conventional properties of the studied blends, penetration at 25°C and softening point values were predicted using rheological data according to (Gershkoff, 1991). Equation 10 was used for predicting penetration whilst predicted softening point values were calculated from G* isochrones at 0.16 Hz and 1.6 Hz to determine the temperature corresponding 1000 Pa and 10,000 Pa respectively.

$$\log(\mathrm{PEN@25°C}) = (-(\log(\mathrm{G} * (0.4\ \mathrm{Hz@25°C})) - 8.8)/1.95) \qquad \textit{Equation 10}$$

Figure 19 illustrates how predicted penetration values align with measured penetration values for a range of conventional (unmodified), polymer modified and aged bitumen sets (Airey and Brown, 1998, Airey, 2003, Airey, 2002a). The excellent fit between measured and predicted penetration for a wide range of binders means that this technique can be used with confidence in this study to determine both the penetration and softening points of the different biobinder blends before and after ageing from the DSR rheological data.

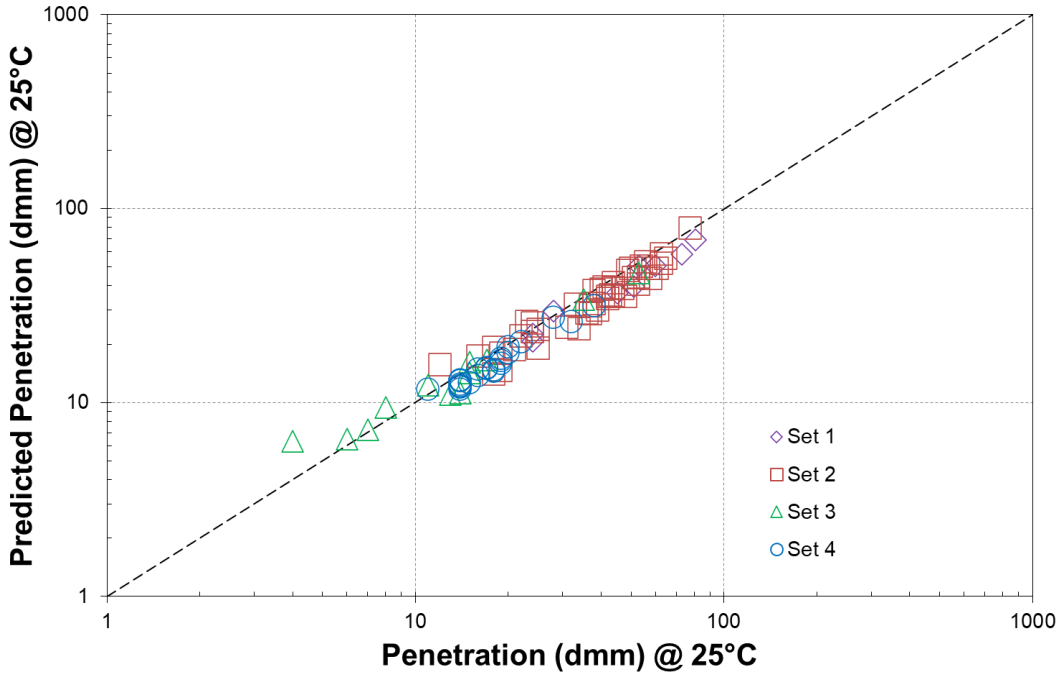

Figure 19: Gershkoff predicted penetration versus measured penetration for a range of unmodified, polymer modified and aged bitumen sets (Airey and Brown, 1998, Airey, 2002a, Airey, 2003).

3.12. Rotational viscosity of BFO materials and control oil sample

Rotational viscometers consist of a cylinder rotating coaxially inside a second static cylinder containing a material, usually a bitumen. The torque of the rotating spindle is used to measure the bitumen's relative resistance to flow at a given temperature. The viscosity of the material is then determined from the torque value. Rotational viscometers are commonly used to determine both viscosity and shear rate dependency of a material over a wide range of temperatures (Taylor and Airey, 2015).

Two methodologies were used to measure rotational viscosity at specific temperatures and with varying shear rate. The first method used was the simple Temperature Sensitivity Test where a rotational speed (shear rate) is kept constant and single point viscosity values are recorded at different temperatures (Brookfield Engineering Laboratories, 2014). Most materials will exhibit decreasing viscosity behaviour with increasing temperature.

A Brookfield viscometer was used to obtain the rotational viscosity from 25 to 100 °C for the BFO initial samples (treated and untreated), keeping a torque range within 10-98% (EN 13302 2010) (British Standards, 2010). The basil-infused vegetable oil was also tested at these temperatures as a control. The liquefied (HTL) samples could not be tested at the lower temperatures as they were semi-solid, so they were tested from 50 – 100 °C. As for the BFO-bitumen blends, the samples were tested following the same procedure from 100 to 200 °C. Two control bitumens, a 10/20 and a 20/30 pen, were also tested at these temperatures for comparison.

The second method used to understand how the viscosity of the starting materials (BFO treated and untreated) change as a function of shear rate from 25 to 100 °C is called the Controlled Rate Ramp method (Brookfield Engineering Laboratories, 2014). The basil oil was also tested as a control. The shear rate was varied using 2 minute intervals.

3.13. Bitumen ageing

Short and long-term laboratory ageing were performed on the base and blended bitumens using the Rolling Thin Film Oven Test (RTFOT, BS EN 12607-1:2014) and the pressure ageing vessel (PAV, BS EN 14769:2012), respectively. For the RTFOT, the standard ageing procedure of 163°C and 75 min was used and for the PAV, 100°C, 2.1 MPa and 20 hr was selected. The aged binders then underwent DMA to evaluate the rheological changes observed after

ageing. Ageing indices (rheological parameter after ageing divided by unaged rheological parameter) were obtained to compare the ageing rate of the bio-modified and non-modified binders.

3.14. Manufacturing of asphalt mixture samples

Asphalt mixtures in the form of gyros have been manufactured following a 14mm asphalt concrete mixture design using granite stone for aggregates. Aggregate gradation and design properties are shown in Table 14 and Figure 20. Only gyros with the treated BFO blends were manufactured.

Table 14: Asphalt mixture design.

Material	Quantity	Description
Binder (bitumen blended with BFO)	5.1 % by mass of mixture	Blend 1: 10/20 pen base bitumen Blends 2 and 3: 20/30 pen base bitumen
Aggregate	94.9% by mass of mixture	Bardon Hill granite gradation used in all mixtures. Maximum size 14mm

The procedure for all samples can be described as follows: the bitumen and biobinder were manually blended in the corresponding proportions prior to starting the asphalt manufacture work. The blended binder and aggregates were pre-heated at 150 °C for 30 min and 8h respectively. The mixtures were manufactured in a gyratory compactor in 1.516 kg batches using the laboratory mixer. 100mm diameter gyro moulds were used with a height of 80mm, giving a volume of 6.28 $x10^{-4}$ m^3. The scaled-up sum of the aggregates and binder totalled 1460 and 78 grams respectively, with a maximum density of 2596 kg/m^3 and 7% target air voids. After cooling overnight, the gyros were weighed, and their bulk density calculated (BS EN 12697). The average density for all gyros was 2.242 Mg/m^3. The samples were then cut in order to fit the NU-14 Cooper Research Technology universal testing machine.

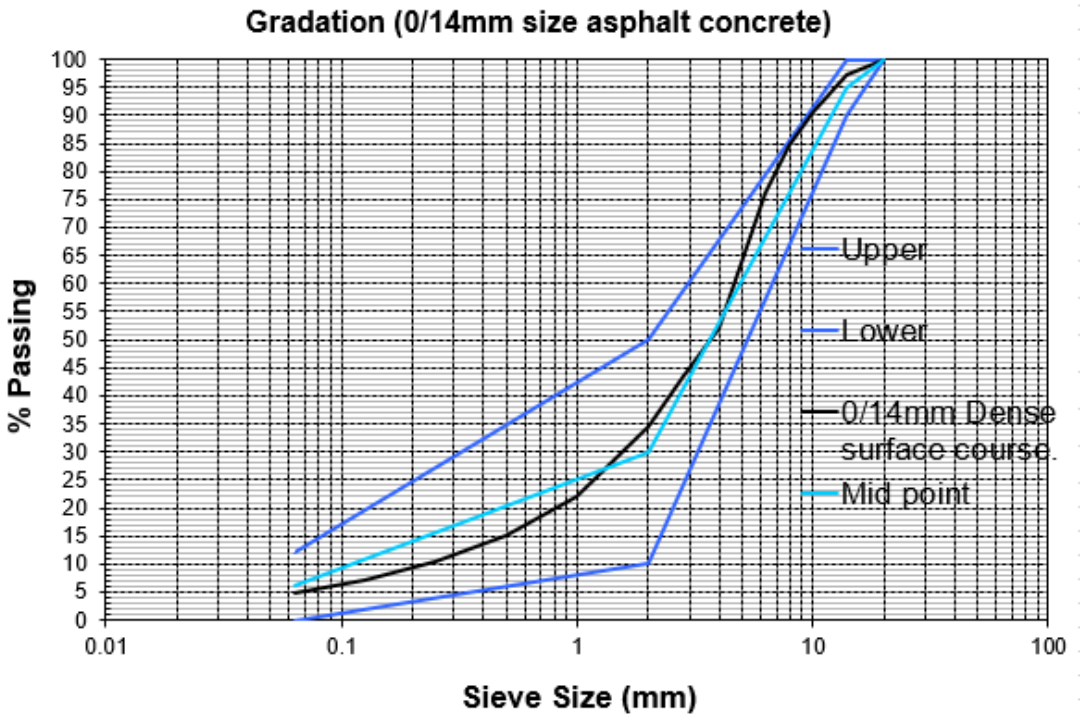

Figure 20: Selected aggregate gradation.

3.15. Performance-based rheological testing of pyrolysed BFO blend with bitumen

3.15.1. Determining the rheological performance properties of the biomodified blend using a DSR

A quick insight into the performance-related properties of binders can be obtained using the AASHTO T 315-10 standard. This test is intended for determining the linear viscoelastic properties of asphalt binders as required for specification testing. It is not considered a comprehensive procedure to characterise the viscoelastic properties of binders, but the results are used to calculate performance-related criteria in accordance with AASHTO M-320, such as the Superpave rheological parameters for rutting ($|G^*|/\sin\delta$) and fatigue ($|G^*|\sin\delta$). These parameters have been used for decades to study the permanent deformation and fatigue response of binders. The rutting parameter defines the high critical temperature for binders with thresholds of 1 kPa for unaged and 2.2 kPa for RTFOT-aged binders (Anderson et al., 1994). Similarly, fatigue behaviour at intermediate temperatures can be studied by the fatigue parameter. This parameter was limited to 5000 kPa and a reduction can represent a better resistance to fatigue (Motamedi et al., 2021). Although useful as a quick evaluation, these widely used parameters have been shown to show poor correlation between them and

the rutting and fatigue performance of asphalt mixtures, particularly for modified binders (Dongré and D'Angelo, 2003). Better tests have been developed in the early 2000s to relate the performance of binders with asphalt mixtures, such as the Multiple Stress Creep Recovery (MSCR) and Linear Amplitude Sweep (LAS) tests. These tests are still used today to characterise the performance of both unmodified and modified binders. In this instance, the rutting and fatigue parameters have been calculated for the biomodified 10% blend made with the pyrolysed untreated BFO (B10HTF+40/60) and compared with a control 40/60 bitumen.

Experimental

Unaged, RTFOT-aged and PAV-aged samples from the biomodified blend (B10HTF + 40/60) and a control 40/60 bitumen were tested on a Kinexus DSR in accordance with AASHTO T 315-10. A 25mm parallel plate geometry and 1mm gap was used for the unaged and RTFOT-aged samples while the PAV-aged samples were tested using the 8mm plate geometry and 2mm gap. During the temperature sweep a constant frequency of 10 rads/s is applied.

3.15.2. Multiple Stress Creep Recovery (MSCR)

Experimental

To study the biomodified blend's response to rutting, the Multiple Stress Creep Recovery (MSCR) test was carried out at 60 °C in a Kinexus DSR using a 25mm parallel plate geometry and 1mm gap, according to AASHTO T350-14. MSCR is an accelerated test where ten creep-recovery cycles are applied to a sample at two specific stress levels: 0.1 and 3.2 kPa. The two stress levels are meant to characterise rutting performance within and outside the LVE region of the binders. The creep (loading) portion of the test lasts for one second followed by a nine-second recovery. Two parameters are derived from the MSCR test: the non-recoverable creep compliance (J_{nr}) and the percent recovery (R%). J_{nr} provides the potential of the binder to suffer permanent deformations. It is the residual strain after a creep and recovery cycle divided by the applied stress. J_{nr} is obtained as Equation 11:

$$J_{nr} = \frac{\sum_{n=1}^{10} J_{nr,n}}{n} = \frac{\sum_{n=1}^{10} \frac{\gamma_{n,10}}{\tau}}{n} \qquad \textit{Equation 11}$$

where J_{nr} is the average non-recoverable creep compliance at the stress level, $J_{nr,n}$ is the non-recoverable compliance at cycle n, and $\gamma_{n,10}$ is the strain after 10 seconds at cycle n (the non-recovered strain). τ is the stress level.

The second parameter, the percent recovery (R%), is a measurement of the elastic response (ability to recover strain) of the binder at a given temperature and applied stress level (Equation 12).

$$R(\%) = \frac{\sum_{n=1}^{10} R_n(\%)}{n} = \frac{\sum_{n=1}^{10} \frac{\gamma_{n,1} - \gamma_{n,10}}{\gamma_{n,1}} \cdot 100}{n} \qquad \textit{Equation 12}$$

where R(%) is the average percentage recovered strain at the stress level, R_n (%) is the percentage of recovered strain at cycle n, $\gamma_{n,1}$ is the strain after 1 second (creep) at cycle n and $\gamma_{n,10}$ is the strain after 10 seconds (recovery) at cycle n.

Short-term aged (RTFOT) samples are tested during this test and compared to their unaged counterparts. MSCR testing provides good correlations with the rutting resistance of asphalt mixtures (Harman et al., 2011). The unaged and RTFOT-aged biomodified blend with pyrolysed untreated BFO added at 10% to a 40/60 binder (B10HTF+40/60) and the control 40/60 bitumen were studied at 0.1 and 3.2 kPa stress levels.

3.15.3. Linear Amplitude Sweep (LAS)

Experimental

The Linear Amplitude Sweep (LAS) test was conducted at 20 °C as per AASHTO TP 101-12 using a Kinexus DSR with the 8mm parallel plate geometry. The unaged and PAV-aged biomodified blend with pyrolysed untreated BFO added at 10% to a 40/60 binder (labelled B10HTF+40/60) and the control 40/60 bitumen were studied. This is an accelerated test lasting approximately 5 minutes and includes a frequency sweep followed by a strain sweep. During the frequency sweep, sinusoidal loadings at multiple frequencies (logarithmic ramp of 0.1 to 30 Hz) are applied to determine the undamaged properties in the LVE region (strain equal to 1%). The strain sweep induces damage by increasing the strain level from 0.1 to 30% in 3,100 loading cycles. The LAS data was analysed using the Viscoelastic Continuum Damage (VECD) theory, a theoretical approach to the analysis of fatigue cracking in asphalt materials including PMBs. It predicts the number of cycles to failure at different strain levels with a single test (Cuciniello

et al., 2020). The VECD theory results in the fatigue power-law damage model given in Equation 13.

$$N_f = A(\gamma_{max})^B \qquad \textit{Equation 13}$$

N_f is defined as the number of cycles to fatigue failure at a user-defined damage level (D_f). γ_{max} is the maximum tensile strain expected in the bitumen phase. A is the value of N_f at a strain level of 1% and depends on the integrity of the material versus the damage on the initial undamaged modulus and the selected failure criterion, B is the slope of the N_f - strain curve and is a function of the logarithmic slope (m) of the storage modulus (G') versus the angular frequency (ω). An increase in B corresponds to an increase in the time-temperature dependency of the material. The analysis was conducted using a fixed damage level of 35% of the undamaged loss modulus (labelled A_{35}), as per Cuciniello et al. (2020). Results are presented in terms of fatigue law parameters (A, B) and fatigue law curves (N_f versus strain). N_f is calculated at γ_{max} equal to 2.5% (typical for thick pavements) and 5% (typical for thin pavements).

4. Lignin-derived residues

The Kraft process is the conversion of wood into wood pulp (cellulose fibre) in order to make paper. The process is based on cooking wood chips under pressure at 130 °C in the presence of sulphide or disulphide (Van Vliet et al., 2016). The process breaks down the bonds that link lignin, cellulose and hemicellulose and produces 98% of the lignin currently available. As lignin is considered a residue of the paper making process, it is an attractive feedstock for biomass energy generation and as an alternative to bitumen. It is one of the most abundant natural polymers available that is hydrophobic and does not easily degrade. Its chemical structure is also similar to that of bitumen (Van Vliet et al., 2016, Hashmi and Jabary, 2020). The phenolic compounds commonly present in lignin (Figure 21) are what makes it resemble the unsaturated, aromatic structures present in bitumen. However, the phenol content in lignin, which is associated with anti-oxidation and adhesive properties, is highly dependent on the pH of the lignin extraction process (Poeran et al., 2017, Faustino et al., 2010). The following sections present the manufacture (via hydrothermal processing) and initial rheological characterisation of the lignin-containing paper waste biobinders in order to examine their behaviour in relation to conventional binders.

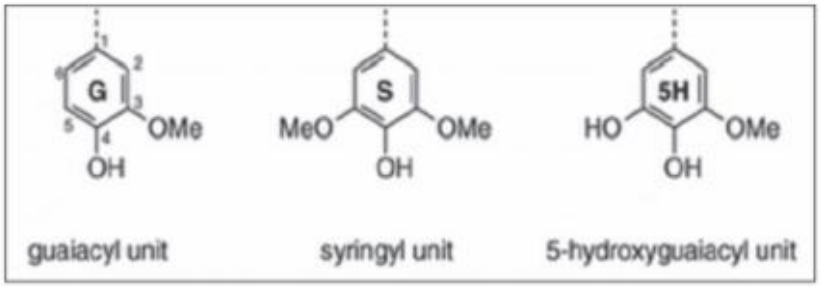

Figure 21: Building blocks of lignin (Poeran et al., 2017).

4.1. Hydrothermal liquefaction of paper waste

Two biobinders were manufactured from the paper waste feedstock via HTL, one at 320 °C and one at 360 °C, in order to study their rheological properties. The experiment details are shown in Table 15.

Table 15: HTL experiments for the paper waste biomass feedstock.

HTL run	Temperature (° C)	Length of run (hours)	Sample weight (+/- 0.5g)	Water weight (+/- 0.5 ml)	Bio-bitumen weight after run (g)	Bio-bitumen yield (%)
B	320	1	10	30	0.5	15.1
C	320	1	10	30	0.5	14.6
D	360	1	20	25	1.0	14.9
E	320	1	32	18	1.7	16.8

From the results in Table 15, it is clear that the bio-bitumen yields are close to one another. Runs B and C have a sample to water added ratio of 1:3 respectively, to ensure that the feedstock is in contact with water vapour during the experiments. It is clear that this ratio did not yield a high percentage of biobinder (other products generated being gas and unconverted paper waste residue). In run D, the sample added to the pressure vessel was doubled and the amount of water added reduced (a 1:2.5 by weight ratio respectively). Similarly this run did not show any increase in yield. A third option was tried in which the amount of sample was further increased (run E). In this run, the moisture content of the as received sample was accounted for and so approximately 20g of dry, moisture-free sample were added alongside its corresponding water content (keeping a 1:2.5 ratio). Bio-bitumen yield increased to 16.8%. This is not a drastic improvement as only 1.7 grams of bio-bitumen was produced. Such small quantities are only sufficient for first-look rheological sweeps but more material would be needed for further testing if this biobinder is to be considered a suitable option in the long term.

Reaction conditions need to be optimised in order to produce as much biobinder as possible. From the literature we know that increasing temperature does increase yield until a certain temperature is reached. As a result, run D was performed at 360 °C to evaluate if this temperature would increase yield. First observation made was that the 360 °C run gave off a stronger ‘bio’ smell compared to the 320 °C run. In this case, an increase in temperature did not significantly increase yield. Preliminary rheological results of the paper waste biobinders are presented below.

4.2. Rheological characterisation of paper waste biobinders

The paper waste biobinders (obtained via HTL at 320 and 360 °C after 1 hour) were subsequently tested on a DSR to characterise the materials in terms of their rheological properties, using the 8mm geometry due to the limited yield produced. Two standard pen bitumens (a 40/60 and a 10/20 pen) were used as controls in this case. Figure 22 and Figure 23 show the Black Diagrams of the binders which allows the different viscoelastic behaviour of the materials to be observed. The control binders exhibit thermorheologically simple behaviour over the range of frequencies and temperatures tested since their curves smoothly overlap for the different temperatures and frequencies. Overall, the two paper waste biobinders display thermorheologically complex behaviour in comparison to the control bitumens. They display more stable phase angles at the lower temperatures, with inconsistencies increasing at the higher temperatures. These inconsistencies have been omitted due to testing the material with the smaller 8mm geometry. The 320 °C biobinder displays stable phase angle values between 52 and 65 °, potentially showing less temperature sensitivity than the control binders. The biobinder obtained at the higher liquefaction temperature (360 °C) displays a more viscous response (higher phase angles) than the control bitumens and the other lignin biobinder (obtained at 320 °C).

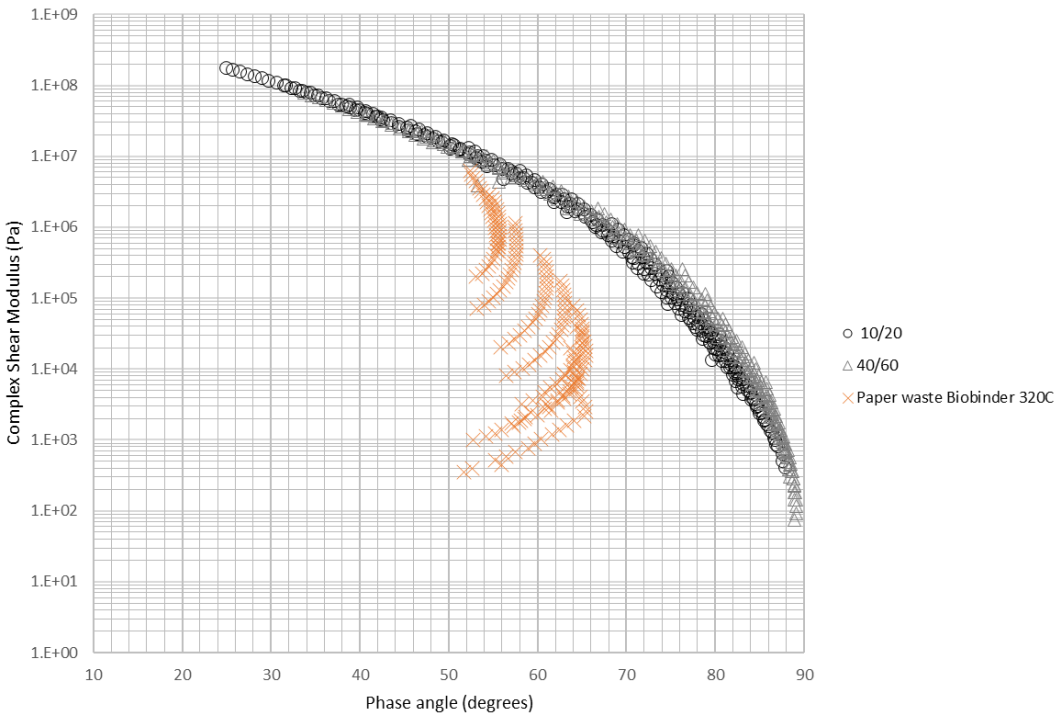

Figure 22: Black diagram of paper waste biobinder manufactured at 320 °C for 1 hour, with control bitumens 10/20 and 40/60 pen.

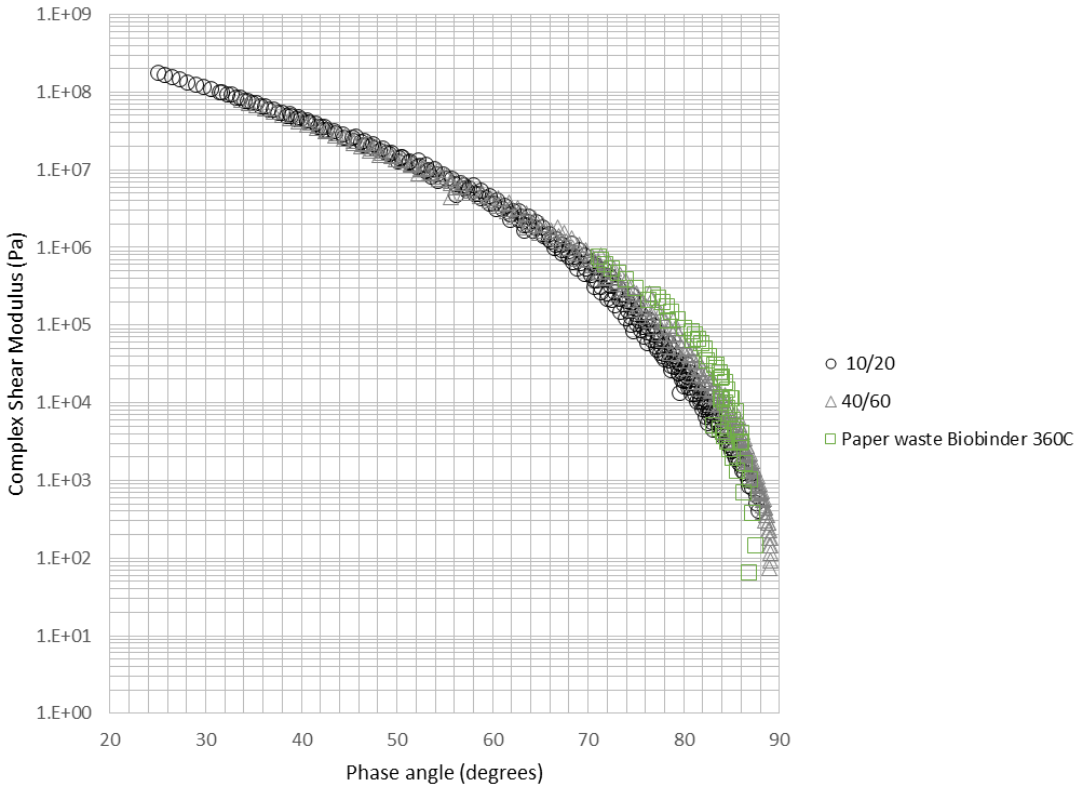

Figure 23: Black diagram of paper waste biobinder manufactured at 360 °C for 1 hour, with control bitumens 10/20 and 40/60 pen.

Complex modulus and phase angle master curves at a reference temperature of 25 °C have been subsequently produced using partial TTSP (Olard and Di Benedetto, 2003) as these biobinders display thermorheological complexity. Figure 24 allows the stiffness of the materials in terms of complex modulus to be compared showing the paper biobinders as softer materials with lower complex modulus at nearly all temperatures than the control bitumens. At the higher temperatures (lower frequencies), the 320 °C paper biobinder shows similar stiffness to that of a 40/60 conventional binder. At this point, they both have the potential of being less brittle than the controls at lower temperatures. The biobinder manufactured at the highest temperature (360 °C) is the softest. This difference in rheological behaviour can be attributed to the increase in reaction temperature and a subsequent change in chemical composition for the paper waste biobinder (from 320 °C to 360 °C). At 360 °C, the biocrude was broken down to lighter molecular weight compounds and subsequently yielded a softer consistency.

In terms of phase angle (Figure 25), the 320 °C biobinder shows a higher elastic component than the control bitumens depending on the temperature/frequency. An opposite response is seen with biobinder manufactured at 360 °C, which shows a more viscous response than the controls (higher phase angle values). As a result, it is important to note that the reaction temperature has a significant influence on the material's rheological behaviour. At low frequencies (high temperatures ranging from 55 and 45 °C for the 320 °C and 360 °C biobinder respectively), the patterns fall apart and the results have been omitted as they present a testing artefact. This is because the sample was only tested using the 8mm geometry due to the limited amounts produced.

When compared to the controls, the paper biobinder manufactured at 320 °C shows an irregular pattern for a wide range of frequencies compared to the control. At low temperatures, phase angle increases revealing a more viscous behaviour. This may be beneficial in preventing low temperature cracking. At high temperatures, phase angle decreases revealing a more elastic response, which could be enhance rutting resistance.

HTL reaction temperature plays a big role in determining the paper waste's rheological properties. The biggest limitation with the paper waste biobinders is the small quantities produced. The manufacture/production of the biobinder was a lengthy process that provided low yields, and so it was difficult to carry out a more detailed rheological characterisation of

these biobinders, including testing with a larger DSR geometry and blending with conventional bitumens. As the BFO materials are readily-available waste residues manufactured at industrial scale and accessible in high quantities, the focus of the thesis shifted to characterising the BFO in terms of its chemical properties, viscosity and rheological characteristics when blended with bitumen.

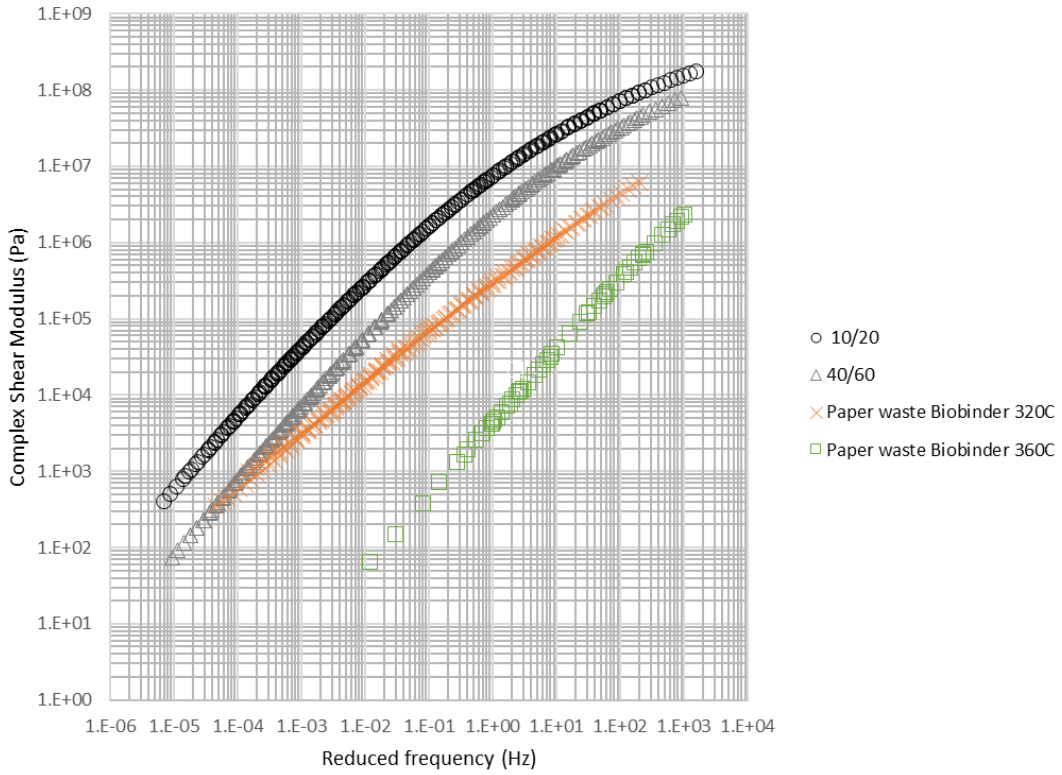

Figure 24: Complex modulus master curves at a reference temperature of 25°C for the paper waste biobinders obtained at 320 and 360 °C through hydrothermal liquefaction, along with the two control bitumens.

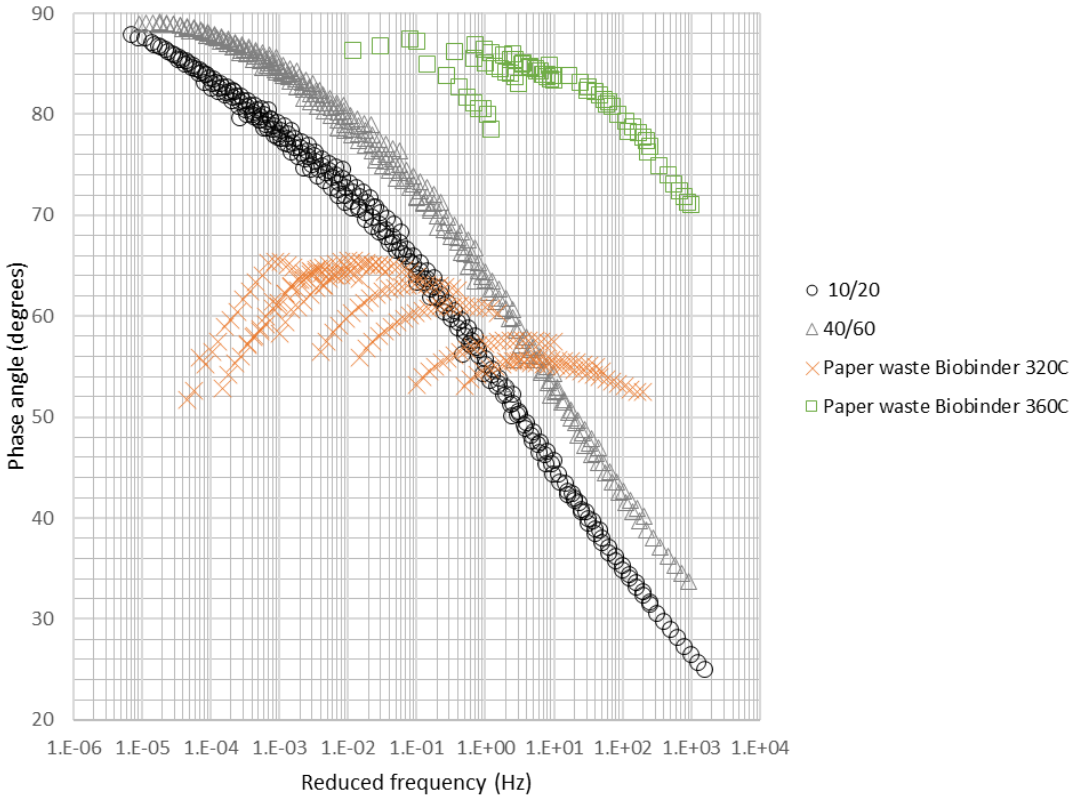

Figure 25: Phase angle master curves at a reference temperature of 25°C for the paper waste biobinders obtained at 320 and 360 °C through hydrothermal liquefaction, along with the two control bitumens.

4.3. Key Points

- The produced paper waste biobinders are softer materials with lower stiffness than the two control bitumens (10/20 and 40/60 pen).
- The biobinder manufactured at 360 °C presents a more viscous response than the controls whereas the lower temperature one has a viscous or elastic response dependent on temperature.
- The biggest limitation with the paper waste is the small quantities produced. The low yields and selectivities make it difficult to consider it a process specifically for bio-bitumen production at this stage and to carry out substantial chemical and rheological characterisation. As a result this was considered preliminary testing and the focus shifted to the mass-produced BFO materials. Based on the results, a potential role the paper waste biobinders could play (with more testing) is enhancing high-temperature (rutting) performance and adding functionality to the base binders. This has been noted with other studies with additions of lignin up to 25% (Van Vliet et al., 2016, Yu et al., 2021).

5. *Biofuel Oil (BFO)*

5.1. Optimisation of recovered HTL biocrudes from the BFO

The BFO hydrothermal liquefaction experimental results are presented in Table 16 and Table 17. As the paper waste yielded such small quantities of biocrude, residence time (length of the experiment) was increased to four hours while maintaining a 1:2.5 BFO:water ratio to ensure contact with water vapour. Reaction temperature was also incrementally increased from 300 to 360 °C to evaluate how the percentage of yield changes with increasing temperature and to drive off low molecular weight compounds in order to leave a heavier, more 'bitumen-like' biocrude product. It was found that at 350 °C, the consistency of the biocrude for both the treated and untreated BFO was the thickest out of all the temperatures tested. At 360 °C, the produced biocrudes were thinner black liquids. This indicates that 350 °C appears to be the optimum temperature to maximise viscosity by hydrothermal treatment. The decreasing recoveries with increasing temperature are due to a combination of evaporative loss and thermal cracking, the latter increasing with temperature. As a result, the biocrudes manufactured at 350 °C were used for further characterisation.

Table 16: Untreated BFO HTL experiments. SD: Standard deviation based on two runs for 340 °C, eight runs for 350 °C, and two runs for the 360 °C experiment. 15g results were normalised to 10g to allow for direct comparisons.

Material	Temperature (°C)	Length of run (hours)	Sample weight (+/- 0.5g)	Water weight (+/- 0.5 ml)	Biocrude weight after run (g) (SD)	Average biocrude yield (%) (SD)
BFO untreated	300	4	10	25	8.3	82.6
	320	4	10	25	9.0	90.0
	340	4	10	25	8.6 (0.1)	86.4 (1.5)
	350	4	10/15	25/37.5	8.4 (0.4)	84.2 (4.0)
	360	4	10	25	8.6 (0.1)	86.2 (1.1)

Table 17: Treated BFO HTL experiments. SD: Standard deviation based on nine runs for the 350 °C experiment. 15g results were normalised to 10g to allow for direct comparisons.

Material	Temperature (°C)	Length of run (hours)	Sample weight (+/- 0.5g)	Water weight (+/- 0.5ml)	Biocrude weight after run (g) (SD)	Average biocrude yield (%) (SD)
BFO treated	300	4	10	25	9.1	90.7
	320	4	10	25	9.0	90.1
	340	4	10	25	8.3	82.9
	350	4	10/15	25/37.5	8.5 (0.5)	84.7 (5.3)
	360	4	10	25	7.7	77.2

5.2. Optimisation of pyrolysis products obtained from the BFO using a high-temperature horizontal furnace

Table 18 and Table 19 display the pyrolysis experiments for the untreated and treated BFO respectively. It is evident that increasing temperature and reaction time (from 1 hr to 5 hrs) increases mass loss percentage. The highest mass loss was achieved during the 300 °C (5 hrs) experiment for both the treated and untreated BFOs. The 'pyrolysed BFO' product obtained from the untreated BFO is shown in Figure 26. The products that produced the three greatest mass losses were subsequently used for both chemical and rheological characterisation (sections 6 and 7). These were the pyrolysed products obtained from the untreated and treated BFO at 300 °C after 1 hr, 275 °C after 5 hrs and 300 °C after 5 hrs. In addition, the pyrolysed material obtained from the untreated BFO at 300 °C after 5 hrs (which produced the greatest mass loss) was used for further rheological characterisation, including blending with bitumen and performance-related rheological characterisation (sections 8.6 and 9). The untreated BFO was chosen as the feedstock of choice for the repeat runs, as it is the crudest version available of the BFO. In addition, according to the manufacturer, Argent Energy, the untreated version of the BFO is less fluid than the treated version, therefore in theory would be more suited as a biomodifier.

Table 18: Untreated BFO pyrolysis experiments. SD: Standard deviation based on 16 runs for the 300 °C, 5 hrs experiment. 15g results were normalised to 10g to allow for direct comparisons.

Material	Temperature (°C)	Length of run (hours)	Sample weight (+/- 0.5g)	Sample weight after run (g) (SD)	Mass loss (%) (SD)
BFO untreated	250	1	10	7.2	31.0
	250	5	10	6.1	41.4
	275	1	10	6.4	38.7
	275	5	10	4.6	55.7
	300	1	10	4.5	56.6
	300	5	10/15	2.9 (0.3)	71.6 (2.4)

Table 19: Treated BFO pyrolysis experiments.

Material	Temperature (°C)	Length of run (hours)	Sample weight (+/- 0.5g)	Sample weight after run (g)	Mass loss (%)
BFO treated	250	5	10	6.8	34.5
	275	5	10	5.4	47.7
	300	1	10	5.2	49.8
	300	5	10	3.7	64.5

Figure 26: Pyrolysis product obtained at 300 °C after 5 hours from the untreated BFO.

5.3. Key Points

- Various hydrothermal liquefaction experiments with increasing temperatures were carried out and the results indicate that 350 °C appears to be the optimal temperature to enhance BFO viscosity via HTL.
- A simpler method of pyrolysis was then tried in a horizontal furnace by varying temperature and residence time. The product obtained at 300 °C after 5 hours removed the most low molecular weight species and yielded a higher viscosity product. The untreated BFO was selected for further experiments as it was the raw (crude) material.

6. Chemical characterisation of BFO materials

6.1. Initial sample characterisation

6.1.1. Thermogravimetric analysis

Thermogravimetric analyses were carried out to accurately measure the mass of the materials as a function of temperature. The original starting materials for both BFO treated and untreated as well as Argent Energy's distilled and crude (undistilled) biodiesel samples were tested for reference. The liquefaction biocrude products obtained at 350 °C for both starting materials were also analysed. The proximate analyses in Table 20 indicate that all the materials tested present very similar results. The TGA profiles of the BFO liquefaction samples are also presented in Figure 27. Moisture level measured at 100 °C for HTL BFO treated and untreated is 1.7 and 1.5 wt% respectively. Volatile matter is the main component of all the samples, with the BFO untreated starting material containing the least amount of moisture (0.5 %) yet the most amount of volatile matter (99.4 %).

At approximately 150 ° C, the thermal degradation of volatiles started and was completed at 500 °C (Figure 27). After 500 °C, the thermal decomposition did not show a significant change as it is already nearly zero, which represents the materials have negligible fixed carbon and ash content, as also seen in Table 20. No residue was left during TGA due to a combination of high flow of gas and higher temperature (up to 950 °C) and heating rate of 20 °C/min. In comparison, the SIMDIS results yielded a residue due to the lower temperature (up to 720 °C) and lower heating rate (15 °C/min), therefore showing consistency between the results.

Table 20: Proximate analysis of the BFO starting materials, their liquefaction products, and the control biodiesel products. M: Moisture, VM: Volatile matter, FC: Fixed carbon.

Sample	Proximate analyses (wt%)			
	M	VM	FC	Ash
Distilled biodiesel	12.6	87.9	<0.1	<0.1
Crude biodiesel	6.1	93.9	<0.1	<0.1
HTL BFO treated	1.7	97.9	0.4	<0.1
HTL BFO untreated	1.5	97.9	0.5	<0.1
BFO treated	1.3	97.9	0.6	0.1
BFO untreated	0.5	99.4	0.1	0.1

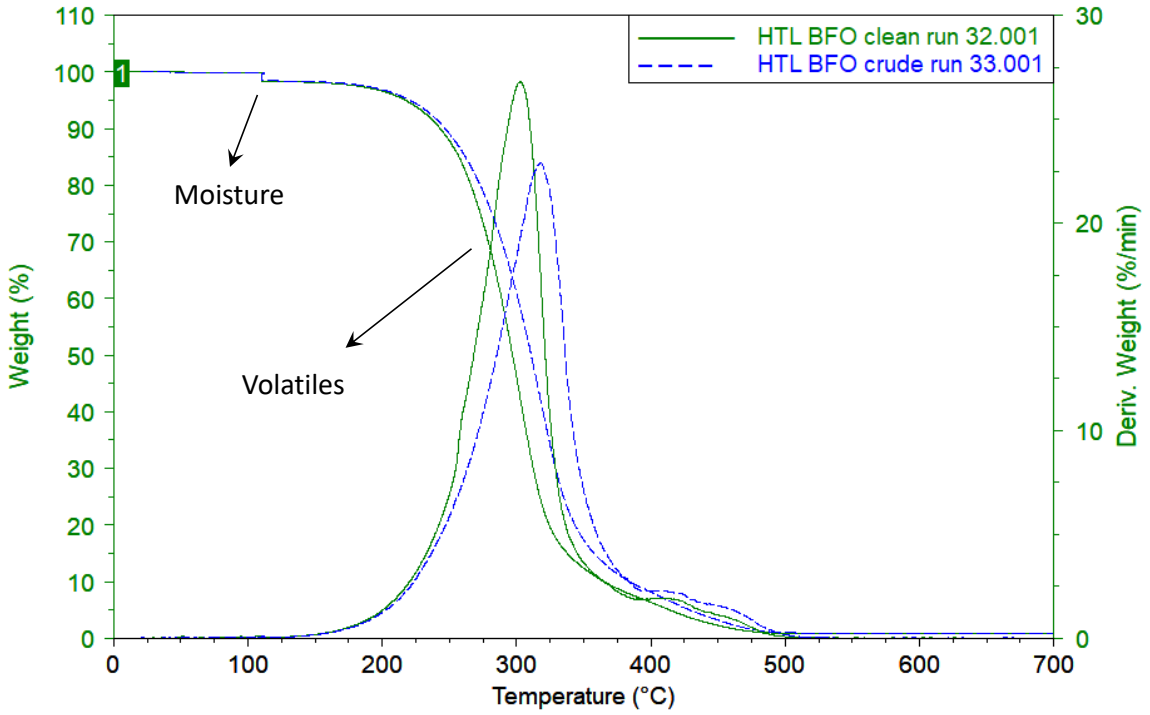

Figure 27: Thermal degradation of the liquefaction (HTL) biocrude products for both BFO treated (clean) and BFO untreated (crude), showing moisture and volatile matter content.

6.1.2. Elemental Analysis

The following samples were analysed:

- BFO untreated (starting material)
- BFO treated (starting material)
- Crude biodiesel
- Distilled biodiesel
- Liquefaction biocrude product obtained from the untreated BFO at 350 °C
- Liquefaction biocrude product obtained from the treated BFO at 350 °C
- Pyrolysed product obtained from the untreated BFO at 300 °C after 5 hrs

There was no evidence to suggest that organic sulphur was present in the samples, and the low ash found meant that sulphate and other inorganic sulphur-containing compounds can be discounted. The averaged ultimate analyses presented in Table 21 and Figure 28 indicate that all the materials tested contain similar hydrogen compositions and minimal nitrogen, and more variations in the carbon and oxygen abundances. The pyrolysed BFO (from the untreated BFO starting material), contains the highest carbon and lowest oxygen content. In

comparison, the crude (unrefined) biodiesel contains the highest oxygen content and the least carbon. This overall trend for decreasing oxygen and increasing carbon content seen in the pyrolysed BFO is favourable for bitumen and bio-bitumen production, as a higher oxygen content can result in faster oxidative hardening (ageing) and lead to embrittlement and cracking (Kliewer et al., 1996).

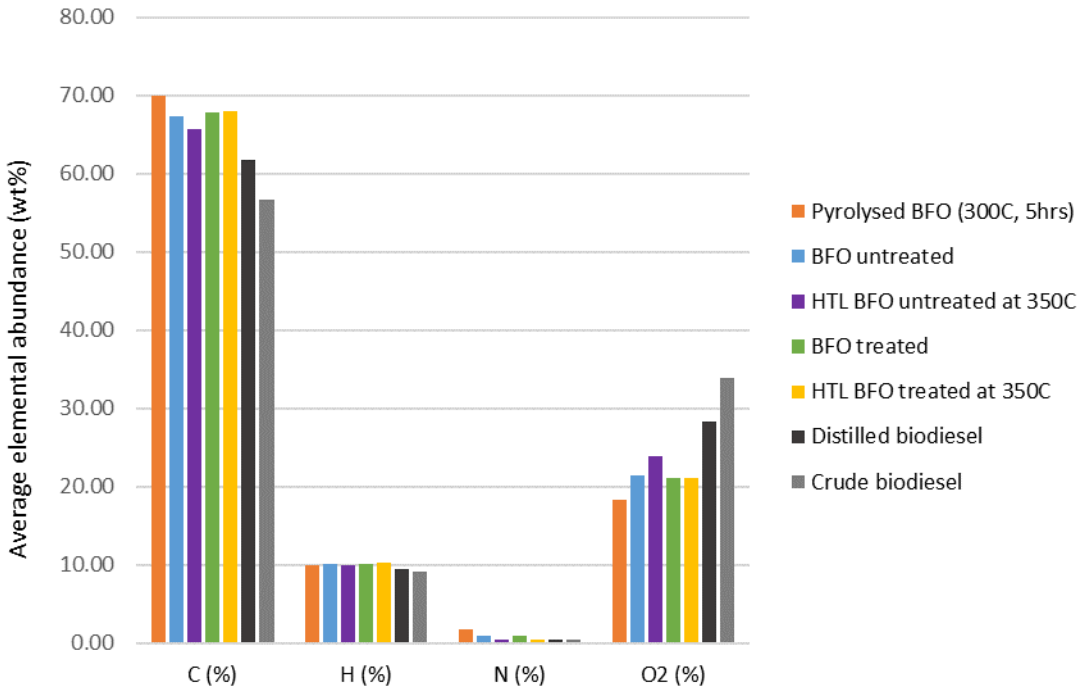

Figure 28: Column plot of elemental analysis of the BFO starting materials, their liquefaction (HTL) products, the pyrolysed BFO and the two biodiesels.

Table 21: Ultimate analysis (wt%) of the BFO starting materials, their liquefaction (HTL) products, the pyrolysed BFO and the two biodiesels. SD: Standard deviation based on three runs, [a] As received basis, [b] Determined by difference.

Ultimate analysis[a] (wt%)	C	H	N	O[b]
Pyrolysed BFO (300 °C, 5hrs) (SD)	70.0 (2.2)	9.9 (0.3)	1.7 (0.1)	18.3 (2.6)
BFO untreated (SD)	67.4 (1.7)	10.2 (0.4)	1.0 (0.0)	21.5 (2.0)
HTL BFO untreated at 350 °C (SD)	65.6 (0.5)	9.9 (0.1)	0.5 (0.0)	23.9 (0.6)
BFO treated (SD)	67.8 (2.3)	10.1 (0.4)	0.9 (0.1)	21.2 (2.8)
HTL BFO treated at 350 °C (SD)	68.1 (0.0)	10.4 (0.0)	0.5 (0.0)	21.1 (0.0)
Distilled biodiesel (SD)	61.8 (1.6)	9.5 (0.2)	0.4 (0.1)	28.4 (1.6)
Crude biodiesel (SD)	56.6 (1.5)	9.1 (0.5)	0.4 (0.1)	33.9 (2.0)

6.2. Gas and liquid product characterisation

6.2.1. Gas characterisation

The paper waste gas fractions were not analysed as it was the preliminary part of the project before the BFOs became the predominant feedstocks for this study. Gases generated during the BFO hydrothermal liquefaction experiments were collected and the results are presented in respectively.

Table 22 and Table 23. Overall, gas yield increases with temperature for both BFO materials. There was a similar increase in hydrocarbon gases (total C_1-C_5) for both BFO treated and untreated. As for the non-hydrocarbon gases (H_2 and CO_2), the treated BFO presented an overall higher increase in H_2 and CO_2 than the untreated BFO, except at 320 °C where the untreated BFO shows higher H_2 and CO_2 gas concentrations. The highest amount of gas was generated at the highest reaction temperature (360 °C). Regarding the total hydrocarbon and non-hydrocarbon gases at 360 °C, approximately 0.9% and 1.1% of the initial untreated and treated BFO were converted to gas, respectively.

Table 22: Gas analysis results from the untreated BFO HTL experiments. SD: Standard deviation based on two runs for 340 °C and 360 °C each and six runs for the 350 °C experiment. HC: Hydrocarbons, NHC: Non-hydrocarbons. 15g results were normalised to 10g to allow for direct comparisons.

Material	HTL conditions	Total C_1-C_5 (g) (SD)	H_2 (g) (SD)	CO_2 (g) (SD)	Total NHC gas (g) (SD)	Sum of hydrocarbons (HC + NHC) (g) (SD)
BFO untreated	300 °C, 4hrs	0.002	0.005	3.111	0.031	0.033
	320 °C, 4 hrs	0.005	0.011	4.252	0.043	0.048
	340 °C, 4hrs	0.010 (0.001)	0.020 (0.005)	5.077 (0.396)	0.051 (0.004)	0.061 (0.005)
	350 °C, 4hrs	0.016 (0.004)	0.029 (0.006)	5.896 (1.279)	0.071 (0.017)	0.087 (0.021)
	360 °C, 4hrs	0.022 (0.000)	0.029 (0.003)	7.618 (0.103)	0.077 (0.001)	0.099 (0.001)

Table 23: Gas analysis results from the treated BFO HTL experiments. SD: Standard deviation based on seven runs for the 350 °C experiment. HC: Hydrocarbons, NHC: Non-hydrocarbons.

Material	HTL conditions	Total C_1-C_5 gas (g) (SD)	H_2 (g) (SD)	CO_2 (g) (SD)	Total NHC gas (g) (SD)	Sum of hydrocarbons (HC + NHC) (g) (SD)
BFO treated	320 °C, 4 hrs	0.005	0.008	3.926	0.039	0.044
	340 °C, 4hrs	0.010	0.023	5.517	0.055	0.065
	350 °C, 4hrs	0.015 (0.001)	0.034 (0.004)	6.670 (0.396)	0.067 (0.004)	0.082 (0.005)
	360 °C, 4hrs	0.024	0.045	8.713	0.087	0.111

6.3. Liquid product characterisation using GC-MS

GC-MS results of the following samples are discussed below:

- BFO untreated (starting material)
- BFO treated (starting material)
- Crude biodiesel
- Distilled biodiesel
- Liquefaction biocrude products obtained from the untreated BFO at 300, 320, 340, 350 and 360 °C
- Liquefaction biocrude products obtained from the treated BFO at 300, 320, 340, 350 and 360 °C
- Pyrolysed products obtained from the untreated BFO at 300 °C after 1 hr, 275 °C after 5 hrs and 300 °C after 5 hrs.

6.3.1. BFO starting materials and control biodiesel samples

Figure 29 presents the total ion chromatogram (TIC) traces for the untreated and treated BFOs. The GC-MS traces show that the BFO (both treated and untreated) mainly contains a mixture of saturated fatty acid methyl esters (sME) and unsaturated fatty acid methyl ester (uME), which are predominantly C_{16} and C_{18} carbon chain length. Larger (C_{20}-C_{26}) saturated and unsaturated fatty acid methyl esters are also present. The GC-MS traces show that there

is no significant difference in chemical composition between the untreated and treated BFO. Fatty acid methyl esters are key components of vegetable oil, consistent with the BFO residue obtained after biodiesel production from vegetable waste. A similar chromatographic distribution was obtained for the distilled and crude biodiesel materials (Figure 30), but there is an enrichment of lower molecular weight (C_8-C_{12}) saturated fatty acid methyl esters (sME) in the crude biodiesel in relation to the distilled biodiesel and both BFO products.

14sME – methyl tetradecanoate, $C_{15}H_{30}O_2$
16uME – 9-hexadecenoic acid methyl ester, $C_{17}H_{32}O_2$
16sME – hexadecanoic acid methyl ester, $C_{17}H_{34}O_2$
18uME – 9-octadecenoic acid methyl ester, $C_{19}H_{36}O_2$
18sME – methyl stearate, $C_{19}H_{38}O_2$
20uME – cis-13-eicosenoic acid methyl ester, $C_{21}H_{40}O_2$
20sME – eicosenoic acid methyl ester, $C_{21}H_{42}O_2$
22uME – 13-docosenoic acid methyl ester, $C_{23}H_{44}O_2$
22sME – docosenoic acid methyl ester, $C_{23}H_{46}O_2$
24uME – 15-tetracosanoic acid methyl ester, $C_{25}H_{48}O$
24sME – tetracosanoic acid methyl ester, $C_{25}H_{50}O_2$
26sME – hexacosanoic acid methyl ester, $C_{27}H_{54}O_2$

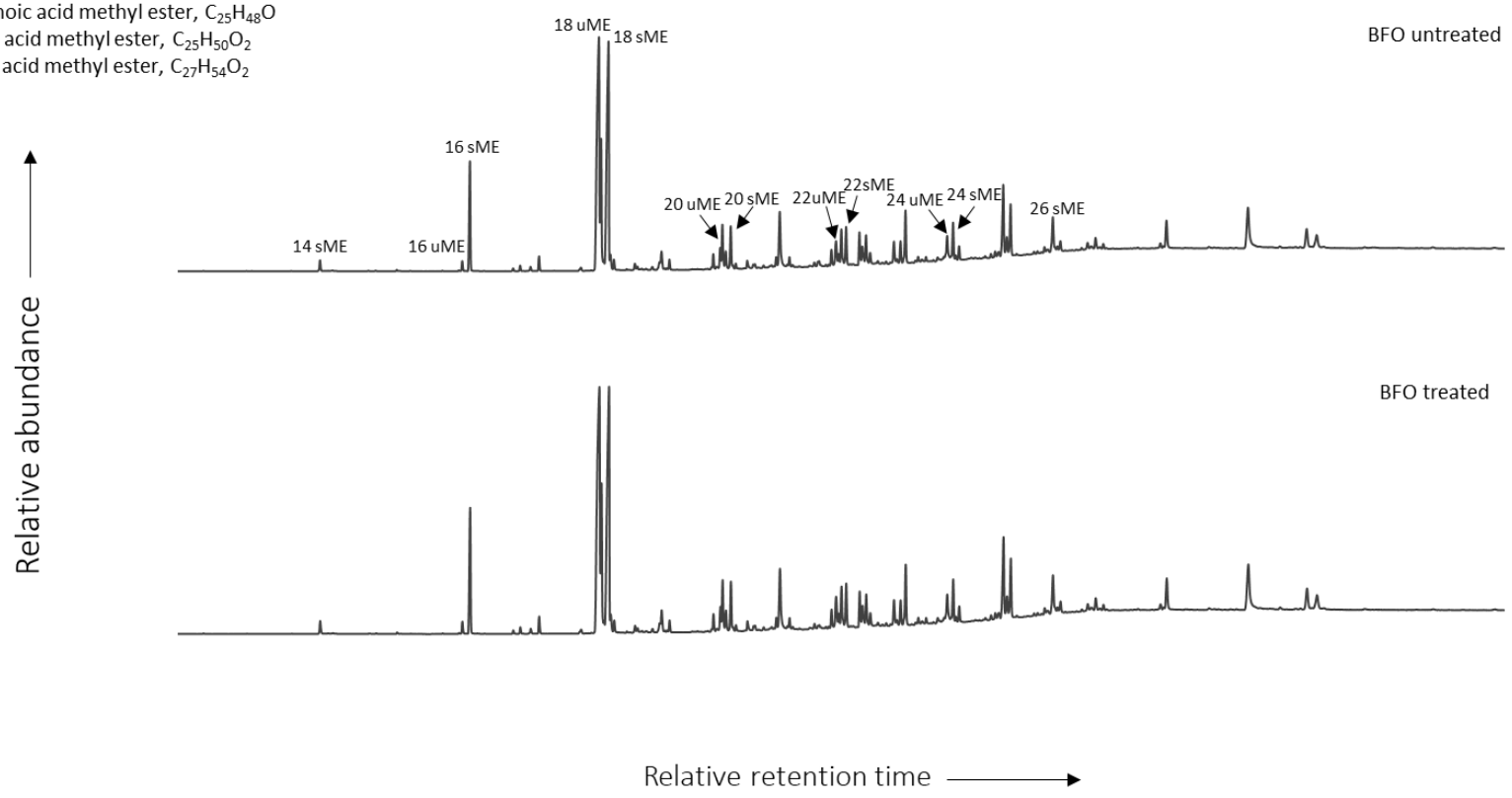

Figure 29: TIC of the untreated and treated BFOs.

8sME – octanoic acid methyl ester, $C_9H_{18}O_2$
10sME – decanoic acid methyl ester, $C_{11}H_{22}O_2$
12sME – dodecanoic acid methyl ester, $C_{13}H_{26}O_2$
14sME – methyl tetradecanoate, $C_{15}H_{30}O_2$
16uME – 9-hexadecenoic acid methyl ester, $C_{17}H_{32}O_2$
16sME – hexadecanoic acid methyl ester, $C_{17}H_{34}O_2$
18uME – 9-octadecenoic acid methyl ester, $C_{19}H_{36}O_2$
18sME – methyl stearate, $C_{19}H_{38}O_2$
20uME – cis-13-eicosenoic acid methyl ester, $C_{21}H_{40}O_2$
20sME – eicosenoic acid methyl ester, $C_{21}H_{42}O_2$
22uME – 13-docosenoic acid methyl ester, $C_{23}H_{44}O_2$
22sME – docosenoic acid methyl ester, $C_{23}H_{46}O_2$
24uME – 15-tetracosanoic acid methyl ester, $C_{25}H_{48}O_2$
24sME – tetracosanoic acid methyl ester, $C_{25}H_{50}O_2$

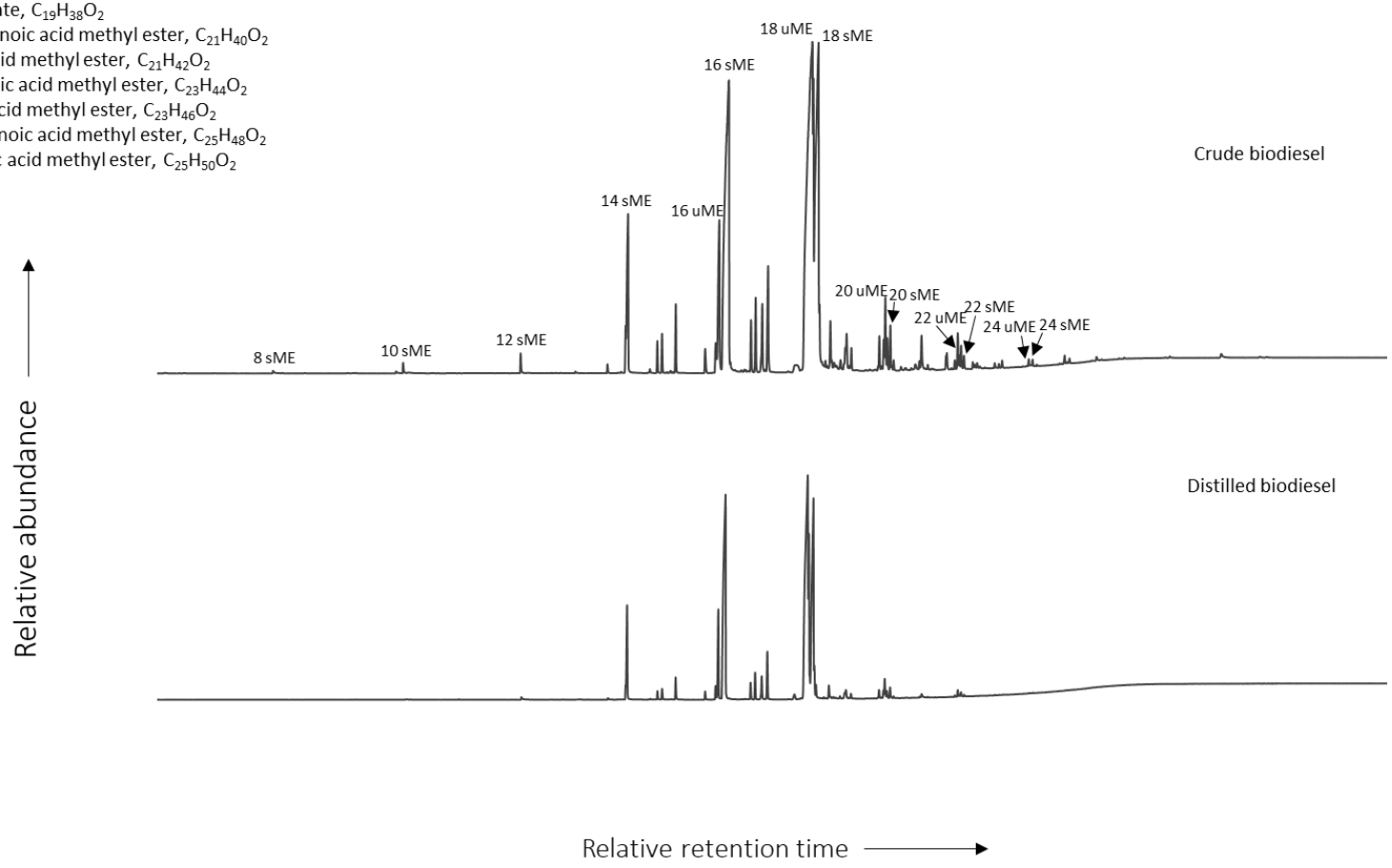

Figure 30: TIC of distilled and crude biodiesels.

6.3.2. Liquefaction products

The GC-MS traces of the untreated BFO starting material and the products obtained after hydrothermal liquefaction (HTL) at 300 °C, 350 °C and 360 °C are presented in Figure 31. Overall there is a greater distribution of higher molecular weight fatty acid methyl esters (FAME) (C_{14}-C_{26}) in the initial BFOs compared to the liquefaction products, where only C_{14}-C_{18} FAME were identified. This is indicative that the higher molecular weight FAME compounds were broken down to lower molecular weight products during the HTL treatment. This correlates with an increase in gas yield as HTL reaction temperature increased in section 6.2.1. The absence of the lower molecular products in the HTL samples (Figure 31) was due to evaporative loss during product recovery and drying. Overall, the liquefaction products obtained at the various temperatures for both the BFO untreated and treated show similar GC-MS distribution, hence the GC-MS traces of the treated HTL samples were not presented.

14sME – methyl tetradecanoate, $C_{15}H_{30}O_2$
16uME – 9-hexadecenoic acid methyl ester, $C_{17}H_{32}O_2$
16sME – hexadecanoic acid methyl ester, $C_{17}H_{34}O_2$
18uME – 9-octadecenoic acid methyl ester, $C_{19}H_{36}O_2$
18sME – methyl stearate, $C_{19}H_{38}O_2$
20uME – cis-13-eicosenoic acid methyl ester, $C_{21}H_{40}O_2$
20sME – eicosenoic acid methyl ester, $C_{21}H_{42}O_2$
22uME – 13-docosenoic acid methyl ester, $C_{23}H_{44}O_2$
22sME – docosenoic acid methyl ester, $C_{23}H_{46}O_2$
24uME – 15-tetracosanoic acid methyl ester, $C_{25}H_{48}O$
24sME – tetracosanoic acid methyl ester, $C_{25}H_{50}O_2$
26sME – hexacosanoic acid methyl ester, $C_{27}H_{54}O_2$

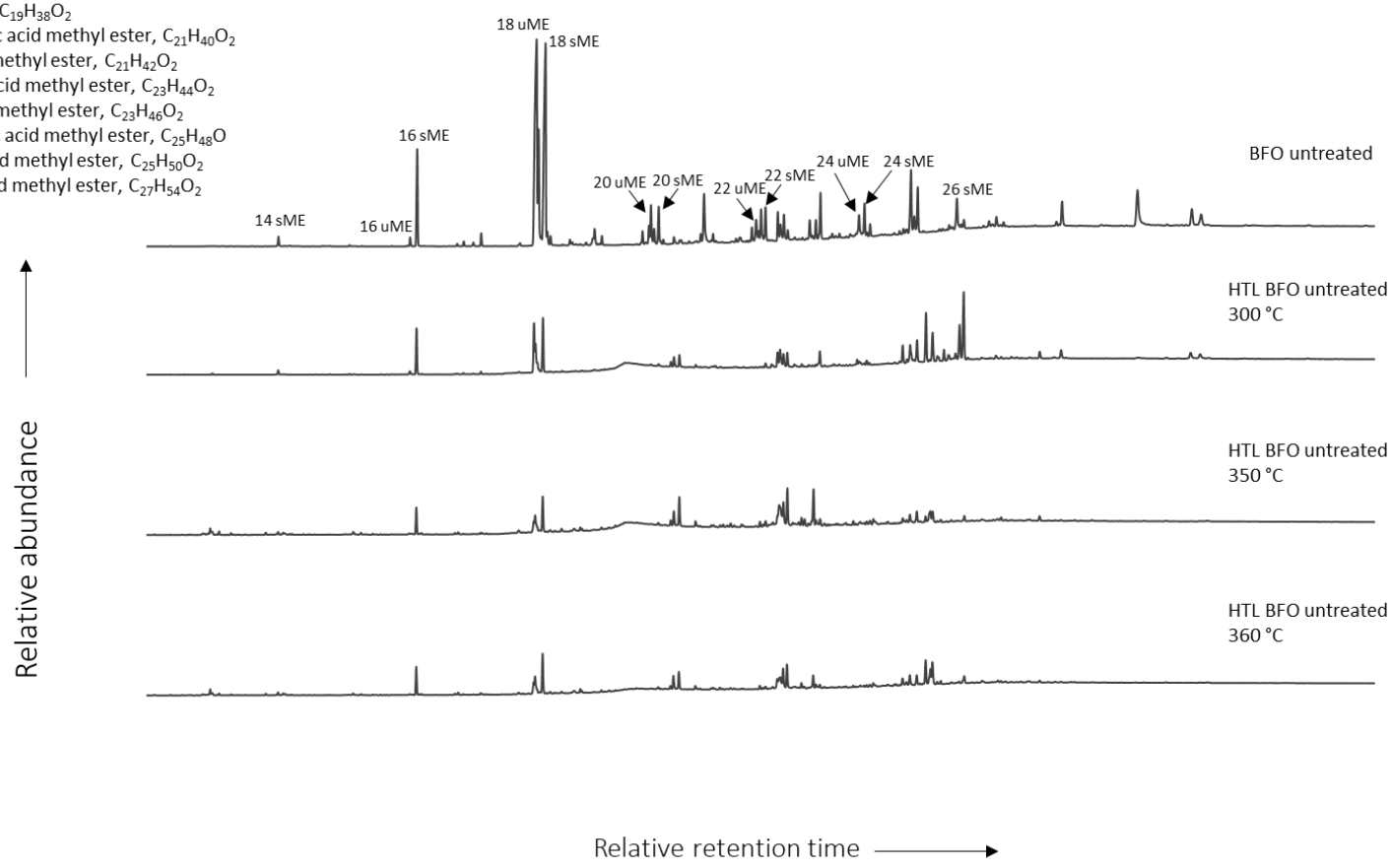

Figure 31: TIC of the untreated BFO and those obtained after HTL at 300 °C, 350 °C and 360 °C.

6.3.3. Pyrolysed BFO products

Figure 32 presents the TIC of the untreated BFO and those products obtained after pyrolysis at 300 °C (1 hr), 275 °C (5 hrs) and 300 ° (5 hrs). Unlike the liquefied BFO materials, no lower molecular weight compounds and FAME were present for the pyrolysed BFO materials (both treated and untreated). Hexasiloxanes ($C_{12}H_{38}O_5Si_6$), organic compounds containing repeating units of silicon and oxygen atoms, cholesta,-3-5-diene and cholesteryl formate ($C_{28}H_{46}O_2$), derivatives of cholesterol were only predominantly present in the chromatograms of all the pyrolysed samples. The same trend was observed for the pyrolysed products obtained from the treated BFO at the same experimental conditions. The absence of lower molecular weight compounds and FAME molecules (C_{14}-C_{26}) in the GC-MS traces obtained after pyrolysis indicates that these compounds have been removed from the initial BFOs via distillation/evaporation and suggests the BFOs can be upgraded to heavier products via pyrolysis in a tubular furnace. This is encouraging for the purpose of bitumen modification.

14sME – methyl tetradecanoate, $C_{15}H_{30}O_2$
16uME – 9-hexadecenoic acid methyl ester, $C_{17}H_{32}O_2$
16sME – hexadecanoic acid methyl ester, $C_{17}H_{34}O_2$
18uME – 9-octadecenoic acid methyl ester, $C_{19}H_{36}O_2$
18sME – methyl stearate, $C_{19}H_{38}O_2$
20uME – cis-13-eicosenoic acid methyl ester, $C_{21}H_{40}O_2$
20sME – eicosenoic acid methyl ester, $C_{21}H_{42}O_2$
22uME – 13-docosenoic acid methyl ester, $C_{23}H_{44}O_2$
22sME – docosenoic acid methyl ester, $C_{23}H_{46}O_2$
24uME – 15-tetracosanoic acid methyl ester, $C_{25}H_{48}O$
24sME – tetracosanoic acid methyl ester, $C_{25}H_{50}O_2$
26sME – hexacosanoic acid methyl ester, $C_{27}H_{54}O_2$

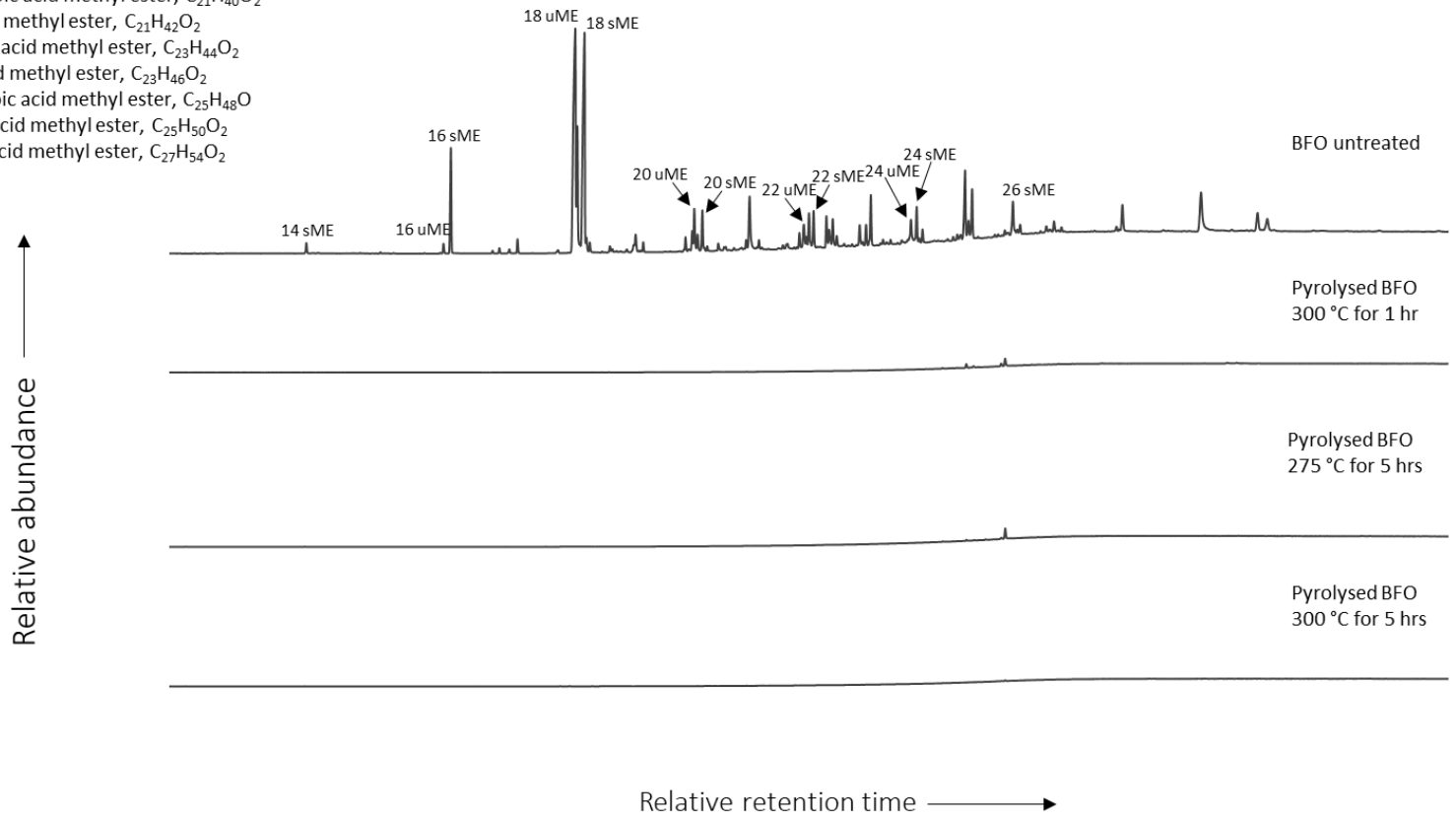

Figure 32: TIC of the untreated BFO and those obtained after pyrolysis at 300 °C (1 hr), 275 °C (5 hrs) and 300 ° (5 hrs).

6.3.4. Unsaturated to saturated FAME ratios

The ratios of unsaturated to saturated fatty acid methyl esters for all the studied samples are presented in Table 24. Both the treated and untreated BFO have similar ratios of unsaturated to saturated C_{16}, C_{18}, C_{20}, C_{22} and C_{24} methyl esters compared to untreated BFO. However, both biodiesel products have higher unsaturated to saturated C_{16}-C_{20} ratios, with the distilled biodiesel containing the highest percentage of C_{20} unsaturated methyl ester. The C_{22} and C_{24} FAME was not detected for the distilled biodiesel, but the crude biodiesel contains C_{22} and C_{24} methyl esters, with a C_{22} unsaturated to saturated ratio of 1.66, approximately double the C_{22} ratio present in both the untreated and treated BFO materials (~ 0.8). One explanation for the biodiesel samples containing higher uMe/sME ratios to the BFOs is that the C_{16}-C_{22} methyl esters were removed via the distillation process. The unsaturated methyl esters were likely preferentially removed to the saturated methyl esters in the BFOs. This would explain why the uMe/sME ratios are lower for the BFO materials compared to the biodiesel samples. In other words, more saturated methyl esters remain in the BFOs than unsaturated methyl esters.

Regarding the liquefied samples from both BFOs, an increase in the C_{16} ratio was observed for the treated BFO as reaction temperature increases up to 340 °C, followed by a decline in the ratio at the higher reaction temperatures (350 °C and 360 °C). The C_{16} ratio stayed about the same for the treated BFO initial to 320 °C, before reducing to 0.07 and 0.06 at 340 °C and 360 °C respectively. There was no C_{16} ratio calculated for the untreated BFO liquefied product obtained at 350 °C because the C_{16} unsaturated carbon peak was not detected. As for the C_{18} FAME ratios, there is a general decrease in the ratios as HTL reaction temperature increases for the products obtained from the untreated BFO. The decrease in the ratio of C_{16} and C_{18} unsaturated to saturated methyl ester suggests that the unsaturated methyl esters are being hydrogenated to saturated methyl esters with increase in HTL temperatures through water donating hydrogen to the BFO. The HTL samples obtained from the treated BFO show a different trend for the C_{18} FAME ratio, where it decreases from the starting material to the 300 °C product, then increases incrementally at 320 °C and 340 °C, followed by a sharp decrease at 350 °C and 360 °C. It is important to note that both the treated and untreated starting materials contain similar C_{18} ratios of 1.21 and 1.18 respectively, before the HTL treatment, and it is not clear why a different trend was observed for the treated BFO

for the C_{18} ratio. Overall, the C_{18} ratios for the HTL treated BFO are higher compared to the untreated BFO, except for the run undertaken at 300 °C. There are no ratios calculated for the pyrolysed BFO, due to the absence of FAME molecules in the chromatogram.

Table 24: Identified FAME compounds and calculated unsaturated to saturated carbon ratios from the GC-MS traces of the two control biodiesels, the BFO starting materials (treated and untreated), the liquefied products and the pyrolysed BFO. Nd: Not detected.

Sample	C_{16} uME/sME	C_{18} uME/sME	C_{20} uME/sME	C_{22} uME/sME	C_{24} uME/sME
Distilled biodiesel	0.18	1.73	2.39	nd	nd
Crude biodiesel	0.19	1.79	1.95	1.66	nd
BFO untreated	0.08	1.18	1.08	0.82	0.88
HTL 300 °C BFO untreated	0.09	0.95	nd	nd	nd
HTL 320 °C BFO untreated	0.09	0.93	nd	nd	nd
HTL 340 °C BFO untreated	0.07	0.88	nd	nd	nd
HTL 350 °C BFO untreated	nd	0.79	nd	nd	nd
HTL 360 °C BFO untreated	0.06	0.68	nd	nd	nd
Pyrolysed BFO	nd	nd	nd	nd	nd
BFO treated	0.09	1.21	1.10	0.83	0.90
HTL 300 °C BFO treated	0.10	0.89	nd	nd	nd
HTL 320 °C BFO treated	0.11	1.01	nd	nd	nd
HTL 340 °C BFO treated	0.12	1.46	nd	nd	nd

HTL 350 °C BFO treated	0.07	0.89	nd	nd	nd
HTL 360 °C BFO treated	0.08	0.85	nd	nd	nd

6.4. ^{13}C Nuclear magnetic resonance

To investigate changes in chemical classification due to pyrolysis (using the high-temperature horizontal furnace) and liquefaction (HTL), ^{13}C NMR spectra of the original BFO materials were obtained to compare with their products. Both the untreated and treated BFO materials were analysed, as well as Argent Energy's distilled biodiesel end-products (both the undistilled/crude and distilled versions), which were used as control samples. The signal intensities were integrated, normalised to 100 % and presented according to the chemical shift ranges in Table 11 and Table 12 from section 3.7. ^{13}C NMR spectra are shown from Figure 33 to Figure 36. Figure 37 presents the carbon distribution of each carbon environment for the BFO products and the biodiesels, based on the integrated area of each chemical shift range and the total integrated area of each spectrum.

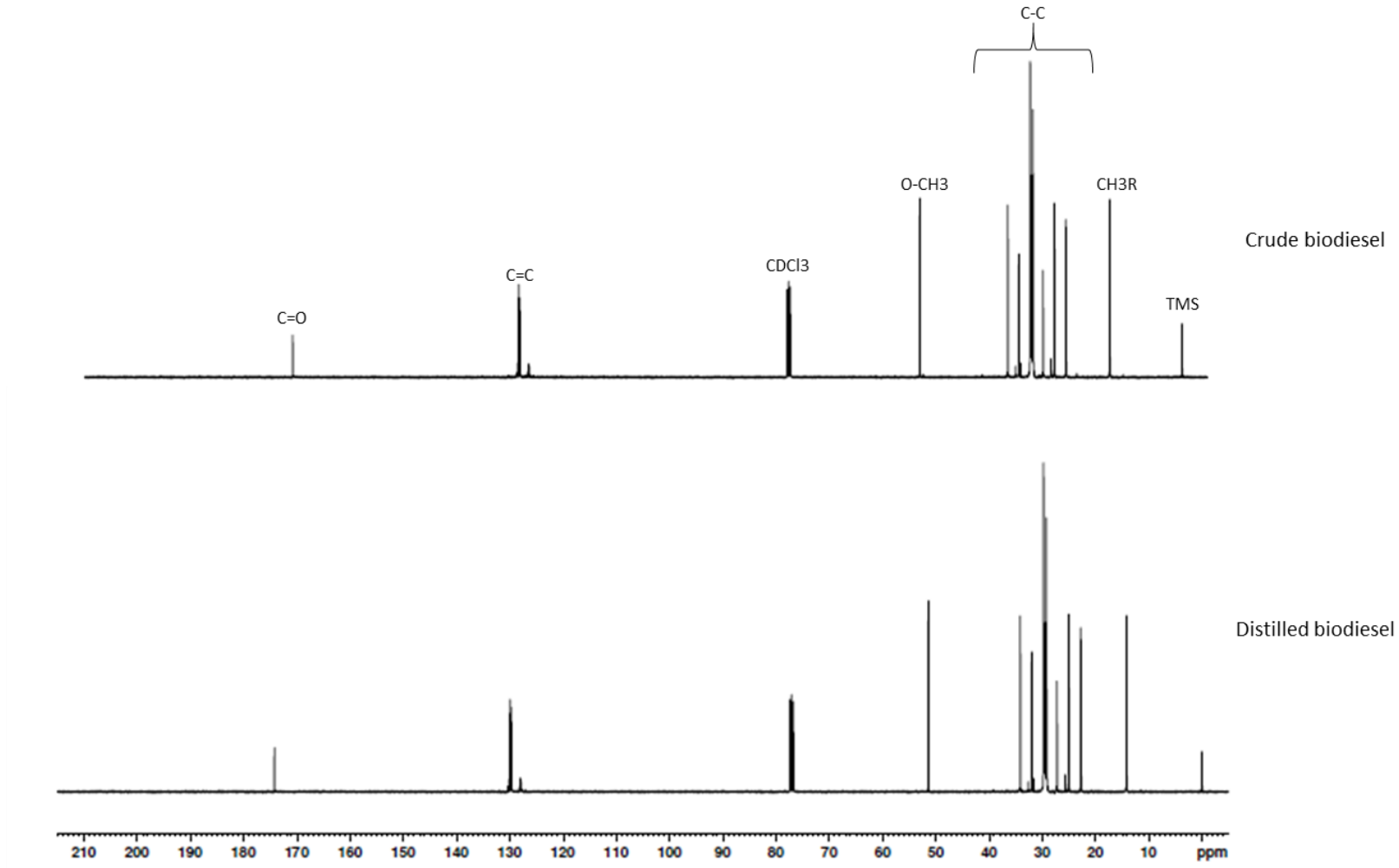

Figure 33: ^{13}C NMR spectra of distilled and crude biodiesels.

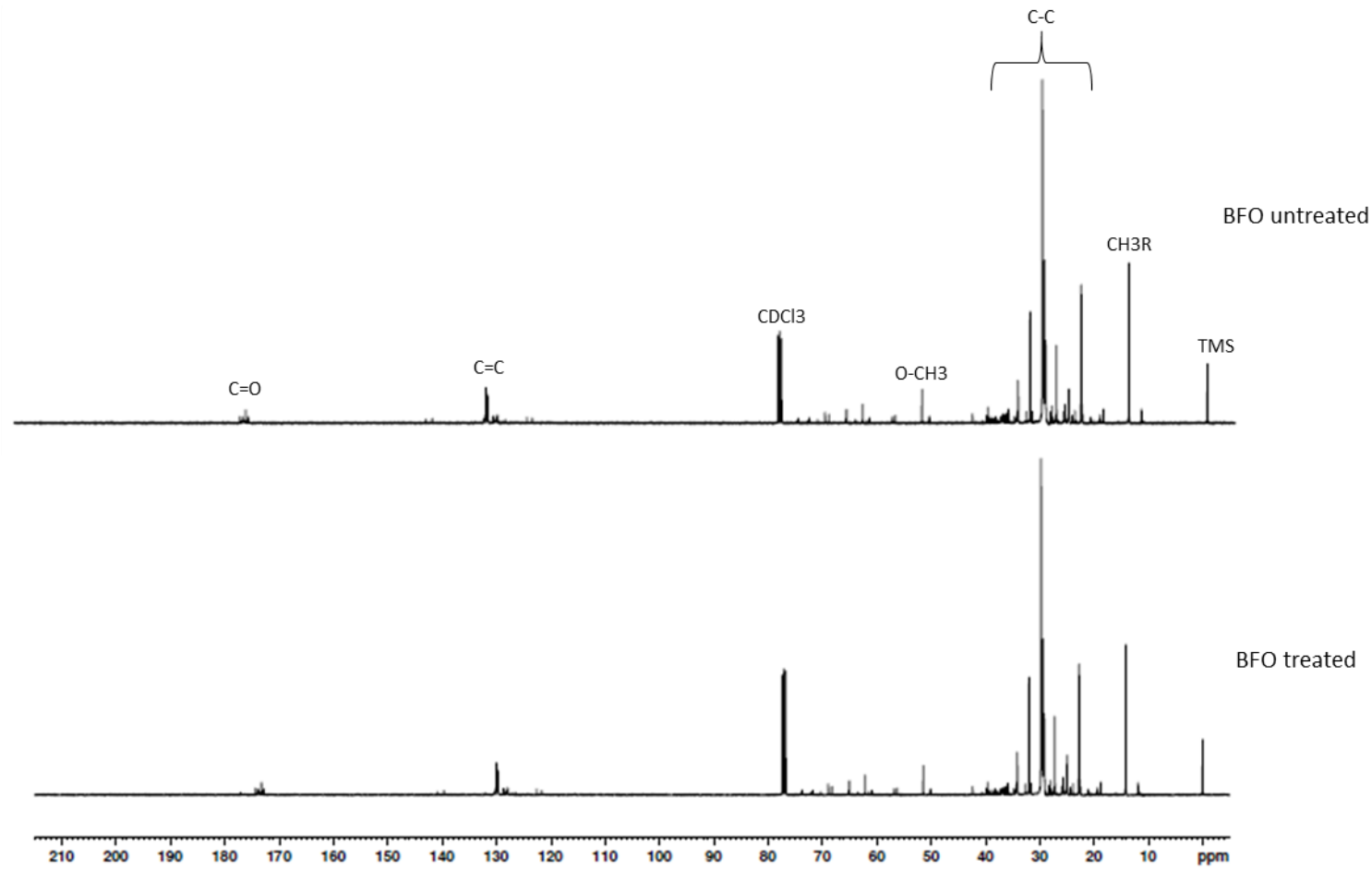

Figure 34: ^{13}C NMR spectra of the untreated and treated BFO starting materials.

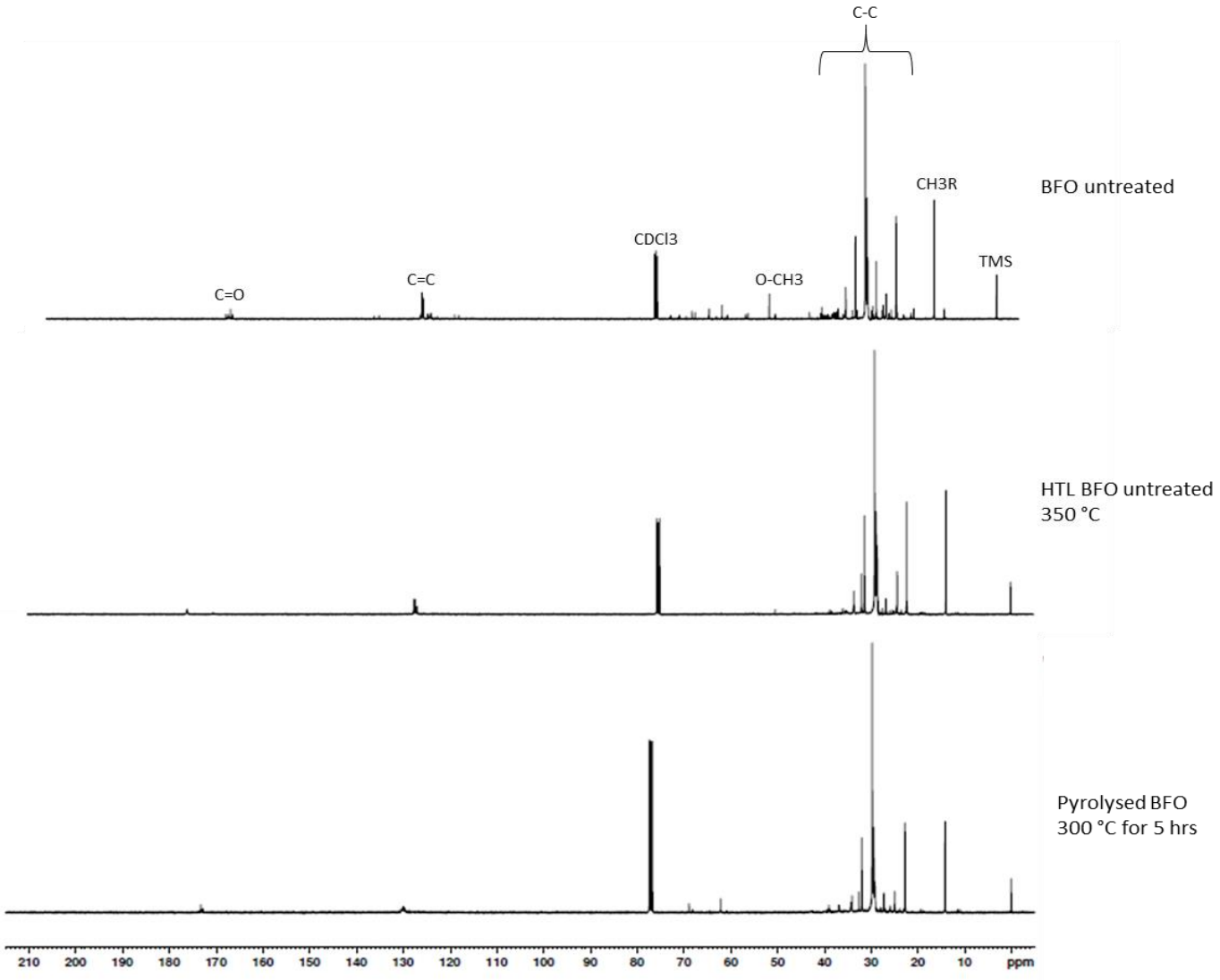

Figure 35: ^{13}C NMR spectra of the untreated BFO starting material, the biocrude obtained after liquefaction at 350 °C and the pyrolysed BFO obtained after pyrolysis at 300 °C (5 hrs).

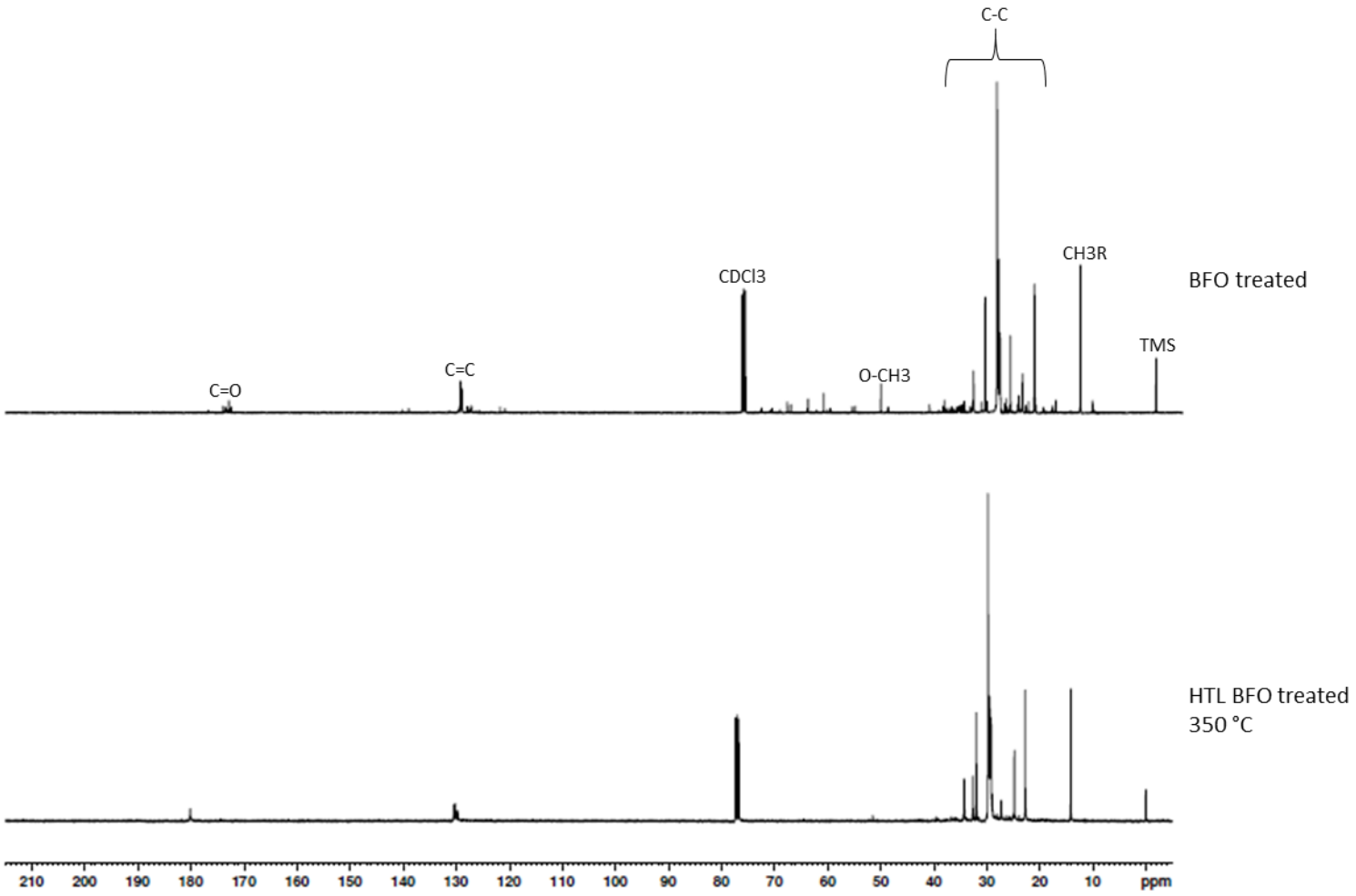

Figure 36: ^{13}C NMR spectra of the treated BFO starting material and the biocrude obtained after liquefaction at 350

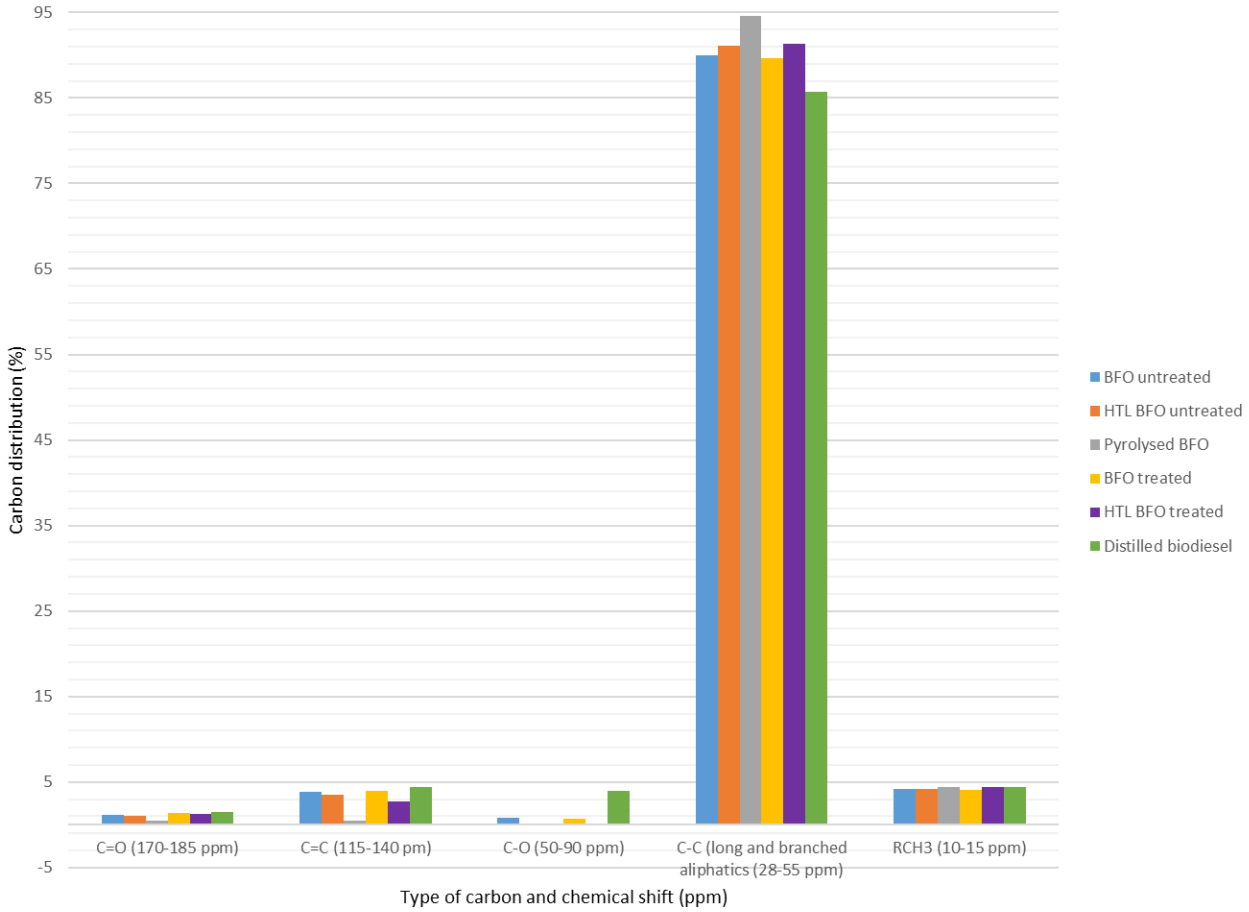

Figure 37: Percentage of carbon distribution in the BFO starting materials and their subsequently treated products – the liquefaction (HTL BFO) and, in the case of the untreated BFO, the additional pyrolysed BFO. For comparison, Argent Energy's end-product, distilled biodiesel, is also presented.

The carboxyl (C=O) environment accounts for less than 2% of all the carbons present. There is a reduction in C=O going from the biodiesel to the BFO, with a further reduction in the liquefied products and the pyrolysed BFO. Regarding the biodiesel sample, the carboxyl group intensity is less than the $–OCH_3$ (C-O), indicating that sp2 hybridised carbon (carbons containing double bonds) is being underestimated. This is due to the fact the experiment was run without a relaxation agent allowing for more variation in signal intensity (Ladner and Snape, 1978). By definition, the carboxyl and OCH_3 concentrations should be equal in biodiesels if 100% transesterification has occurred.

Regarding the unsaturated carbon bonds (C=C), both the BFO treated and untreated starting materials contain broadly similar amounts of alkenes, which are in turn similar to the biodiesel. The liquefaction products (both treated and untreated) contain similar alkene distributions that are slightly lower than those in the original BFO materials, whereas the

pyrolysed BFO has the lowest concentration of unsaturated carbon bonds overall. This reduction in alkenes could arise either naturally from being less abundant in the pyrolysed BFO or due to cross-linking reactions occurring through the double bonds during pyrolysis. This would enhance strength and elasticity in the heavier material (pyrolysed BFO).

The OCH_3 functional group from methyl esters (present between 50-60 ppm) is the only aliphatic C-O present, mostly in the biodiesel and but also in both BFO starting materials at a lower level. It is marginally present in the liquefaction products (both BFO treated and untreated) and not present in the pyrolysed BFO. Pyrolysis in the horizontal furnace has removed OCH_3 from the methyl esters in the BFOs, confirming thermal decomposition. New peaks also appear in the BFOs between 60 and 75 ppm which are not present in the biodiesels, indicating possible CH_2 (methylene groups).

The majority carbons present in all the samples originate from the long and branched aliphatic (C-C) hydrocarbons, with most peaks present in the region of 28-55 ppm, accounting for approximately 85-95% of all carbons. This is expected due to the long C_{12}-C_{26} chain molecules present. Various peaks are observed in this region due to the different positions in the alkyl chains, with the largest at about 29.7 ppm. The biodiesel contains the lowest concentration of aliphatic compounds, followed by the BFO starting materials. Liquefaction and pyrolysis seem to increase the concentration of C-C hydrocarbons slightly. This is possibly due to decreases in the methoxy (OCH_3) and sp2 hybridised carbon functionalities (C=O, C=C).

The methyl group attached to the rest of the molecule (R group) distributions are very similar across the samples, indicating that the distinctive methyl ester functional groups are present across the materials.

The most marked changes are observed with the pyrolysis and liquefaction of BFO (pyrolysed BFO and HTL BFO treated and untreated), at the C-O environment, which has been removed compared to the biodiesel. In addition, Argent Energy's treatment to the BFO, has not drastically altered the carbon distributions compared to the crude (untreated) BFO.

6.4.1. Unsaturated to saturated FAME ratios

The ratios of unsaturated to saturated carbons for the studied samples are presented in Table 25. Although the biodiesel samples contain the highest unsaturated to saturated ratios, the BFO starting materials and the liquefied products contain similar C=C to C-C distributions, while the pyrolysed BFO contains the least amount of unsaturated carbon. This correlates with the uMe/sMe ratios obtained from the GC-MS results (section 6.3.4), which indicate that overall the biodiesels contain higher unsaturated methyl esters. However, the GC-MS ratios are higher than the ^{13}C NMR ones, highlighting the fact that NMR has underestimated sp2 hybridised carbon. For instance, looking at the C_{18} methyl esters, the distilled biodiesel has a ratio of 1.73 obtained from GC-MS whereas ^{13}C NMR indicates a lower ratio of 0.05. In addition, it is clear that both the GC-MS and ^{13}C NMR suggest a high degree of saturation in the thermally treated materials (both liquefied and pyrolysed BFO) compared to both the BFO and biodiesels.

Table 25: Calculated unsaturated to saturated carbon ratios from the ^{13}C NMR integrals. The pyrolysed BFO refers to the one obtained at 300 °C after 5 hours using the untreated BFO.

Sample	C=C to C-C ratio
Undistilled (crude) biodiesel	0.05
Distilled biodiesel	0.05
BFO treated	0.04
BFO untreated	0.04
HTL 350 °C BFO untreated	0.04
HTL 350 °C BFO treated	0.03
Pyrolysed BFO	0.01

6.5. Laser desorption ionisation mass spectrometry

6.5.1. BFO untreated starting material

LDI-MS was used to examine the relative amounts of fatty acid methyl esters (FAME) present in the original BFO untreated and its subsequent pyrolysed sample (pyrolysed BFO), by obtaining a fingerprint of the desorbed (ionised) molecules that reflect their relative abundance in the mixture. In order to identify the expected FAME species, the analysis was carried out by searching for molecules with a double bond equivalence (DBE) value of less than 6 with 1 to 4 oxygen atoms present. These parameters should detect the FAME compounds and any dimeric products formed through fatty acid methyl esters combining. The results are displayed in Table 26 and Table 27 for the original untreated BFO and the pyrolysed BFO samples respectively, with unidentified ions labelled. Potential assignments are noted in the tables, however these are not unique due to the number of isomers having the same molecular formula. The spectra shown are not the full spectrum mode but those of the oxygenated ions after searching. Two ionization processes are possible, one where association of a proton to the molecule, generating an $[M+H]^+$ ion, and one with where a positive radical is generated without association of an extra proton.

More oxygenated species with higher DBE values (higher degree of unsaturation) were found in the pyrolysed BFO compared to the untreated BFO starting material, as shown in Figure 38 and Figure 39. This contrasts the ^{13}C NMR results, which show a reduction in unsaturated carbons in the pyrolysed material. It is likely that the highly selective nature of ionisation during LDI-MS has created bias in the results. As presented in Figure 40, the untreated BFO starting material also contains lower intensity peaks for the oxygenated species considered (relative abundance) than the pyrolysed BFO (Figure 41). This could be an experimental or sampling effect and therefore unlikely to be representative of the concentration of ion in the sample.

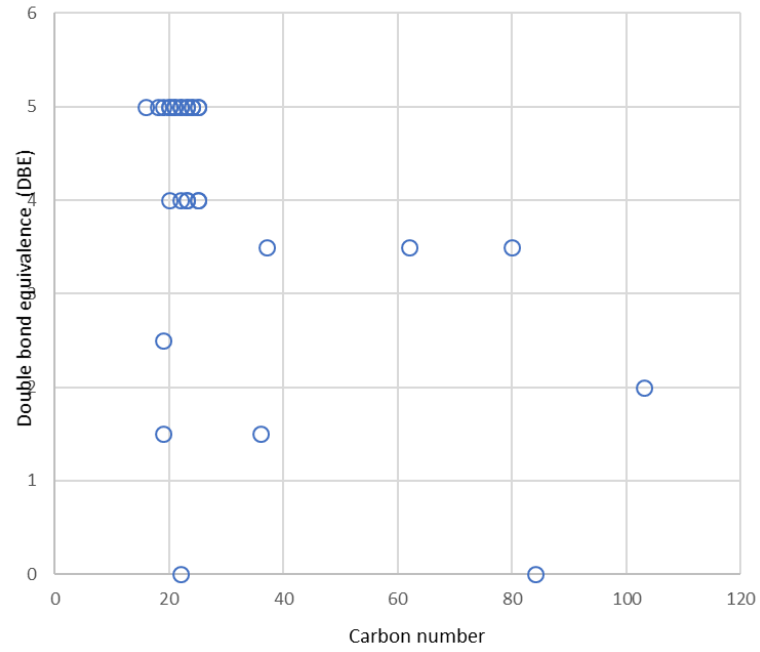

Figure 38: DBE vs carbon number (<5 O atoms) for the original BFO untreated sample.

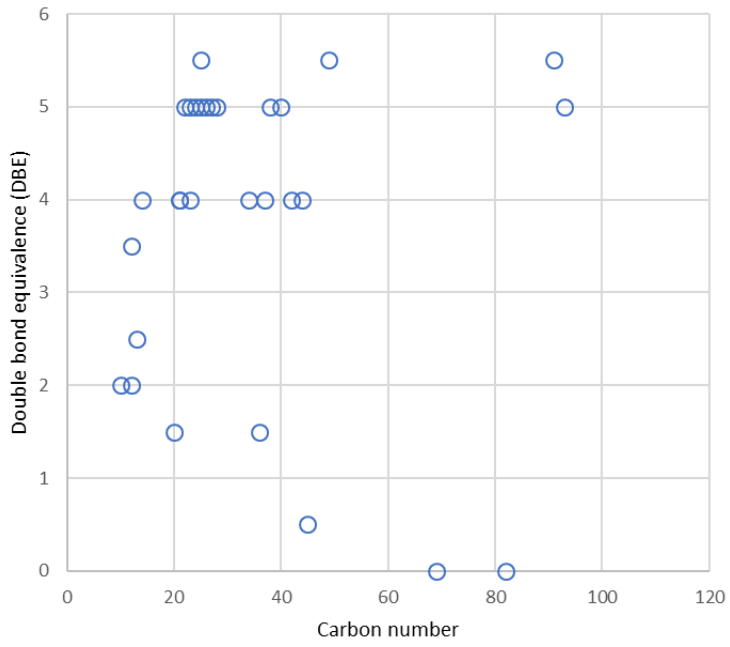

Figure 39: DBE vs carbon number (<5 O atoms) for the pyrolysed BFO sample.

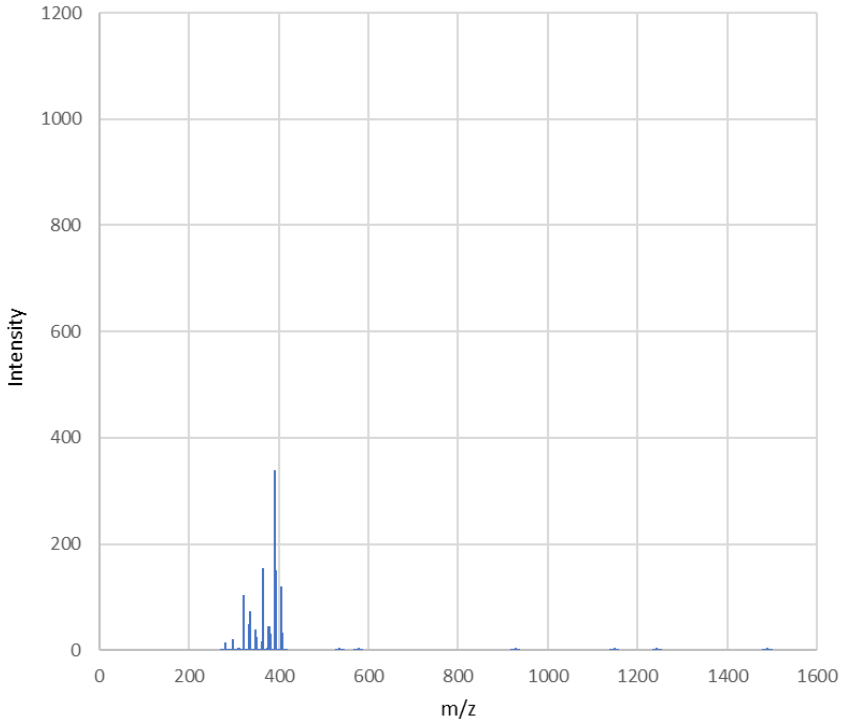

Figure 40: LDI-MS spectra (<5 O atoms) for the original BFO untreated sample. This spectrum is representative of the oxygenated ions after performing molecular formula prediction (MFP) on the raw data to assign ions containing C, H (any value) and O (<5) (Edney et al., 2022).

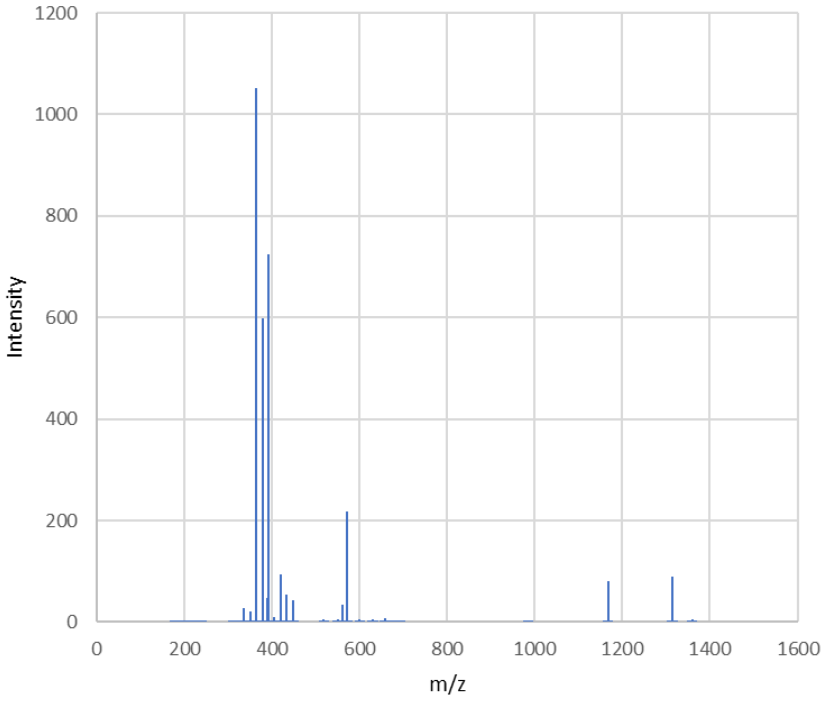

Figure 41: LDI-MS spectra (<5 O atoms) for the pyrolysed BFO sample. This spectrum is representative of the oxygenated ions after performing molecular formula prediction (MFP) on the raw data to assign ions containing C, H (any value) and O (<5) (Edney et al., 2022).

The most intense peak for the untreated BFO sample corresponds to 19-(4-Hydroxyphenyl)nonadecanoic acid, a monocarboxylic acid derivative of nonadecanoic acid, one of the C_{19} straight-chain saturated fatty acids that can be found in fats and vegetable oils. The expected FAME with 0-3 DBE values per C_{16}/C_{18}/C_{20} chains do not appear as major constituents in the untreated BFO, indicating the bias that has occurred in the ionisation process. The LDI-MS analysis shows that the original BFO contains one FAME molecule (highlighted in green in Table 26): methyl oleate (intensity 20.3), which is derived from oleic acid ($C_{18}H_{34}O_2$), a monounsaturated omega-9 fatty acid naturally found in animal and vegetable fats and oils. A potential chemical structure that fits the formula is shown in Figure 42. Although not a FAME, icosyl hexadecenoate, an ester is derived from hexadecanoic (palmitic) acid, was also present in the BFO. Palmitic acid is considered a major component of palm oil, dairy and meats.

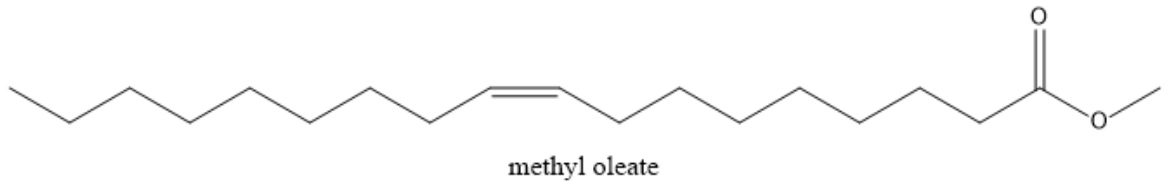

methyl oleate

Figure 42: Potential chemical structure of methyl oleate, $C_{19}H_{36}O_2$, found in the original untreated BFO. The position of the double bond in the chain is not known.

While no other FAME ions were identified in the original BFO, a range of carboxylic acid species have been annotated including bile acids such as homoursodeoxycholic acid, dinorhyodeoxycholic acid and chenodeoxycholic acid (Figure 43). Other ester and ether species were identified such as 2-arachidonyl glycerol ether and 2-arachidonoylglycerol, derived from arachidonic acid (a polyunsaturated omega-6 fatty acid) and glycerol. Lipids and steroids such as phenolic phthiocerol and tetrahydrocorticosterone respectively were also identified in the BFO.

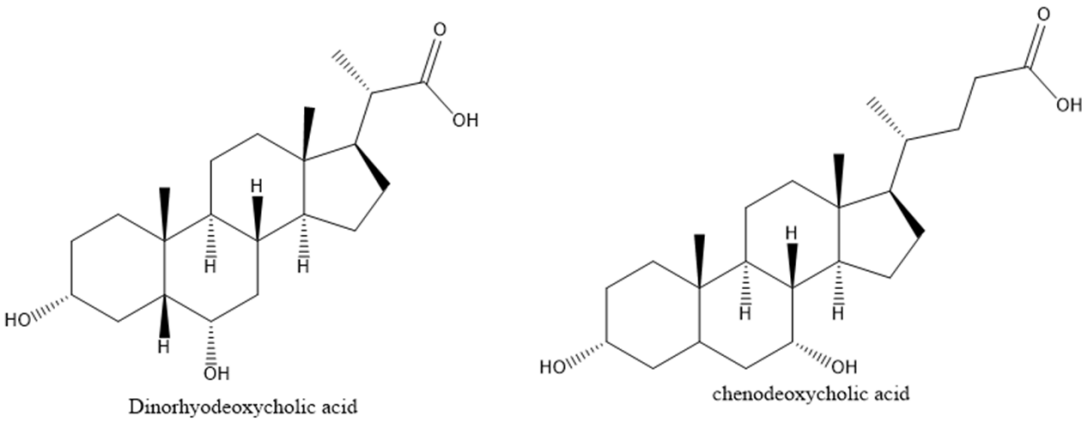

Figure 43: Potential chemical structures of dinorhyodeoxycholic acid ($C_{22}H_{36}O_4$) and chenodeoxycholic acid ($C_{24}H_{40}O_4$) found in both the original untreated BFO.

6.5.2. Pyrolysed BFO

Similarly to the untreated BFO material, FAME molecules have not yielded major ions from the pyrolysed BFO sample. Eicosenoic acid, $C_{20}H_{38}O_2$, a monounsaturated fatty acid was identified in the pyrolysed BFO. Eicosenoic acid may result from 13-eicosenoic (paullinic) acid found in guarana fruit, 11-eicosenoic (gondoic) acid found in jojoba oil and nuts or 9-eicosenoic (gadoleic) acid, commonly found in fish oil. Another fatty acid, 3-oxododecanoic acid, was also found post pyrolysis. 3-oxododecanoic acid is derived from dodecanoic (lauric) acid, which is found in coconut fatty acids.

The most intense peak in the pyrolysed BFO sample corresponds to the bile acid dinorhyodeoxycholic acid (intensity 1052.4), which is also found in the original BFO, but at a much lower intensity (34.9) (Figure 43). Only four other ions were present in both materials, which suggests that pyrolysis has significantly altered the molecular composition of the BFO for the ions generated. The overlapping ions are highlighted in blue in Table 27. 19-(4-Hydroxyphenyl)nonadecanoic acid, 2-arachidonoylglycerol and chenodeoxycholic acid were noted as overlapping assignments. Persin ($C_{23}H_{40}O_4$), an oil-soluble toxin present in avocado which is similar to a fatty acid, is also found in both materials. Possible chemical structures of cis-11-eicosenoic acid, found in the pyrolysed BFO, and the overlapping ion 19-(4-Hydroxyphenyl)nonadecanoic acid are presented in Figure 44.

Due to pyrolysis, different ions have formed to those seen in the original BFO. An example is glycerol 2-linolenate, a monoglyceride derived from alpha-linolenic acid, commonly found in seeds and oils like flaxseed and walnuts. Sebacic acid, $C_{10}H_{18}O_4$, a derivative of castor oil, is also present in the pyrolysed BFO.

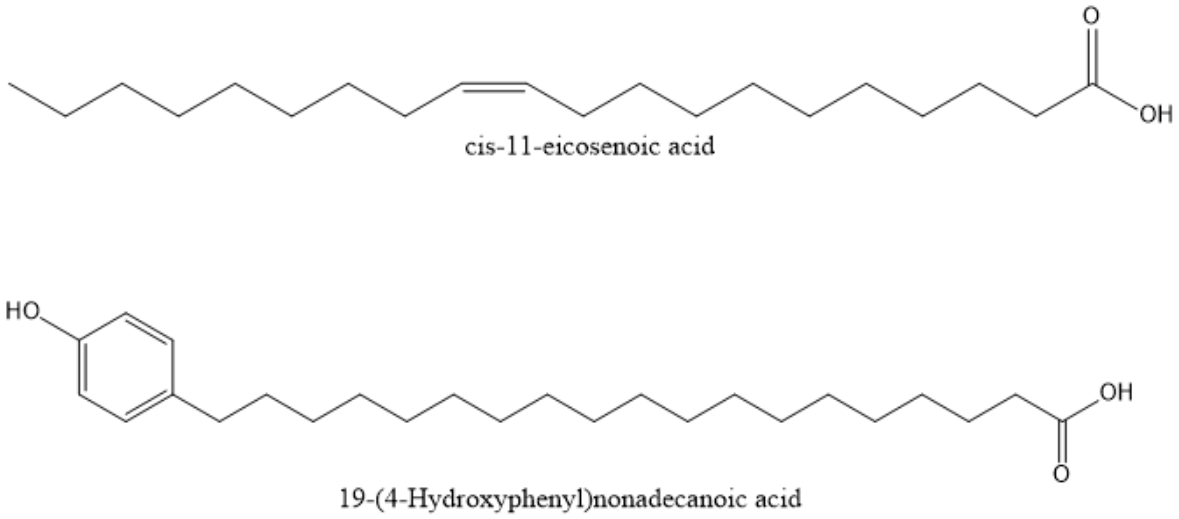

Figure 44: Potential chemical structures of cis-11-eicosenoic (gondoic) acid ($C_{20}H_{38}O_2$), found in the pyrolysed BFO, and 19-(4-Hydroxyphenyl)nonadecanoic acid ($C_{25}H_{42}O_3$), found in both the original and pyrolysed BFO.

Table 26: LDI-MS data for the BFO untreated sample. FAME molecule highlighted in green.

Error (ppm)	DBE	DBE $[M+H]^+$	m/z	Intensity (AU)	Formula	Name and example origin
1.2	5	x	390.3133	339.3	$C_{25}H_{42}O_3^+$	19-(4-hydroxyphenyl)nonadecanoic acid (found in fats and veg oils)
0.8	4	x	364.2975	155.6	$C_{23}H_{40}O_3^+$	2-arachidonyl glycerol ether (arachidonic acid - polyunsaturated omega-6 fatty acid
1.5	4	x	392.3291	151.1	$C_{25}H_{44}O_3^+$	miaolinolide
0.8	5	x	406.3081	120.3	$C_{25}H_{42}O_4^+$	homoursodeoxycholic acid (bile acid from animal origin)
2.2	5	x	320.2353	103.6	$C_{20}H_{32}O_3^+$	isocupressic acid (present in conifer needles i.e. ponderosa pine)
1.8	5	x	336.2301	73.6	$C_{20}H_{32}O_4^+$	arachidonic acid 5-hydroperoxide or hepoxilin or leukotriene B4
2.0	5	x	334.2509	48.5	$C_{21}H_{34}O_3^+$	tetrahydrodeoxycorticosterone (steroid)
0.8	5	x	376.2975	46.0	$C_{24}H_{40}O_3^+$	lithocholic acid (bile acid)
1.2	5	x	378.2769	44.7	$C_{23}H_{38}O_4^+$	2-arachidonoylglycerol
1.7	5	x	348.2665	38.5	$C_{22}H_{36}O_3^+$	dinorlithocholic acid (bile acid) or anacardic acid (found in cashew nuts, cashew oil and mangos)
1.3	5	x	364.2613	34.9	$C_{22}H_{36}O_4^+$	dinorhyodeoxycholic acid (bile acid)
1.4	4	x	408.3240	33.7	$C_{25}H_{44}O_4^+$	Diacarnoxide C
0.8	4	x	380.2924	31.4	$C_{23}H_{40}O_4^+$	persin
1.5	5	x	350.2457	24.4	$C_{21}H_{34}O_4^+$	Tetrahydrocorticosterone (hydroxy steroid found in animals)
0.7	1.5	2	297.2790	20.3	$C_{19}H_{36}O_2^+$	FAME, methyl oleate, derived from oleic acid
2.0	4	x	322.2509	17.7	$C_{20}H_{34}O_3^+$	3,4-dimethyl-5-propyl-2-furanundecanoic Acid (derived from furan fatty acids which can be found in fish but also products like butter
1.5	5	x	362.2821	17.7	$C_{23}H_{38}O_3^+$	cetyl salicylate (salicylates found naturally in some plants such as white willow bark)

2.1	5	x	280.1675	15.7	$C_{16}H_{24}O_4^+$	cyanein - a fungal metabolite
2.0	5	x	392.2929	10.2	$C_{24}H_{40}O_4^+$	chenodeoxycholic acid (bile acid)
-0.1	4	x	350.2815	9.4	$C_{22}H_{38}O_3^+$	10-undecenoic anhydride or 2,6-Dioctoxyphenol
0.7	5	x	322.2141	5.7	$C_{19}H_{30}O_4^+$	8-gingerol (from ginger)
1.8	3.5	4	577.5201	5.2	$C_{37}H_{68}O_4^+$	phenolic phthiocerol (-H) a lipid
1.6	3.5	4	1148.2040	5.2	$C_{80}H_{154}O_2^+$	unidentified
0.3	5	x	308.1983	5.1	$C_{18}H_{28}O_4^+$	dihydrocapsiate (from pepper)
2.4	0	x	1243.3124	5.0	$C_{84}H_{170}O_4^+$	unidentified
1.7	2.5	3	311.2586	4.6	$C_{19}H_{34}O_3^+$	methoprene (used in the production of foods including meat and milk and also used as an insecticide)
0.6	0	x	374.3393	4.4	$C_{22}H_{46}O_4^+$	Ceteth-3 or 1,8-Octanediol, 1,8-bis(heptyloxy)-
1.9	2	x	1489.5833	4.2	$C_{103}H_{204}O_3^+$	unidentified
0.9	3.5	4	927.9111	4.0	$C_{62}H_{118}O^{4+}$	docosanoyl (Z)-19-oxotetracont-9-enoate (-H)
1.8	1.5	2	535.5458	3.8	$C_{36}H_{70}O_2^+$	Icosyl hexadecenoate (-H) from palmitic acid (hexadecanoic acid)

Table 27: LDI-MS data for the pyrolysed BFO sample. FAME molecule highlighted in green and overlapping ions present in both materials highlighted in blue.

Error (ppm)	DBE	DBE $[M+H]^+$	m/z	Intensity (AU)	Formula	Name and example origin
2.4	5		364.2617	1052.4	$C_{22}H_{36}O_4^+$	dinorhyodeoxycholic acid (bile acid)
2.3	5		392.2930	724.3	$C_{24}H_{40}O_4^+$	chenodeoxycholic acid (bile acid)
2.5	5		378.2774	598.7	$C_{23}H_{38}O_4^+$	2-arachidonoylglycerol (derived from arachidonic acid which is found in animal and human fat)
2.1	5		572.5175	217.0	$C_{38}H_{68}O_3^+$	2-(4-hydroxyphenyl)ethyl triacontanoate from melissic acid - found in beeswax
1.2	5		420.3239	94.4	$C_{26}H_{44}O_4^+$	Dihomoursodeoxycholic acid
2.0	5.5	6	1314.3410	89.1	$C_{91}H_{172}O_3^+$	unidentified
1.5	0		1167.2950	80.1	$C_{82}H_{166}O^+$	unidentified
1.0	5		434.3395	54.2	$C_{27}H_{46}O_4^+$	3a,7a-dihydroxycoprostanic acid (bile acid) - precursor of chenodeoxycholic acid (another bile acid)
2.4	5		390.3138	47.9	$C_{25}H_{42}O_3^+$	19-(4-hydroxyphenyl)nonadecanoic acid (found in fats and veg oils)
0.9	5		448.3551	44.0	$C_{28}H_{48}O_4^+$	teasterone (steroid)
0.9	4		560.5168	33.9	$C_{37}H_{68}O_3^+$	1-(15-methyl-tridecanyl)-2-(8-[3]-ladderane-octanyl)-sn-glycerol
1.8	4		336.2665	27.1	$C_{21}H_{36}O_3^+$	isolinderanolide (found in THF)
2.0	4		352.2615	21.1	$C_{21}H_{36}O_4^+$	glyceryl 2-linolenate (derived from alpha-linolenic acid)
-1.6	5.5	6	405.2993	9.0	$C_{25}H_{40}O_4^+$	isononyl isooctyl phthalate
1.0	4		658.6265	6.9	$C_{44}H_{82}O_3^+$	ethylhexyl linoleoyl stearate
1.3	4		518.4700	6.4	$C_{34}H_{62}O_3^+$	unidentified
0.3	5		600.5478	6.2	$C_{40}H_{72}O_3^+$	unidentified
1.8	4		630.5957	6.0	$C_{42}H_{78}O_3^+$	unidentified
-1.0	5		1359.3710	6.0	$C_{93}H_{178}O_4^+$	unidentified

-1.9	1.5	2	551.5387	4.7	$C_{36}H_{70}O_3^+$	stearic anhydride (-H) - from stearic acid (octadecanoic acid)
2.4	2.5	3	195.1748	4.3	$C_{13}H_{22}O^+$	solanone (-H) found in tobacco leaves and in blackcurrant buds
1.8	4		380.2928	4.2	$C_{23}H_{40}O_4^+$	persin
0.7	2		202.1201	3.7	$C_{10}H_{18}O_4^+$	sebacic acid (derivative of castor oil)
-0.4	0.5	1	679.6960	3.7	$C_{45}H_{90}O_3^+$	hydroxyphthioceranic acid (C45) (-H) plant source - sesterterpenoid
-2.1	1.5	2	311.2938	3.5	$C_{20}H_{38}O_2^+$	Eicosenoic acid
1.9	4		238.1568	3.4	$C_{14}H_{22}O_3^+$	cyclohexanecarboxylic anhydride
0.4	0		985.0903	3.2	$C_{69}H_{140}O^+$	unidentified
1.7	5.5	6	693.6920	3.1	$C_{49}H_{88}O^+$	unidentified
1.4	3.5	4	179.1433	3.0	$C_{12}H_{18}O^+$	unidentified
2.1	2		214.1568	3.0	$C_{12}H_{22}O_3^+$	3-oxododecanoic acid (derivative of dodecanoic (lauric) acid, found in coconut fatty acids (milk and oil), laurel oil and palm kernel oil)

6.6. Simulated Gas Chromatography Distillation

The simulated distillation analysis was performed to determine the boiling point distribution of the samples listed below, in order to compare with the GC-MS results.

- BFO untreated (starting material)
- Liquefaction biocrude product obtained from the untreated BFO at 350 °C
- Pyrolysed product obtained from the untreated BFO at 300 °C after 5 hrs
- Distilled biodiesel
- Crude biodiesel

Only the samples originating from the untreated BFO as well as the two control biodiesels were studied and sent to the Czech Republic for analysis and it was clear that at this point, they were the materials of interest to identify the sample that has the potential to be applied as a bitumen modifier. Table 28 presents the SIMDIS results.

Sample	IBP	FBP	% non-distillable residue	% recovery
BFO untreated	332.72	>720	19.16	80.84
HTL BFO untreated	268.75	>720	16.24	83.76
Pyrolysed BFO	355.62	>720	29.61	70.39
Crude biodiesel	302.75	594.74	not detected	not detected
Distilled biodiesel	300.87	413.34	not detected	not detected

Table 28: Simulated distillation analysis results for the untreated BFO starting material, the liquefaction BFO product at 350 °C, the pyrolysed BFO (at 300 °C after 5hrs) and the two control biodiesel samples. IBP: Initial boiling point, FBP: Final boiling point.

The untreated BFO starting material has a final boiling point (FBP) > 720, and approximately 80% of the material was recovered after distillation. The chromatogram in Figure 45 shows a distribution of compounds eluted at a maximum to about 20 minutes with the first peak eluted just before 7 minutes. In comparison, the liquefaction (HTL) BFO sample presents a shift to lighter materials with a maximum elution of approximately 11 minutes, and the first peak appearing at around 6 minutes (Figure 46), with a lower initial boiling point (IBP) and higher percentage recovery than that of the starting BFO. It is interesting to note that the HTL product has the lowest IBP out of all the samples tested, including the two control biodiesels. This suggests that cracking reactions broke down the higher carbon chain FAME material to lower carbon chain material and confirm the GC-MS results, which show that the BFO starting

materials have an overall heavier carbon chain of FAME than the liquefaction products, for both BFO treated and untreated.

A shift to heavier materials was observed for the pyrolysed BFO sample, where the lighter ends have been lost due to distillation, with the constituents present in the material eluting between 14 and 24 minutes (Figure 47). There is also an increase in IBP and percentage residue compared to the starting BFO material, suggesting that lighter materials have been distilled off during pyrolysis, leaving heavier materials remaining in the product. This result is consistent with the GC-MS chromatographic distribution of the pyrolysed BFO, which shows no FAME material present (Figure 32), indicating a shift to heavier constituents that could not be eluted from the GC-MS column.

Regarding the distilled and crude biodiesel samples in Figure 48 and Figure 49 respectively, both contain lower IBP and FBPs compared to the other materials investigated, with the undistilled (crude) biodiesel containing slightly heavier FAME compounds than the distilled biodiesel with no residue obtained for both the distilled and crude biodiesel.

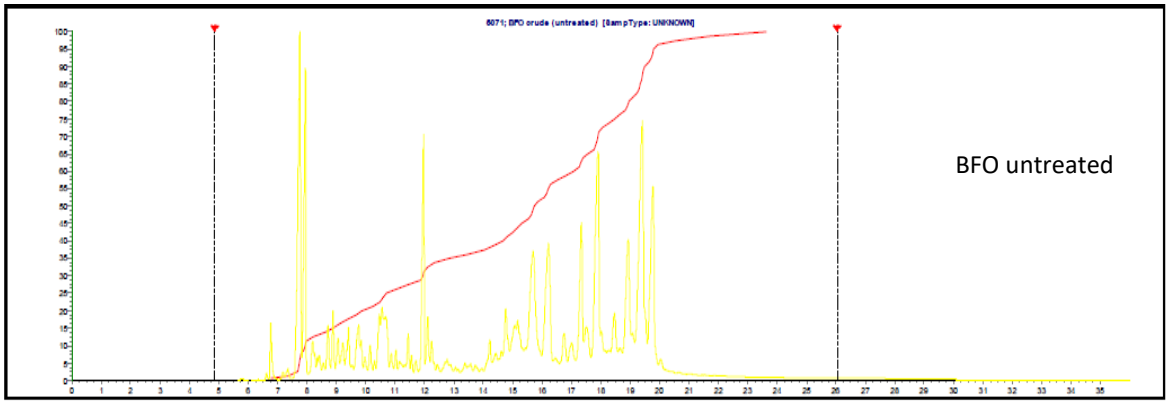

Figure 45: SIMDIS chromatogram for the BFO untreated starting material

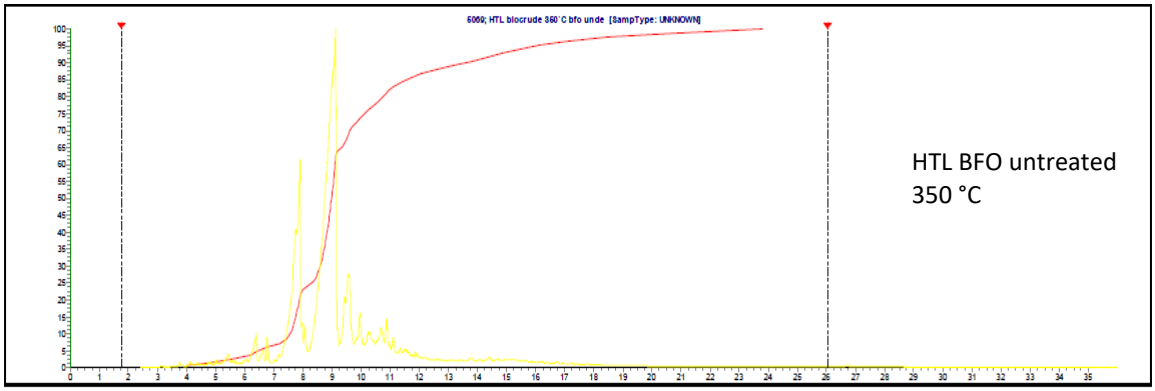

Figure 46: SIMDIS chromatogram for the liquefaction product obtained from the untreated BFO, at 350 °C.

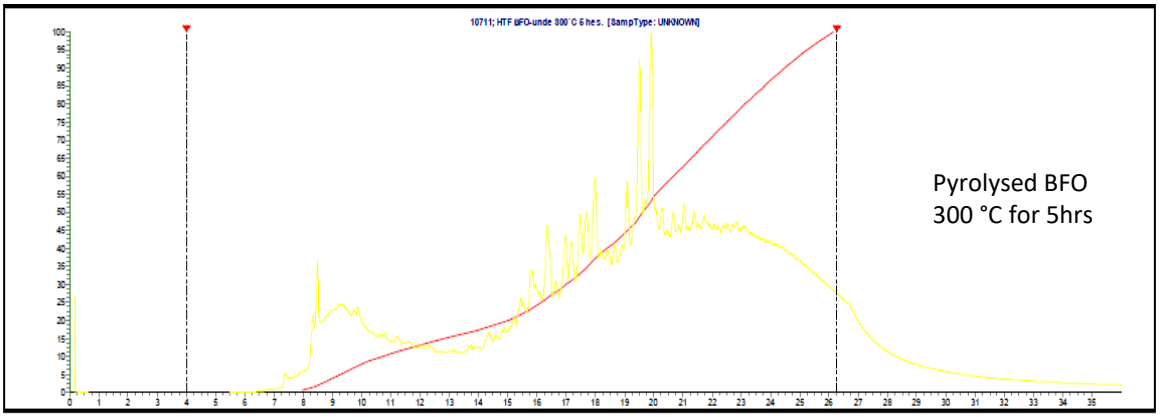

Figure 47: SIMDIS chromatogram for the pyrolysed BFO obtained at 300 °C after 5 hrs.

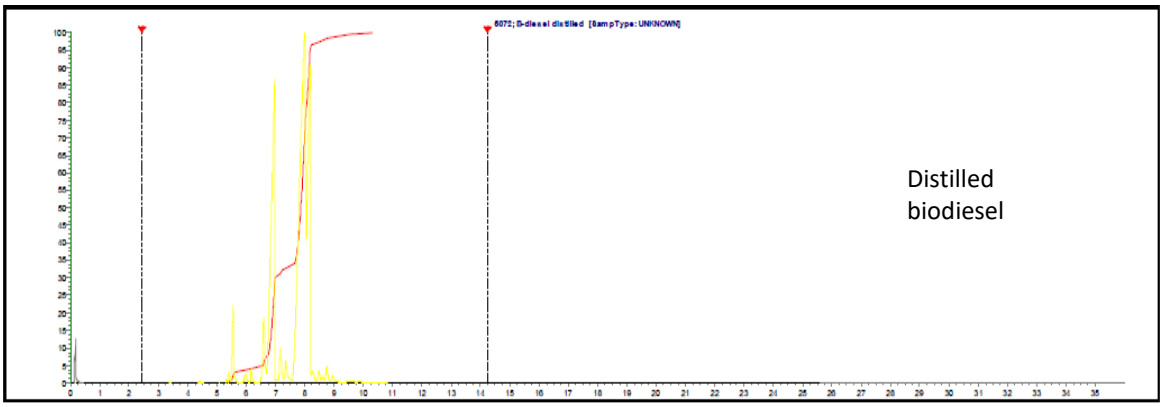

Figure 48: SIMDIS chromatogram for the distilled biodiesel.

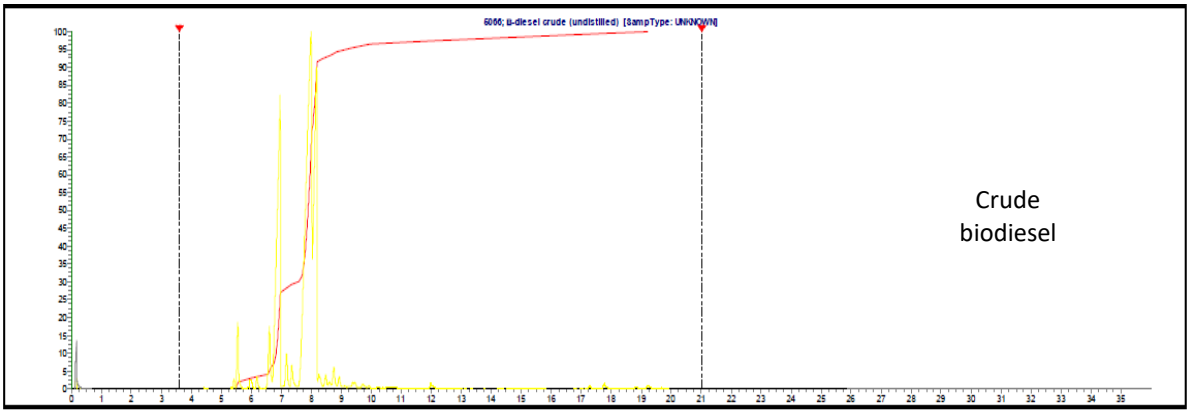

Figure 49: SIMDIS chromatogram for the crude biodiesel.

6.7. Key Points

- TGA results show that volatile matter is the main component of all the samples while no residue was obtained. This is expected due to the higher heating rate and temperature seen in the TGA.
- As for the EA, the pyrolysed BFO contains the lowest oxygen content and highest carbon. This lower oxygen content could be favourable for bio-bitumen production to avoid accelerated ageing.
- GC-MS: In summary, the BFOs and the biodiesel control samples have higher carbon chains of FAME than their liquefaction counterparts. This reveals that hydrothermal liquefaction did not work to produce a heavier biocrude from the BFO. On the other hand, no FAME were seen on the GC-MS spectra of the pyrolysed samples, suggesting that the BFO can be upgraded to heavier products via pyrolysis.
- ^{13}C NMR: The key takeaway from the ^{13}C NMR results is the reduction of methoxy (C-O) and carboxyl (C=O) groups in the BFO materials compared to the biodiesel. OCH_3 virtually disappears from the HTL and pyrolysed BFO products. This correlates with the higher concentration of CO_2 in the gas analysis from the HTL experiments, indicating that decarboxylation is occurring. In addition, there is a drastic decrease in alkenes (C=C) in the pyrolysed BFO which could be due to naturally being less abundant or due to cross-linking reactions taking place. Although sp2 hybridised carbon is underestimated in ^{13}C NMR, the results for the unsaturated to saturated carbon ratios align with the GC-MS ratios.

- LDI-MS: The highly selective ionisation process has indicated that FAME molecules were not predominantly found in the untreated BFO starting material or the pyrolysed BFO. A range of carboxylic acids were predominant but not many overlapping species were seen between the two materials tested. This matrix-free method did not identify the expected FAME species that are clearly seen with the GC-MS and ^{13}C NMR results.
- SIMDIS: HTL product (obtained at 350 °C from BFO untreated) has the lowest boiling point out of the materials tested, including the two biodiesels. This result confirms the GC-MS results and show that the liquefaction products are lightweight materials with lower carbon chain. In comparison, the pyrolysed BFO material has the highest boiling point (representative of a heavier product present).

7. Rheological characterisation of BFO materials

In order to characterise the newly produced BFO materials, viscosity was studied. Two types of tests were carried out to investigate this parameter – one was using rotational viscometry testing carried out using a Brookfield viscometer and the second one was using a DSR to understand the viscosity and temperature relationship of the BFO materials with the use of log complex viscosity vs temperature plots.

7.1. Viscosity-temperature relationship of neat (unblended) BFO materials

The following samples were studied in a Kinexus DSR (using parallel plate geometry) in order to investigate the relationship between viscosity and temperature using log complex viscosity versus temperature plots. The results are presented for one frequency (1 Hz) in order to compare differences:

- BFO untreated (starting material)
- BFO treated (starting material)
- Liquefaction biocrude product obtained from the untreated BFO at 350 °C
- Liquefaction biocrude product obtained from the treated BFO at 350 °C
- Pyrolysed products obtained from the untreated and treated BFOs at 300 °C after 1 hr, 275 °C after 5 hrs and 300 °C after 5 hrs

The viscosity-temperature relationship for the treated BFO, its liquefaction product at 350 °C, and the three pyrolysed BFOs at a fixed frequency of 1 Hz are presented in Figure 50. The liquefaction product has the highest complex viscosity at the lowest temperature studied (10 °C). In addition, the pyrolysed BFO obtained at 300 °C after 1 hr was approximately one order of magnitude less than the HTL BFO (at about 1039000 Pa.s) at this temperature. This was followed by the pyrolysed BFO attained at 300 °C after 5 hrs, the BFO treated starting material and the pyrolysed product obtained at 275 °C after 5 hrs respectively. The viscosity at 10 °C for the pyrolysis run done at 275 °C and 5 hrs is approximately 4 orders of magnitude lower to that of the liquefied product.

Viscosity gradually decreases as temperature increases for the BFO treated initial material. As expected, the liquid starting material shows the lowest viscosities at ambient temperature (20 °C - 35 °C). The same decreasing viscosity trend is observed for the liquefied (HTL) product until about 50 °C, but more drastically. Viscosity values start to plateau slightly at the higher

temperatures until 70 °C for the HTL sample. In general, the highest viscosities are seen with the pyrolysed BFO products throughout the tested temperatures, about two orders of magnitude greater than those seen in the HTL product. These results also agree with the chemical characterisation of the pyrolysed BFO which indicate that it is comprised of heavier material. All three pyrolysed products show similar viscosity profiles and decrease in viscosity gradually as temperature increases, plateauing at around 50 °C.

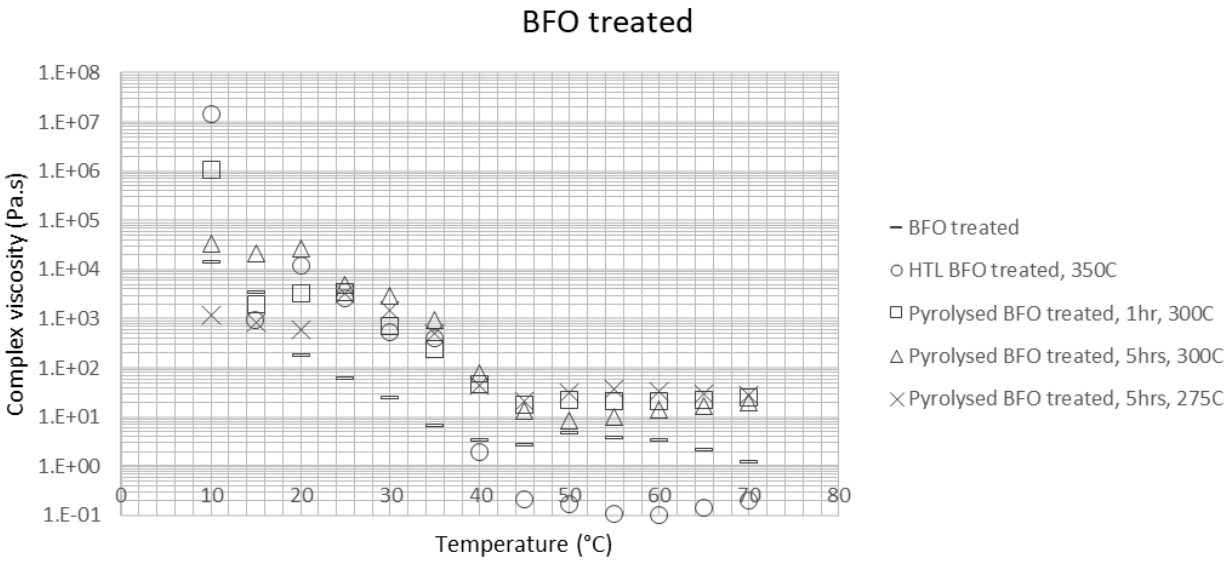

Figure 50: Viscosity-temperature relationship at 1 Hz for the BFO treated, the HTL BFO product obtained at 350 °C, and the pyrolysed BFO products obtained at 300 °C (1 hr), 300 °C (5 hrs) and 275 °C (5 hrs).

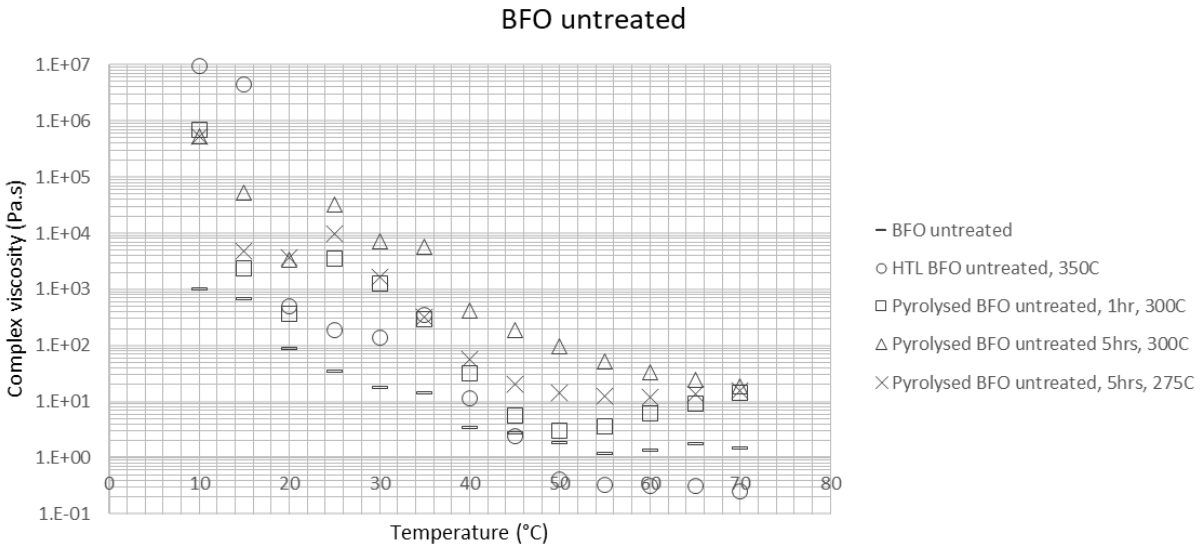

Figure 51: Viscosity-temperature relationship at 1 Hz for the BFO untreated, the HTL BFO product obtained at 350 °C, and the pyrolysed BFO products obtained at 300 °C (1 hr), 300 °C (5 hrs) and 275 °C (5 hrs).

The viscosity-temperature relationship for the untreated BFO, its liquefaction product at 350 °C, and the three pyrolysed BFOs at 1 Hz is presented in Figure 51. Similarly to the treated BFO results, the liquefaction product has the highest viscosity observed at 10 °C and 15 °C, with complex viscosities close to 1.00E+07. At 10 °C, unlike the treated BFO, the three pyrolysed BFO products have almost identical complex viscosity just below 1.00E+06, approximately one order of magnitude less than the HTL material. In this case, the lowest complex viscosity at 10 °C comes from the starting material (approximately 4 orders of magnitude less than HTL product and 3 orders of magnitude less than the pyrolysed products). There is more variation in the viscosity profile of the pyrolysed BFO untreated samples compared to the treated BFO ones. The product obtained at 300 °C after 5 hrs (highest mass loss seen during pyrolysis at 66%) shows the highest increase in viscosity out of all the samples studied. The same trends observed for the treated BFO are seen here for the HTL product and the original BFO.

7.1.1. Comparison of viscosity-temperature plots between BFO treated and untreated

The results in Figure 50 and Figure 51 above display the trends observed for each BFO and its subsequent produced samples. The following plots in Figure 52 to Figure 56 show the differences in the viscosity-temperature relationship between the treated and untreated counterparts at 1 Hz. For the starting materials (Figure 52), viscosity gradually decreases as temperature increases. Viscosity for the treated BFO is approximately 1 order of magnitude higher at 10 °C and 15 °C than the untreated BFO. Both materials display similar viscosities in the mid-range temperatures (20 °C to 45 °C). At 50 - 60 °C, the treated BFO displays higher viscosities, but these are once again similar at the highest temperatures of 65 °C and 70 °C (very low viscosities in the range of 1 and 10 Pa.s). From 50 °C, viscosity values seem to stabilise for the untreated BFO material. Overall, although there are subtle differences, the viscosities and the pattern of viscosity versus temperature for both the untreated and treated BFO are the same. Argent Energy's treatment of the BFO does not seem to make a big difference. This was unexpected as Argent Energy claim the treatment makes the treated BFO more fluid at ambient temperature. This resemblance in viscosity agrees with the chemical characterisation of the BFO, particularly the GC-MS and ^{13}C NMR results which display the similarities in chemical composition between the two materials.

The liquefied BFO materials in Figure 53 display a similar pattern of behaviour. In general, at low temperatures, the liquefied treated BFO seems to have higher viscosity while the opposite is true at the higher temperatures. Both materials have similar high viscosities at 10 °C (around 1.00E+07 Pa.s), however differences are seen already from 15 °C, which shows a significant drop in viscosity for treated BFO (~4 orders of magnitude lower), whereas the untreated BFO's viscosity remains high between 1.00E+07 and 1.00E+06 Pa.s at this temperature. From 20 °C to 30 °C, the treated BFO's viscosity is higher than untreated BFO (between 1000 and 10,000 Pa.s). At these temperatures, there is a gradual decrease as temperature increases with treated BFO sample. A similar trend is seen with the untreated BFO but at viscosities around 100 and 1000 Pa.s. Viscosity slightly increases at 35 °C for the untreated BFO, showing a similar viscosity to that of the treated BFO. From 40 °C onwards, very low viscosities are seen with both HTL materials, with the treated BFO displaying slightly lower viscosity values overall. The observed stark transition from low to high temperature may relate to possible molecular-level effects, such as crystallization or glass transition. Crystallization describes melting temperature and transition of a solid into a liquid phase, mostly dependant on the types of chemical bonding of molecules present in the material. On the other hand, glass transition refers to the temperature at which an amorphous, hard material in a 'glassy' state passes to a soft, 'rubbery' molten state. This depends mainly on the chemical structure of the material itself. Partially crystalline materials contain a mixture of both crystalline and amorphous structures (Santos et al., 2014, Whisnant, 2021). Viscosities for both samples plateau at around 50 °C and stay constant until 70 °C. The low viscosities of the liquefied products agree with the GC-MS results which show they are comprised of lower molecular weight fatty acid compounds which were then lost during sample drying, leaving behind a lighter material with lower viscosity.

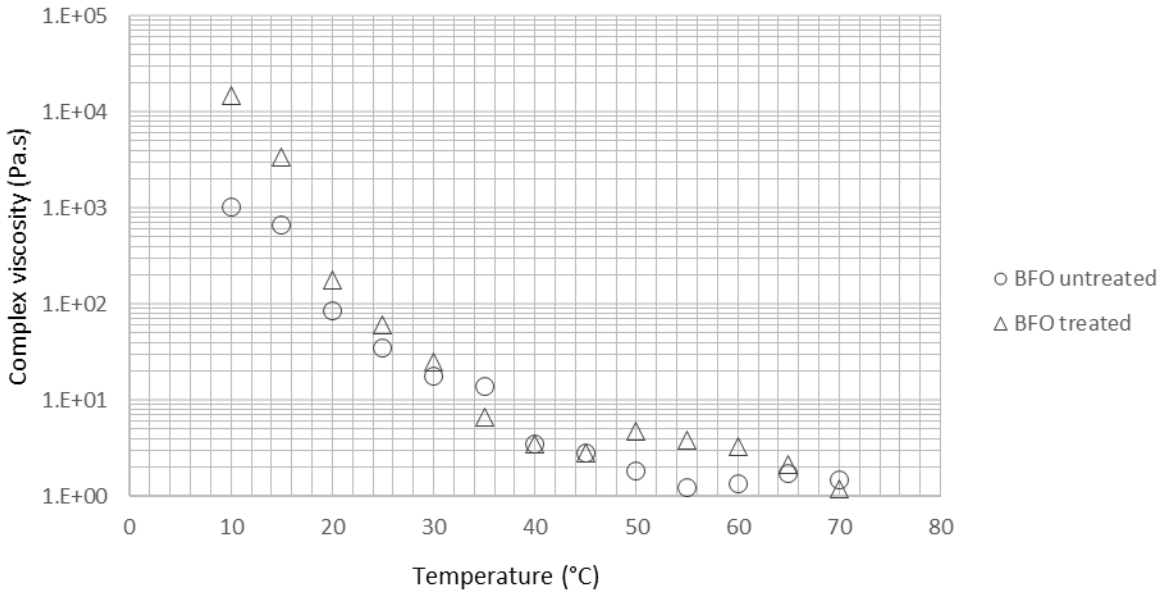

Figure 52: Viscosity-temperature relationship at 1 Hz for the BFO untreated and BFO treated starting materials.

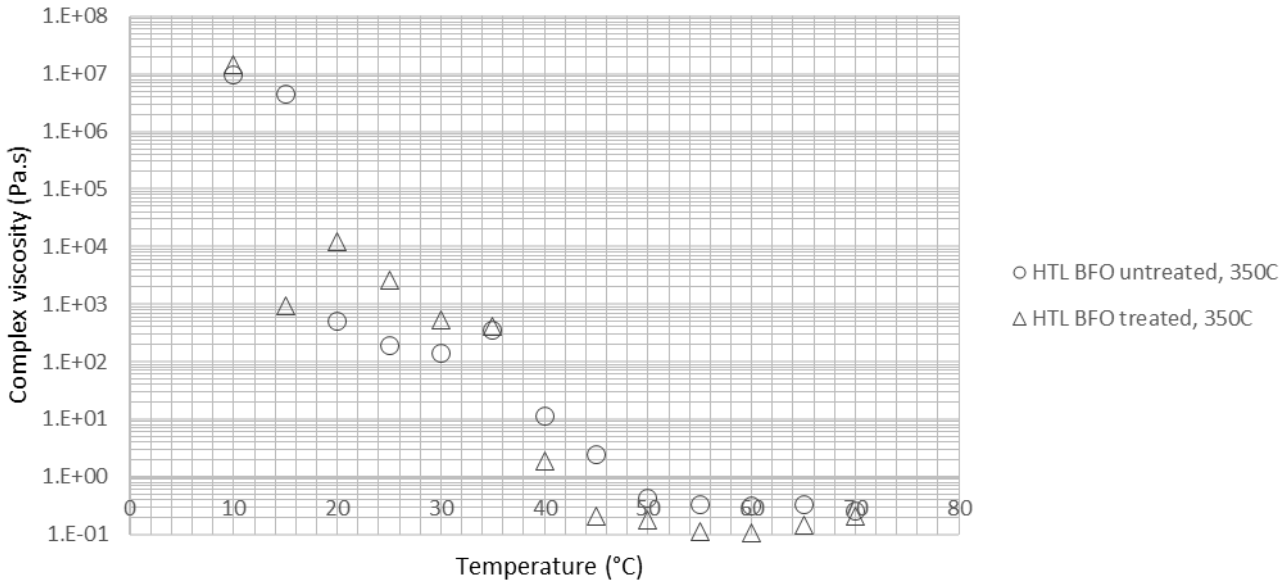

Figure 53: Viscosity-temperature relationship at 1 Hz for the liquefaction (HTL) BFO untreated and BFO treated products, obtained at 350 °C.

The complex viscosity-temperature plots for the pyrolysed samples from both treated and untreated BFOs are displayed in Figure 54 to Figure 56. For the product obtained at 275 °C after 5 hrs (Figure 54), the pyrolysed BFO from the untreated BFO has a much higher viscosity at 10 °C than that of the product obtained from the treated BFO (~3 orders of magnitude higher). Viscosities remain less than an order of magnitude higher until 25 °C for the pyrolysed BFO untreated. From 30 °C until 45 °C, both products display very similar viscosities, but at

the higher temperatures (50 °C onwards), the pyrolysed BFO treated exhibits slightly higher viscosities than those from the untreated product.

A similar trend is observed for the products obtained at 300 °C after 1 hr (Figure 55) to that of those from the 275 °C experiment, with two major differences. At 10 °C, the viscosities for both products are almost identical, with the pyrolysed BFO untreated product having just slightly lower viscosity. In the mid-range temperatures (25 – 35 °C), both pyrolysis products display more similar viscosities than at these temperatures for the 275 °C experiment.

The pyrolysis products obtained at 300 °C after 5 hrs produced the heaviest products out of the pyrolysis experiments, with the greatest mass losses observed (64.5% and 71.6% for BFO treated and untreated respectively). Overall, the product obtained from the untreated BFO during these conditions result in the highest viscosities across all the tested temperatures, except only at 20 °C, where the pyrolysed BFO treated has ~1 order of magnitude higher viscosity (Figure 56). There is a steady decrease in viscosities at temperature increases for the pyrolysed BFO untreated, whereas viscosities stabilise at around 50 °C and slightly increase towards 70 °C for the treated BFO product.

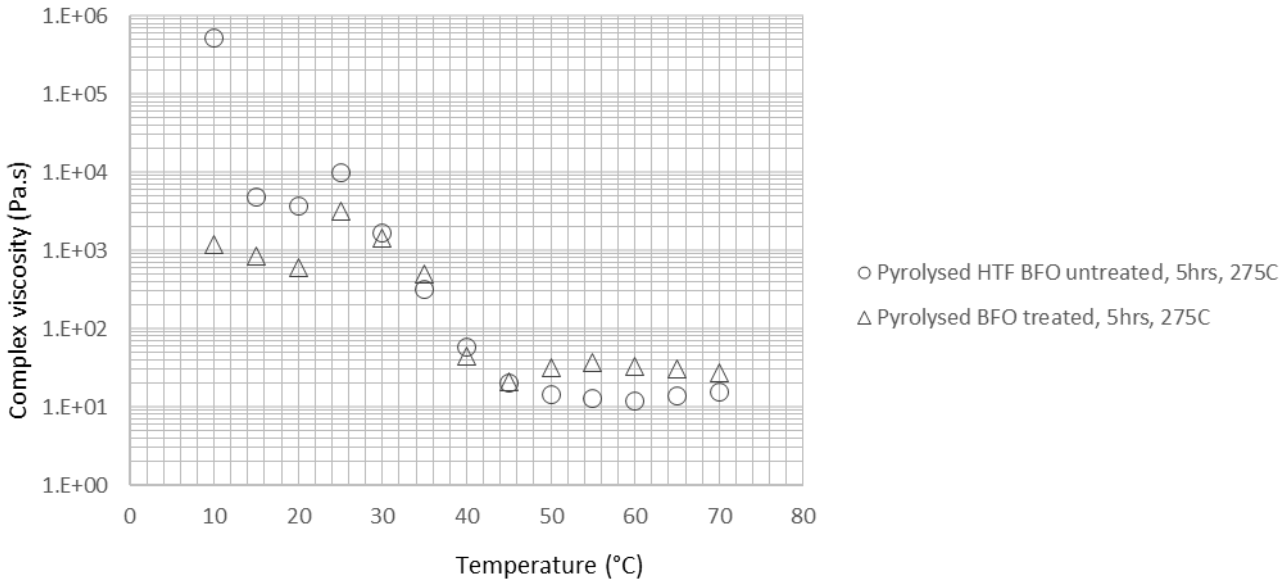

Figure 54: Viscosity-temperature relationship at 1 Hz for the pyrolysed BFO products obtained at 275 °C after 5 hrs, from both treated and untreated BFOs.

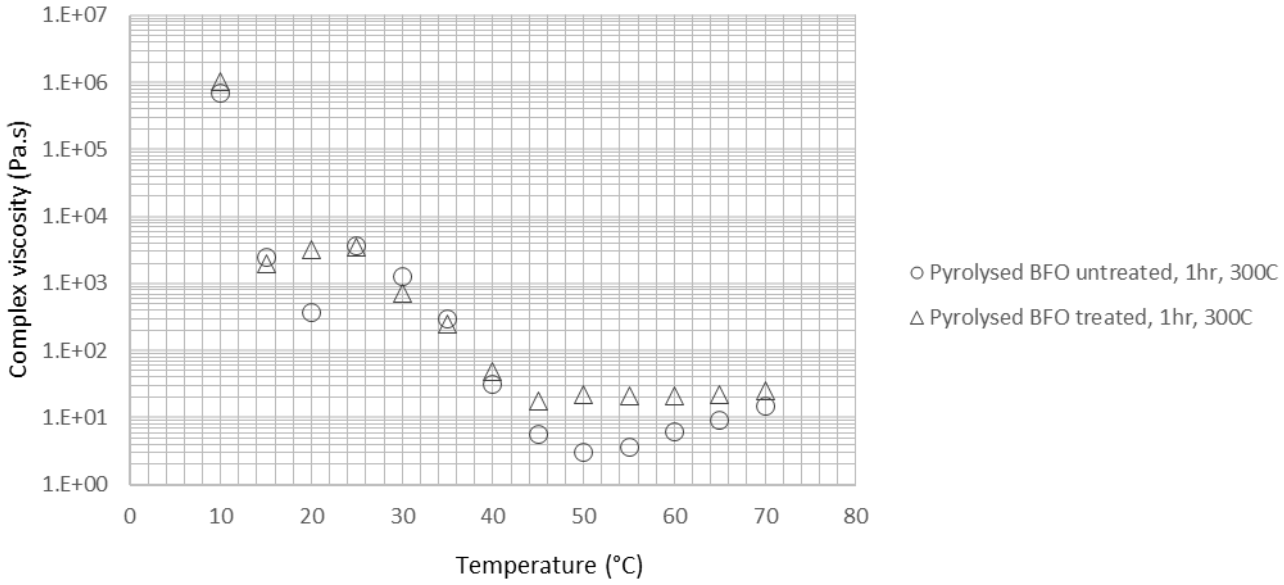

Figure 55: Viscosity-temperature relationship at 1 Hz for the pyrolysed BFO products obtained at 300 °C after 1 hr, from both treated and untreated BFOs.

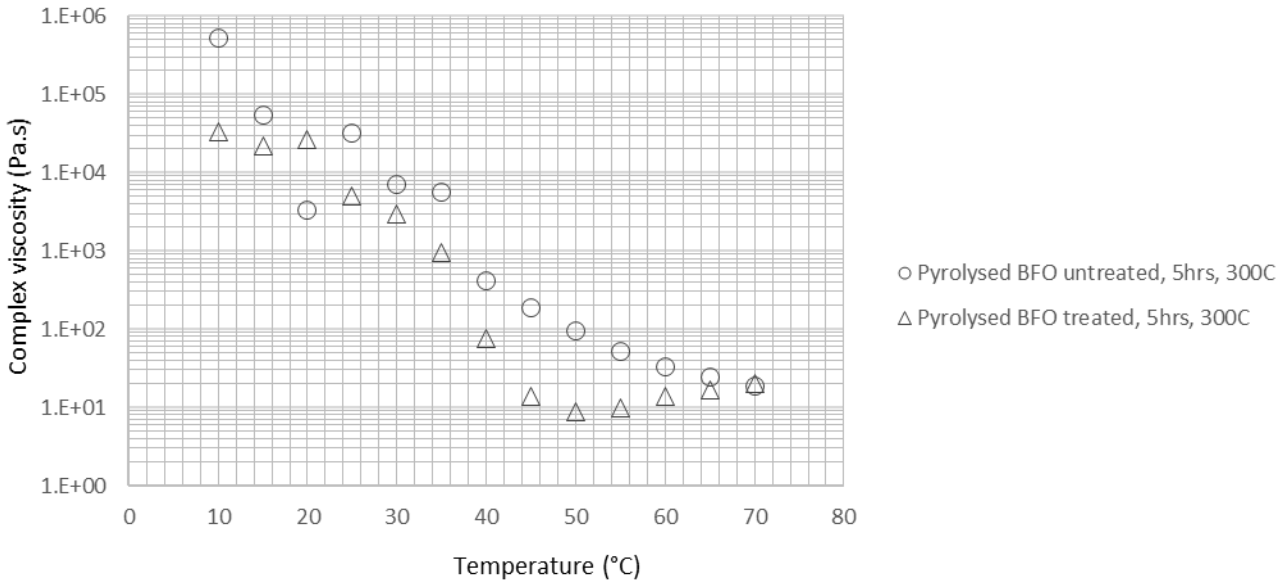

Figure 56: Viscosity-temperature relationship at 1 Hz for the pyrolysed BFO products obtained at 300 °C after 5 hrs, from both treated and untreated BFOs.

7.1.2. Comparison of viscosity profiles of BFO materials to conventional bitumens

For comparison, the two starting materials and their liquefaction products are compared to two conventional bitumen binders (10/20 and 20/30 pen) in Figure 57 and Figure 58, this time with the full range of frequencies from 0.1 to 10 Hz. It is obvious that both starting materials

are much softer materials (lower viscosities) compared to the control bitumens (Figure 57). The HTL products have similar viscosities at the lower temperatures to those of the bitumens, but very quickly lose their viscosity from 15 °C onwards (Figure 58).

All three of the pyrolysed BFOs obtained from the untreated BFO had greater mass losses during pyrolysis, indicating that a higher proportion of lighter ends were distilled off and a heavier product remained, compared to the treated BFO products. As a result, the products obtained from the untreated BFO were subsequently compared to complex viscosity-temperature plots of the two control bitumens (shown in Figure 59 to Figure 61). All pyrolysed products (from both treated and untreated BFOs) have higher viscosities than the starting materials. Interestingly, the product obtained at 300 °C after 1 hr (Figure 60) indicates lower viscosities at the higher temperatures (40 °C and above) compared to the two other pyrolysed BFO products (Figure 59 and Figure 61), which were done over 5 hrs. This suggests that in this case, reaction time has a considerable effect on distillation of lighter material, even more so than an increase in temperature. However, a higher temperature (300 °C) and longer reaction time (5 hrs) combined give the highest viscosities through all the temperatures tested and produced a more 'bitumen-like' material in terms of viscosity.

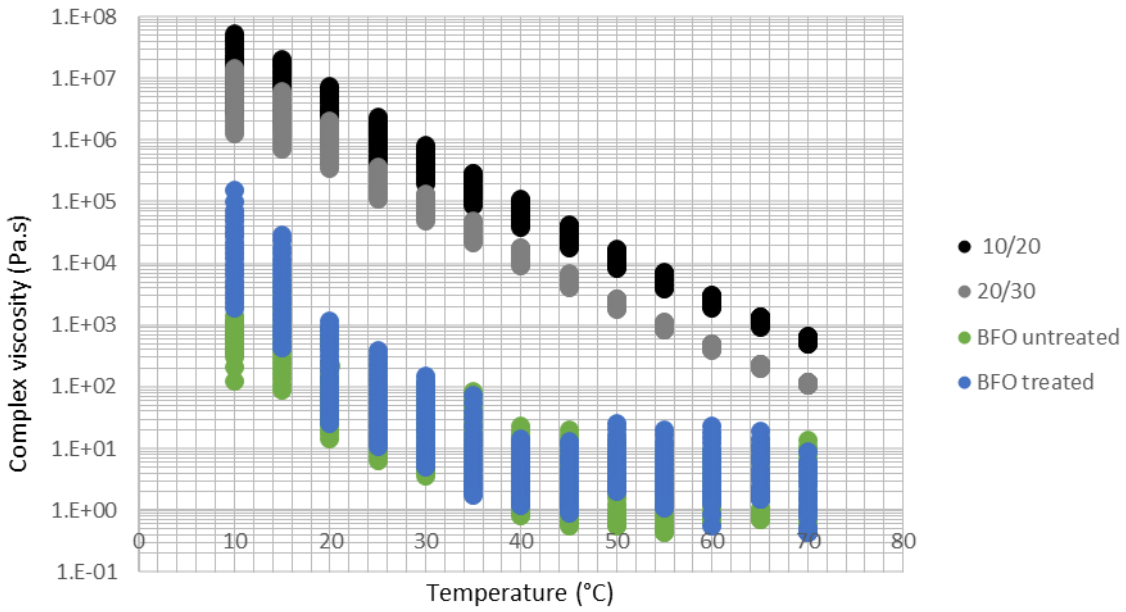

Figure 57: Viscosity-temperature relationship from 0.1 to 10 Hz for the BFO starting materials (treated and untreated) and two conventional bitumens, a 10/20 pen and a 20/30 pen binder.

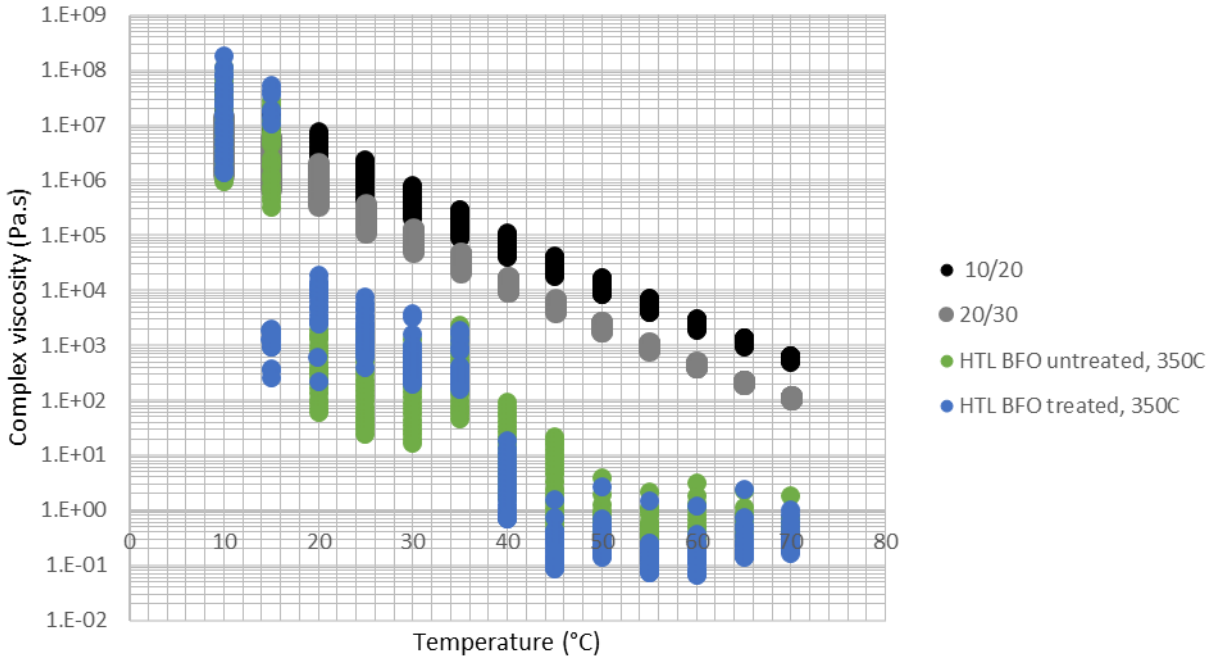

Figure 58: Viscosity-temperature relationship from 0.1 to 10 Hz for the HTL products obtained at 350 ° (treated and untreated) and two conventional bitumens, a 10/20 pen and a 20/30 pen binder.

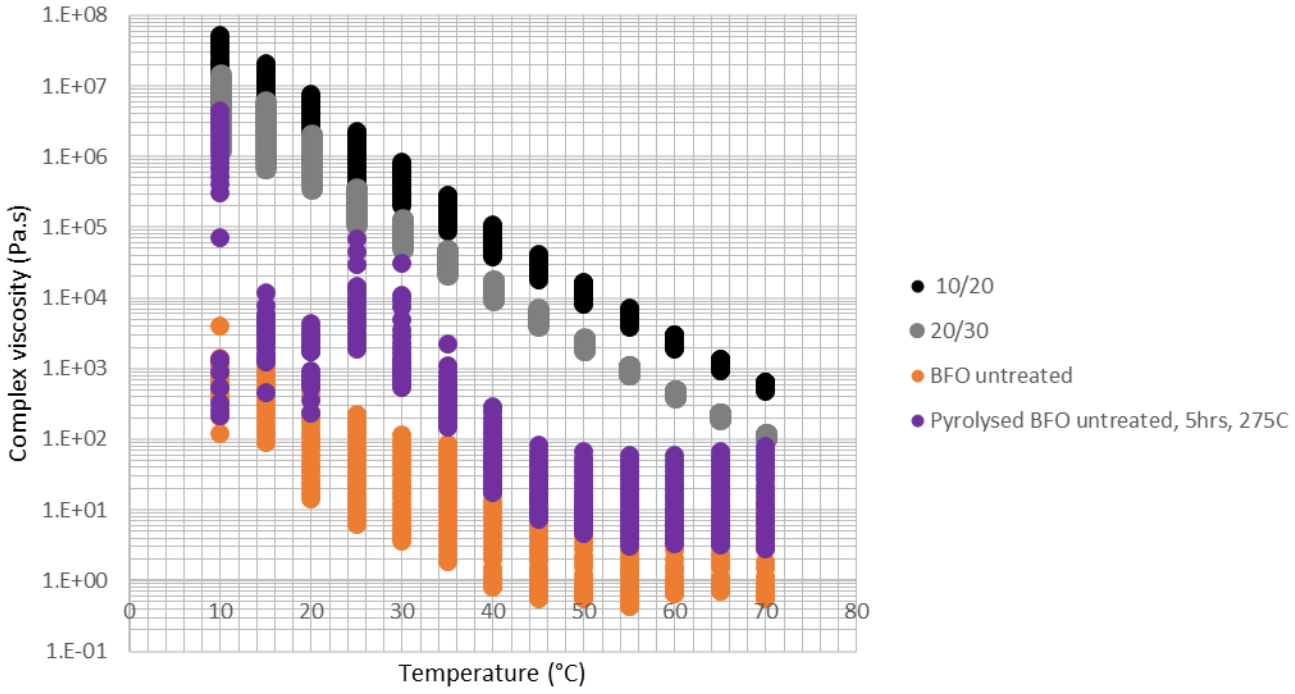

Figure 59: Viscosity-temperature relationship from 0.1 to 10 Hz for the pyrolysed BFO product obtained from the untreated BFO at 275 °C after 5 hrs, the BFO untreated starting material and two conventional bitumens, a 10/20 pen and a 20/30 pen binder.

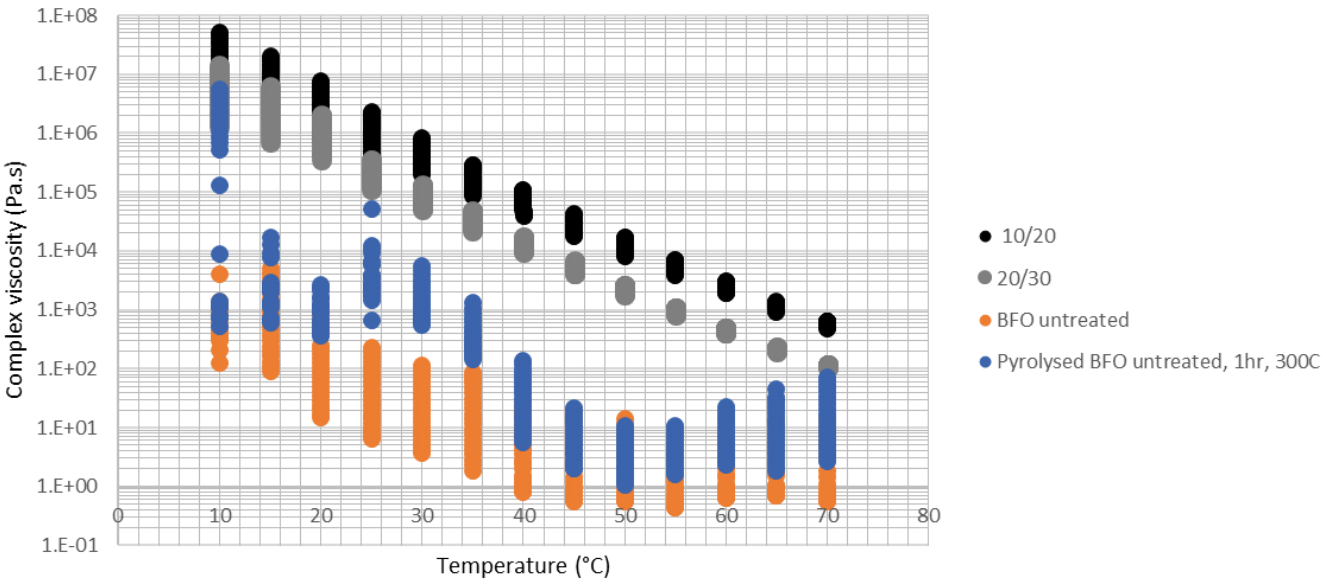

Figure 60: Viscosity-temperature relationship from 0.1 to 10 Hz for the pyrolysed BFO product obtained from the untreated BFO at 300 °C after 1 hr, the BFO untreated starting material and two conventional bitumens, a 10/20 pen and a 20/30 pen binder.

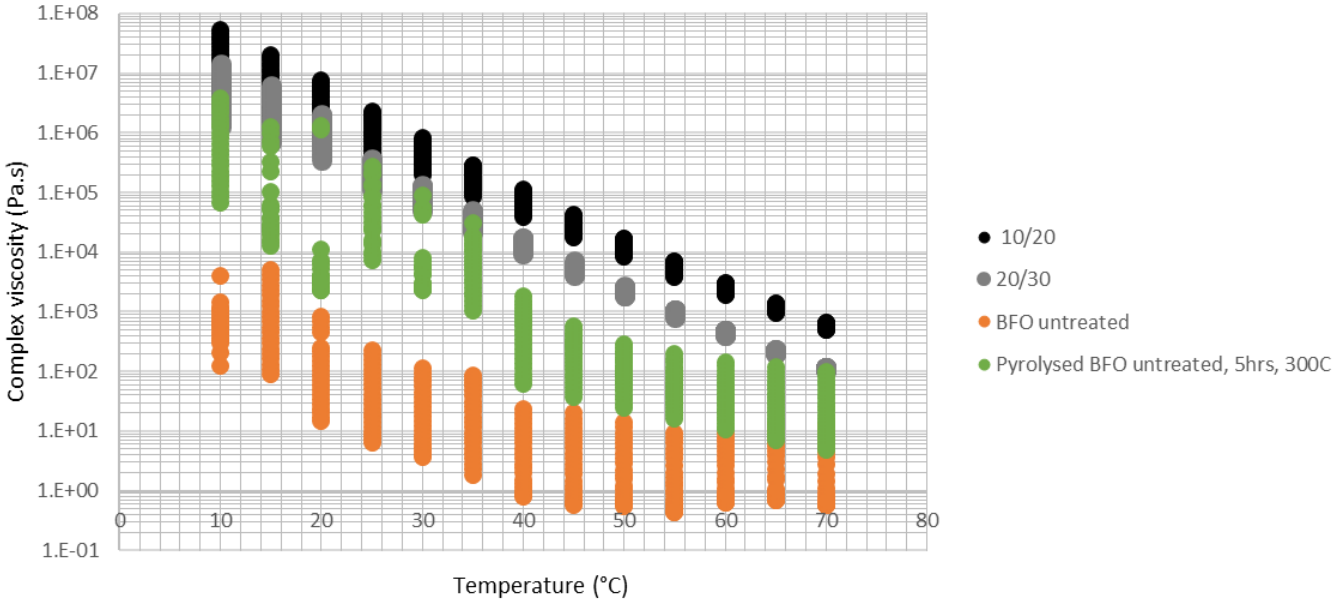

Figure 61: Viscosity-temperature relationship from 0.1 to 10 Hz for the pyrolysed BFO product obtained from the untreated BFO at 300 °C after 5 hrs, the BFO untreated starting material and two conventional bitumens, a 10/20 pen and a 20/30 pen binder.

7.2. Rotational viscosity results

Figure 62 and Figure 63 display the results of the viscosity of the BFO starting materials and liquefaction products respectively at different temperatures. For reference, viscosity values at 40 °C provided by the BFO's manufacturer, Argent Energy, are also shown on Figure 62. All

the materials display similar viscosity characteristics, with the BFO untreated sample having slightly higher viscosity than the treated BFO, with viscosities becoming essentially identical at the higher temperatures (80 and 100 °C). These results agree with Argent Energy's values at 40 °C, which show that the BFO treated is more fluid than the untreated at this temperature. However, at the lower temperatures (< 40 °C), the DSR results (Figure 52, Figure 57) show that treated BFO has higher viscosities, whereas the opposite is seen with the rotational viscosity results (at 25 °C). Despite this, the viscosity differences are very minimal. The HTL products (both treated and untreated) display even more similar viscosity trends with one another, but both have slightly lower viscosities than the starting materials at the measured temperatures. These observations agree with the DSR complex viscosity-temperature plots shown in section 7.1 above (as seen on Figure 57 and Figure 58). Additionally, the results agree with both the GC-MS and SIMDIS results in sections 6.3 and 6.6 respectively, which indicate that the HTL materials have a lower initial boiling point and a lower carbon chain FAME material than the initial BFOs.

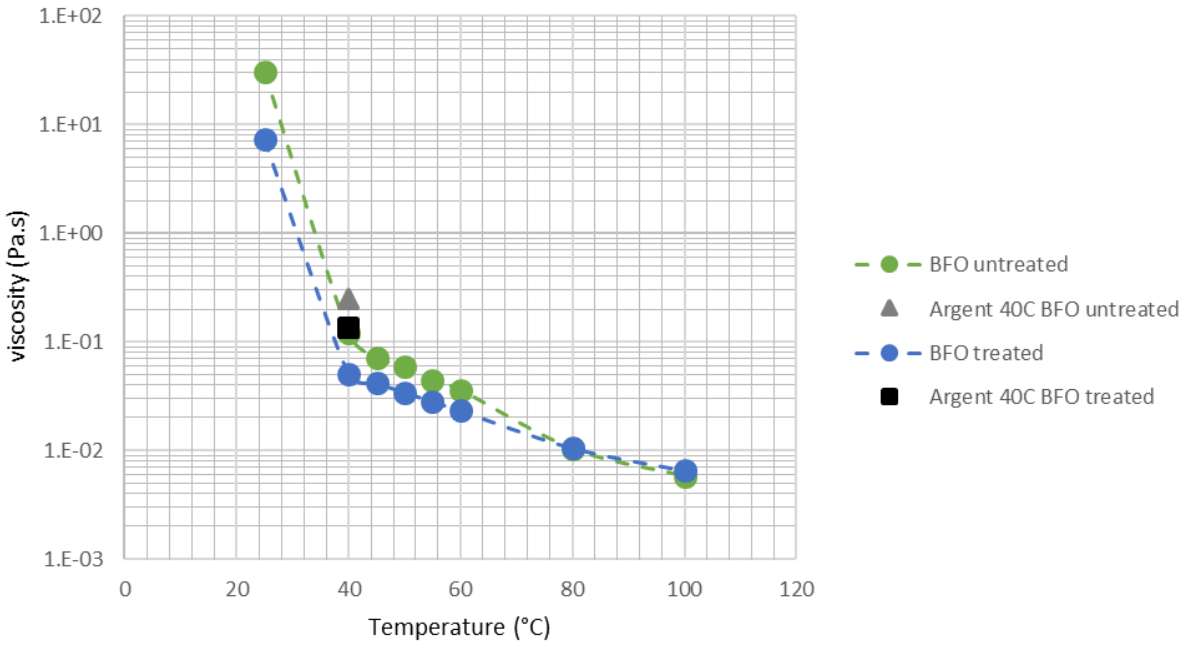

Figure 62: Starting materials' rotational viscosity results, as well as Argent Energy's provided viscosity value at 40 °C.

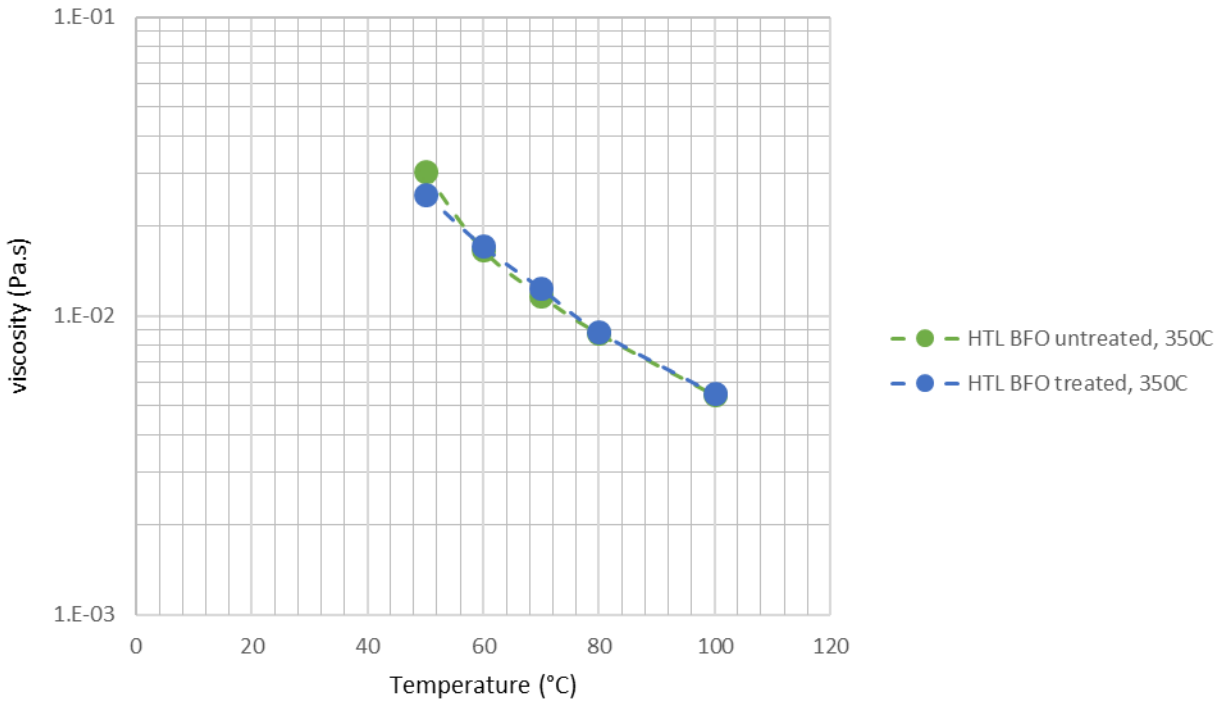

Figure 63: HTL BFO materials' rotational viscosity results.

7.3. Comparison of BFO with other oils

The BFO initial materials were subsequently compared to other oils to further understand their viscosity behaviour. The canola and sunflower oil data was taken from Fasina et al. (2006), and the basil oil was run as a control. The results in Figure 64 show that at the higher temperatures (above 40 °C), both the treated and untreated BFO behave more like conventional vegetable oils. At the lower temperatures, there is a distinct viscosity discrepancy between the BFOs and the other oils. The conventional oils see a gradual decline in viscosity from 20 °C onwards, whereas the BFOs see a steep decline from ambient temperature as their viscosity is initially much higher.

Table 29 displays these viscosities at 25, 55 and 80 °C, with the addition of the liquefaction products, sesame and corn oils and a biodiesel-derived product from waste cooking oil (from literature). The conventional vegetable oil and biodiesel-derived product were taken from Fasina et al. (2006) and Sun et al. (2016) respectively. The biodiesel by-product is described as a black and oily liquid (similar to what the BFO looks like).

The BFO starting materials display very high viscosities at 25 °C compared to the biodiesel-derived product from the literature. At 55 °C, the viscosities values are closer, but it is clear that the liquefaction materials are more closely aligned to the other oils than the initial BFO. At 80 °C, both the starting materials and the HTL products display lower viscosities than the conventional oils, with the HTL products having the lowest viscosities.

According to its manufacturer, the BFO is made up of a combination of waste material and so it does not come from a single origin. Perhaps at different temperatures, the viscosity value is determined by different dominating components within the material. At higher temperatures, the components in the BFO that are dominating the viscosity measurement align with the oils which behave in a similar way to a 'sunflower-like' oil. However, at the lower temperatures, something more viscous, perhaps a heavier waste fat, is determining this parameter.

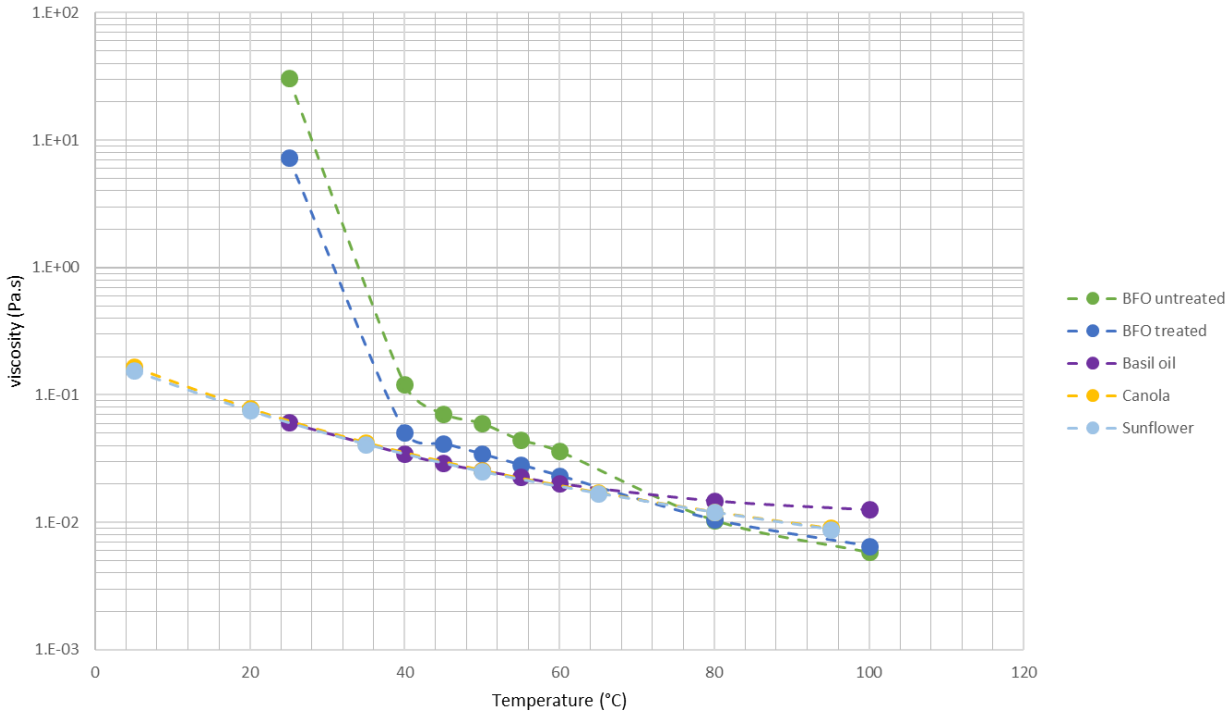

Figure 64: Starting materials' rotational viscosity results, compared against a basil-infused vegetable oil, canola and sunflower oils. Viscosity data for the canola and sunflower oils was acquired from Fasina et al. (2006).

Table 29: Viscosities (cP) of the BFO materials (starting materials/HTL products) and other vegetable and biodiesel-derived oils at different temperatures, adapted from Sun et al. (2016) and Fasina et al. (2006). X: not recorded.

Sample	Sample temperature (°C)		
	25	55	80
BFO untreated	30,759	60	10
BFO treated	7,346	34	11
BFO HTL untreated, 350 °C	x	30	9
BFO HTL treated, 350 °C	x	26	9
Sunflower	x	25	12
Sesame	x	25	12
Corn	x	23	11
Basil (control)	63	24	12
Biodiesel by-product from waste cooking oil	146	x	x

7.4. Viscosity of BFO materials as a function of shear rate

The two BFO starting materials and a basil-infused vegetable salad oil were further tested on the Brookfield to observe their viscosity changes with varying shear rate every 2 minutes. The results are presented in the form of viscosity vs shear rate plots below.

The Brookfield viscometer results present the control salad oil (Figure 65) as having non-Newtonian (shear-thinning) tendencies, as viscosity seems to decrease with increasing shear rate. This is unexpected as it has been clearly documented in literature that vegetable oils are Newtonian fluids (Hashempour-Baltork et al., 2018, Diamante and Lan, 2014).

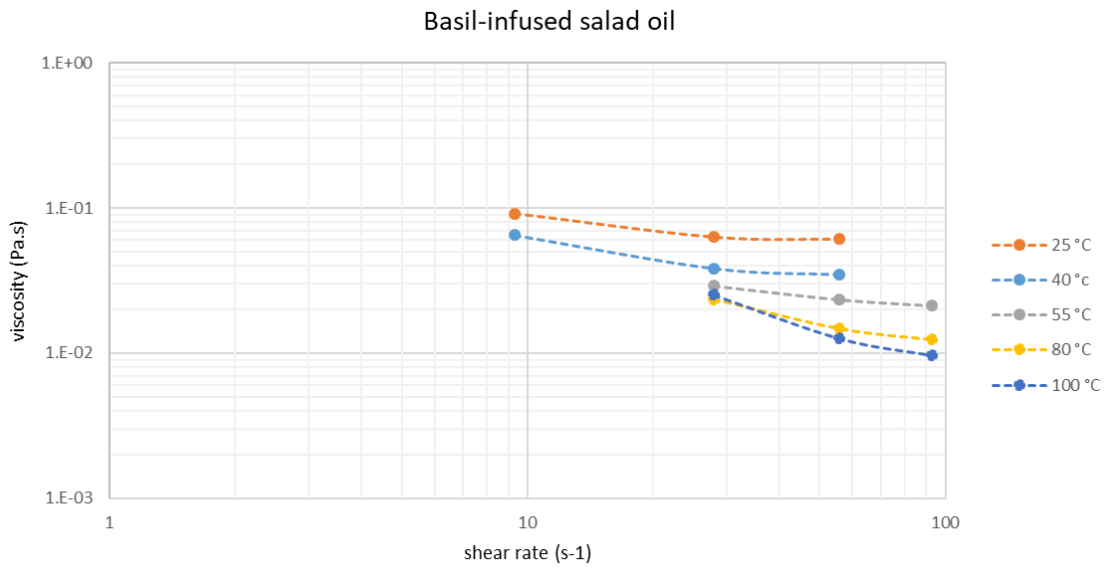

Figure 65: Rotational viscometry shear rate results for the basil-infused salad oil (control sample) from 25 to 100 °C.

A viscosity profile test was subsequently run on the Kinexus DSR in order to verify whether the salad oil was indeed Newtonian. The test was run from 25 to 140 °C using the cup and bob geometry, varying the shear rate from 0.1 to 100 s^{-1}. The results displayed on Figure 66 show a constant viscosity with increasing shear rates, confirming that the salad oil is Newtonian.

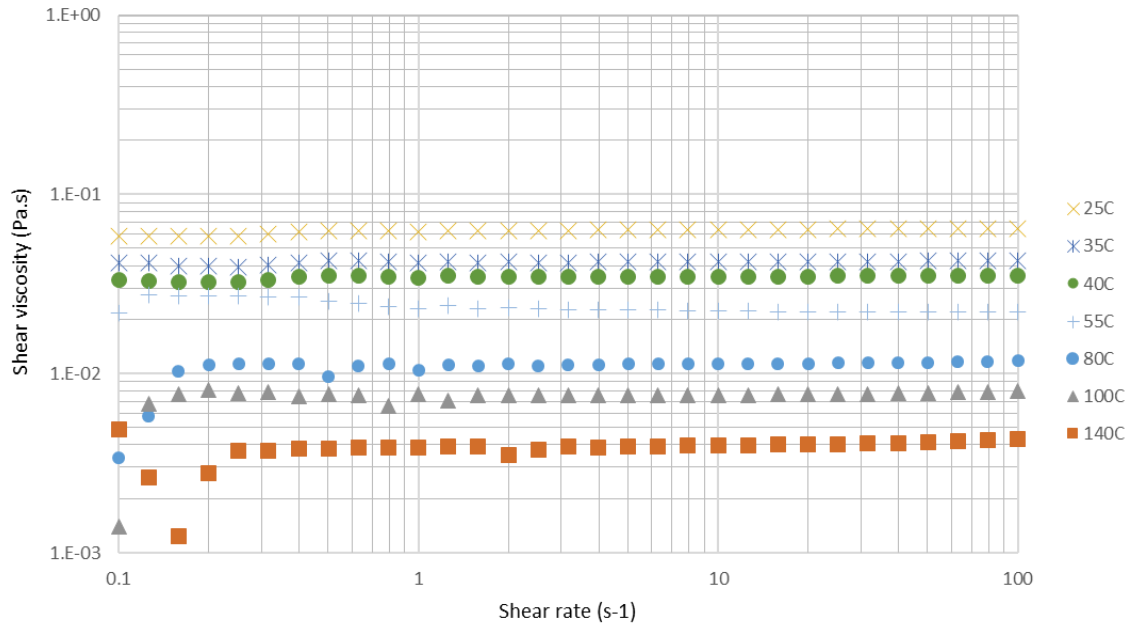

Figure 66: Salad oil viscosity profile DSR test using the cup and bob geometry, from 25 to 140 °C, with 0.1 – 100 $^{s-1}$ shear rates.

The BFO rotational viscosity shear rate results are shown in Figure 67 and Figure 68. The results from the 25 °C data are shown separately on Figure 69 for both BFOs, as these were done at much lower shear rates due to the low temperature. The gradients in the viscosity vs shear rate plots suggest non-Newtonian behaviour for the BFO materials. However, these gradients are generally very similar to the ones seen in the rotational viscosity results of the control salad oil above. For example, for the 80 °C temperature, when plotting the log of both shear rate and viscosity, a linear trend was found and the gradient measured for the BFO treated, untreated and the control basil oil (Figure 70). The gradients are all very similar, suggesting that, like the basil-infused salad oil, the BFO materials are also Newtonian. This gradient may be due to a testing artefact from the Brookfield equipment. As a result, the shear rate testing was not indicative of the BFO's fluid behaviour.

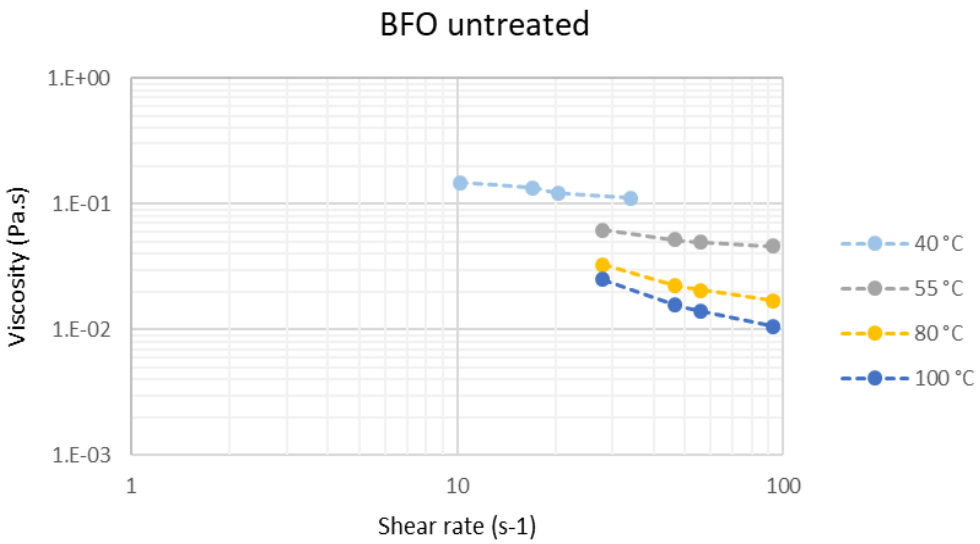

Figure 67: Rotational viscometry shear rate results for the BFO untreated starting material from 40 to 100 °C.

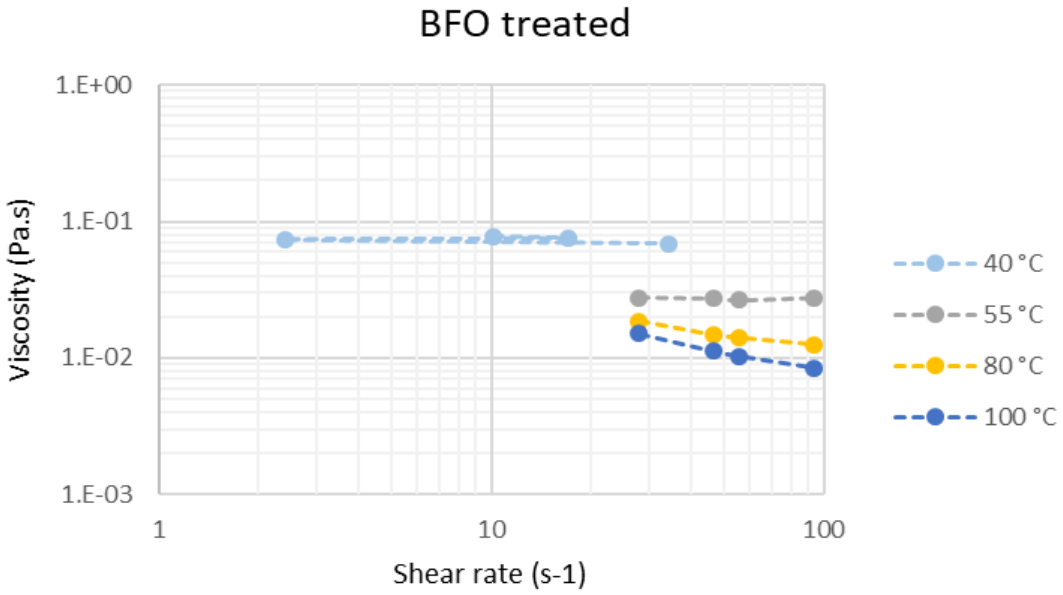

Figure 68: Rotational viscometry shear rate results for the BFO treated starting material from 40 to 100 °C.

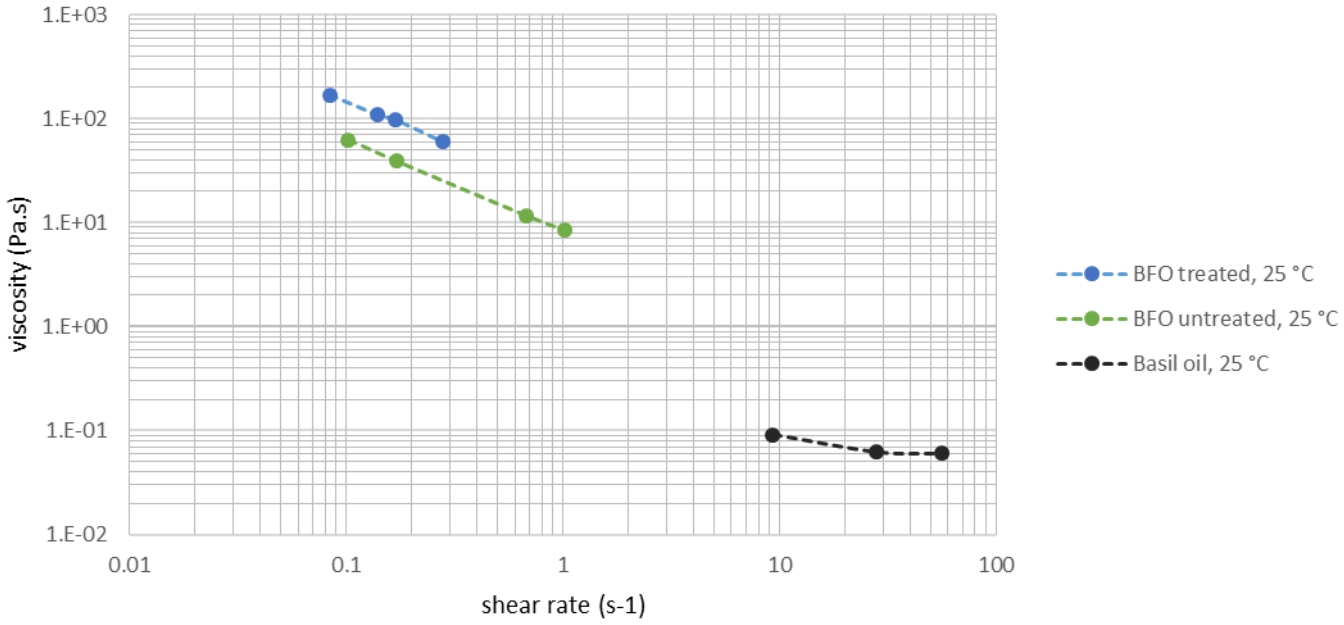

Figure 69: Rotational viscometry shear rate results for the BFO untreated and treated starting materials and the control salad oil at 25 °C.

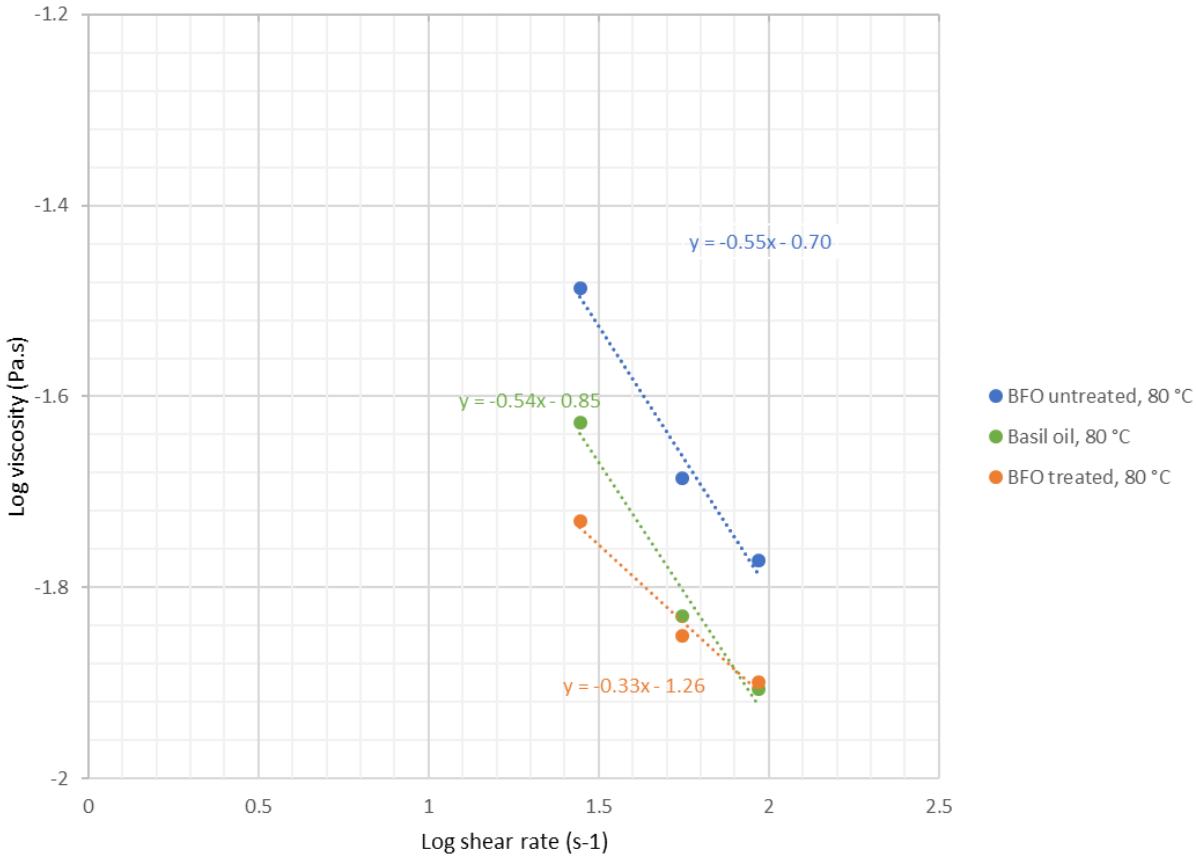

Figure 70: Log viscosity vs log shear rate results for the BFO treated and untreated and the control salad oil taking at 80 °C. The same shear rates were used to plot the results.

7.5. Key Points

- Although there are subtle differences, the viscosity pattern for both the treated and untreated BFO are the same as temperature increases.
- Argent Energy's treatment of the BFO does not alter the viscosity profile. This correlates with the chemical characterisation of the BFO materials (especially the GC-MS and ^{13}C NMR results), which display the similarities in chemical composition between treated and untreated BFO.
- The HTL treated materials display a similar pattern of behaviour. At low temperatures, both the liquefied products display high viscosities but from 40 °C onwards, they exhibit the lowest viscosities, with the treated liquefied BFO displaying slightly lower viscosities.

- In general, the highest viscosities are seen with the pyrolysed BFO samples. The product obtained at 300 °C after 5 hrs from the untreated BFO, which produced the greatest mass loss, had the highest viscosities overall.
- Rotational viscosity results confirm that the liquefied products are lower viscosity than the BFO starting materials. Although more viscous at ambient temperature, the BFO (both treated and untreated) display similar viscosities at high temperatures to conventional oils like canola and sunflower. The BFO materials follow a similar pattern of viscosity to conventional vegetable oils therefore it is likely to be Newtonian.

8. Rheological characterisation of blended bitumens with BFO

The first BFO-bitumen blends to be studied in terms of rheological and ageing properties are presented in Table 30.

Table 30: Composition of BFO and bitumen blends.

Blend name	Bitumen type	BFO type	BFO content
B10T+10/20	10/20 pen	Treated	10%
B10U+10/20	10/20 pen	Untreated	10%
B5T+20/30	20/30 pen	Treated	5%
B5U+20/30	20/30 pen	Untreated	5%
B2.5T+20/30	20/30 pen	Treated	2.5%
B2.5U+20/30	20/30 pen	Untreated	2.5%

Figure 71 shows the complex modulus master curves comparing the treated and untreated blends (10% BFO with 10/20 pen bitumen) as well as the 2S2P1D predicted complex modulus master curves of various control penetration grade bitumens (solid lines in plot). The untreated BFO blend (B10U+10/20) has the lowest G* values (lowest stiffness) with a softer consistency than the control 100/150 pen bitumen (probably equivalent to a 160/220 pen bitumen). The treated blend (B10T+10/20) has higher complex modulus values over the master curve frequency range and is almost identical to a 70/100 pen bitumen. In this instance, the treatment of the BFO has resulted in a higher viscosity (higher stiffness) oil that has softened the 10/20 pen base bitumen to a considerably lesser extent than the lower viscosity untreated BFO. This has affected the final rheology of the blends and resulted in the higher complex modulus master curve demonstrated by the B10T+10/20 blend relative to the B10U+10/20 blend.

The same trends are observed for the B5+20/30 and B2.5+20/30 blends in Figure 72 but are evidently not as marked due to the lower content of BFO. B5U+20/30 has the lowest stiffness (lower G* values), most similar to a 100/150 pen bitumen, whereas its treated counterpart resembles the 70/100 pen bitumen control. The change in stiffness is less obvious with less modification in the binders, although in all the blends, the untreated BFO blends are less stiff than the treated BFO blends. Of the four BFO biobinder blends shown in Figure 72, B5T+20/30 and B2.5U+20/30 show almost identical complex modulus master curves due to the combined effects of BFO dosage and BFO consistency (viscosity). The higher dosage of the higher

viscosity treated BFO having the same softening effect on the 20/30 pen base bitumen as the lower dosage but lower viscosity untreated BFO.

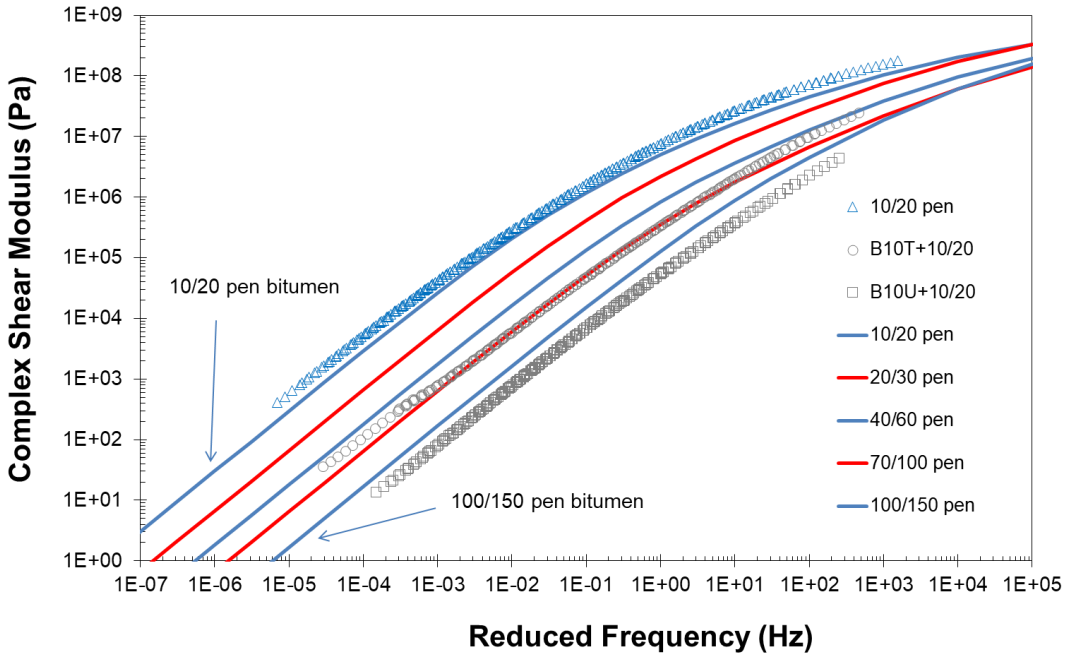

Figure 71: Complex modulus master curves at a reference temperature of 25°C for BFO binder blends with 10/20 pen bitumen.

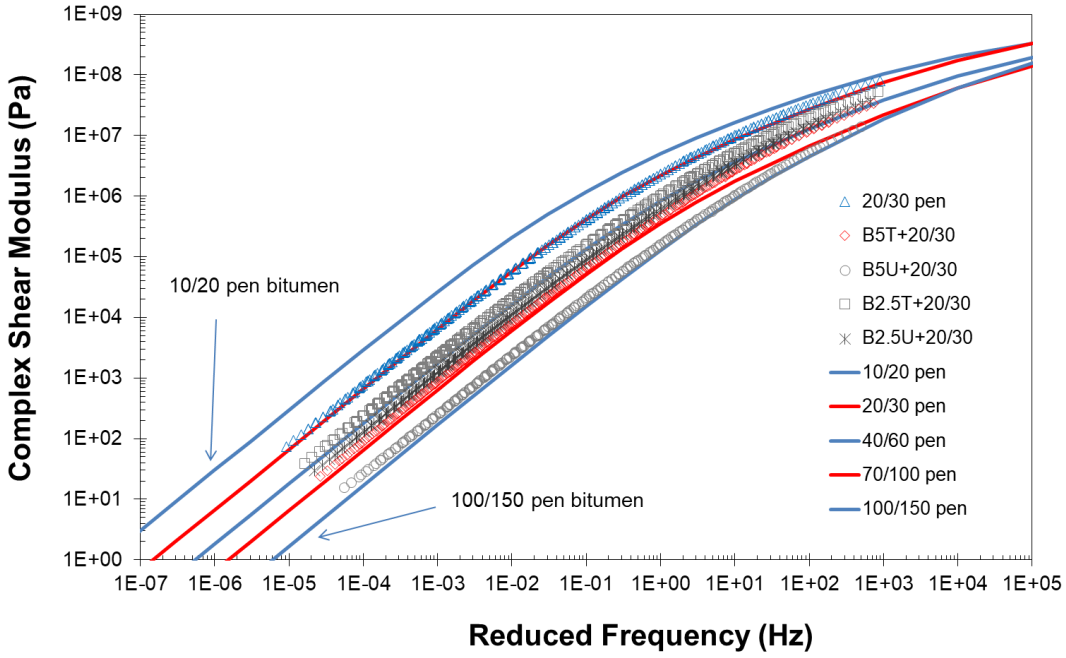

Figure 72: Complex modulus master curves at a reference temperature of 25°C for BFO binder blends with 20/30 pen bitumen.

In regard to the phase angle (viscoelastic balance), master curves are shown in Figure 73 and Figure 74 for the biobinder blends as well as the 2S2P1D predicted phase angle master curves

of various control penetration grade bitumens (solid lines in plot). All the treated blends display similar phase angle values at the higher temperatures (lower frequencies), with an increase in viscous response (phase angles approaching 90°) as the percentage of BFO increases (Figure 73). All three blends fall between the phase angle master curves of the 100/150 pen and 70/100 pen control bitumens. A more elastic response (lower phase angles) is seen at the lower temperatures (higher frequencies), with B2.5T+20/30 displaying the most elastic rheological response, similar to that of a 70/100 pen bitumen.

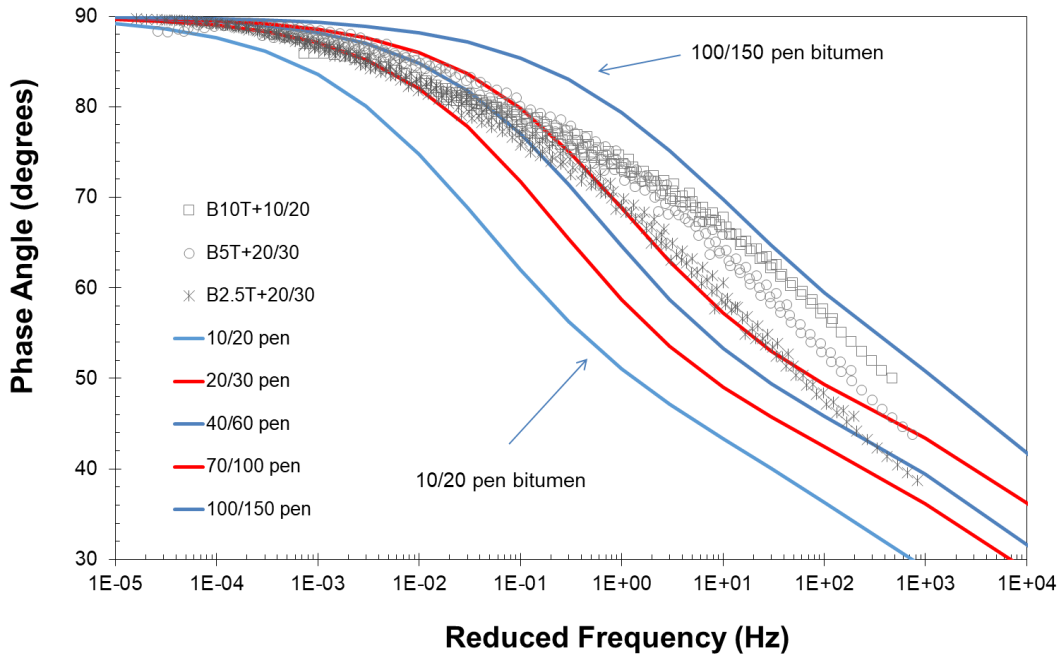

Figure 73: Phase angle master curves at a reference temperature of 25°C for BFO treated binder blends.

A similar increase in viscous rheological response with increasing BFO content is also seen with the untreated blends (Figure 74), although the master curves are less grouped together than the treated samples indicating a wider range of rheological behaviour for these BFO blends. B10U+10/20 reveals the highest viscous response over a wide range of frequencies, whereas B5U+20/30 mimics the response of the 100/150 pen bitumen. The similarities between the 70/100 pen bitumen and B2.5U+20/30 are not as marked at the lower temperatures as compared to B2.5T+20/30.

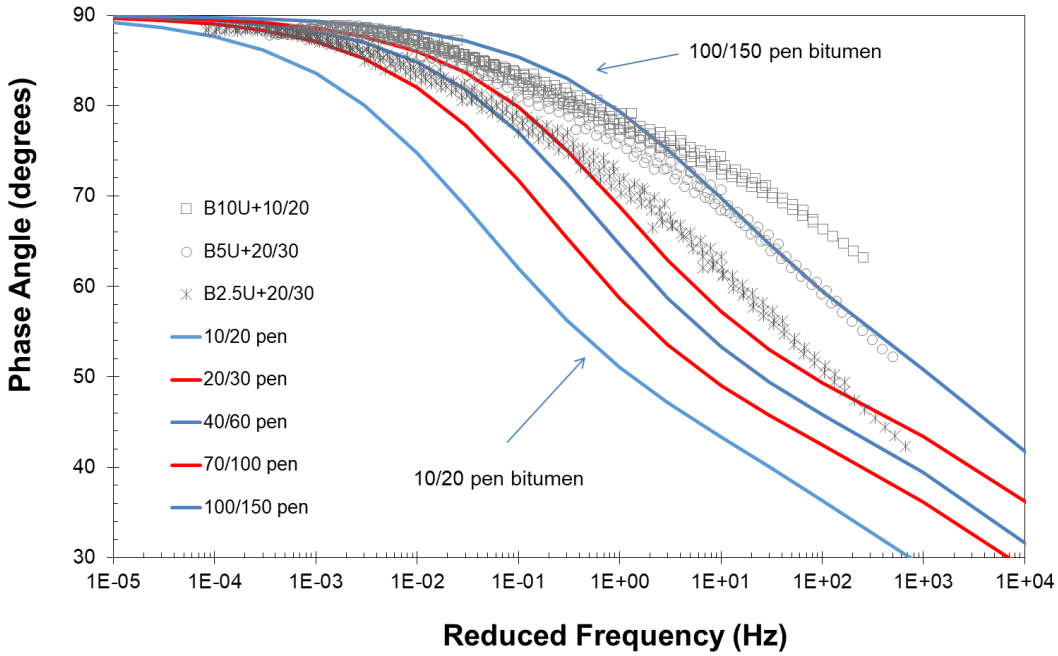

Figure 74: Phase angle master curves at a reference temperature of 25°C for BFO untreated binder blends.

All the untreated samples have a higher viscous component than the treated ones. Similarly to stiffness, the less modified the blend, the more similar to the controls the results seem to be. The BFO modification results in an overall increase in viscous response (increased phase angles) and lower stiffness values than the two base bitumens (10/20 pen and 20/30 pen). Other biodiesel-based biobinders have shown similar rheological performance when blended with bitumen at <10%, having therefore the potential to improve low temperature performance and fatigue resistance in comparison to base bitumens (Sun et al., 2016, Gong et al., 2016). In particular, these are two of the desired properties for rejuvenators that are used in recycled asphalt mixtures in order to rejuvenate recycled asphalt (RA) (Hill et al., 2018, Hill et al., 2013, Jiménez del Barco Carrión et al., 2015), revealing that the studied BFO could be a suitable rejuvenator for RA.

8.1. Changes in rheological properties after ageing

8.1.1. Predicted conventional blend properties

Table 31 shows the results for the predicted penetration and softening point for the BFO blends and base bitumens. The predicted softening point is shown as the average of the values obtained at 0.16 Hz and 1.6 Hz (maximum relative standard deviation of 2.22%). The

penetration and softening point results are presented for the unaged binders as well as after RFTOT and PAV ageing. Similar to conventional binders, there is a consistent decrease in penetration and increase in softening point temperatures for all the biobinder blends.

Table 31: Conventional properties of biobinder blends.

Binders	Predicted penetration at 25 °C (dmm)			Predicted softening point (°C)		
	Unaged	RTFOT	PAV	Unaged	RTFOT	PAV
10/20 pen	13.0	9.1	7.6	66.9	73.1	78.0
20/30 pen	25.1	18.2	11.8	55.3	61.3	68.3
B10T+10/20	71.1	48.4	32.5	47.9	53.9	59.6
B10U+10/20	184.4	74.3	40.2	38.0	48.9	58.3
B5T+20/30	60.3	38.1	24.4	46.5	52.9	59.0
B5U+20/30	106.1	50.5	28.5	42.8	49.7	57.9
B2.5T+20/30	39.6	26.6	17.7	50.2	56.7	63.1
B2.5U+20/30	51.7	25.8	18.5	48.3	55.7	61.8

The changes in penetration and softening point are shown graphically in Figure 75 and Figure 76. With ageing, predicted penetration and softening point values decrease and increase respectively, corresponding to the oxidative hardening effect of conventional bitumens. For the blends with an addition of 10% BFO, the untreated blend (B10U+10/20) shows the most drastic change in penetration and softening point (Figure 75) from ~ 184 dmm unaged to ~ 40 dmm PAV aged (softening point from 38 °C to 58 °C). B10T+10/20 has a similar range of change to that of the 10/20 pen base bitumen, although much higher penetration values and lower softening points. Both blends have a much softer consistency than the harder 10/20 pen binder, with a predicted penetration similar to that of a 70/100 pen bitumen for the treated, and a 160/220 pen for the untreated blend.

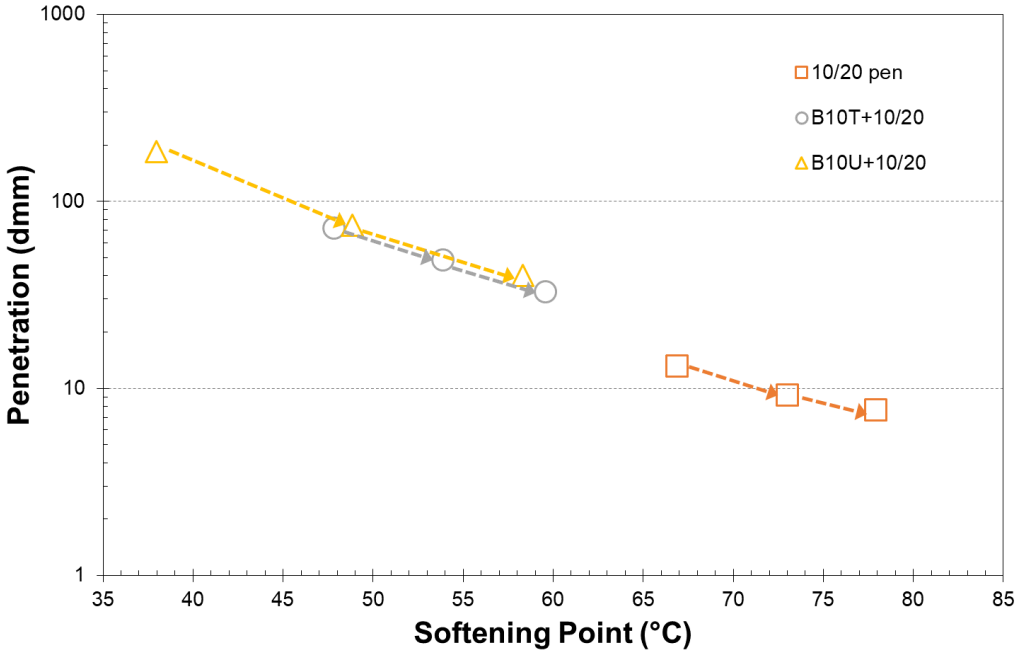

Figure 75: Changes in penetration and softening point with RTFOT and PAV ageing for BFO blends produced with a 10/20 pen bitumen.

Similarly, the untreated blends with the lower BFO contents also demonstrate severe changes with RTFOT and PAV ageing (Figure 76). The use of a linear penetration scale in Figure 76 allows the severe changes for the untreated BFO blends with ageing to be identified. The changes in penetration and softening point decrease with decreasing BFO content with the relative changes in penetration and softening point being more consistent with those shown for the control 20/30 pen bitumen.

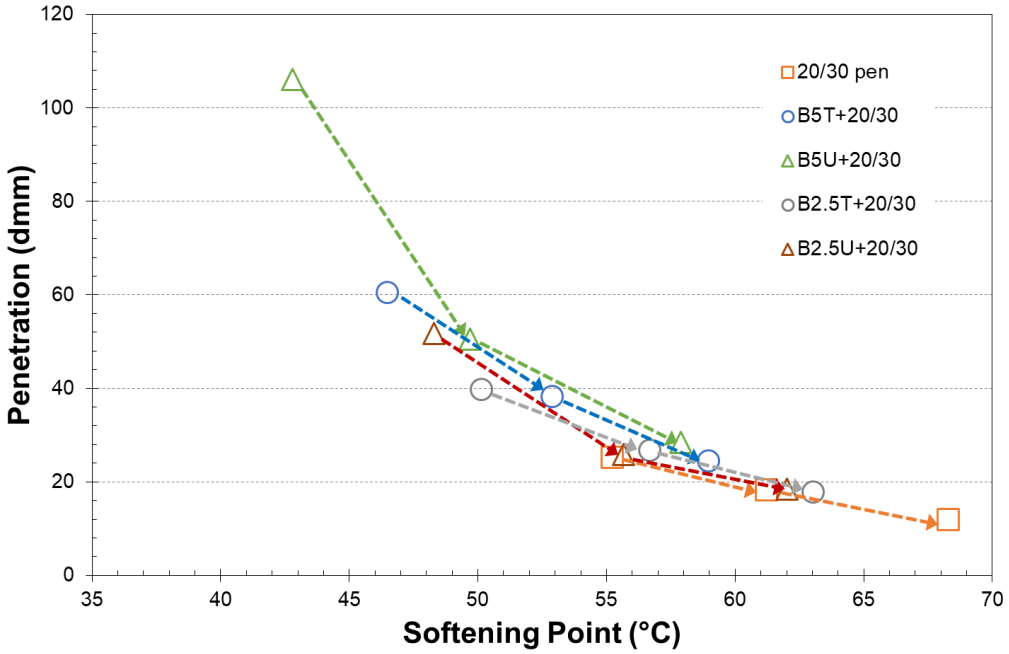

Figure 76: Changes in penetration and softening point with RTFOT and PAV ageing for BFO blends produced with a 20/30 pen bitumen.

8.1.2. Complex modulus and phase angle changes with ageing

For conventional bitumens, the effect of oxidative ageing is seen as a constant increase in complex modulus and decrease in phase angles as demonstrated in rheological master curves and a combined increase in G* with a shift in the Black Space diagram curves towards lower phase angles (Airey and Brown, 1998). As a result, the rheological behaviour after ageing consists of an increase in stiffness and a greater proportion of elastic behaviour (rheological response) compared to the unaged binder (Airey, 2002b).

The effect of ageing is shown in the form of complex modulus and phase angle master curves for samples modified with 5% BFO (B5T+20/30 and B5U+20/30) in Figure 77 and Figure 78. Similar plots were produced for the 10% and 2.5% BFO binders but have not shown here for brevity. In all the samples, the complex modulus increases and the aged binders become more elastic (lower phase angles) at the lower temperatures (higher frequencies), indicating a similar hardening effect to that of petroleum bitumens (Airey, 2003). The significant difference between the treated and untreated BFO binders in Figure 77 and Figure 78 is the greater change (differences between) the complex modulus and phase angle master curves

for the untreated BFO binders (B5U+20/30 in this case). Overall the changes in the rheological properties are not as marked as biobinder content decreases.

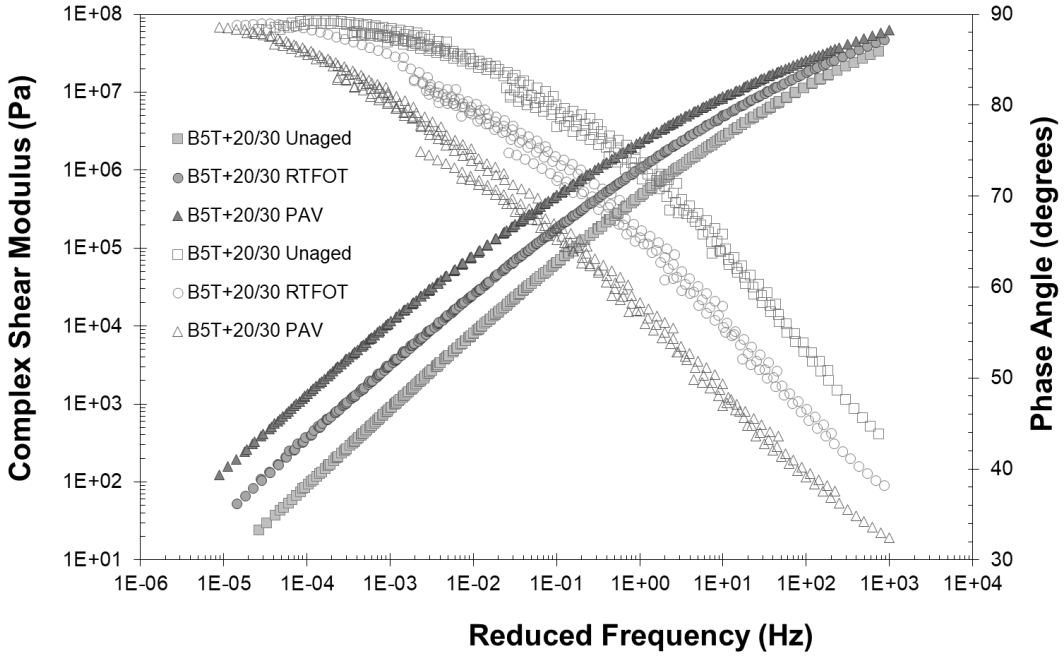

Figure 77: Complex modulus and phase angle master curves at a reference temperature of 25°C for unaged, RTFOT and PAV aged BFO treated binders at 5% BFO content.

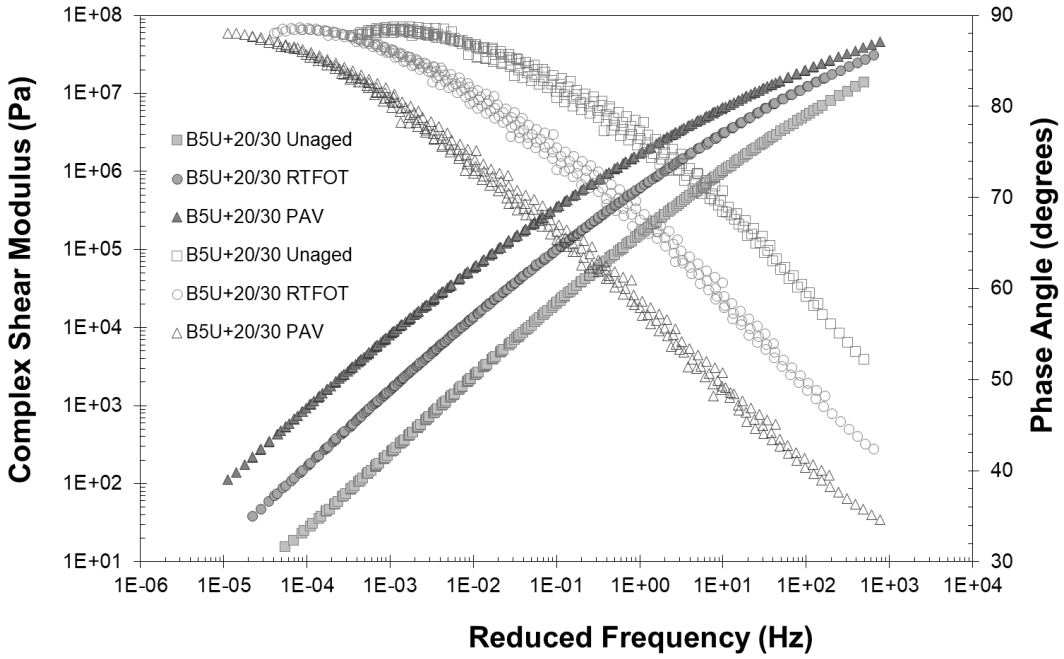

Figure 78: Complex modulus and phase angle master curves at a reference temperature of 25°C for unaged, RTFOT and PAV aged BFO untreated binders at 5% BFO content.

8.1.3. Ageing indices

Bitumen ageing can be evaluated (quantified) by means of an ageing index, which is defined as the ratio of a physical/rheological parameter of the aged bitumen to that of the unaged bitumen. Higher values of the ratio typically indicate a higher degree of hardening for conventional bitumens (Lu and Isacsson, 1998), which has also been observed for both polymer modified bitumens and bio-modified bitumens (Lu and Isacsson, 1998, Yang et al., 2013). Ageing indices based on predicted softening point (SP) and complex modulus values obtained during DMA (G* values @ 20 °C and 60 °C both at a loading frequency of 10 Hz) are illustrated in Figure 79 to Figure 81 for the three sets of BFO content.

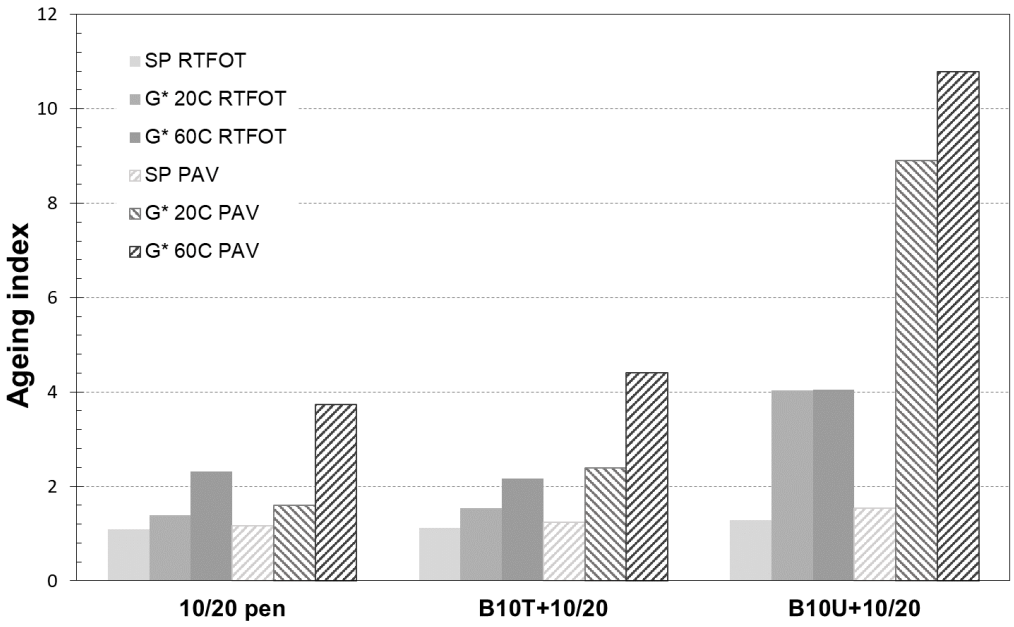

Figure 79: Ageing indices based on softening point and complex modulus rheological parameters for BFO treated and untreated binder blends at 10% BFO content.

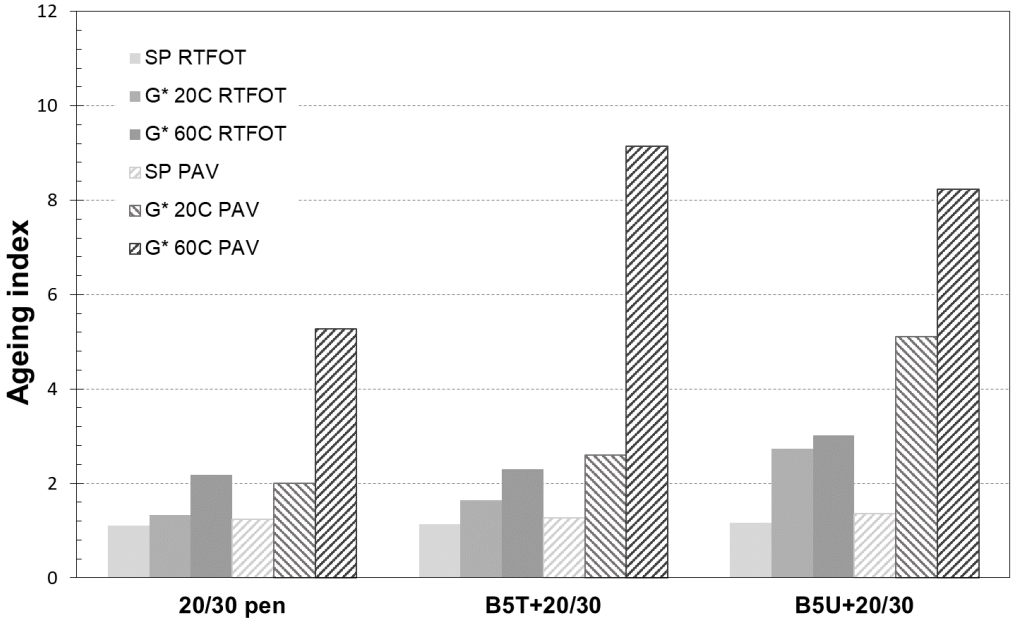

Figure 80: Ageing indices based on softening point and complex modulus rheological parameters for BFO treated and untreated binder blends at 5% BFO content.

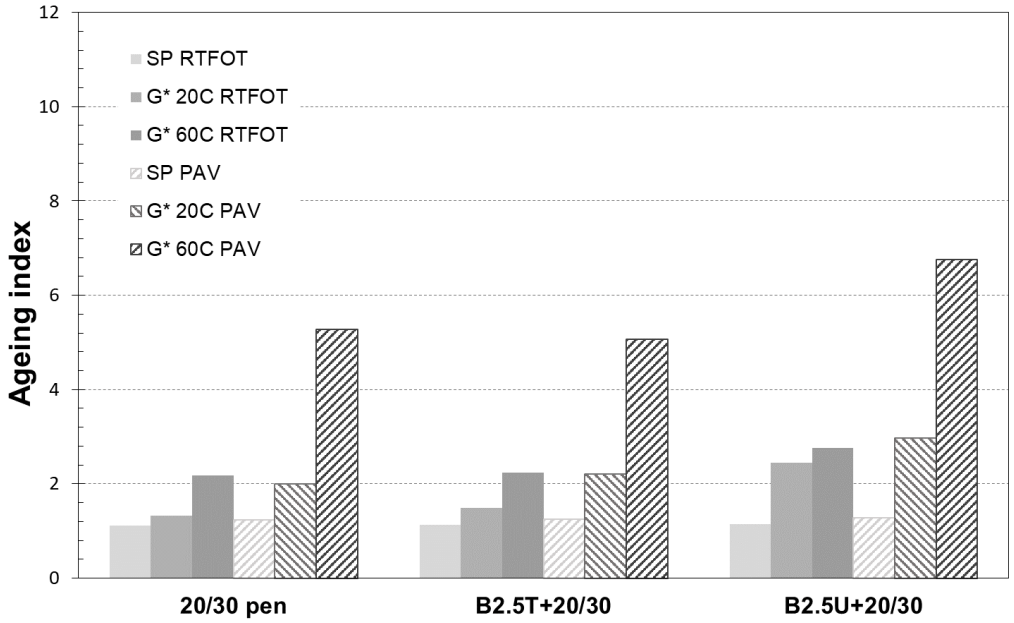

Figure 81: Ageing indices based on softening point and complex modulus rheological parameters for BFO treated and untreated binder blends at 2.5% BFO content.

The untreated blend at 10% BFO addition (B10U+10/20) shows the highest ageing indices after RTFOT and PAV ageing across the entire binder data set and for all three rheological parameters (SP as well as G* @ 20 °C and 60 °C). Figure 79 shows that the ageing indices for

B10T+10/20 are similar to those seen for the control 10/20 pen bitumen and considerably less than B10U+10/20. As expected, the ageing indices calculated for the three different rheological parameters differ in terms of the actual values as also seen by other researchers (Lu and Isacsson, 2002, Wu et al., 2014, Wu and Airey, 2009). The results also support the general trend that ageing indices tend to be higher for softer (higher penetration grade) binders compared to harder (lower penetration grade) binders (Wu and Airey, 2009, Wu et al., 2014).

With regards to the G* ageing indices, a higher degree of ageing is seen at the higher temperature of 60 °C compared to the values seen at 20 °C. In general, lower ageing indices are seen as the biobinder concentrations decrease as shown in Figure 80 and Figure 81. It is also clear that at the same BFO level, binders with treated BFO have tended to have lower ageing indices than those with untreated BFO.

As the rheological master curves showed that binders B5T+20/30 and B2.5U+20/30 are very similar in terms of their rheology (also shown in terms of predicted penetration and softening point in Table 31), it is interesting to compare their degrees of ageing. Both binders show similar ageing indices after RTFOT and PAV ageing in terms of all three rheological parameters (SP and G* @ 20 °C and 60 °C). This would indicate that the ageing of the BFO biobinder blends is consistent for similar rheological property blends irrespective of how the blends were produced (increased BFO dosage for higher viscosity BFO or decreased dosage for lower viscosity BFO). Overall, the two base bitumens (10/20 pen and 20/30 pen) showed the lowest levels of ageing (lowest ageing indices).

Relationships between the different ageing indices have been compared in terms of age ranking in Table 32 with a ranking of '1' given for the highest ageing index (most ageing) and '8' for the lowest (least ageing). Regardless of the parameter used to measure the ratio, the untreated blend with 10% BFO (B10U+10/20) ages the most. Generally, the untreated samples show higher susceptibility to ageing than the treated blends, with ageing generally increasing with increasing BFO content. As suggested by Lu and Isacsson (2002), there is a weak correlation between the ageing indices, indicating that ageing susceptibility may be ranked differently when different parameters are used. It is interesting to note the similarity

in ranking for the B5T+20/30 and B2.5U+20/30 blends with both these binders having a similar overall ranking of approximately ‘4’.

Table 32: Ranking of ageing indices obtained from rheological measurements.

Binder	G* 20°C RTFOT	G* 20°C PAV	G* 60°C RTFOT	G* 60°C PAV	SP RTFOT	SP PAV
10/20 pen	7	8	4	8	8	7
20/30 pen	8	7	7	5	7	6
B10T+10/20	5	5	8	7	6	5
B10U+10/20	1	1	1	1	1	1
B5T+20/30	4	4	5	2	4	3
B5U+20/30	2	2	2	3	2	2
B2.5T+20/30	6	6	6	6	5	4
B2.5U+20/30	3	3	3	4	3	8

8.2. Indirect Tensile Stiffness Modulus

The blends using the treated BFO were subsequently tested as binders for asphalt mixtures. The asphalt mixtures were tested to obtain their stiffness modulus at 20 °C (ITSM test – BS EN 12697-26 Annex C). The samples were pre-conditioned at 20 °C overnight before testing. The influence of biobinder content on the asphalt stiffness modulus is shown in Figure 82. Overall, stiffness decreases in the asphalt mixtures with increasing amount of BFO. Compared to the 10/20 pen control, the stiffness modulus of B10T+10/20 decreases by ~77%. B5T+20/30 and B2.5T+20/30 (5% and 2.5% blended biobinders respectively) produced similar results with an average of 47% decrease in their stiffness. Despite the difference in biobinder content, B5T+20/30 and B2.5T+20/30 have similar stiffness values with only a difference in 1.4%. There is an approximately 18% decrease in stiffness between these samples and the asphalt mixture with 10% treated BFO with the harder binder (B10T+10/20). This ITSM data aligns with the rheological binder data as stiffness decreases in the asphalt mixtures with increasing BFO content.

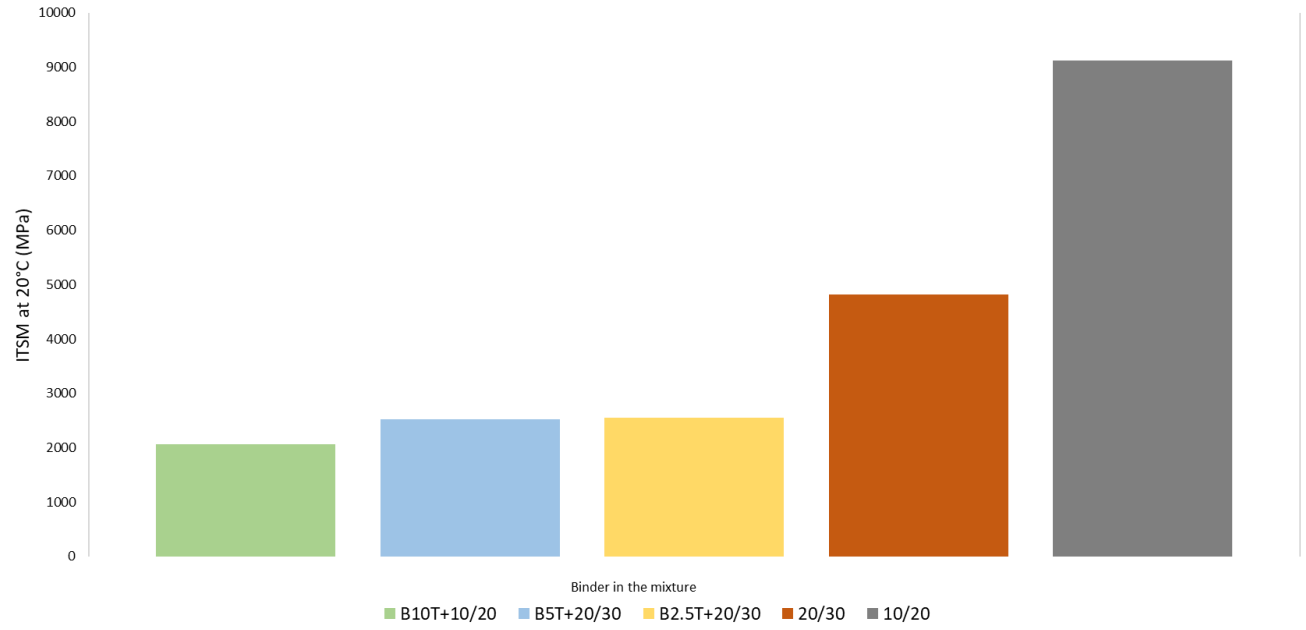

Figure 82: Stiffness modulus of the treated BFO asphalt mixtures.

8.3. Viscosity-temperature relationship of BFO-bitumen blends

The following blends were tested on a Kinexus DSR and a Brookfield rotational viscometer to investigate changes in viscosity as a function of temperature (Table 33). A hard 10/20 pen and a 20/30 pen bitumen were used as controls. The 2.5% blend (B2.5+20/30) was omitted as the amount of modifier used was very low and the rheological changes on the bitumen were minimal. A 50% addition of BFO was subsequently tested (labelled B50+20/30) in order to study the effects on the original binder when a significant portion of BFO is added.

Table 33: Composition of BFO and bitumen blends.

Blend name	Bitumen type	BFO type	BFO content
B10T+10/20	10/20 pen	Treated	10%
B10U+10/20	10/20 pen	Untreated	10%
B5T+20/30	20/30 pen	Treated	5%
B5U+20/30	20/30 pen	Untreated	5%
B50T+20/30	20/30 pen	Treated	50%
B50U+20/30	20/30 pen	Untreated	50%

The viscosity-temperature relationship for the treated and untreated B10+10/20 blends and the two control bitumens are shown in Figure 83. Overall the treated blend displays higher viscosities, similar to a 70/100 pen binder. The viscosity range at the various frequencies is

more compact and becomes more unified as temperature increases, as seen similarly with the conventional bitumens. A similar trend is seen with the BFO blends at 5% (B5+20/30) (Figure 84). At the lower temperatures (10-25 °C), the viscosities are more closely aligned to that of the 20/30 bitumen. This is expected as this blend contains the least amount of BFO. Both the 5 and 10% blends show conformance with bitumen trends, however increasing the BFO content towards 50% changes the viscosity response of the blend drastically (Figure 85). The viscosity range is much wider overall. The untreated B50+20/30 displays higher viscosities than the treated up until around 55 °C, where the viscosities are more aligned. Above this temperature, there is a slight trend of the treated blend showing higher viscosities.

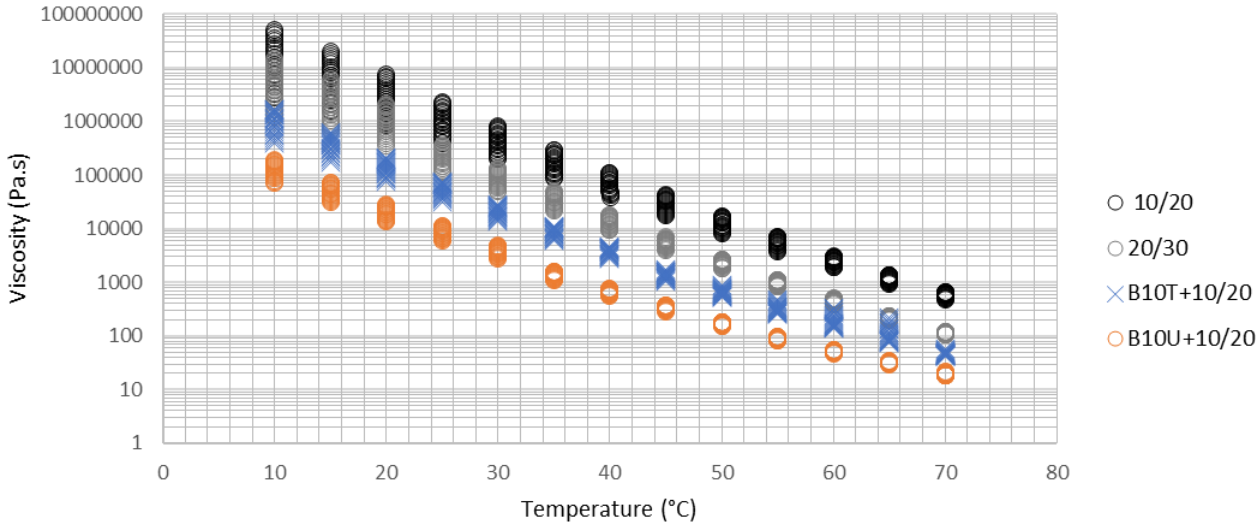

Figure 83: Viscosity-temperature relationship from 0.1 to 10 Hz for the 10% blend with 10/20 bitumen (B10+10/20 treated and untreated) and two conventional bitumens, a 10/20 pen and a 20/30 pen binder.

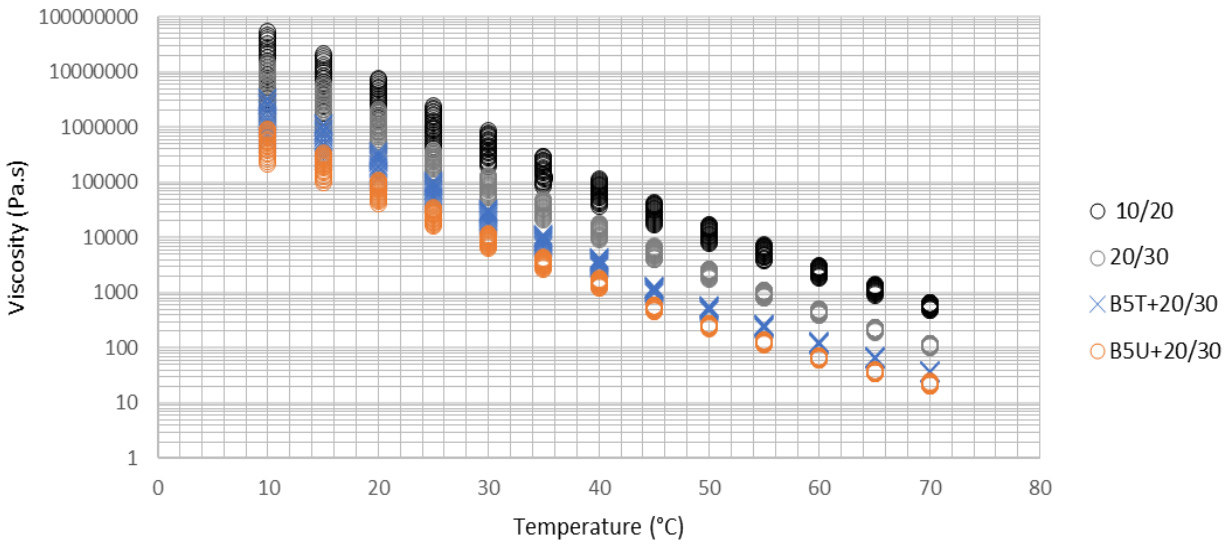

Figure 84: Viscosity-temperature relationship from 0.1 to 10 Hz for the 5% blend with 20/30 bitumen (B5+20/30 treated and untreated) and two conventional bitumens, a 10/20 pen and a 20/30 pen binder.

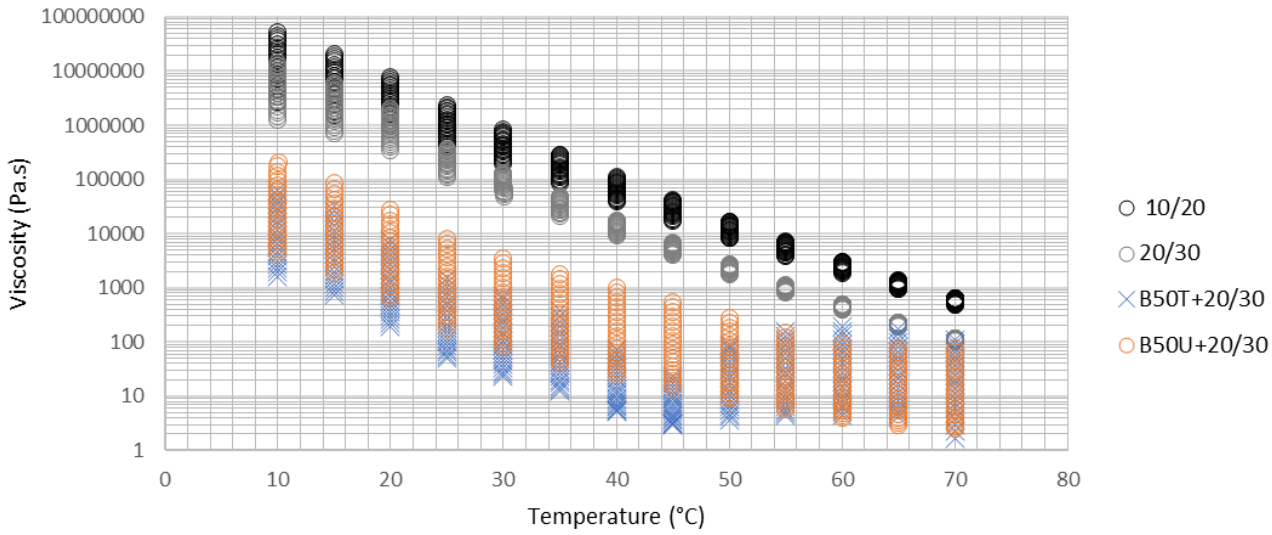

Figure 85: Viscosity-temperature relationship from 0.1 to 10 Hz for the 50% blend with 20/30 bitumen (B50+20/30 treated and untreated) and two conventional bitumens, a 10/20 pen and a 20/30 pen binder.

8.4. Rotational viscosity results for BFO-bitumen blends

Figure 86 and Figure 87 present the rotational viscosity results for the BFO untreated and treated blends respectively. All blends display a similar fluid behaviour as the conventional bitumens but at lower viscosities. Both the B10+10/20 and B5+20/30 treated and untreated blends present almost identical viscosity trends (ranging from approximately 10,000 cP to below 100 cP) and are very similar to the 20/30 control bitumen. It is not surprising that the harder binder (10/20) with more BFO presents similar viscosities to the softer binder (20/30)

with less BFO. In addition, both the treated and untreated B10+10/20 blends have similar viscosities to that of a 50/70 pen blend with 3% waste soybean oil at 135 and 150 °C found in the literature (Portugal et al., 2018). More differences in viscosity are seen as the BFO percentage increases in the blends.

Both B50+20/30 (50% BFO) blends have much lower viscosities (between 100 to just below 10 cP) than the other blends. B50U+20/30 is more fluid (lower viscosity) overall than the treated BFO blend at this percentage (Figure 88). At 100 °C, viscosities for both B50+20/30 blends are most similar. There is more discrepancy as temperature increases. The B50T+20/30 (treated) blend viscosities seem to slightly plateau between 120 and 150 °C. This is not the case for the B50U+20/30 (untreated) results, which show more of a gradual decrease in viscosity as temperature increases. When comparing with the DSR viscosity results in section 8.3, it is clear that there is a discrepancy in these results. The untreated B50+20/30 blend was higher in viscosity for the DSR experiment (Figure 85). However, above 55 °C, the two blends start to converge. Taking the two experiments together, this implies that around 55 °C, there is a viscosity crossover between the two BFOs. This behaviour is not necessarily expected due to the similarity in chemical composition but may be due to various physical and physico-chemical effects that have not been determined. Unlike the 50%, the blends at 5 and 10% BFO display almost identical viscosity profiles and also the same trend as the control bitumens. This agrees with the DSR results which show that blending at 50% ratio severely changes the viscosity response.

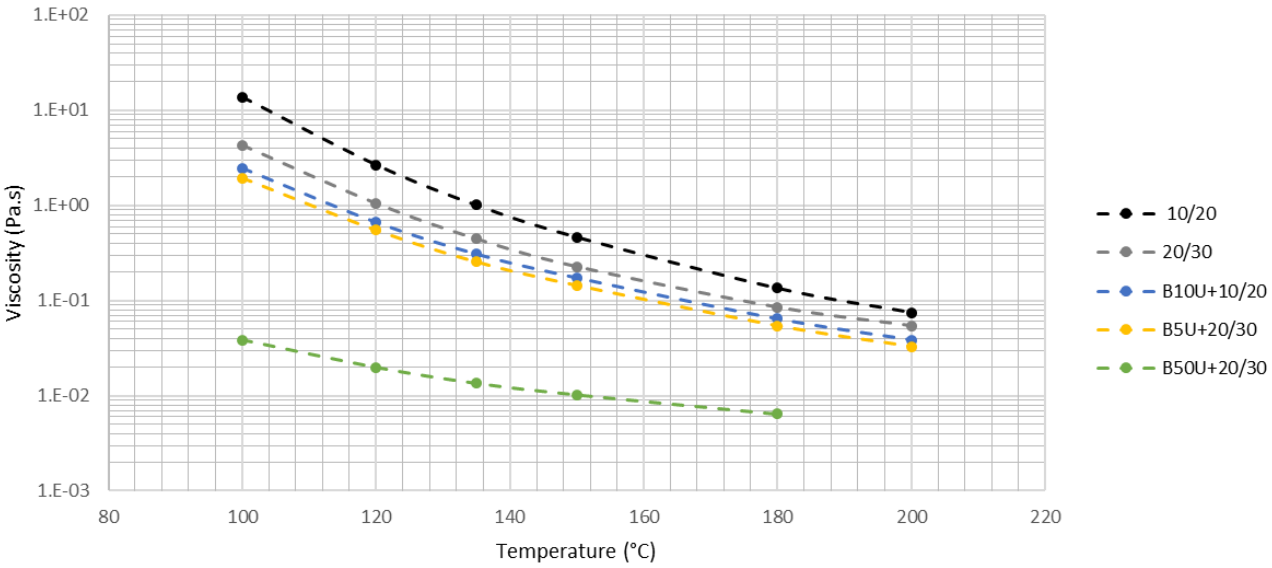

Figure 86: Rotational viscosity results of the BFO-bitumen blends (from the untreated BFO), as well as 10/20 and 20/30 pen bitumens.

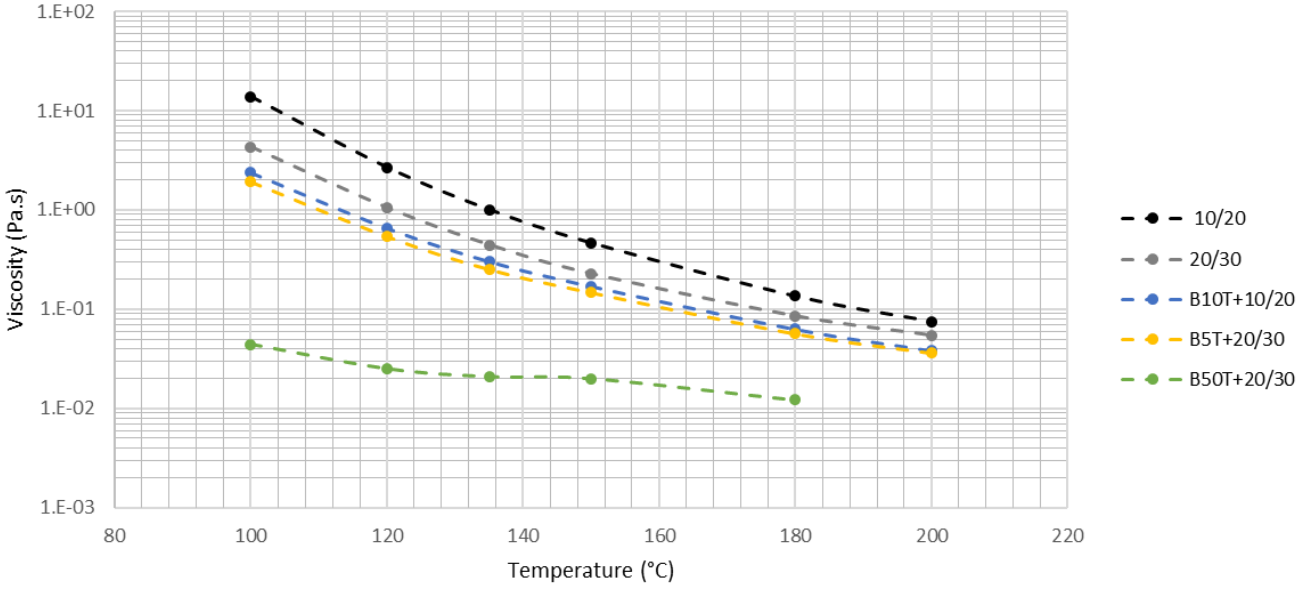

Figure 87: Rotational viscosity results of the BFO-bitumen blends (from the treated BFO), as well as 10/20 and 20/30 pen bitumens.

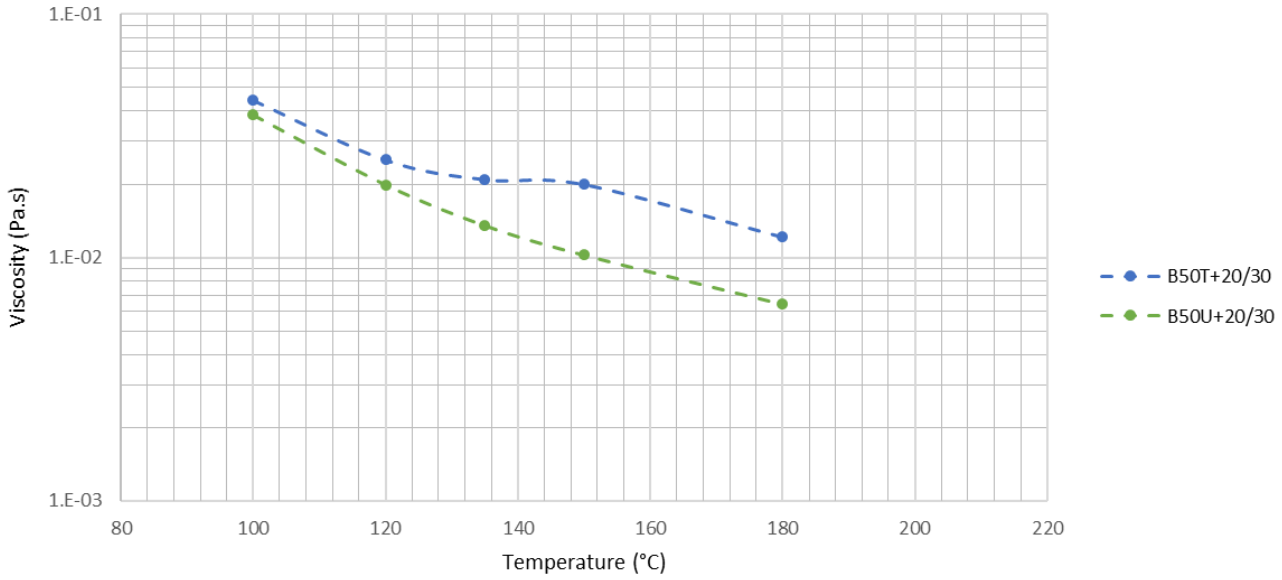

Figure 88: Rotational viscosity results of the BFO-bitumen 50% + 20/30 blends from both the treated and untreated BFO.

8.5. Summary of observations

DSR rheological testing shows that the treated B10+10/20 and B5+20/30 have a higher complex modulus and lower phase angles than the softer untreated blends when tested over 10-70 °C. This suggests that the treated BFO-bitumen blends are higher in viscosity. The complex viscosity DSR plots also show that the treated B10+10/20 and B5+20/30 blends are higher in viscosity over this temperature range.

Rotational viscosity testing carried out on the Brookfield over 100-200 °C show that viscosities are almost identical for the treated and untreated blends B10+10/20 and B5+20/30. This agrees with the Brookfield results for the neat BFO materials at 80 and 100 °C, where they were found to be almost identical.

At higher temperatures (80-100 °C for the neat BFO materials and 100-200 °C for B10+10/20 and B5+20/30 blends), viscosities for all materials are very similar between treated and untreated. The 10% addition to the harder binder and 5% addition to the softer binder makes little difference to the viscosity profile.

At the lower temperatures (25-60 °C), the untreated neat BFO material is shown to have higher viscosities with the rotational viscometer than the treated BFO (as claimed by Argent

Energy). This does not agree with the rheological master curves of the blends, which show the treated blends as having higher viscosity.

The 50% untreated blend shows lower viscosities than the treated blend in the Brookfield testing over the temperatures 100-200 °C. The DSR complex viscosity testing shows the B50U+20/30 blend has higher viscosities than the treated up to about 55 °C. Above this temperature, the untreated and treated blends start to converge. Taking the two experiments together, this implies that around 55 °C, there is a viscosity crossover between the two materials.

8.6. Pyrolysed BFO blend rheological characterisation

The heavier, pyrolysed material (obtained from the original untreated BFO) was subsequently blended with a 40/60 pen bitumen at 10%. This blend is called B10HTF+40/60, and HTF signals that it has been pyrolysed in a horizontal furnace to remove lower molecular weight FAME compounds. Complex modulus and phase angle master curves and complex viscosity vs temperature plots were generated to examine the rheological behaviour of this new blend.

Figure 89 shows the complex modulus master curves for the pyrolysed BFO blend (B10HTF+40/60) with four conventional bitumens as controls: 10/20, 20/30, 40/60 and 70/100 pen bitumens. Compared to the control bitumens, B10HTF+40/60 has the lowest stiffness and is still softer than the control bitumens. Although the addition of the pyrolysed BFO lowers the stiffness of the original binder, there is an increase in complex modulus when compared to the non-pyrolysed BFO blends. The removal of low molecular weight FAME via pyrolysis has resulted in a higher viscosity oil that has softened the 40/60 pen bitumen to a lesser extent than the lower viscosity B10U+10/20 blend which used the original BFO. A 10% addition of the original BFO to a hard 10/20 binder lowers the stiffness more so than adding the same percentage of pyrolysed BFO to a softer binder such as 40/60. This suggests that the pyrolysed BFO could be added at higher quantities without compromising on stiffness as much. Phase angle master curves are shown in Figure 90. The pyrolysed BFO blend (B10HTF+40/60) displays lower phase angles at higher temperatures (lower frequencies) revealing the higher elastic rheological response. This elastic behaviour at the higher temperatures is not seen with the conventional bitumens and the previous blends with the original BFO materials, such as the B10+10/20 blend which shows an increase in viscous

response (phase angles approaching 90°) at the higher temperatures (lower frequencies). There is an increase in viscous behaviour (higher phase angles) at the mid-range temperatures for the pyrolysed BFO blend, followed by a gradual decrease in phase angle values at the lower temperatures (higher frequencies), similar to the control bitumens and the other BFO blends. This increased elastic response seen in the pyrolysed BFO blend at higher temperatures might be beneficial in preventing rutting.

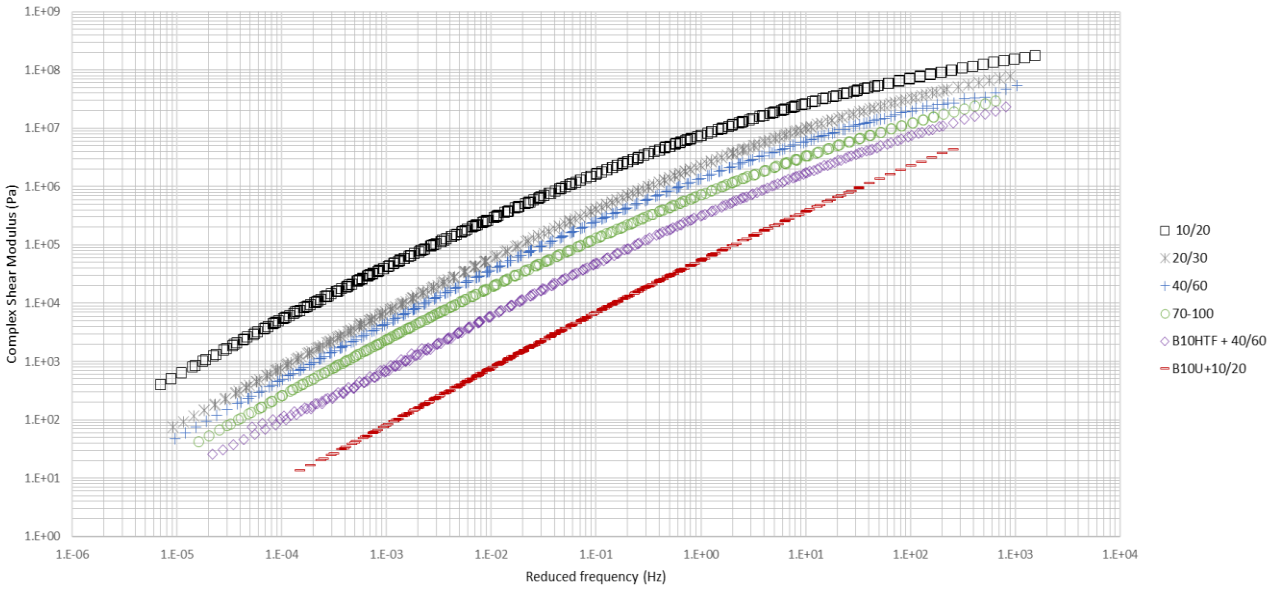

Figure 89: Complex modulus master curves at a reference temperature of 25°C for the pyrolysed BFO blend with 40/60 bitumen (B10HTF+40/60) and the original BFO untreated blend with 10/20 (B10U+10/20).

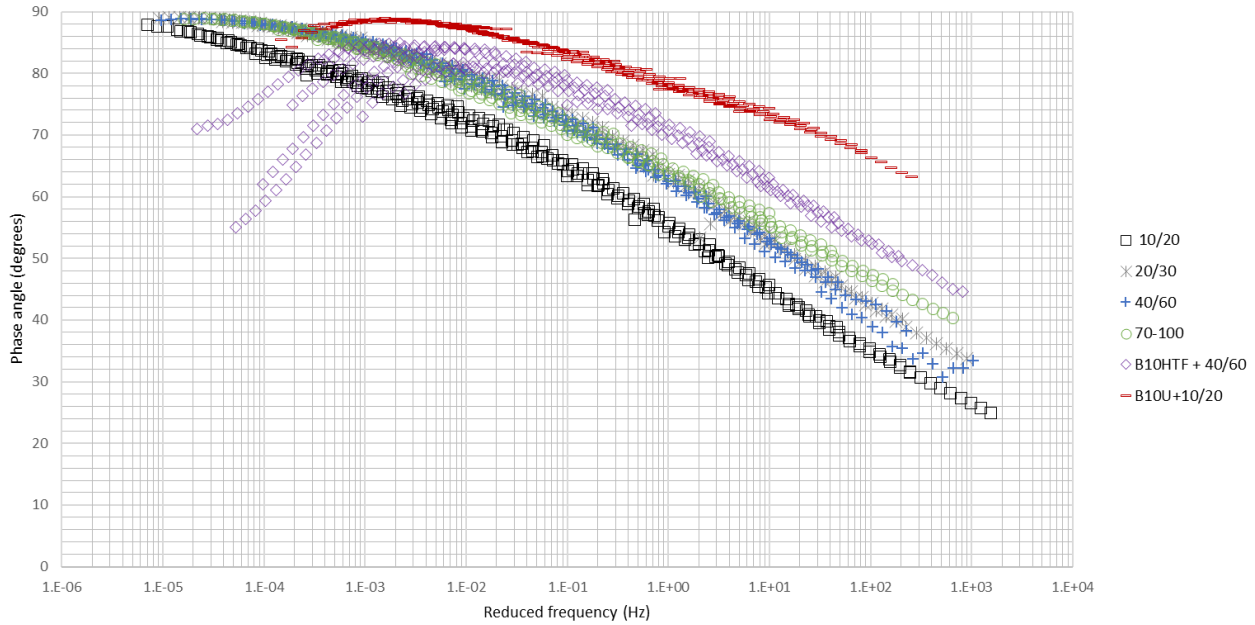

Figure 90: Phase angle master curves at a reference temperature of 25°C for the pyrolysed BFO blend with 40/60 bitumen (B10HTF+40/60) and the original BFO untreated blend with 10/20 (B10U+10/20).

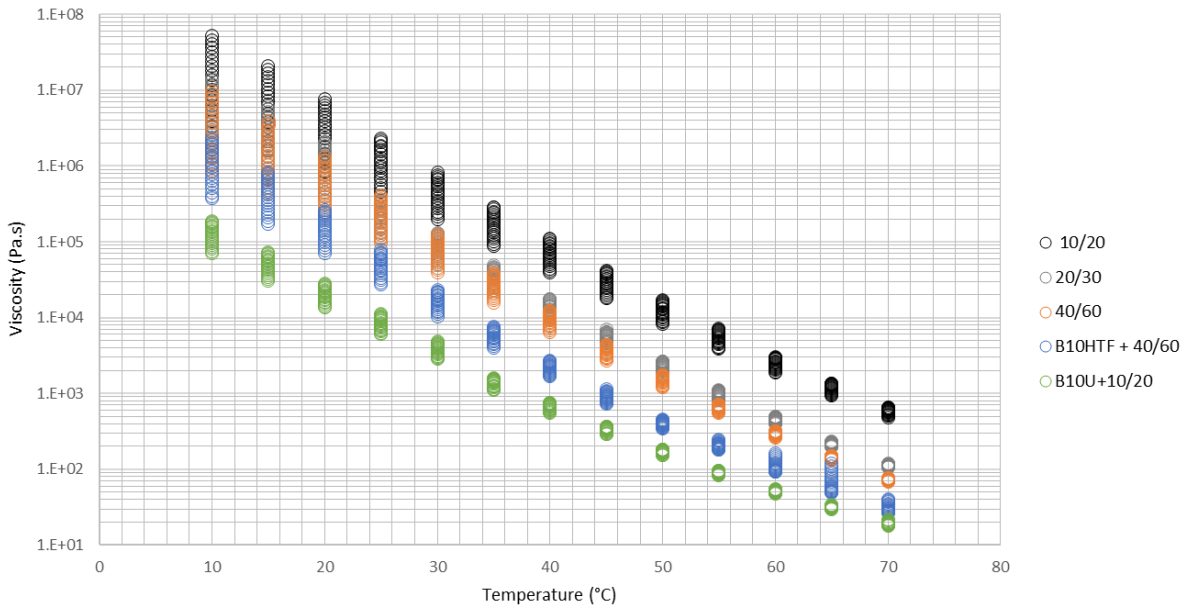

Figure 91: Viscosity-temperature relationship from 0.1 to 10 Hz for the pyrolysed BFO blend with 40/60 bitumen (B10HTF+40/60) and the original BFO untreated blend with 10/20 (B10U+10/20).

The complex viscosity vs temperature plot for the pyrolysed BFO blend added to the 40/60 binder (B10HTF+40/60) also shows its increased viscosity compared to the original blend with the same percentage of untreated BFO added to a hard 10/20 binder (B10U+10/20) (Figure 91). The original B10U+10/20 has a wider range of viscosity values at the lower temperatures (10-40 °C) which progressively unify as temperature increases, similarly to the conventional binders. The heavier, pyrolysed BFO blend (B10HTF+40/60) shows this trend up to about 55 °C, where viscosity values stretch slightly at the higher temperatures.

8.6.1. Changes in rheological properties after ageing

The effect of ageing is shown in the form of complex modulus and phase angle master curves for the blend modified with 10% pyrolysed BFO (B10HTF+40/60) (Figure 92 and Figure 93 respectively). Similar to the 40/60 conventional bitumen, the complex modulus increases and the aged blend becomes more elastic (lower phase angles) at the lower temperatures (higher frequencies). The PAV-aged B10HTF+40/60 sample and the RTFOT-aged 40/60 binder have almost identical stiffness and elastic response, with the PAV-aged pyrolysed BFO blend having slightly lower phase angles (higher elastic response) over the range of frequencies than the RTFOT-aged 40/60 bitumen. The RTFOT-aged B10HTF+40/60 blend shows a similar elastic response at the higher temperatures (lower frequencies) to its unaged counterpart. The PAV-

aged B10HTF+40/60 shows an increase in viscous response at the higher temperature, similar to petroleum binders.

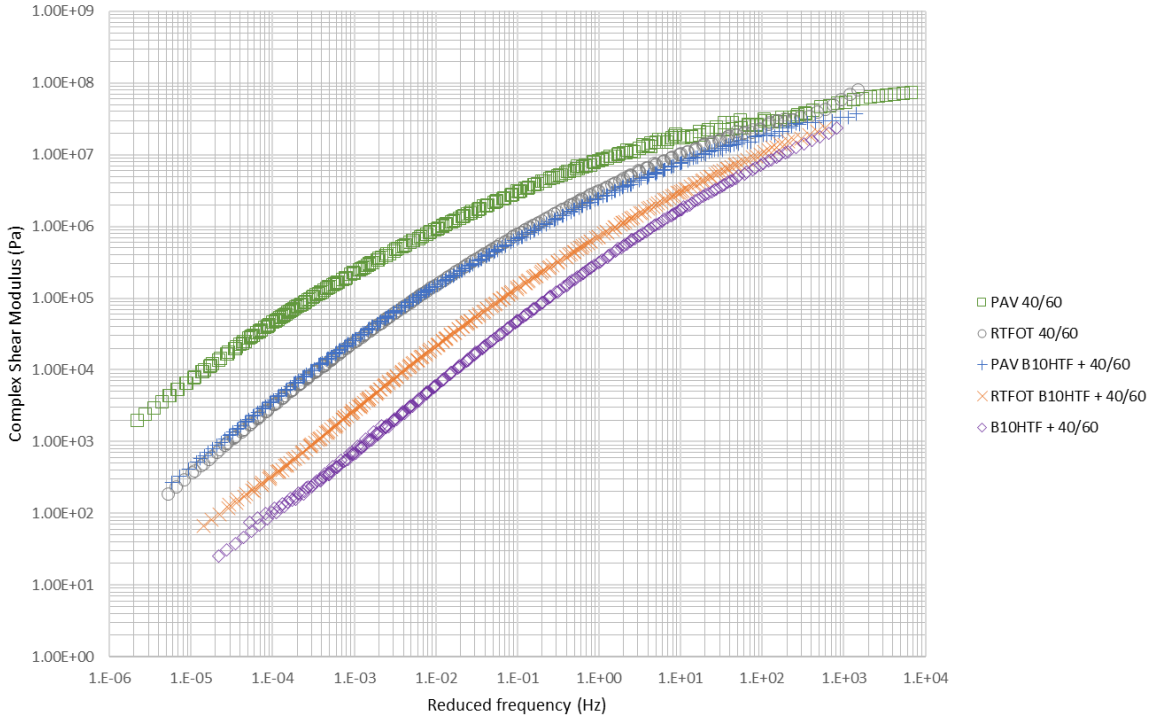

Figure 92: Complex modulus master curves at a reference temperature of 25°C for the unaged, RTFOT and PAV aged pyrolysed BFO blends with 40/60 bitumen (B10HTF+40/60) and 40/60 control binder.

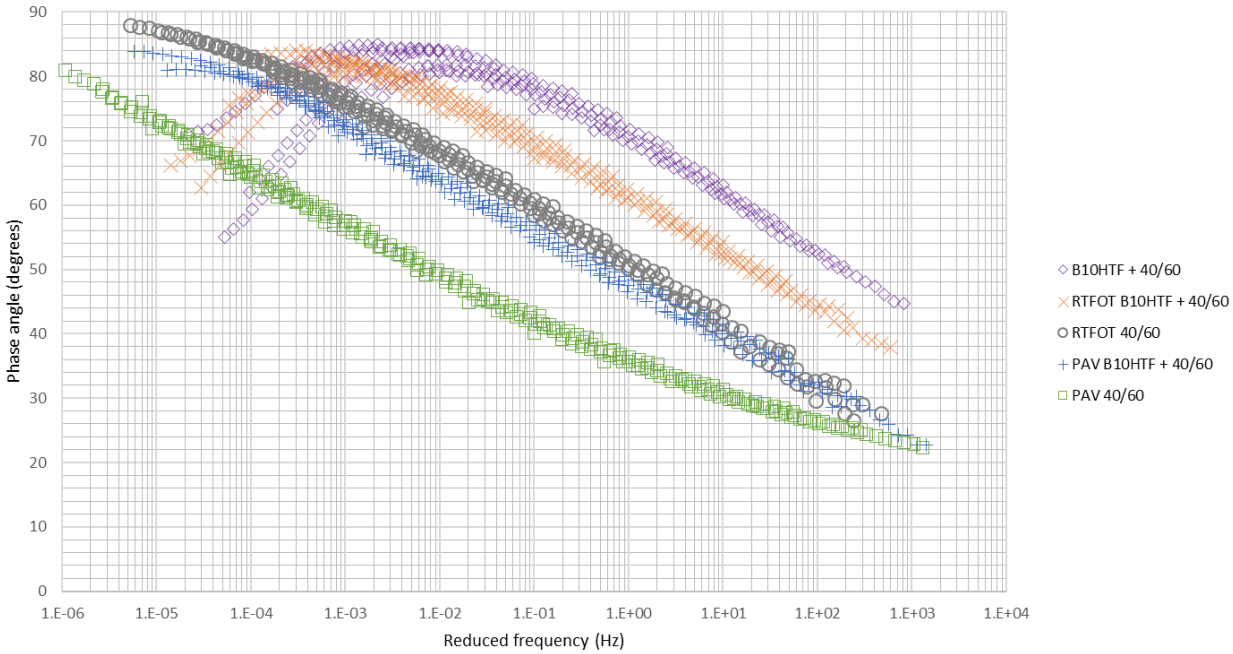

Figure 93: Phase angle master curves at a reference temperature of 25°C for the unaged, RTFOT and PAV aged pyrolysed BFO blends with 40/60 bitumen (B10HTF+40/60) and 40/60 control binder.

8.7. Key Points

- Once blended with bitumen, the treated and untreated blends display various changes in rheology and ageing. Similar to other biomaterials, the addition of BFO (at any percentage) softens the original binder and lowers viscosity and stiffness. This change is more marked as biobinder content increases.
- The untreated blends are generally softer (lower complex modulus values and higher phase angles) compared to the same blend proportions produced with the higher viscosity treated biobinder. Stiffness also decreases in asphalt mixtures with increasing BFO content. The 5 and 2.5% blends are overall very similar. This correlates with rheological master curve results.

- In terms of aged samples, the rheological behaviour indicates a similar oxidative effect to that of conventional binders. The ageing indices confirm that the untreated blends age the most and that ageing increases with increasing BFO content.

- There are subtle changes in viscosity, complex modulus and phase angle response that have been identified by both DSR and Brookfield testing. While the 5 and 10% BFO bitumen blends conform to conventional bitumen trends, increasing the BFO towards 50% changes the viscosity profile drastically, with a much wider viscosity range. Viscosities between the treated and untreated BFO blends are generally the same at the higher temperatures.
- Overall there is an increase in stiffness and decrease in phase angles (higher elastic response) in the pyrolysed BFO (B10HTF+40/60) blend than in the lower viscosity blends using the original BFOs. Regarding ageing, it follows a similar pattern to conventional bitumens with the more severely-aged blend (PAV B10HTF+40/60) having almost identical complex modulus and phase angle values to a lesser-aged RTFOT 40/60 bitumen.

9. Performance-based rheological testing of pyrolysed BFO blend with bitumen

Table 34 displays the temperatures at which the rutting and fatigue parameters were achieved for the biomodified blend and the 40/60 binder. B10HTF + 40/60 reaches the rutting limit at a lower temperature (58 °C for the unaged and RTFOT-aged blend) than the 40/60 pen bitumen (64 °C for the unaged, 70 °C for the RTFOT-aged control binder). Since the biomodified binder is inherently softer, it has a lower rutting resistance than the control bitumen.

Regarding the PAV-aged samples, the biomodified binder reaches the fatigue limit at a lower temperature (22 °C) than the 40/60 pen bitumen (28 °C). A softer consistency and a lower stiffness is seen with the biomodified binder after PAV ageing than the 40/60 binder. The PAV-aged control bitumen achieved the fatigue limit at a higher temperature, showing higher stiffness (due to the fact that it is a harder binder) and a decreased fatigue resistance compared to the biomodified binder. This correlates with the master curves which show the PAV-aged biomodified binder as having a lower complex modulus and overall higher phase angle values than the PAV-aged 40/60.

Table 34: Temperatures at which the rutting and fatigue parameter limits were achieved.

Sample	Parameter	Limit (kPa)	Temperature where limit was achieved (°C)
B10HTF + 40/60	G* / sin(delta)(kPa)	≥ 1	58
RTFOT B10HTF + 40/60	G* / sin(delta)(kPa)	≥ 2.2	58
PAV B10HTF + 40/60	G* x sin(delta)	≤ 5000	22
40/60	G* / sin(delta)(kPa)	≥ 1	64
RTFOT 40/60	G* / sin(delta)(kPa)	≥ 2.2	70
PAV 40/60	G* x sin(delta)	≤ 5000	28

9.1. Multiple Stress Creep Recovery (MSCR)

The results of the MSCR test at 60 °C in terms of J_{nr} and recovery (R%) are shown in Figure 94 and Figure 95. The unaged biomodified blend (B10HTF+40/60) shows higher susceptibility to rutting due to its higher J_{nr} values (Figure 94). This is not surprising as the biomodified blend is a softer binder with a higher deformation, which might perform similarly to other soft binders such as 70/100 pen. RTFOT ageing enhances rutting performance significantly by about two-thirds of the unaged blend, although not nearly as well as the conventional 40/60

bitumen. The RTFOT-aged biomodified blend has a similar J_{nr} to that of the unaged 40/60 binder.

Overall, the percentage recovery is lower for the biomodified blend (B10HTF+40/60) than the conventional binder, which is more flexible and elastic at the tested temperature (60 °C) (Figure 95). The R% plot shows the sensitivity of the recovery (R%) of the blend to the two stress levels. At the lower stress level (0.1 kPa), the unaged blend exhibits a similar, slightly higher elastic recovery to the unaged 40/60. However, the RTFOT-aged 40/60 has about 40% greater recovery than the RTFOT-aged blend. On the other hand, for the 3.2 kPa stress level, a negative elastic recovery is seen for the unaged blend and 40/60 bitumen. The value of percentage recovery should in theory be positive for asphalt binders as the residual strain at the end of the recovery section should be no more than the accumulated strain at the end of the creep section. However, researchers have reported negative recoveries commonly observed for both unmodified and modified binders due to a combination of the high stress level (3.2 kPa) and high temperature (Liu et al., 2021). This negative response is probably caused by inertia effects dominating on soft bitumens and has been commonly observed in binders with lower viscosities. It can be regarded to equal to 'zero recovery' under these conditions (Zhu et al., 2021, Liu et al., 2021). The RTFOT-aged blend shows a slight increase in recovery whereas the RTFOT-aged 40/60 recovers more efficiently. In light of the hardening of the binder, this is to be expected due to the increased viscosity effects from the ageing process. The higher strain level significantly worsens the blend's ability to recover. B10HTF+40/60 (unaged and RTFOT-aged) is a poor binder choice for enhancing damage caused by rutting due to its low recovery and high J_{nr} values in comparison to the control bitumen. This correlates with the rutting parameter calculated above which indicates the biomodified is less resistant to permanent deformation than the 40/60 binder. However, the rheological phase angle master curves in section 8.6 present an increased elastic response (a shift to lower phase angles) from 55 °C onwards for both the unaged and RTFOT-aged B10HTF+40/60 blend (important for rutting resistance). This elastic behaviour could be attributed to the low torque used during standard DSR frequency sweeps compared to the significant deformation applied during MSCR testing. At 60 °C, the DSR frequency sweep has an average complex shear stress of 0.007 and 0.017 kPa for the unaged and RTFOT-aged biomodified blend respectively. This is dramatically lower than the stress applied with MSCR

at 0.1 and 3.2 kPa. Although the biomodified blend seems to have some rutting resistance at very low deformations, and even at 0.1 kPa, in reality it is a poor binder choice for high-temperature performance compared to a conventional 40/60 binder due to its more fluid characteristics.

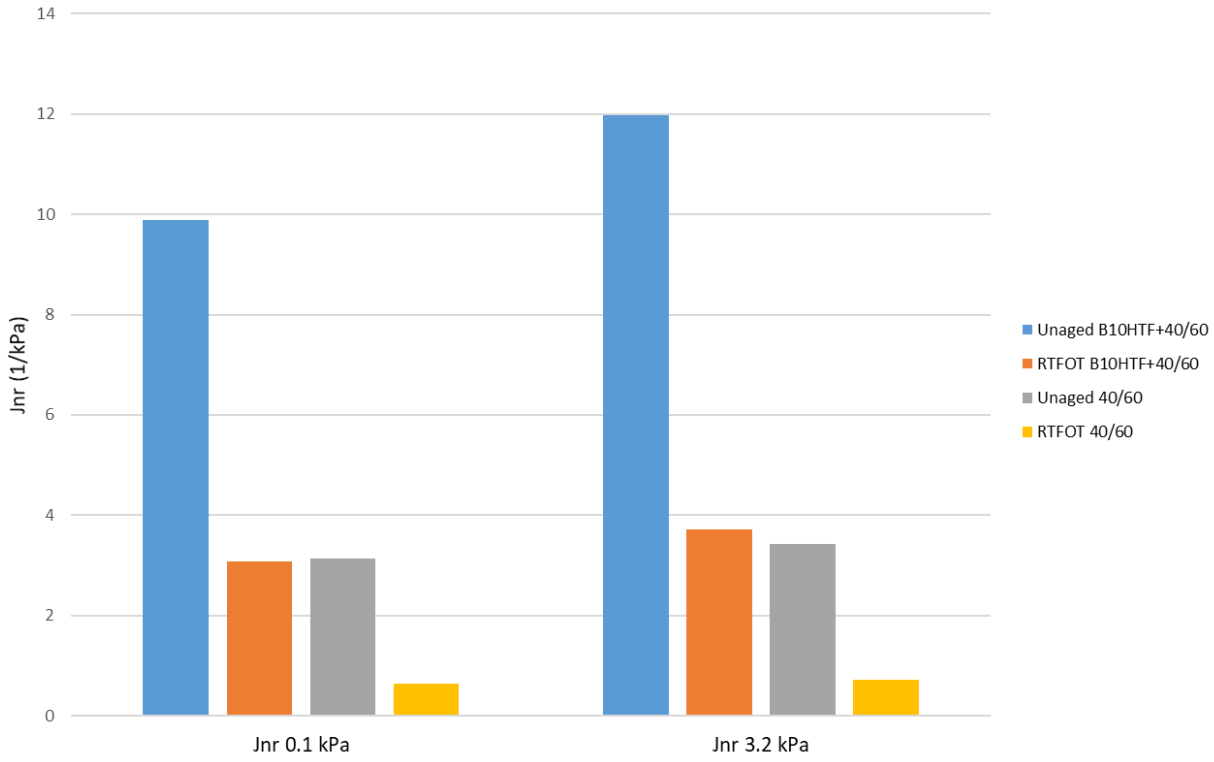

Figure 94: Non-recoverable creep compliance (J_{nr}) values at 0.1 and 3.2 kPa for the unaged and RTFOT-aged biomodified blend B10HTF+40/60 and 40/60 conventional binder.

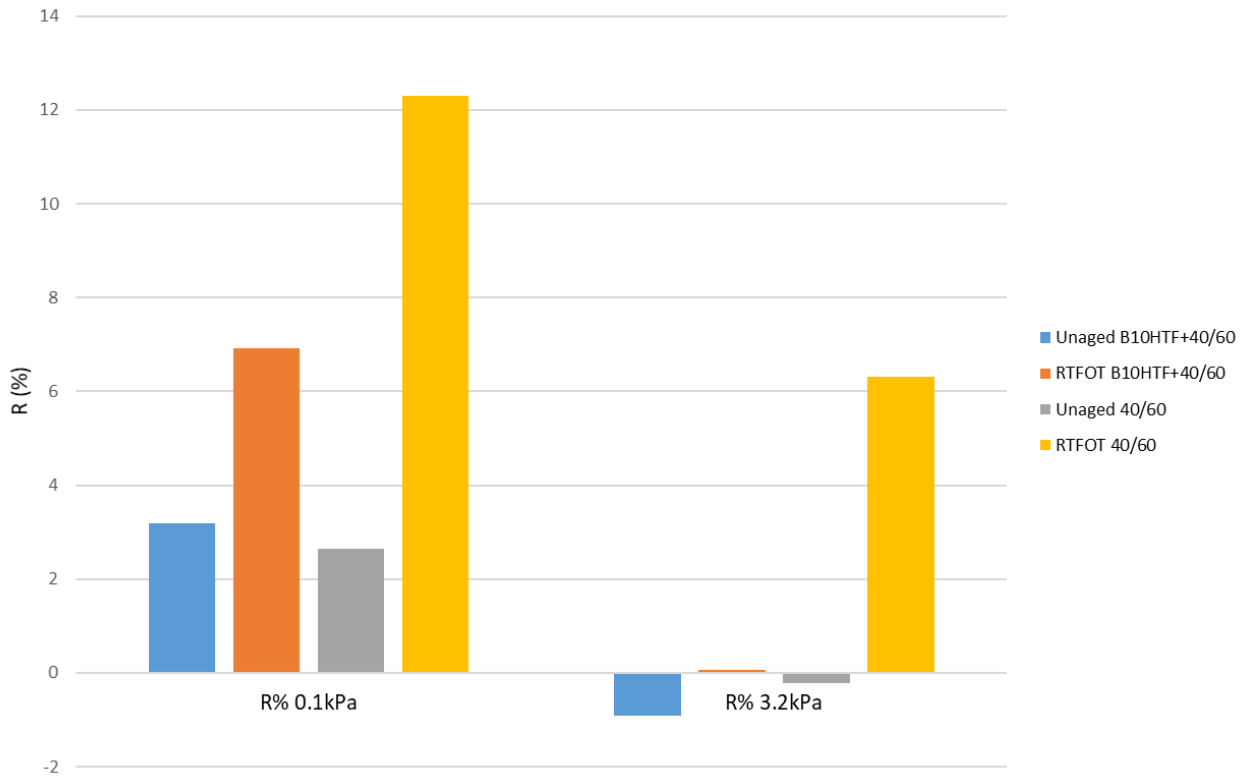

Figure 95: Percentage recovery (R%) at 0.1 and 3.2 kPa for the unaged and RTFOT-aged biomodified blend B10HTF+40/60 and 40/60 conventional binder.

9.2. Linear Amplitude Sweep (LAS)

The LAS test results are presented in Table 35 and Figure 96 for the unaged and PAV-aged biomodified blend using the pyrolysed untreated BFO (B10HTF+40/60) and the 40/60 control bitumen. At the lower strain levels, the PAV-aged samples show higher number of cycles to failure (N_f) than the unaged samples (Figure 96). In other words, they show a better fatigue resistance compared to the unaged samples as they are stiffer and therefore more resistant to damage at low strain levels. This is also seen with an increase in the A_{35} parameter with ageing (Table 35). At the higher strain levels the curves converge and the ageing seems to worsen fatigue resistance. This is seen with an increase in the magnitude of the slope in the power law curves for the aged samples, and a reduction in the B parameter, correlating with a reduction in time-temperature susceptibility. At the highest strain level, the PAV-aged blend and control bitumen have slightly higher N_f values compared to the unaged samples. In addition, the unaged biomodified blend shows slightly better fatigue resistance than the unaged 40/60 binder. Both the unaged blend and 40/60 binder have lower gradients so the change in fatigue with increasing strain is lower relative to the PAV-aged samples. At 2.5%

strain, the PAV-aged blend has a worse fatigue resistance than the PAV-aged 40/60 binder. At 5% (highest strain), the PAV-aged biomodified blend shows comparable fatigue resistance to the aged bitumen. This result correlates with the fatigue parameter and the rheological master curves of the PAV-aged blend and 40/60 binder (section 8.6.1).

Two key observations can be drawn from these results: PAV-ageing increases tolerance to fatigue damage but also the pyrolysed BFO in the bitumen blend (B10HTF+40/60) slightly enhances fatigue resistance at the higher strain level (5%). Fatigue cracking is more likely to happen at 5% strain for thin pavements, so B10HTF+40/60 would be better suited when the strain is higher, as brittle fracture would be likely avoided as the binder is softer. This would have to be confirmed by carrying out asphalt mixture fatigue testing and subsequently pilot-scale experiments to evaluate long-term fatigue performance.

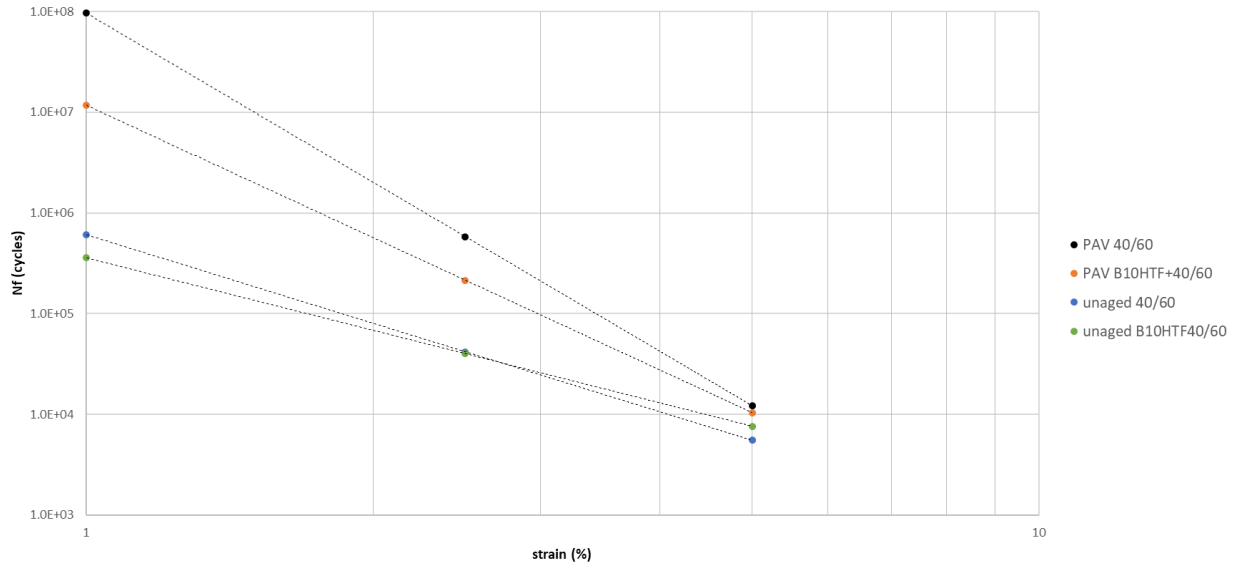

Figure 96: Power law fatigue curve at A_{35} (35% fixed damage) for the unaged and PAV-aged B10HTF+40/60 blend and 40/60 binder.

Table 35: Values of fatigue law parameters A_{35} and B for the unaged and PAV-aged biomodified blend and control 40/60 bitumen. A_{35}: the value of N_f (number of cycles to failure) at 35% damage level. B: the slope of the N_f - strain curve correlating to the time-temperature dependency of the material (Cuciniello et al., 2020).

Sample	A_{35}	B
Unaged 40/60	6.08E+05	-2.9
PAV 40/60	9.68E+07	-5.6
Unaged B10HTF+40/60 blend	3.59E+05	-2.4
PAV B10HTF+40/60 blend	1.18E+07	-4.4

9.3. Key Points

- The rutting parameter and MSCR show that the biomodified blend has lower rutting resistance than the 40/60 binder.
- The Superpave rheological fatigue parameter (AASHTO T-315) indicates that the PAV-aged pyrolysed BFO blend has higher fatigue resistance than the control binder. From the LAS results, it is clear that that PAV-ageing increases tolerance to fatigue damage and the PAV-aged 40/60 conventional binder has better fatigue resistance at the lower strain levels. However, the pyrolysed BFO in the bitumen blend (B10HTF+40/60) slightly enhances fatigue resistance at the higher strain level (5%).

10. Conclusions

The main objective of this study was to investigate the suitability of lignin and biodiesel-derived waste materials as potential bitumen modifiers by manufacturing a high-viscosity biobinder and investigating their chemical and/or rheological properties. The vast majority of biobinder studies that use oils as bitumen modifiers do detailed analysis once the oil or biobinder is mixed with bitumen. As a result, the bulk of work done in this thesis centred around a thorough chemical and rheological characterisation of the neat biomaterials. In addition to this, further investigations were conducted on the biomodified bituminous blends. Another motivation behind this study was to focus on waste materials available in high volumes. The reason for this is twofold: firstly, availability for experiments is necessary, and secondly the potential ability for large scale-up in road construction applications.

The paper waste and BFO materials underwent various thermal treatments with a range of times and temperatures in order to maximise viscosity. The biocrude products obtained were subsequently characterised before blending with bitumen. As for the BFO materials, samples before and after treatment were characterised through a variety of different techniques to quantify any induced changes. The results in the final chapter (performance based rheological testing) help to suggest possible applications of the BFO materials in asphalt engineering.

Given the results obtained, the following conclusions can be drawn:

1. Paper waste: Two biobinders at two different temperatures (320 and 360 °C) were manufactured via hydrothermal liquefaction from a paper waste residue. The produced materials are softer materials with lower complex modulus than the control bitumens (10/20 and 40/60 pen). The biobinder manufactured at 320 °C presents a similar stiffness to that of a 40/60 bitumen. Regarding phase angle, the softer biobinder (obtained at 360 °C) has a higher viscous response, indicating its low stiffness. The lower temperature biobinder has a viscous or elastic response dependent on temperature but has an increased elastic response compared to the biobinder manufactured at 360 °C. Due to the low yields produced, HTL does not seem to be the right process for the production of a bio-bitumen from this paper waste residue. With more testing, a potential role for this material could be enhancing high-temperature performance and preventing permanent deformation.

2. BFO: The chemical characterisation of the BFO materials prior to blending indicates that both the treated and untreated BFOs have a similar chemical makeup of fatty acid methyl esters, which are readily found in vegetable oils. Although there are subtle differences, the viscosities and viscosity patterns of the BFOs are the same. Once blended with bitumen, the treated and untreated blends display various changes in rheology and ageing. Similar to other biomaterials, the addition of BFO (at any percentage) softens the original binder and lowers viscosity and stiffness. This change is more marked as biobinder content increases. The untreated BFO blends are generally softer than the treated BFO blends. There is a similar ageing trend seen with the BFO blends as there is with conventional bitumens, with ageing increasing with increasing BFO content. An addition of 50% BFO drastically changes the viscosity response indicating that such a high proportion of BFO is unlikely to be beneficial in a binder blend.

3. HTL BFO materials: Both the chemical and rheological characterisation reveal that the hydrothermally-treated BFO materials are softer materials than the original BFO. The presence of higher molecular weight FAME compounds is reduced or absent in the HTL BFOs. As HTL reaction temperature increased from 300 to 360 °C, the high molecular weight compounds thermally decomposed to lower molecular weight compounds which were then evaporated off during sample drying. Hydrothermal treatment does not seem to be the appropriate thermochemical technique for the production of a higher viscosity biobinder from the BFOs. As a result, no bitumen blending was undertaken with these materials.
4. Pyrolysed BFO: BFO can still be upgraded to a more 'bitumen-like' product via pyrolysis using a horizontal furnace. This method which distils off lower molecular weight compounds is a simpler and more suitable process for producing a higher viscosity product with the BFO. The characterisation of the pyrolysed BFO indicates that 300 °C and a longer reaction time of 5 hours increases viscosity of the BFO. There is an increased stiffness and elastic response in the pyrolysed BFO compared to the original materials. As for ageing, a similar pattern to conventional binders is observed. From the performance-based rheological testing, rutting resistance decreases for the biomodified blend with the pyrolysed BFO. At higher strain levels (5%), PAV-ageing

enhances fatigue resistance similar to a 40/60 bitumen. This suggests that B10HTF+40/60 is better suited for thinner pavements when the strain is higher, as the softening effect would help avoid brittle fracture.

11. Wider significance of the findings

It is evident that the materials studied in this thesis are at an early stage of development and therefore this document can be considered a starting point for future research for both waste lignin and biodiesel-derived residues to be used as biobinders in pavement engineering. The key benefit of utilising waste biomass feedstocks like the BFO and the paper waste is the large quantities available. BFO could offer a potential improvement in low temperature cracking and fatigue performance due to the decrease in stiffness and increase in viscous response compared to aged or high modulus (low penetration) base bitumens. As a result, using these as potential rejuvenators in RA mixtures could be a possible application for these biobinders. A possible applicability for the higher viscosity pyrolysed BFO with further research could be as a warm mix asphalt (WMA) additive for thinner pavements. WMA offers a range of benefits such as lower mixing temperatures and reduced paving costs as less energy is required. WMA also allows for improved workability and compaction and better working conditions due to lower emissions of fumes being produced.

11.1. Future work

The following points are recommended for future research work:

- A range of experimental techniques were utilised to study the chemical and rheological properties of these materials, and some were more appropriate than others. For instance, GC-MS is not a suitable technique to fully characterise the chemical makeup of the pyrolysed BFO. The pyrolysed material did not contain compounds that are GC-MS amenable as these were distilled/evaporated off during treatment. Higher molecular weight molecules left in the pyrolysed BFO could not be detected by the GC-MS. This is a common limitation found with the equipment and as a result, size-exclusion chromatography (SEC) would help complement the simulated distillation results. LDI-MS would also help obtain representative results for the whole sample.

- In this study, sp2 hybridised carbons were underestimated in ^{13}C NMR. A suggestion for further work is to utilise a relaxation agent such as chromium acetylacetonate to reduce longitudinal relaxation times and therefore improve quantitative results.
- As for LDI-MS, the matrix-free approach used was not selective enough to identify the FAME compounds. Perhaps using matrix-assisted laser desorption ionisation mass spectrometry (MALDI MS) and utilising a matrix capable of identifying FAME ions, such as iron (III) porphyrins (F20TPP), could help detect ions dominated by these molecules.

11.2. Scale-up of biobinder production

- It might be useful to thermally treat the paper waste residue using the horizontal tube furnace to see whether a heavier material can be produced. This method is simpler than liquefaction so if successful it could facilitate laboratory-scale production.
- Manufacturing more pyrolysed BFO material using a simple horizontal furnace and blending with a wider range of bitumens to investigate how the pyrolysed BFO affects their rheology. Focusing on harder and more brittle bitumens would be ideal as these biobinders are softeners and therefore might have the potential to replace softer bitumens in the industry and reduce bitumen demand.
- A limitation of this study was the low yield produced per experiment. This meant that many repeat runs were necessary. Therefore, a key point of study could be investigating how to scale up the pyrolysis treatment to produce higher yields of pyrolysed BFO.

11.3. Rheological testing and ageing

- Testing the BFO using the cup and bob geometry to confirm Newtonian behaviour would be beneficial, similar to the control salad oil.
- As only one blend was studied with the pyrolysed BFO, it would be interesting to study new blends with various proportions. This would find the threshold percentage of pyrolysed BFO that can be added without compromising bitumen functionality. A range of 2 to 20% may be considered.
- Ageing is the most pressing issue that biobinders face as they naturally age faster than petroleum bitumens, meaning that there is a reduction of years of service life. Standard bitumen ageing testing does not necessarily simulate the ageing process of biobinders, therefore new laboratory protocols need to be developed that are capable

of reproducing the ageing of biobinders during the manufacturing of asphalt mixtures and service life. The addition of other additives such as crumb rubber could help improve the ageing behaviour of a biobinder blend/mixture, as crumb rubber has been shown to improve ageing resistance of conventional binders. The interactions between the biobinder, specific modifier and bitumen would also be a key area to study.

- Carry out more detailed rheological performance testing and asphalt mixture work and correlate with blending study. For instance, using the Bending Beam Rheometer (BBR) to study low temperature performance is key to confirm if the BFO prevents low temperature cracking. Moisture damage of both the binders and asphalt mixtures could also be studied. Two common tests are the Binder Bond Strength (BBS) test and the Indirect Tensile Strength (ITS) test. BBS analyses the adhesive properties of the binder to aggregates using a pneumatic adhesive testing instrument (PATTI device). The ITS Test (EN 12697-12 (2008)) is commonly used to study the moisture damage of asphalt mixtures.

- Full-scale experiments with prototype road sections would be a last step for the development of biobinder asphalt mixtures, as they would provide real-world results.

References

AFLAKI, S., HAJIKARIMI, P., FINI, E. H. & ZADA, B. 2014. Comparing effects of biobinder with other asphalt modifiers on low-temperature characteristics of asphalt. *Journal of Materials in Civil Engineering,* 26**,** 429-439.

AIREY, G. 1997. *Rheological characteristics of polymer modified and aged bitumens.* University of Nottingham.

AIREY, G., GRENFELL, J., APEAGYEI, A., SUBHY, A. & LO PRESTI, D. L. 2016. Time dependent viscoelastic rheological response of pure, modified and synthetic bituminous binders. *Mechanics of Time-Dependent Materials,* 20**,** 455-480.

AIREY, G. D. 2002a. Rheological evaluation of ethylene vinyl acetate polymer modified bitumens. *Construction and Building Materials,* 16**,** 473-487.

AIREY, G. D. 2002b. Use of black diagrams to identify inconsistencies in rheological data. *Road Materials and Pavement Design,* 3**,** 403-424.

AIREY, G. D. 2003. Rheological properties of styrene butadiene styrene polymer modified road bitumens☆. *Fuel,* 82**,** 1709-1719.

AIREY, G. D. & BROWN, S. F. 1998. Rheological performance of aged polymer modified bitumens. *Journal of the Association of Asphalt Paving Technologists,* 67.

AIREY, G. D. & MOHAMMED, M. H. 2008. Rheological properties of polyacrylates used as synthetic road binders. *Rheologica Acta,* 47**,** 751-763.

AIREY, G. D., MOHAMMED, M. H. & FICHTER, C. 2008. Rheological characteristics of synthetic road binders. *Fuel,* 87**,** 1763-1775.

AKHTAR, J. & AMIN, N. A. S. 2011. A review on process conditions for optimum bio-oil yield in hydrothermal liquefaction of biomass. *Renewable and Sustainable Energy Reviews,* 15**,** 1615-1624.

AL-QADI, I. L., ELSEIFI, M. & CARPENTER, S. H. 2007. Reclaimed asphalt pavement—a literature review.

AL CHAMI, Z., AMER, N., SMETS, K., YPERMAN, J., CARLEER, R., DUMONTET, S. & VANGRONSVELD, J. 2014. Evaluation of flash and slow pyrolysis applied on heavy metal contaminated Sorghum bicolor shoots resulting from phytoremediation. *biomass and bioenergy,* 63**,** 268-279.

ALI, A. H., MASHAAN, N. S. & KARIM, M. R. 2013. Investigations of physical and rheological properties of aged rubberised bitumen. *Advances in Materials Science and Engineering,* 2013.

ALLEN, S. G., KAM, L. C., ZEMANN, A. J. & ANTAL, M. J. 1996. Fractionation of sugar cane with hot, compressed, liquid water. *Industrial & Engineering Chemistry Research,* 35**,** 2709-2715.

ANDERSON, D. A., CHRISTENSEN, D. W., BAHIA, H. U., DONGRE, R., SHARMA, M., ANTLE, C. E. & BUTTON, J. 1994. Binder characterization and evaluation, volume 3: Physical characterization. *Strategic Highway Research Program, National Research Council, Washington, DC*.

ARGENT, E. 2022. *Argent Energy* [Online]. Available: https://argentenergy.com/ [Accessed November 2021].

ASTM D7169, A. S. O. T. A. M. I. 2020. ASTM D7169, Standard Test Method for Boiling Points Distributions of Samples with Residues Such as Crude Oils and Atmospheric and Vacuum Residues by High Temperature Gas Chromatography. West Conshohocken, PA-USA.

AUDO, M., PARASCHIV, M., QUEFFÉLEC, C. M., LOUVET, I., HÉMEZ, J., FAYON, F., LÉPINE, O., LEGRAND, J., TAZEROUT, M. & CHAILLEUX, E. 2015. Subcritical hydrothermal liquefaction of microalgae residues as a green route to alternative road binders. *ACS Sustainable Chemistry & Engineering,* 3**,** 583-590.

AVANTIUM. 2018. *Asphalt composition comprising humins obtained from dehydration of carbohydrates*. The Netherlands patent application 135941 AI.

AZAHAR, W. N. A. W., BUJANG, M., JAYA, R. P., HAININ, M. R., MOHAMED, A., NGAD, N. & JAYANTI, D. S. 2016. The potential of waste cooking oil as bio-asphalt for alternative binder–an overview. *Jurnal Teknologi,* 78.

AZIZ, M. M. A., RAHMAN, M. T., HAININ, M. R. & BAKAR, W. A. W. A. 2015. An overview on alternative binders for flexible pavement. *Construction and Building Materials,* 84**,** 315-319.
BACHLER, C., SCHOBER, S. & MITTELBACH, M. 2010. Simulated distillation for biofuel analysis. *Energy & fuels,* 24**,** 2086-2090.
JIMENEZ DEL BARCO CARRIÓN, A., LO PRESTI, D. & AIREY, G. 2015. Binder design of high RAP content hot and warm asphalt mixture wearing courses. *Road materials and pavement design,* 16**,** 460-474.
JIMENEZ DEL BARCO CARRIÓN, A., LO PRESTI, D., POUGET, S., AIREY, G. & CHAILLEUX, E. 2017. Linear viscoelastic properties of high reclaimed asphalt content mixes with biobinders. *Road Materials and Pavement Design,* 18**,** 241-251.
BENSAID, S., CONTI, R. & FINO, D. 2012. Direct liquefaction of ligno-cellulosic residues for liquid fuel production. *Fuel,* 94**,** 324-332.
BIRD, M., KEITEL, C. & MEREDITH, W. 2017. Analysis of biochars for C, H, N, O and S by elemental analyser. *Biochar: a guide to analytical methods,* 39.
BIRD, R., CLARKE, R., DONELLY, T., HEIDRICH, O. & HUANG, Y. 2004. Life cycle and sustainability indices for road paving materials [unpublished report]. School of Civil Engineering and Geosciences, University of Newcastle upon Tyne.
BLANC, J., CHAILLEUX, E., HORNYCH, P., WILLIAMS, R. C., LO PRESTI, D., JIMENEZ DEL BARCO CARRION, A., POROT, L., PLANCHE, J.-P. & POUGET, S. 2019a. Bio materials with reclaimed asphalt: from lab mixes properties to non-damaged full scale monitoring and mechanical simulation. *Road Materials and Pavement Design,* 20**,** S95-S111.
BLANC, J., HORNYCH, P., SOTOODEH-NIA, Z., WILLIAMS, C., POROT, L., POUGET, S., BOYSEN, R., PLANCHE, J.-P., LO PRESTI, D. & JIMENEZ, A. 2019b. Full-scale validation of bio-recycled asphalt mixtures for road pavements. *Journal of cleaner production,* 227**,** 1068-1078.
BOATENG, A. & MULLEN, C. 2013. Fast pyrolysis of biomass thermally pretreated by torrefaction. *Journal of Analytical and Applied Pyrolysis,* 100**,** 95-102.
BORGHOL, I., QUEFFÉLEC, C., BOLLE, P., DESCAMPS, J., LOMBARD, C., LÉPINE, O., KUCMA, D., LORENTZ, C., LAURENTI, D. & MONTOUILLOUT, V. 2018. Biosourced analogs of elastomer-containing bitumen through hydrothermal liquefaction of Spirulina sp. microalgae residues. *Green Chemistry,* 20**,** 2337-2344.
BRIDGWATER, A. V. 2012. Review of fast pyrolysis of biomass and product upgrading. *Biomass and bioenergy,* 38**,** 68-94.
BRITISH STANDARDS 1990. *BS 3690. Bitumens for building and Civil Engineering. Part 3. Specification for mixtures of bitumen with pitch, tar and Trinidad Lake asphalt.*
BRITISH STANDARDS 2005. *EN 13108-8. Bituminous mixtures — Material specifications — Part 8: Reclaimed asphalt.*
BRITISH STANDARDS 2007. *BS EN 15323. Bitumen and bituminous binders — Accelerated long-term ageing / conditioning by the rotating cylinder method (RCAT).*
BRITISH STANDARDS 2009. *EN 12591. Bitumen and bituminous binders - Specifications for paving grade bitumens.*
BRITISH STANDARDS 2010. *BS EN 13302:2010. Bitumen and bituminous binders — Determination of dynamic viscosity of bituminous binder using a rotating spindle apparatus*
BRITISH STANDARDS 2012. *BS EN 14769. Bitumen and bituminous binders — Accelerated long-term ageing conditioning by a Pressure Ageing Vessel (PAV).*
BRITISH STANDARDS 2014a. *BS EN 12607-2. Bitumen and bituminous binders — Determination of the resistance to hardening under influence of heat and air Part 2 : TFOT method.*
BRITISH STANDARDS 2014b. *BS EN 12607-1. Bitumen and bituminous binders — Determination of the resistance to hardening under influence of heat and air Part 1 : RTFOT method.*

BROOKFIELD ENGINEERING LABORATORIES. 2014. More solutions to sticky problems Available: https://www.academia.edu/34377304/MORE_SOLUTIONS_TO_STICKY_PROBLEMS.

BROWN, R. C. & ZHANG, X. 2019. Chapter 1: Introduction to Thermochemical Processing of Biomass into Fuels, Chemicals and Power. *Thermochemical Processing of Biomass : Conversion into Fuels, Chemicals and Power, John Wiley & Sons, Incorporated, 2nd ed.*

CARO, S., VEGA, N., HUSSERL, J. & ALVAREZ, A. E. 2016. Studying the impact of biomodifiers produced from agroindustrial wastes on asphalt binders. *Construction and Building Materials,* 126**,** 369-380.

CHAILLEUX, E., AUDO, M., BUJOLI, B., QUEFFELEC, C., LEGRAND, J. & LEPINE, O. Alternative binder from microalgae: Algoroute project. Workshop alternative binders for sustainable asphalt pavements, 2012. pp 7-14.

CHAILLEUX, E., BESSMANN, E., HORNYCH, P., BLANC, J., GAUDEFROY, V., SOTOODEH-NIA, Z. & OLARD, F. Biorepavation: Innovation in bio-recycling of old asphalt pavements, comparison between EU and US mix design specification systems. International ISAP Conference, 2018.

CHENG, S., D'CRUZ, I., WANG, M., LEITCH, M. & XU, C. 2010. Highly efficient liquefaction of woody biomass in hot-compressed alcohol− water co-solvents. *Energy & Fuels,* 24**,** 4659-4667.

CLARK, J. 2014. *Chemguide: Interpreting C-13 NMR spectra* [Online]. Available: https://www.chemguide.co.uk/analysis/nmr/interpretc13.html#top [Accessed 15-11-2021, 2021].

COLAS. 2004a. *Liant de nature végétale pour la réalisation de matériaux pour le bâtiment et/ou les travaux publics*. EP1466878(A1).

COLAS. 2004b. *Obtention de liants routiers a`base de bitume et d'une nouvelle gamme de fluxantsd'origine naturelle fonctionnalises*. EP1645595 (A1).

COLLARD, F.-X. & BLIN, J. 2014. A review on pyrolysis of biomass constituents: Mechanisms and composition of the products obtained from the conversion of cellulose, hemicelluloses and lignin. *Renewable and Sustainable Energy Reviews,* 38**,** 594-608.

COUNCIL, N. R. 2009. *Liquid transportation fuels from coal and biomass: technological status, costs, and environmental impacts*, National Academies Press.

CUCINIELLO, G., LEANDRI, P., LOSA, M. & AIREY, G. 2020. Effects of ageing on the damage tolerance of polymer modified bitumens investigated through the LAS test and fluorescence microscopy. *International Journal of Pavement Engineering***,** 1-12.

D'MELO, D. R. T. 2015. Constitution and structure of bitumens. *In:* R.N. HUNTER, A. S., J. READ (ed.) *The Shell Bitumen Handbook.* 6 ed. London: ICE Publishing.

DE TOULOUSE, I. 2010. *Coating material for road construction*. WO2010/003838 (A1).

DELAPORTE, B., DI BENEDETTO, H., CHAVEROT, P. & GAUTHIER, G. 2007. Linear viscoelastic properties of bituminous materials: from binders to mastics (with discussion). *Journal of the Association of Asphalt Paving Technologists,* 76.

DEMIRBAS, A. 2005. Pyrolysis of ground beech wood in irregular heating rate conditions. *Journal of Analytical and Applied Pyrolysis,* 73**,** 39-43.

DEMIRBAŞ, A. 2001. Biomass resource facilities and biomass conversion processing for fuels and chemicals. *Energy conversion and Management,* 42**,** 1357-1378.

DHASMANA, H., OZER, H., AL-QADI, I. L., ZHANG, Y., SCHIDEMAN, L., SHARMA, B. K., CHEN, W.-T., MINARICK, M. J. & ZHANG, P. 2015. Rheological and chemical characterization of biobinders from different biomass resources. *Transportation Research Record,* 2505**,** 121-129.

DI BENEDETTO, H., OLARD, F., SAUZÉAT, C. & DELAPORTE, B. 2004. Linear viscoelastic behaviour of bituminous materials: From binders to mixes. *Road Materials and Pavement Design,* 5**,** 163-202.

DIAMANTE, L. M. & LAN, T. 2014. Absolute viscosities of vegetable oils at different temperatures and shear rate range of 64.5 to 4835 s− 1. *Journal of food processing,* 2014.

DIMITRIADIS, A. & BEZERGIANNI, S. 2017. Hydrothermal liquefaction of various biomass and waste feedstocks for biocrude production: a state of the art review. *Renewable and Sustainable Energy Reviews,* 68**,** 113-125.

DING, X., CHEN, L., MA, T., MA, H., GU, L., CHEN, T. & MA, Y. 2019. Laboratory investigation of the recycled asphalt concrete with stable crumb rubber asphalt binder. *Construction and Building Materials,* 203**,** 552-557.

DOASSANS-CARRÈRE, N., FERRASSE, J.-H., BOUTIN, O., MAUVIEL, G. & LÉDÉ, J. 2014. Comparative study of biomass fast pyrolysis and direct liquefaction for bio-oils production: products yield and characterizations. *Energy & Fuels,* 28**,** 5103-5111.

DOBSON, G., MONISMITH, C., PUZINAUSKAS, V. & BUSCHING, H. The dynamic mechanical properties of bitumen. Association of Asphalt Paving Technologists Proc, 1969.

DONGRÉ, R. & D'ANGELO, J. 2003. Refinement of Superpave high-temperature binder specification based on pavement performance in the accelerated loading facility. *Transportation research record,* 1829**,** 39-46.

EAPA 2020. Asphalt in Figures 2019. *Asphalt in Figures.* Brussels, Belgium: European Asphalt Pavement Association.

ECOBIOPAVE™. 2004a. *Acknowledgement of organizations involved in the evaluation of GEO320™ and MRH™ over the years* [Online]. Australia. Available: http://www.owerhall.bigpondhosting.com/biopave/bio_bitumen_asphalt_concrete_research_eco-biopave_australia_006.htm [Accessed May 2021].

ECOBIOPAVE™. 2004b. *GEO320 MRH Research Line Marking field testing* [Online]. Australia. Available: http://www.owerhall.bigpondhosting.com/biopave/boral_geo320_field_trial/eco-biopave_geo320_bio_bitumen_asphalt_concrete_testing_007.htm [Accessed May 2021].

EDNEY, M. K., KOTOWSKA, A. M., SPANU, M., TRINDADE, G. F., WILMOT, E., REID, J., BARKER, J., AYLOTT, J. W., SHARD, A. G. & ALEXANDER, M. R. 2022. Molecular formula prediction for chemical filtering of 3D OrbiSIMS Datasets. *Analytical Chemistry*.

EDNEY, M. K., LAMB, J. S., SPANU, M., SMITH, E. F., STEER, E., WILMOT, E., REID, J., BARKER, J., ALEXANDER, M. R. & SNAPE, C. E. 2020. Spatially Resolved Molecular Compositions of Insoluble Multilayer Deposits Responsible for Increased Pollution from Internal Combustion Engines. *ACS Applied Materials & Interfaces,* 12**,** 51026-51035.

EIFFAGE. 2007. *Composition comprenant une fraction organique pour la réalisation d'une couche et/ou d'un revêtement de voie ou de bâtiment*. FR2915204 (A1).

ELLIOTT, D., BECKMAN, D., BRIDGWATER, A., DIEBOLD, J., GEVERT, S. & SOLANTAUSTA, Y. 1991. Developments in direct thermochemical liquefaction of biomass: 1983-1990. *Energy & Fuels,* 5**,** 399-410.

ELLIOTT, D. C., BILLER, P., ROSS, A. B., SCHMIDT, A. J. & JONES, S. B. 2015. Hydrothermal liquefaction of biomass: developments from batch to continuous process. *Bioresource technology,* 178**,** 147-156.

ELLIOTT, D. C., HART, T. R., NEUENSCHWANDER, G. G., ROTNESS, L. J., ROESIJADI, G., ZACHER, A. H. & MAGNUSON, J. K. 2014. Hydrothermal processing of macroalgal feedstocks in continuous-flow reactors. *ACS Sustainable Chemistry & Engineering,* 2**,** 207-215.

ELLIOTT, D. C., HART, T. R., SCHMIDT, A. J., NEUENSCHWANDER, G. G., ROTNESS, L. J., OLARTE, M. V., ZACHER, A. H., ALBRECHT, K. O., HALLEN, R. T. & HOLLADAY, J. E. 2013. Process development for hydrothermal liquefaction of algae feedstocks in a continuous-flow reactor. *Algal Research,* 2**,** 445-454.

ELLIOTT, D. C., NEUENSCHWANDER, G. G., HART, T. R., BUTNER, R. S., ZACHER, A. H., ENGELHARD, M. H., YOUNG, J. S. & MCCREADY, D. E. 2004. Chemical processing in high-pressure aqueous environments. 7. Process development for catalytic gasification of wet biomass feedstocks. *Industrial & engineering chemistry research,* 43**,** 1999-2004.

EUROPEAN BITUMEN ASSOCIATION 2012. Life Cycle Inventory: Bitumen. 2 ed. Eurobitume, Brussels, Belgium.
EUROPEAN STANDARDS 2015. *EN 1426. Bitumen and bituminous binders — Determination of needle penetration.*
EUROVIA. 2010. *Liant synthétique essentiellement à base de matières issues de ressources renouvelables, en particulier d'origine végétale, et ses applications en technique routière*. FR2955586 (A1).
FASINA, O., HALLMAN, H., CRAIG-SCHMIDT, M. & CLEMENTS, C. 2006. Predicting temperature-dependence viscosity of vegetable oils from fatty acid composition. *Journal of the American Oil Chemists' Society,* 83**,** 899.
FAUSTINO, H., GIL, N., BAPTISTA, C. & DUARTE, A. P. 2010. Antioxidant activity of lignin phenolic compounds extracted from kraft and sulphite black liquors. *Molecules,* 15**,** 9308-9322.
FERRY, J. D. 1980. *Viscoelastic properties of polymers*, John Wiley & Sons.
FIFIELD, F. W. & KEALEY, D. 2000. *Principles and practice of analytical chemistry*, Cambridge.
FINI, E. H., AL-QADI, I. L., YOU, Z., ZADA, B. & MILLS-BEALE, J. 2012. Partial replacement of asphalt binder with bio-binder: characterisation and modification. *International Journal of Pavement Engineering,* 13**,** 515-522.
FINI, E. H. & BUEHLER, M. J. Reducing asphalt's low temperature cracking by disturbing its crystallization. 7th RILEM International Conference on Cracking in Pavements, 2012. Springer, 911-919.
FINI, E. H., HOSSEINNEZHAD, S., OLDHAM, D. J., CHAILLEUX, E. & GAUDEFROY, V. 2017. Source dependency of rheological and surface characteristics of bio-modified asphalts. *Road Materials and Pavement Design,* 18**,** 408-424.
FINI, E. H., KALBERER, E. W., SHAHBAZI, A., BASTI, M., YOU, Z., OZER, H. & AURANGZEB, Q. 2011. Chemical characterization of biobinder from swine manure: Sustainable modifier for asphalt binder. *Journal of Materials in Civil Engineering,* 23**,** 1506-1513.
FINI, E. H., OLDHAM, D. J. & ABU-LEBDEH, T. 2013. Synthesis and characterization of biomodified rubber asphalt: Sustainable waste management solution for scrap tire and swine manure. *Journal of Environmental Engineering,* 139**,** 1454-1461.
GERSHKOFF, J. C. 1991. *A study of the rheological behaviour of some surface dressing binders (MSc thesis).* School of Civil Engineering, The University of Nottingham.
GOLLAKOTA, A., KISHORE, N. & GU, S. 2018. A review on hydrothermal liquefaction of biomass. *Renewable and Sustainable Energy Reviews,* 81**,** 1378-1392.
GONDIM, L., SOARES, S., BARROSO, S., ALECRIN, C. 2017. Chemical and physical properties of an asphalt binder modified by the sap of Euphorbia Tirucalli plant: Application in bituminous prime coat. *10th International Conference on the Bearing Capacity of Roads, Railways and Airfields.* Athens, Greece.
GONG, M., YANG, J., ZHANG, J., ZHU, H. & TONG, T. 2016. Physical–chemical properties of aged asphalt rejuvenated by bio-oil derived from biodiesel residue. *Construction and Building Materials,* 105**,** 35-45.
GONG, M., ZHU, H., PAULI, T., YANG, J., WEI, J. & YAO, Z. 2017. Evaluation of bio-binder modified asphalt's adhesion behavior using sessile drop device and atomic force microscopy. *Construction and Building Materials,* 145**,** 42-51.
GOYAL, H., SEAL, D. & SAXENA, R. 2008. Bio-fuels from thermochemical conversion of renewable resources: a review. *Renewable and sustainable energy reviews,* 12**,** 504-517.
GUO, M., SONG, W. & BUHAIN, J. 2015. Bioenergy and biofuels: History, status, and perspective. *Renewable and Sustainable Energy Reviews,* 42**,** 712-725.
HAARLEMMER, G., GUIZANI, C., ANOUTI, S., DÉNIEL, M., ROUBAUD, A. & VALIN, S. 2016. Analysis and comparison of bio-oils obtained by hydrothermal liquefaction and fast pyrolysis of beech wood. *Fuel,* 174**,** 180-188.
HAMZAH, M. O., KAKAR, M. R. & HAININ, M. R. 2015. An overview of moisture damage in asphalt mixtures. *Jurnal Teknologi,* 73.

HARMAN, T., YOUTCHEFF, J. & BUKOWSKI, J. 2011. The multiple stress creep recovery (MSCR) procedure. United States. Federal Highway Administration.
HASHEMPOUR-BALTORK, F., TORBATI, M., AZADMARD-DAMIRCHI, S. & SAVAGE, G. P. 2018. Chemical, rheological and nutritional characteristics of sesame and olive oils blended with linseed oil. *Advanced pharmaceutical bulletin,* 8**,** 107.
HASHMI, S. & JABARY, A. 2020. Introduction of a Sustainable Alternative for Bitumen: Case study of lignin-based asphalt for the Swedish market.
HILL, B., OLDHAM, D., BEHNIA, B., FINI, E. H., BUTTLAR, W. G. & REIS, H. 2013. Low-temperature performance characterization of biomodified asphalt mixtures that contain reclaimed asphalt pavement. *Transportation Research Record,* 2371**,** 49-57.
HILL, B., OLDHAM, D., BEHNIA, B., FINI, E. H., BUTTLAR, W. G. & REIS, H. 2018. Evaluation of low temperature viscoelastic properties and fracture behavior of bio-asphalt mixtures. *International Journal of Pavement Engineering,* 19**,** 362-369.
HUANG, Y., BIRD, R. & HEIDRICH, O. 2009. Development of a life cycle assessment tool for construction and maintenance of asphalt pavements. *Journal of Cleaner Production,* 17**,** 283-296.
HVEEM, F. N., ZUBE, E. & SKOG, J. Proposed new tests and specifications for paving grade asphalts. Association of Asphalt Paving Technologists Proceedings, 1963.
INGRASSIA, L. P., LU, X., FERROTTI, G. & CANESTRARI, F. 2019. Renewable materials in bituminous binders and mixtures: Speculative pretext or reliable opportunity? *Resources, Conservation and Recycling,* 144**,** 209-222.
ISA, K. M. 2015. *High conversions of biomass and pyrolysis oil using sub- and supercritical water above 400 °C.* University of Nottingham.
JAZRAWI, C., BILLER, P., ROSS, A. B., MONTOYA, A., MASCHMEYER, T. & HAYNES, B. S. 2013. Pilot plant testing of continuous hydrothermal liquefaction of microalgae. *Algal Research,* 2**,** 268-277.
JIMENEZ DEL BARCO CARRION, A. 2017. *Design and characterisation of reclaimed asphalt mixtures with biobinders.* University of Nottingham.
JIMÉNEZ DEL BARCO CARRIÓN, A., CARVAJAL-MUÑOZ, J. S., LO PRESTI, D. & AIREY, G. 2019. Intrinsic adhesive and cohesive assessment of the moisture sensitivity of bio-rejuvenated recycled asphalt binders. *Road Materials and Pavement Design,* 20**,** S347-S364.
JIMÉNEZ DEL BARCO CARRIÓN, A., PÉREZ-MARTÍNEZ, M., THEMELI, A., LO PRESTI, D., MARSAC, P., POUGET, S., HAMMOUM, F., CHAILLEUX, E. & AIREY, G. 2017. Evaluation of bio-materials' rejuvenating effect on binders for high-reclaimed asphalt content mixtures. *Materiales de Construcción,* 67**,** 1-11.
JIN, B., DUAN, P., XU, Y., WANG, F. & FAN, Y. 2013. Co-liquefaction of micro-and macroalgae in subcritical water. *Bioresource technology,* 149**,** 103-110.
KALANTAR, Z. N., KARIM, M. R. & MAHREZ, A. 2012. A review of using waste and virgin polymer in pavement. *Construction and Building Materials,* 33**,** 55-62.
KARLSSON, R. & ISACSSON, U. 2006. Material-related aspects of asphalt recycling—state-of-the-art. *Journal of Materials in Civil Engineering,* 18**,** 81-92.
KLIEWER, J. E., ZENG, H. & VINSON, T. S. 1996. Aging and low-temperature cracking of asphalt concrete mixture. *Journal of Cold Regions Engineering,* 10**,** 134-148.
KLUTTZ, R. Considerations for Use of Alternative Binders in Asphalt Pavements. TRB 91st Annual Meeting, Alternative Binders for Sustainable Asphalt Pavements, Washington, DC, 2012. Citeseer, 2-6.
KOENDERS, B. 2015. Routine testing and mechanical properties of bitumens. *In:* R.N. HUNTER, A. S., J. READ (ed.) *The Shell Bitumen Handbook.* 6 ed. London: ICE Publishing.
LADNER, W. R. & SNAPE, C. E. 1978. Application of quantitative 13C nuclear magnetic resonance spectroscopy to coal-derived materials. *Fuel,* 57**,** 658-662.
LÉDÉ, J., BROUST, F., NDIAYE, F.-T. & FERRER, M. 2007. Properties of bio-oils produced by biomass fast pyrolysis in a cyclone reactor. *Fuel,* 86**,** 1800-1810.

LESUEUR, D. 2009. The colloidal structure of bitumen: Consequences on the rheology and on the mechanisms of bitumen modification. *Advances in colloid and interface science,* 145**,** 42-82.
LI, Q., LIU, D., SONG, L., WU, P., YAN, Z. & LI, M. 2016. Investigation of solvent effect on the hydro-liquefaction of sawdust: an innovative reference approach using tetralin as chemical probe. *Fuel,* 164**,** 94-98.
LIU, H., ZEIADA, W., AL-KHATEEB, G. G., SHANABLEH, A. & SAMARAI, M. 2021. Use of the multiple stress creep recovery (MSCR) test to characterize the rutting potential of asphalt binders: A literature review. *Construction and Building Materials,* 269**,** 121320.
LIU, Z. & ZHANG, F.-S. 2008. Effects of various solvents on the liquefaction of biomass to produce fuels and chemical feedstocks. *Energy conversion and management,* 49**,** 3498-3504.
LO PRESTI, D., JIMENEZ DEL BARCO CARRIÓN, A., AIREY, G. & HAJJ, E. 2016. Towards 100% recycling of reclaimed asphalt in road surface courses: binder design methodology and case studies. *Journal of cleaner production,* 131**,** 43-51.
LU, X. & ISACSSON, U. 1998. Chemical and rheological evaluation of ageing properties of SBS polymer modified bitumens. *Fuel,* 77**,** 961-972.
LU, X. & ISACSSON, U. 2000. Artificial aging of polymer modified bitumens. *Journal of applied polymer science,* 76**,** 1811-1824.
LU, X. & ISACSSON, U. 2002. Effect of ageing on bitumen chemistry and rheology. *Construction and Building materials,* 16**,** 15-22.
M. VONDENHOF, N. C. 2015. Specifying bitumens and checking their quality. *In:* R.N. HUNTER, A. S., J. READ (ed.) *The Shell Bitumen Handbook.* 6 ed. London: ICE Publishing.
MAHSSIN, Z. Y., HASSAN, N. A., YAACOB, H., PUTEH, M. H., AMIN, N. A. S., ZAINOL, M. M. & HAININ, M. R. Characterization of asphalt binder containing hydrothermal liquefied composition extracted from food waste. IOP Conference Series: Earth and Environmental Science, 2019. IOP Publishing, 012013.
MAMAT, R., HAININ, M. R., HASSAN, N. A., RAHMAN, N. A. A., WARID, M. N. M. & IDHAM, M. K. 2015. A review of performance asphalt mixtures using bio-binder as alternative binder. *Jurnal Teknologi,* 77.
MANKE, N. D., WILLIAMS, R. C., SOTOODEH-NIA, Z., COCHRAN, E. W., POROT, L., CHAILLEUX, E., POUGET, S., OLARD, F., JIMENEZ DEL BARCO CARRION, A. & PLANCHE, J.-P. 2019. Performance of a sustainable asphalt mix incorporating high RAP content and novel bio-derived binder. *Road Materials and Pavement Design***,** 1-23.
MARATEANU, M. & ANDERSON, D. 1996. Time-temperature dependency of asphalt binders--An improved model (with discussion). *Journal of the Association of Asphalt Paving Technologists,* 65.
MARTÍNEZ-ECHEVARRÍA-ROMERO, M., GARCÍA-TRAVÉ, G., RUBIO-GÁMEZ, M., MORENO-NAVARRO, F. & PÉREZ-MIRA, D. 2015. Valorization of vinasse as binder modifier in asphalt mixtures. *Dyna,* 82**,** 52-56.
MCKENDRY, P. 2002a. Energy production from biomass (part 1): overview of biomass. *Bioresource technology,* 83**,** 37-46.
MCKENDRY, P. 2002b. Energy production from biomass (part 2): conversion technologies. *Bioresource technology,* 83**,** 47-54.
METWALLY, M. & RAOUF, M. A. 2010. Development of non-petroleum binders derived from fast pyrolysis bio-oils for use in flexible pavement.
MILLS-BEALE, J., YOU, Z., FINI, E., ZADA, B., LEE, C. H. & YAP, Y. K. 2012. Aging influence on rheology properties of petroleum-based asphalt modified with biobinder. *Journal of Materials in Civil Engineering,* 26**,** 358-366.
MOGAWER, W. S., BOOSHEHRIAN, A., VAHIDI, S. & AUSTERMAN, A. J. 2013. Evaluating the effect of rejuvenators on the degree of blending and performance of high RAP, RAS, and RAP/RAS mixtures. *Road Materials and Pavement Design,* 14**,** 193-213.

MOGAWER, W. S., FINI, E. H., AUSTERMAN, A. J., BOOSHEHRIAN, A. & ZADA, B. 2016. Performance characteristics of high reclaimed asphalt pavement containing bio-modifier. *Road Materials and Pavement Design,* 17**,** 753-767.
MOHAMMAD, L. N., ELSEIFI, M. A., COOPER III, S. B., CHALLA, H. & NAIDOO, P. 2013. Laboratory evaluation of asphalt mixtures that contain biobinder technologies. *Transportation Research Record,* 2371**,** 58-65.
MOTAMEDI, M., SHAFABAKHSH, G. & AZADI, M. 2021. Evaluation of fatigue and rutting properties of asphalt binder and mastic modified by synthesized polyurethane. *Journal of Traffic and Transportation Engineering (English Edition),* 8**,** 1036-1048.
NAYAK, P. & SAHOO, U. C. 2017a. A rheological study on aged binder rejuvenated with Pongamia oil and Composite castor oil. *International Journal of Pavement Engineering,* 18**,** 595-607.
NAYAK, P. & SAHOO, U. C. 2017b. Rheological, chemical and thermal investigations on an aged binder rejuvenated with two non-edible oils. *Road Materials and Pavement Design,* 18**,** 612-629.
OLAOYE, T. S., DEWSBURY, M. & KUNZEL, H. 2021. A method for establishing a hygrothermally controlled test room for measuring the water vapor resistivity characteristics of construction materials. *Energies,* 14**,** 4.
OLARD, F. & DI BENEDETTO, H. 2003. General "2S2P1D" model and relation between the linear viscoelastic behaviours of bituminous binders and mixes. *Road materials and pavement design,* 4**,** 185-224.
OLARD, F., DI BENEDETTO, H., ECKMANN, B. & TRIQUIGNEAUX, J.-P. 2003. Linear viscoelastic properties of bituminous binders and mixtures at low and intermediate temperatures. *Road materials and pavement design,* 4**,** 77-107.
OWERHALL, E. J., MALMBERG, S. J. & PELTONEN, S. T. 2016. *Bio Bitumen Binder Composition*. Australia patent application AU2016100073 (A4).
PALM. 2022. *Palm* [Online]. Papierfabrik Palm GmbH & Co KG. Available: https://www.palm.de/en.html [Accessed February 2022].
PASQUIER, M. 1997. *Liant bitumineux, composition et utilisation*. FR2768150 (A1).
PAVEMENT INTERACTIVE 2013. Aggregate.
PELLINEN, T., ZOFKA, A., MARASTEANU, M. & FUNK, N. Asphalt mixture stiffness predictive models. Asphalt Paving Technology: Association of Asphalt Paving Technologists-Proceedings of the Technical Sessions, 2007. Association of Asphalt Paving Technologist, 575-625.
PERALTA, J., WILLIAMS, R. C., ROVER, M. & SILVA, H. M. R. D. D. 2012. Development of a rubber-modified fractionated bio-oil for use as noncrude petroleum binder in flexible pavements. *Transportation Research Circular***,** 23-36.
PERLACK, R. D., STOKES, B.J. 2011. US billion-ton update: biomass supply for a bioenergy and bioproducts industry. *In:* LABORATORY, O. R. N. (ed.). Oak Ridge, TN: US Department of Energy.
PETERSON, J., ROBERTSON, R., BRANTHAVER, J., HARNSBERGER, P., DUVALL, J. & KIM, S. 1994. Binder Characterization and Evaluation, Volume 4: Test Methods. SHRP.
PINOMAA, O. 1991. *Dyeable pavement material*. US5021476 (A).
POERAN, N., SLUER, B., VAN DE VEN, M. & GARD, W. 2017. Improving the raveling resistance of porous asphalt with kraft lignin modified bitumen. *Bearing Capacity of Roads, Railways and Airfields.* CRC Press.
PORTUGAL, A. C. X., LUCENA, L. C. D. F. L., LUCENA, A. E. D. F. L. & BESERRA DA COSTA, D. 2018. Rheological performance of soybean in asphalt binder modification. *Road Materials and Pavement Design,* 19**,** 768-782.
POUGET, S. & LOUP, F. 2013. Thermo-mechanical behaviour of mixtures containing bio-binders. *Road Materials and Pavement Design,* 14**,** 212-226.
PRESTON, N. & O'NIONS, L. 2015. Durability of bitumens and asphalts. *In:* R.N. HUNTER, A. S., J. READ (ed.) *The Shell Bitumen Handbook.* 6 ed. London: ICE Publishing.
QU, Y., WEI, X. & ZHONG, C. 2003. Experimental study on the direct liquefaction of Cunninghamia lanceolata in water. *Energy,* 28**,** 597-606.

RAOUF, M. A. & WILLIAMS, C. R. 2010a. General rheological properties of fractionated switchgrass bio-oil as a pavement material. *Road Materials and Pavement Design,* 11**,** 325-353.
RAOUF, M. A. & WILLIAMS, R. C. 2010b. General rheological properties of fractionated switchgrass bio-oil as a pavement material. *Road Materials and Pavement Design,* 11**,** 325-353.
RAOUF, M. A. & WILLIAMS, R. C. 2010c. Temperature and shear susceptibility of a nonpetroleum binder as a pavement material. *Transportation research record,* 2180**,** 9-18.
READ, J. M. 1996. *Fatigue Cracking of bituminous paving mixtures.* University of Nottingham.
RODRIGUES, C. & HANUMANTHGARI, R. 2015. Polymer modified bitumens and other modified binders. *In:* R.N. HUNTER, A. S., J. READ (ed.) *The Shell Bitumen Handbook.* 6 ed. London: ICE Publishing.
ROMBERG, J., NESMITH, S. & TRAXLER, R. 1959. Some Chemical Aspects of the Components of Asphalt. *Journal of Chemical and Engineering Data,* 4**,** 159-161.
RUAN, Y., DAVISON, R. R. & GLOVER, C. J. 2003. The effect of long-term oxidation on the rheological properties of polymer modified asphalts☆. *Fuel,* 82**,** 1763-1773.
SAMIEADEL, A., SCHIMMEL, K. & FINI, E. H. 2018. Comparative life cycle assessment (LCA) of bio-modified binder and conventional asphalt binder. *Clean Technologies and Environmental Policy,* 20**,** 191-200.
SANTOS, E. F., OLIVEIRA, R. V. B., REIZNAUTT, Q. B., SAMIOS, D. & NACHTIGALL, S. M. B. 2014. Sunflower-oil biodiesel-oligoesters/polylactide blends: Plasticizing effect and ageing. *Polymer Testing,* 39**,** 23-29.
SANTOS, J., BRESSI, S., CEREZO, V., LO PRESTI, D. & DAUVERGNE, M. 2018. Life cycle assessment of low temperature asphalt mixtures for road pavement surfaces: A comparative analysis. *Resources, Conservation and Recycling,* 138**,** 283-297.
SANTOS, J., FLINTSCH, G. & FERREIRA, A. 2017. Environmental and economic assessment of pavement construction and management practices for enhancing pavement sustainability. *Resources, Conservation and Recycling,* 116**,** 15-31.
SARKER, N. 2015. Design of Asphalt Mixtures. *In:* R.N. HUNTER, A. S., J. READ (ed.) *The Shell Bitumen Handbook.* 6 ed. London: ICE Publishing.
SEIDEL, J. C. & HADDOCK, J. E. 2012. Soy fatty acids as sustainable modifier for asphalt binders. *Alternative Binders for Sustainable Asphalt Pavements Washington DC*.
SELF, A. 2015. Introduction. *In:* R.N. HUNTER, A. S., J. READ (ed.) *The Shell Bitumen Handbook.* 6 ed. London: ICE Publishing.
SHELL. 2010. *Binder composition and asphalt mixture*. WO2010128105 (A1).
SILINA, Y. E. & VOLMER, D. A. 2013. Nanostructured solid substrates for efficient laser desorption/ionization mass spectrometry (LDI-MS) of low molecular weight compounds. *Analyst,* 138**,** 7053-7065.
SINGH, M., KUMAR, P. & MAURYA, M. R. 2013. Strength characteristics of SBS modified asphalt mixes with various aggregates. *Construction and Building Materials,* 41**,** 815-823.
SINGH, R., BHASKAR, T. & BALAGURUMURTHY, B. 2015. Effect of solvent on the hydrothermal liquefaction of macro algae Ulva fasciata. *Process Safety and Environmental Protection,* 93**,** 154-160.
SOMÉ, S. C., GAUDEFROY, V. & DELAUNAY, D. 2016. Effect of vegetable oil additives on binder and mix properties: laboratory and field investigation. *Materials and structures,* 49**,** 2197-2208.
SOTOODEH-NIA, Z., MANKE, N., WILLIAMS, R. C., COCHRAN, E. W., POROT, L., CHAILLEUX, E., LO PRESTI, D., JIMENEZ DEL BARCO CARRIÓN, A. & BLANC, J. 2019. Effect of two novel bio-based rejuvenators on the performance of 50% RAP mixes–a statistical study on the complex modulus of asphalt binders and asphalt mixtures. *Road Materials and Pavement Design***,** 1-18.
SUN, D., LU, T., XIAO, F., ZHU, X. & SUN, G. 2017a. Formulation and aging resistance of modified bio-asphalt containing high percentage of waste cooking oil residues. *Journal of Cleaner Production,* 161**,** 1203-1214.

SUN, D., SUN, G., DU, Y., ZHU, X., LU, T., PANG, Q., SHI, S. & DAI, Z. 2017b. Evaluation of optimized bio-asphalt containing high content waste cooking oil residues. *Fuel,* 202**,** 529-540.
SUN, P., HENG, M., SUN, S. & CHEN, J. 2010. Direct liquefaction of paulownia in hot compressed water: Influence of catalysts. *Energy,* 35**,** 5421-5429.
SUN, Z., YI, J., HUANG, Y., FENG, D. & GUO, C. 2016. Investigation of the potential application of biodiesel by-product as asphalt modifier. *Road Materials and Pavement Design,* 17**,** 737-752.
TAO, J., LI, J., YAN, B., CHEN, G., CHENG, Z., LIN, F., MA, W. & CRITTENDEN, J. C. 2020. Biomass combustion: Environmental impact of various precombustion processes. *Journal of Cleaner Production***,** 121217.
TAYLOR, R. & AIREY, G. 2015. Rheology of bitumens. *In:* R.N. HUNTER, A. S., J. READ (ed.) *The Shell Bitumen Handbook.* 6 ed. London: ICE Publishing.
TEWS, I. J., ZHU, Y., DRENNAN, C., ELLIOTT, D. C., SNOWDEN-SWAN, L. J., ONARHEIM, K., SOLANTAUSTA, Y. & BECKMAN, D. 2014. Biomass Direct Liquefaction Options. TechnoEconomic and Life Cycle Assessment. Pacific Northwest National Lab.(PNNL), Richland, WA (United States).
THE FREEDONIA GROUP. 2021. *World Asphalt (Bitumen)* [Online]. Cleveland, USA. Available: https://www.freedoniagroup.com/industry-study/world-asphalt-bitumen-3351.htm [Accessed January 2022].
THOM, N. 2008. *Principles of pavement engineering*, Thomas Telford London.
TOOR, S. S., ROSENDAHL, L. & RUDOLF, A. 2011. Hydrothermal liquefaction of biomass: a review of subcritical water technologies. *Energy,* 36**,** 2328-2342.
TRAN, N., TAYLOR, A., TURNER, P., HOLMES, C. & POROT, L. 2017. Effect of rejuvenator on performance characteristics of high RAP mixture. *Road Materials and Pavement Design,* 18**,** 183-208.
TRAXLER, R. 1936. The Physical Chemistry of Asphaltic Bitumen. *Chemical reviews,* 19**,** 119-143.
VALAGRO. 2011. *Procédé de préparation d'une composition tensioactive à base de bio-tensioactifs non-ioniques d'origine naturelle*. FR2972191 (A1).
VALDEZ, P. J., NELSON, M. C., WANG, H. Y., LIN, X. N. & SAVAGE, P. E. 2012. Hydrothermal liquefaction of Nannochloropsis sp.: Systematic study of process variables and analysis of the product fractions. *Biomass and Bioenergy,* 46**,** 317-331.
VAN VLIET, D., SLAGHEK, T., GIEZEN, C. & HAAKSMAN, I. Lignin as a green alternative for bitumen. Proceedings of the 6th Euroasphalt & Eurobitume Congress, Prague, Czech, 2016. 1-3.
VASSILEV, S. V., VASSILEVA, C. G. & VASSILEV, V. S. 2015. Advantages and disadvantages of composition and properties of biomass in comparison with coal: An overview. *Fuel,* 158**,** 330-350.
WANG, Y., WANG, H., LIN, H., ZHENG, Y., ZHAO, J., PELLETIER, A. & LI, K. 2013. Effects of solvents and catalysts in liquefaction of pinewood sawdust for the production of bio-oils. *Biomass and bioenergy,* 59**,** 158-167.
WEIR, A., JIMÉNEZ DEL BARCO CARRIÓN, A., QUEFFÉLEC, C., BUJOLI, B., CHAILLEUX, E., UGUNA, C. N., SNAPE, C. & AIREY, G. 2022. Renewable binders from waste biomass for road construction: A review on thermochemical conversion technologies and current developments. *Construction and Building Materials,* 330**,** 127076.
WEIR, A. I., AIREY, G., SNAPE, C. & JIMÉNEZ DEL BARCO CARRIÓN, A. Rheological Characterisation of Modified Bitumens with Biodiesel-Derived Biobinders. RILEM International Symposium on Bituminous Materials, 2020. Springer, 1563-1569.
WEN, H., BHUSAL, S. & WEN, B. 2012. Laboratory evaluation of waste cooking oil-based bioasphalt as an alternative binder for hot mix asphalt. *Journal of Materials in Civil Engineering,* 25**,** 1432-1437.
WEST, R. 2010. Reclaimed asphalt pavement management: best practices. *Auburn, AL: National Center for Asphalt Technology, NCAT Draft Report*.
WHISNANT, D. 2021. *Polymer Chemistry: The Glass Transition* [Online]. LibreTexts. Available:

https://eng.libretexts.org/Bookshelves/Materials_Science/Supplemental_Modules_(Materials_Science)/Polymer_Chemistry/Polymer_Chemistry%3A_Transitions/Polymer_Chemistry%3A_The_Glass_Transition [Accessed September 2022].
WILLIAMS, R. C., FERREIRA PERALTA, E. J. J. F. & NG PUGA, K. L. N. 2015. Development of non-petroleum-based binders for use in flexible pavements–Phase II.
WILLIAMS, R. C., METWALLY, M. A. R. M. & BROWN, R. C. 2017. *Bio-oil formulation as an asphalt substitute*. US patent application 9,546,276 B2.
WILLIAMS, R. C., SATRIO, J., ROVER, M., BROWN, R. C. & TENG, S. Utilization of fractionated bio oil in asphalt. 88th annual meeting of the Transportation Research Board, Washington, DC, 2009.
WU, J. & AIREY, G. 2009. The influence of aggregate interaction and aging procedure on bitumen aging. *Journal of testing and evaluation,* 37**,** 402-409.
WU, J., HAN, W., AIIEY, G., YUSOFF, M. & IZZI, N. 2014. The Influence of Mineral Aggregates on Bitumen Ageing. *International Journal of Pavement Research & Technology,* 7.
WU, S.-P., PANG, L., MO, L.-T., CHEN, Y.-C. & ZHU, G.-J. 2009. Influence of aging on the evolution of structure, morphology and rheology of base and SBS modified bitumen. *Construction and Building Materials,* 23**,** 1005-1010.
XU, C. & ETCHEVERRY, T. 2008. Hydro-liquefaction of woody biomass in sub-and super-critical ethanol with iron-based catalysts. *Fuel,* 87**,** 335-345.
XU, C. & LANCASTER, J. 2008. Conversion of secondary pulp/paper sludge powder to liquid oil products for energy recovery by direct liquefaction in hot-compressed water. *Water research,* 42**,** 1571-1582.
XU, S., WANG, K., WAYIRA, A. & LU, J. 2015. Influence of binder properties on the performance of asphalts. *The Shell Bitumen Handbook.* 6 ed. London: ICE Publishing.
XUE, Y., WU, S., CAI, J., ZHOU, M. & ZHA, J. 2014. Effects of two biomass ashes on asphalt binder: Dynamic shear rheological characteristic analysis. *Construction and Building Materials,* 56**,** 7-15.
YADAV, L. D. S. 2013. *Organic spectroscopy*, Springer Science & Business Media.
YANG, S.-H. & SUCIPTAN, T. 2016. Rheological behavior of Japanese cedar-based biobinder as partial replacement for bituminous binder. *Construction and Building Materials,* 114**,** 127-133.
YANG, X., MILLS-BEALE, J. & YOU, Z. 2017. Chemical characterization and oxidative aging of bio-asphalt and its compatibility with petroleum asphalt. *Journal of cleaner production,* 142**,** 1837-1847.
YANG, X. & YOU, Z. 2015. High temperature performance evaluation of bio-oil modified asphalt binders using the DSR and MSCR tests. *Construction and Building Materials,* 76**,** 380-387.
YANG, X., YOU, Z. & DAI, Q. 2013. Performance Evaluation of Asphalt Binder Modified by Bio-oil Generated from Waste Wood Resources. *International Journal of Pavement Research & Technology,* 6.
YANG, X., YOU, Z., DAI, Q. & MILLS-BEALE, J. 2014. Mechanical performance of asphalt mixtures modified by bio-oils derived from waste wood resources. *Construction and Building Materials,* 51**,** 424-431.
YILDIRIM, Y. 2007. Polymer modified asphalt binders. *Construction and Building Materials,* 21**,** 66-72.
YOU, Z., MILLS-BEALE, J., FINI, E., GOH, S. W. & COLBERT, B. 2011. Evaluation of low-temperature binder properties of warm-mix asphalt, extracted and recovered RAP and RAS, and bioasphalt. *Journal of materials in Civil Engineering,* 23**,** 1569-1574.
YU, J., VAIDYA, M., SU, G., ADHIKARI, S., KOROLEV, E. & SHEKHOVTSOVA, S. 2021. Experimental study of soda lignin powder as an asphalt modifier for a sustainable pavement material. *Construction and Building Materials,* 298**,** 123884.
YUSOFF, N. I. M., MOUNIER, D., MARC-STÉPHANE, G., HAININ, M. R., AIREY, G. D. & DI BENEDETTO, H. 2013. Modelling the rheological properties of bituminous binders using the 2S2P1D Model. *Construction and Building Materials,* 38**,** 395-406.

YUSOFF, N. I. M., SHAW, M. T. & AIREY, G. D. 2011. Modelling the linear viscoelastic rheological properties of bituminous binders. *Construction and Building Materials,* 25**,** 2171-2189.
YVELINES, C. G. 2011. Catalogue des revêtements adaptés aux véloroutes, voies vertes, pistes cyclables et bandes cyclables. Mission Politique Technique

Direction des Routes et des Transports.
ZAUMANIS, M., MALLICK, R. B. & FRANK, R. 2014a. 100% recycled hot mix asphalt: A review and analysis. *Resources, Conservation and Recycling,* 92**,** 230-245.
ZAUMANIS, M., MALLICK, R. B., POULIKAKOS, L. & FRANK, R. 2014b. Influence of six rejuvenators on the performance properties of Reclaimed Asphalt Pavement (RAP) binder and 100% recycled asphalt mixtures. *Construction and Building Materials,* 71**,** 538-550.
ZHANG, Q., CHANG, J., WANG, T. & XU, Y. 2007. Review of biomass pyrolysis oil properties and upgrading research. *Energy conversion and management,* 48**,** 87-92.
ZHANG, R., WANG, H., GAO, J., YOU, Z. & YANG, X. 2017. High temperature performance of SBS modified bio-asphalt. *Construction and Building Materials,* 144**,** 99-105.
ZHANG, X. 2016. Essential scientific mapping of the value chain of thermochemically converted second-generation bio-fuels. *Green Chemistry,* 18**,** 5086-5117.
ZHONG, C. & WEI, X. 2004. A comparative experimental study on the liquefaction of wood. *Energy,* 29**,** 1731-1741.
ZHU, H., XU, G., GONG, M. & YANG, J. 2017. Recycling long-term-aged asphalts using bio-binder/plasticizer-based rejuvenator. *Construction and Building Materials,* 147**,** 117-129.
ZHU, J., AHMED, A. & DINEGDAE, Y. 2021. *Bitumen properties and the shear resistance of asphalt mixtures: towards a tool for bitumen selection*, Statens väg-och transportforskningsinstitut.
ZOFKA, A. & YUT, I. 2012. Investigation of rheology and aging properties of asphalt binder modified with waste coffee grounds. *Transportation Research E-Circular***,** 61-72.

Appendix A. Summary of the influence of biobinder composition on bituminous binders' properties and performance

↓	Decrease compared to conventional materials
↑	Increase compared to conventional materials
✓	Better comparison to conventional materials
x	Worse comparison to conventional materials
~	Similar performance to conventional materials
-	Not known/specified

Thermochemical Technology used	Ref.	Biobinder	Replacement (%)	Biobinder used as	Rheology	Viscosity	Complex Modulus	Phase Angle	Rutting resistance	Fatigue resistance	Thermal cracking resistance	Moisture Damage	Temperature susceptibility	Ageing resistance	Durability in field
Pyrolysis	(Peralta et al., 2012)	Oakwood and crumb rubber	100	Binder replacement	-	~	-	-	-	-	-	-	-	-	-
	(Williams et al., 2015)	Oakwood and crumb rubber	20	Bitumen extender	~	~	~	~	~	✓	~	✓	-	~	-
	(Raouf and Williams, 2010b)	Switchgrass oil	100	Binder replacement	-	~	-	-	-	-	-	-	↑	-	-
	(Mohammad et al., 2013)	Pine wood biomass	Up to 50%	Bitumen extender	-	↓	-	-	✓	-	✓	~	-	-	-
	(Yang and Suciptan, 2016)	Japanese cedar chips	2 and 8% And 25 and 50%	Bitumen modifier and extender	-	↑	~	↑	✓	-	↓	-	↓	-	-
	(Williams et al., 2009)	Oakwood, switchgrass and corn stover oils	3-9%	Bitumen modifier	-	-	-	-	✓	-	x	-	-	-	-
	(Yang et al., 2014)	Waste wood resources	5 and 10%	Bitumen modifier	-	-	-	-	~	✓	-	-	-	-	-
	(Yang and You, 2015)	Waste wood resources	5 and 10%	Bitumen modifier	-	-	↑	↓	✓	-	-	-	✓	-	-
	(Yang et al., 2017)	Waste wood resources in the form of wood chips, sawdust and shavings	2, 5 and 10%	Bitumen modifier	-	-	-	-	-	-	-	-	-	x	-
	(Zhang et al., 2017)	SBS-modified bio-oil	1% SBS, 5-20% bio-oil	Bitumen modifier and extender	-	↓ with increase in bio-oil content	-	-	~ slightly weaker than base binder ✓ Stronger rutting resistance after RTFOT ageing	-	-	-	✓less temperature sensitive than base binder. Sensitivity ↓ with increase in bio-oil content both before and after RTFOT ageing	✓	-

Liquefaction	(Fini et al., 2011)	Biocrude from swine manure	2, 5 and 10%	Bitumen modifier	-	↓	↓ as biobinder content increased	-	~	-	✓	-	-	-	-
	(Fini et al., 2012)	Biocrude from swine manure	2, 5 and 10%	Bitumen modifier	-	↓	↓	-	-	-	✓	-	-	✓	-
	(You et al., 2011)	Biocrude from swine manure	2, 5 and 10%	Bitumen modifier	-	-	-	-	-	-	✓	-	-	-	-
	(Fini and Buehler, 2012)	Biocrude from swine manure	2, 5 and 10%	Bitumen modifier	✓for low temperature properties	-	-	-	-	-	✓	Potential to improve	-	-	-
	(Fini et al., 2013)	Biocrude from swine manure with crumb rubber	5, 10 and 15% crumb rubber blended with 5% biobinder	Bitumen modifier	-	↓ than a common crumb-rubber modified binder. This is less significant at higher temperatures	-	-	-	-	✓	-	↓	-	-
	(Aflaki et al., 2014)	Biocrude from swine manure	2, 5 and 10%	Bitumen modifier	-	-	-	-	-	-	✓	-	-	-	-
	(Mills-Beale et al., 2012)	Biocrude from swine manure	5%	Bitumen modifier	✓	↓	↓	↓	✓	-	✓	-	~ can potentially enhance both the high- and low-temperature susceptibility of typical binders	✓ potential to reduce ageing without compromising rutting performance	-
	(Fini et al., 2017)	Swine manure, miscanthus pellets, corn stover and wood pellets	10%	Bitumen modifier	Ranked differently before and after ageing	↓ in unaged biobinders to that of control but ↑ after ageing	↑ after ageing except for swine manure biobinder (only ↑ at low frequencies after ageing)	↓ for swine manure biobinder after ageing but ~ behaviour at high frequencies ↓ for Miscanthus, and corn stover than control Wood pellet lowest phase angle	✓	-	-	-	Wood pellet most susceptible to temperature and miscanthus least susceptible	Wood pellet highest susceptibility to ageing followed by miscanthus, corn stover, control and then swine manure	-
	(Samieadel et al., 2018)	Biocrude from swine manure	10%	Bitumen modifier	-	-	-	-	-	-	-	-	-	-	-
	(Dhasmana et al., 2015)	*Spirulina* sp. algae (microalgae), swine manure, and nanoalgae	Studied as virgin biobinder and blended biobinder with PG 64-22 bitumen in a 1:8 ratio	Bitumen modifier	~ but more work needed	~	↓ before ageing for virgin biobinders ~ behaviour to aged base binder when blended with bitumen and aged	↓ after ageing for virgin samples ~ behaviour when blended	-	-	✓	↓	-	Stiffer virgin biobinders after ageing, algal feedstocks stiffer than swine manure ~ behaviour to aged base binder	-

Liquefaction	(Audo et al., 2015)	*Scenedesmus* sp. Microalgae	100%	Binder replacement	~ similar properties to that of bitumen	-	~	~	-	-	-	-	-	-	-
	(Borghol et al., 2018)	*Spirulina* sp. residues	100%	Binder replacement	~ viscoelastic profile to an elastomer-containing bitumen composed of ca. 8% SBS dispersed in bitumen	-	↓	↓	-	-	-	-	↓ water-insoluble fraction appears to be less temperature sensitive than conventional bitumen, particularly at high temperatures	-	-
	(Mahssin et al., 2019)	Household food waste	5 and 10%	Bitumen modifier	-	~	-	-	-	-	-	-	↓	-	-
Recycled Asphalt	(Blanc et al., 2019a)	Bio-rejuvenator SYLVAROAD™ Biobinder Biophalt® Bio-additive Epoxidized Soybean Soyate (EMS)	Up to ~5% added to mixtures with 50% RA	Bitumen modifier	✓	-	✓	✓	-	✓	-	-	-	-	-
	(Jimenez del Barco Carrión et al., 2015)	Rejuvenator A (regenerated oil and a Fischer-Tropsch wax) and Rejuvenator B (highly viscous material free of polycyclic aromatic hydrocarbons)	6,12 and 18% Rejuvenator A and 9, 18 and 27% Rejuvenator B added to RA mixture	Bitumen modifier and extender	-	↓	-	-	✓	✓	✓	-	-	-	-
	(Blanc et al., 2019b)	Bio-rejuvenator SYLVAROAD™ Biobinder Biophalt® Bio-additive Epoxidized Soybean Soyate (EMS)	Up to ~5% added to mixtures with 50% RA	Bitumen modifier	✓	-	-	-	✓	✓	✓	-	-	-	✓
	(Zaumanis et al., 2014b)	Waste vegetable oil, waste vegetable grease, organic oil, distilled tall oil, aromatic extract and waste engine oil	12% added to RA mixture	Bitumen modifier	✓	↓	-	-	↑	↑	↑	↑	-	↓	-

Recycled Asphalt	(Tran et al., 2017)	Bio-rejuvenator SYLVAROAD™	6.8% added to mixtures with 50% RA	Bitumen modifier	-	-	-	-	✓	-	✓	-	-	✓in short-term laboratory testing	-
	(Mogawer et al., 2013)	Rejuvenators BituTech RAP SonneWarmix RJT and RJ	9.28% added to mixtures containing 35 and 40% RA	Bitumen modifier	✓	↓	-	-	x	✓	✓	x	-	✓	-
	(Ding et al., 2019)	Crumb rubber with a commercial rejuvenator	3, 5 and 7% rejuvenator added to mixtures containing 0, 30 and 50% RA	Bitumen modifier	-	-	-	-	↓	✓	✓	✓	-	-	-
	(Sotoodeh-Nia et al., 2019)	Crude tall oil and soybean oil derivative	3 and 6% added to mixtures containing 50% RA	Bitumen modifier	✓	-	↓ at high temperatures	↓ as dynamic modulus |E*| decreases	~	~	✓	-	-	↓	-
	(Chailleux et al., 2018)	Bio-rejuvenator SYLVAROAD™ Biobinder Biophalt® Bio-additive Epoxidized Soybean Soyate (EMS)	Up to 2.8% biobinder added to mixtures containing 50% RA	Bitumen modifier	✓	-	✓	-	✓	✓	✓	✓	-	↑	-
	(Manke et al., 2019)	Biobinder Biophalt®	1.7% added to mixtures containing 50% RA	Bitumen modifier	-	-	-	~ at low temperatures/high frequency, ↓ at high temperatures/low frequency and ↑ at intermediate temperatures and 1 Hz frequency	✓	~	✓	~	-	-	-
	(Mogawer et al., 2016)	Swine manure	5% biobinder added to mixtures containing 40% RA	Bitumen modifier	-	↓	-	-	~	✓	✓	~	↓	-	↑
	(Hill et al., 2013)	Swine manure	5% biobinder added to mixtures of 0, 15 and 45% RA	Bitumen modifier	-	↓	-	-	-	-	✓	-	↓	-	-
	(Hill et al., 2018)	Swine manure, corn stover, miscanthus and wood pellets	5 and 10% biobinder added to mixtures with 0, 15 and 45% RA	Bitumen modifier	↑ viscoelastic response found to be superior than hot-mix asphalt	↓	-	-	-	-	↑	-	↓	✓potential to perform better than hot-mix asphalt except for corn stover	-
	(Nayak and Sahoo, 2017a, Nayak and Sahoo, 2017b)	Pongamia oil and a composite oil made from castor oil and coke oven gas	5, 10 and 15%	Bitumen modifier	✓	↓	↓	-	✓	✓	-	-	✓	-	-

Miscellaneous	(Chailleux et al., 2012)	Microalgae	100%	Binder replacement	~	-	~	~	-	-	-	-	~	-	-
	(Pouget and Loup, 2013)	Forestry industry by-products	5.7%	Bitumen modifier	~	↓	~	↓	-	-	~	-	-	x	-
	(Wen et al., 2012)	Waste cooking oil	10, 30 and 60%	Bitumen modifier and extender	✓	-	-	-	x	x	✓	-	-	~	-
	(Sun et al., 2016)	Biodiesel by-product from waste cooking oil (as aged binder rejuvenator)	2-8%	Bitumen modifier	-	↓	↓	-	x	✓	✓	-	-	-	-
	(Gong et al., 2016)	Biodiesel by-product from waste cooking oil (as aged binder rejuvenator)	1.5,1.75 and 2%	Bitumen modifier	✓	↓	✓	-	x	✓	✓	x	-	-	-
	(Seidel and Haddock, 2012)	Soy fatty acids	1 and 3%	Bitumen modifier	✓	↓	↓	-	-	-	-	-	-	-	-
	(Zofka and Yut, 2012)	Waste coffee grounds	2 to 8%	Bitumen modifier	-	↓	-	-	-	-	-	-	~	↓ oxidation rate increase with an increase of coffee ground content but does not exceed that one of the base binder	-
	(Martínez-Echevarría-Romero et al., 2015)	Vinasse	10%	Bitumen modifier	✓	-	-	-	-	✓	-	~	-	-	-
	(Xue et al., 2014)	Rice husk and wood sawdust	10 and 20%	Bitumen modifier and extender	✓	↑	↑	↓	✓	-	-	-	-	↓	-
	(Somé et al., 2016)	Plant resin fluxed with monoalkyl esters from vegetable and animal oils	0.5 and 5%	Bitumen modifier	-	↓	✓	↑	-	-	-	-	-	x	✓good after 5 years but not enough to draw definite conclusions
	(Caro et al., 2016)	Sugarcane bagasse, corncobs and rice husk	1 and 2%	Bitumen modifier	✓	-	↑	-	✓	-	-	x	-	↑ with the exception of a rice husk biobinder, age-related hardening effects were smaller at low dosages than the control	-

														although this trend changed at higher dosages	
	(Gong et al., 2017)	Natural bean oil	1-3%	Bitumen modifier	-	-	-	-	-	-	-	Depends on base bitumen	-	-	-
Synthetic	(Airey and Mohammed, 2008)	Polyethyl acrylate (PEA), polymethyl acrylate (PMA) and polybutyl acrylate (PBA)	100%	Binder replacement	✓except for PBA	-	✓ except for PBA	✓ except for PBA	-	-	-	-	-	-	-
	(Airey et al., 2008)	Polyethyl acrylate (PEA), polymethyl acrylate (PMA) and polybutyl acrylate (PBA)	25-75%	Bitumen extenders	✓the blends produced similar but not identical rheological properties to SBS PMBs	-	✓	✓	-	-	-	-	-	-	-
	(Zhu et al., 2017)	Cotton oil by-product and dibutylphthalate (DBP) (as aged binder rejuvenator)	5 and 10%	Bitumen modifier	✓	~ 10% bio-rejuvenator is enough to restore the viscosity of the PAV-aged bitumen to its original level	↓	-	x	✓	✓	-	-	-	-